Contribution to Chiral Discrimination in the Solid State and Access to Pure Enantiomer via Crystallization

François-Xavier Gendron

THÈSE

Pour obtenir le diplôme de doctorat

Spécialité Physique

Préparée au sein de l'Université
De Rouen Normandie

Contribution to Chiral Discrimination in the Solid State & Access to Pure Enantiomer via Crystallization

Présentée et soutenue par
François-Xavier GENDRON

Thèse soutenue publiquement le 29 Juin 2018 devant le jury composé de		
M. Richard M. KELLOGG	Prof. University of Groningen	Rapporteur
M. Jean-Jacques COUNIOUX	Prof. University of Lyon I	Rapporteur
Mme. Christine MARTIN	Dr. University of Caen	Examinateur
M. Gérard COQUEREL	Prof. University of Rouen	Directeur de thèse

Thèse dirigée par Gérard COQUEREL, professeur des universités au laboratoire Sciences et Méthodes Séparatives (EA 3233 SMS)

A la pépite Agathe,

arrivée au début de la fin.

&

A ma famille, qui m'a

accompagné depuis 6 ans

&

A mon grand-père André,

parti à la fin du début.

“Don’t the great tales never end?”

“No, they never end as tales,” said Frodo, “but the people in them come, and go when their part’s ended. Our part will end later – or sooner.”

J. R. R. Tolkien, The Two Towers

"If more of us valued food and cheer and song
above hoarded gold, it would be a merrier world."

J. R. R Tolkien, <u>The Hobbit</u>

Remerciements

Bien que cette thèse ait été rédigée dans la langue de Shakespeare, j'ai souhaité ici retourner à ma langue maternelle, celle de Molière, et ce afin de pouvoir pleinement y exprimer mes intentions.

Mes tout premiers remerciements sont pour le Professeur Gérard Coquerel pour, le temps d'une pause lors d'un cours, avoir reçu, lu et finalement accepté ma demande de stage. Ce fut le 1er pas d'un voyage de 6 ans à vos côtés.

I would like to thank the members of the jury committee for accepting the review of my thesis and for their questions and comments during the defense: Prof. Richard M. Kellogg, Prof. Jean-Jacques Counioux and Dr. Christine Martin.

Thanks also to the Prof. Reiko Kuroda to be the source of the last chapter of this thesis.

5 ans et 3 mois se sont donc écoulés depuis mes 1ers pas au sein du laboratoire. Comme pour toute thèse, des hauts et des bas sont venus « enrichir » cette expérience. Je remercie les différents permanents du laboratoire pour leurs aides, scientifique ou non, et en particulier lors de ces derniers mois : Clément Brandel, Morgane Sanselme, Nicolas Couvrat, Yohann Cartigny, Gabin Gbabobe, Valérie Dupray et Samuel Petit pour l'équipe Crist, ainsi que Pascal Cardinael et Valérie Peulon-Agasse pour l'équipe Chro.

Beaucoup d'autres membres du laboratoire SMS sont également à remercier, et ce pour différentes raisons.

La précédente gestionnaire Ghislaine Chevalier (pour ton aide administrative) et l'actuelle, Lucie Dautréaux (pour mes erreurs administratives résiduelles) ainsi que Marie Vaccaro et Céline Bensakoun (mes camarades du Pays de Caux) et Françoise Ringot (Framboise).

La 1ère génération de doctorants que j'ai connue : Julien Mahieux (encadrement du 1er stage), Simon Clevers (Loulou), J.C Debray & Florent Simon (mon 1er surnom au labo : FootX).

La 2ème génération : Emilie Bobo (je léguerai notre place à une âme digne), Benjamin Schammé (quand tu veux pour le full), Mélanie Mignot (la Folle Mignot), Quentin Viel (mon 2ème surnom au labo : ChouppFx) et Aurélien Curat.

Une autre génération avec Lina Yuan (quand même) et Antoine Burel (Bibu).

Arrive enfin ma génération avec Bienvenu Atawa et Clément De Saint JoreS, mon tour est passé et vous êtes les prochains !!!

Les générations suivantes : Manon Schindler (Super SchinMan !!), CORE Project Lina Harfouch, Alyou Mbodjy &Ryusei Oketani, Kangli Li et enfin Chloé Sainlaud.

Et les stagiaires : Manon Poupard (PoupaMan !!), Maxime Charpentier, Aurélien Lemercier & Marine Hoquante. Mon cousin Valentin Aubert (3ème surnom évité : Gendron Beurre), Béranger Cardinot et Mélanie Canu.

Je tiens également à remercier un autre groupe qui se fait connaître sous le nom de « Les Dignes Fils de Gégé », nom que je n'approuve pas, pour leurs « soutiens » et leurs « compréhensions » tout au long de ma thèse : Antonin, Hervé, Charlotte, Aurélie & Ségolène. A partir de maintenant, je fais les fins de soirées avec vous.

Enfin je souhaite remercier ma famille. Les discussions ne sont pas l'un de nos points forts, et j'en suis un digne représentant, mais il n'empêche que vous avez toujours été là pour moi et cette thèse vous est dédié à vous : Papa, Maman, Aurélie & Camille & Agathe, Quentin & Camille, Mamie et tout le monde.

F.x

Contribution to Chiral Discrimination in the Solid State &
Access to Pure Enantiomer via Crystallization

Table of contents

Laboratoire SMS, Université de Rouen Normandie

François-Xavier Gendron

29/06/2018

Chapter 2 – Preferential Crystallization of a solid/solid demixing system

Chapter 3 – Racemic isoplethal section between two atropisomers & Chirality Induced by Dissymmetric Distribution

Contribution to Chiral Discrimination in the Solid State &
Access to Pure Enantiomer via Crystallization

General Introduction

Laboratoire SMS, Université de Rouen Normandie

François-Xavier Gendron

29/06/2018

The key word of this PhD manuscript is *chirality*. Since its discovery in the 19th century, chirality has been found to be involved in a large panel of domains: biology, pharmacy, chemistry, physico-chemistry, physics, etc. Thus, *chirality* is not sufficient to describe this thesis. More specifically, we have been interested in the phase equilibria involving chirality, and the opportunity of separation of the enantiomers that results from them.

The need for access to pure enantiomers has been accelerated since the nineties when new pharmaceutical restrictions imposed by medicinal agencies resulted in a strict control of the difference in activity and side effects between the enantiomers. The importance, and demand, for new, cheap, efficient and robust processes to obtain pure enantiomers are thus more important than ever.

Among the possible route for the access to pure enantiomers, one can directly synthesize the desirable enantiomer (asymmetric synthesis, synthesis from chiral pool, etc) or can use a process to separate the enantiomers from a racemic mixture (chromatography, Pasteurian resolution, …).

In this work, we focus only on processes using crystallization of chiral components, in particular *via* Preferential Crystallization or Deracemization.

After the recall of basic notions in Chapter 1, two studies will be presented.

The first one, the Chapter 2, is the basic application of an already well-known resolution process to a molecule of pharmaceutical interest. Baclofen, already used as muscle relaxant, has been undergoing an increase of its demand since recent results against addictions. Application of a low-cost separation method being relevant, Preferential Crystallization has been carry on its hydrogenomaleate salt. Even if the resolution of a conglomerate forming system by Preferential Crystallization is a well-known process, its application to mirror image partial solid solutions is more unusual.

The third chapter of this thesis is devoted to the phase equilibria existing between the racemic composition of two couples of atropisomers. This study is not directly related to the separation of enantiomers, but it could result in a facile deracemization. Through this chapter would be investigated:

- Three different quaternary equilibria (stable, metastable and apparent).
- A new simple recrystallization accelerator.
- A new kind of chirality (*Chirality Induced by Dissymmetric Distribution*) will be presented and theoretical cases will be discussed.
- The various possibilities of total or partial deracemization at different compositions of the system will be pointed out.

Contribution to Chiral Discrimination in the Solid State & Access to Pure Enantiomer via Crystallization

Chapter 1 – Thermodynamics, Crystallogenesis & Chirality

Laboratoire SMS, Université de Rouen Normandie

François-Xavier Gendron

29/06/2018

Introduction

In this chapter, generalities about crystalline state, thermodynamics of heterogeneous equilibria and chirality will be briefly detailed. The aim is not to treat thoroughly those different domains, but to give a general overview of them to ensure to the neophyte readers, as far as possible, a pleasant lecture of this work.

Part.I Thermodynamics & Heterogeneous Equilibria

I Thermodynamic phase and states of the matter

A *system* is a part of the universe delimited by real or fictive boundaries. *Open systems* exchange both matter and energy with surroundings, *closed systems* exchange only energy and *isolated systems* exchange nothing.

A *phase* is a part of a thermodynamic system that can be considered as homogeneous in properties (e.g composition, density, temperature, …) and constant in time.[1,2]

Crystalline is applied to phases that exhibit a periodic, three dimensional and strict arrangement of particles (atom(s), ions and/or molecule(s)). Those phases, called *crystals*, present a *Long Range Order* (LRO). Instead of crystal, in the contest of thermodynamics and heterogenous equilibria, we prefer to use the term of *solid* to describe this state of the matter.

In the gas or vapor phase, molecules have no interaction one with the other. In the liquid phase, molecules interact with their neighborhoods with certain conformations leading to the formation of a *Short Range Order* (SRO) (Figure 1).

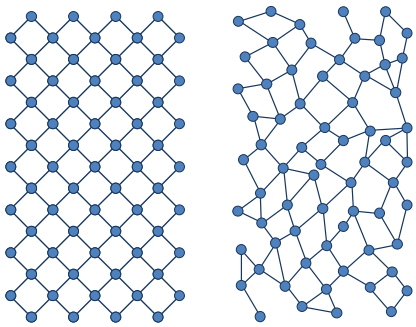

Figure 1. Schematic 2 dimensions representation of LRO (left) and a SRO (right).

According to the United States Pharmacopeia, the *amorphous solid* (or *glassy state*) is defined as "*a solid containing the maximum possible density of imperfections, such that all long-range order is lost while only the short-range order imposed by its nearest neighbors remains*". They present an "infinite" viscosity and a very low diffusion of particles. They are characterized by a *glass transition temperature* corresponding to the transition of the frozen glassy state to a *supercooled liquid*.[3] This glass transition temperature is not a thermodynamic transition since it depends on different conditions such as the heating condition, the solvent content (plastizing effect), the history of the sample, etc.

Thus, from thermodynamics point of view, amorphous solids are considered as a liquid-like state and not as a solid-like state.

II Phase equilibria

II.1 Energy of a system

The state of a system is given by its energy respecting one simple rule: the lower the energy, the better. To describe this energetic state, the *molar free enthalpy* or *Gibb's free energy* $\boldsymbol{G}$ is commonly used.[4]

$$\boldsymbol{G = U + PV - TS} \qquad \textit{Eq. 1}$$

Where $\boldsymbol{U}$ is the *molar internal energy* of the system, $\boldsymbol{V}$ the *molar volume*, $\boldsymbol{S}$ the *molar entropy* and $\boldsymbol{P}$ and $\boldsymbol{T}$ the pressure and the temperature.

Gibb's free energy can also be written as:

$$\boldsymbol{G = H - TS} \qquad \textit{Eq. 2}$$

Where $\boldsymbol{H}$ is the *molar enthalpy* of the system which represents the total amount of heat of the system whereas the entropy is associated to its disorder.[5]

The pre-mentioned rule concerning the energy of a system can be formalized by:[6,7]

- A single transformation of a system is made spontaneous when the free energy of the final state is lower than that of the initial one.

$$\Delta G = G_{final} - G_{initial} = \Delta H - T\Delta S < 0 \qquad Eq.\ 3$$

- The most stable state of a thermodynamic system is attained when its molar free energy is at its lowest possible value. A mixture of different phases can be necessary to fulfill this condition.

II.2 Equilibrium and stability

When concomitant thermal (δT), mechanical (δP) and chemical (δn_i) equilibria are reached, the system is at equilibrium and at a minimum value of free energy.

Several levels of equilibria can be reached. Thus, one can define (Figure 2):

- *Instable* state: when the free enthalpy is not at a minimum value, the system is unstable and will evolve to reach the nearest equilibrium.
- *Metastable equilibrium*: if the system reaches a local minimum of the free enthalpy, it is at a metastable state. It is at equilibrium but not the lowest one. System would need activation energy (E_a or ΔG_a) to leave this equilibrium to a more stable one (metastable or stable).
- *Stable equilibrium*: the global free energy minimum corresponds to the stable equilibrium.

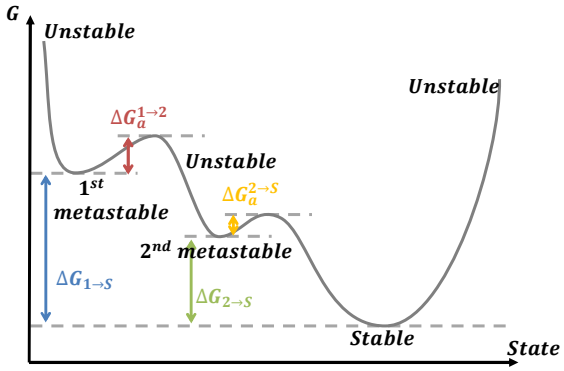

Figure 2. Energetic landscape for a system with two metastable equilibria.

Ostwald rule of stage[8,9] sets that an out of equilibrium system will undergo transformation(s) (phase transition(s)) between intermediate metastable state(s) before to reach the stable equilibrium.

II.3 Variance

The variance corresponds to the *number of degrees of freedom.* If $\boldsymbol{C}$ corresponds to the number of *independent component(s)* of a system (not linked by any chemical reaction), $\boldsymbol{N}$ the number of *extensive variable(s)* and $\boldsymbol{\varphi}$ the number of phase(s) in equilibrium, so the *variance* $\boldsymbol{v}$ is given by:

$$\boldsymbol{v = C + N - \varphi} \qquad \textit{Eq. 4}$$

This equation is known as the *Gibbs' phase rule.*[4] It is the number of the $\boldsymbol{C - 1 + N}$ variables (pressure, temperature and/or composition(s)) that can be changed without modifying the equilibrium.

For $\boldsymbol{v = 0}$, the equilibrium is *invariant*, *monovariant* for $\boldsymbol{v = 1}$, *bivariant* for $\boldsymbol{v = 2}$, and so on…

III Phase diagram

This part is mainly based on the book of John Ettore Ricci, The phase rule and heterogeneous equilibrium published in 1966.[10]

Heterogenous equilibria studied and presented in this work concern the condensed liquid and solid phases. The gas phase would be represented in the low order systems but we will not discuss its equilibria. Solid lines represent stable equilibria whereas dotted lines represent metastable equilibria.

III.1 Unary phase diagram

A phase diagram dealing with chemically pure component ($\boldsymbol{C = 1}$) is called *unary phase diagram*. The extensive variables are the temperature and the pressure ($\boldsymbol{N = 2}$). It can be represented in 2D ($\boldsymbol{P}$,$\boldsymbol{T}$) diagram:

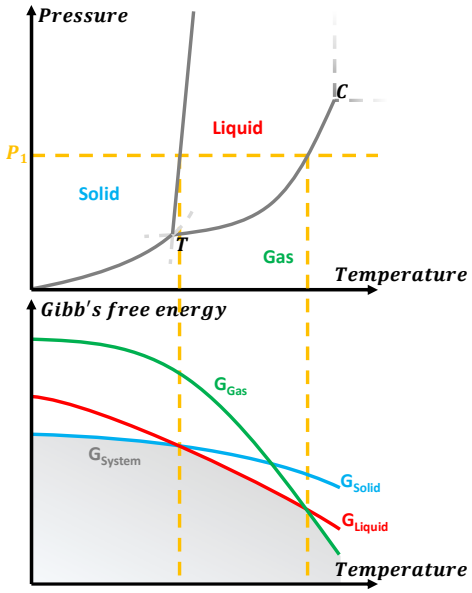

Figure 3. Unary phase diagram (top) and $\boldsymbol{P_1}$ *corresponding* ($\boldsymbol{G}$,$\boldsymbol{T}$) *diagram.*

The variance for such a system is given by the Eq. 5 and the shape of each domain, according to the variance, is listed in Table 1.[6]

$$\boldsymbol{v = 3 - \varphi} \qquad \textit{Eq. 5}$$

Table 1. Domains shape for unary phase diagram.

Type of domain	(P,T) representation	
	Variance $v = 3 - \varphi$	Domain's shape
Monophasic ($\varphi = 1$)	2	Surface
Biphasic ($\varphi = 2$)	1	Line
Triphasic ($\varphi = 3$)	0	Point

Phases repartition and domains shapes are determined by the minimization of the free energy $\boldsymbol{G}$ (Figure 3). Linear combinations of two free energies give rise to a biphasic domain and linear combinations of three free energies to a triphasic domain (*triple point* for unary system).

Over a certain **P** and **T** value, *super-critical fluid* appears that corresponds to both liquid and gas phases merging into a unique one.

Moreover, several solid phases may exist for the same component (atom(s), ions and/or molecule(s)). This behavior is known as *allotropism* or *polymorphism*[11–13] defined by Mc Crone as "*a solid crystalline phase of a given compound, resulting from the possibility of at least two different arrangements of the molecules of that compound in the solid state*". As polymorphs present different structural packings, their physicochemical properties, related to their structures, are different.

As shown in Figure 4, when two polymorphs have their own domains of stability, they have an *enantiotropic* behavior. There is a reversible transition, between the two polymorphs, at defined temperatures and pressures.

Otherwise they have a *monotropic* behavior: one polymorph is metastable while the other one is the stable solid phase.

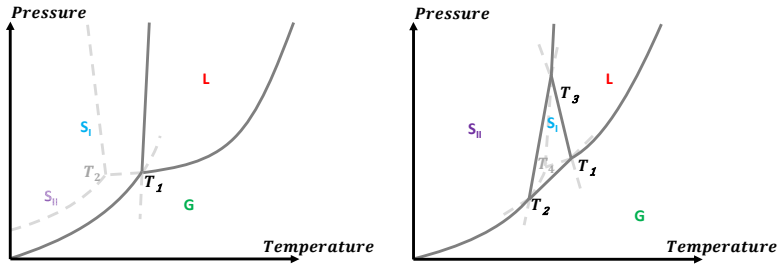

Figure 4. Monotropic (left) and enantiotropic (right) behavior in unary phase diagrams.

III.2 Binary phase diagram

In addition of the pressure and the temperature, another variable appears for binary system: the composition between the $\boldsymbol{A}$ and $\boldsymbol{B}$ components ($\boldsymbol{C-1=1}$). Compositions can be expressed in *weight* ($\boldsymbol{x_i}$) (Eq. 6) or in *molar* ($\boldsymbol{X_i}$) (Eq. 7) *fraction*.

$$x_A = \frac{m_A}{m_A+m_B} \quad \text{and} \quad x_B = \frac{m_B}{m_A+m_B} \quad \text{with} \quad x_A + x_B = 1 \qquad \textit{Eq. 6}$$

$$X_A = \frac{n_A}{n_A+n_B} \quad \text{and} \quad X_B = \frac{n_B}{n_A+n_B} \quad \text{with} \quad X_A + X_B = 1 \qquad \textit{Eq. 7}$$

General expression can be made for a $\boldsymbol{j}$-order system ($\boldsymbol{j}$ components):

$$x_i = \frac{m_i}{\sum_{k=1}^{j} m_k} \quad \text{and} \quad X_i = \frac{n_i}{\sum_{k=o}^{j} n_k} \quad \text{with} \quad \sum_{i=1}^{j} x_i = \sum_{i=1}^{j} X_i = 1 \qquad \textit{Eq. 8}$$

J. E. Ricci wrote that "*A binary system is completely defined, in representation, by a three-dimensional figure with the coordinates P, T, c, where c is the composition in weight percentage or mole fraction.*"[10] (Figure 5).

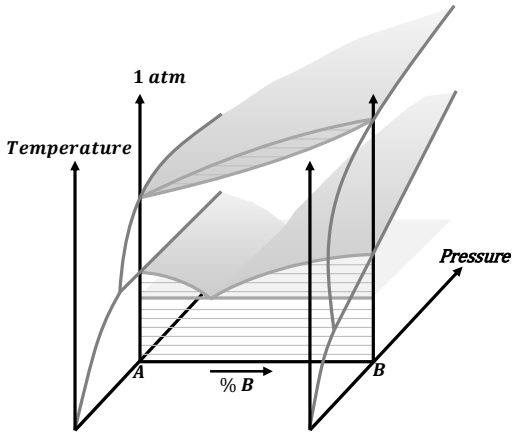

Figure 5. Completely defined binary system exploring pressure, temperature and composition variables. Domains boundaries are in bold line, tie-lines are in thin lines.

Due to the difficulties of pressure exploration and 3D representation and visualization, binary phase diagrams are, most of the time, represented by their *isobaric* representation ($\boldsymbol{T}$,%$\boldsymbol{B}$) at $\boldsymbol{P} = 1\ atm$ (Figure 6).

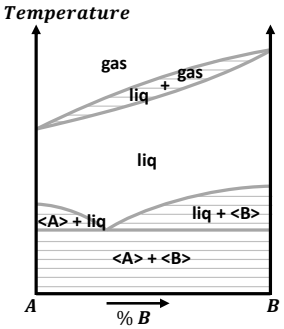

Figure 6. Isobaric binary section. Domains boundaries are in bold line, tie-lines are in thin lines.

The expression of the variance for a binary system is:

$$\boldsymbol{v = 4 - \varphi} \qquad \textit{Eq. 9}$$

Nevertheless, the isobaric sections permit a new expression of the variance (with $\boldsymbol{N = 1}$):

$$\boldsymbol{v' = 3 - \varphi} \qquad \textit{Eq. 10}$$

Table 2. Domains shape for binary phase diagram

Type of domain	Isobaric (T,%B) representation		Complete (P,T,%B) representation	
	Variance $v' = 3 - \varphi$	Domain's shape	Variance $v = 4 - \varphi$	Domain's shape
Monophasic **($\varphi = 1$)**	**2**	**Free surface**	**3**	**Free volume**
Biphasic **($\varphi = 2$)**	**1**	**2D bundle of tie-lines**	**2**	**3D bundle of tie-lines**
Triphasic **($\varphi = 3$)**	**0**	**Point**	**1**	**Line**

The different domains listed in Table 2 are obtained by free energy minimization (Figure 7). In binary systems, the stable state of a domain is often the mixture of several phases. Those phenomena appear when those phases, at different compositions, share the same slope break of the free energy:

$$\frac{\partial G_{phase\,1}(X_1)}{\partial X} = \frac{\partial G_{phase\,2}(X_2)}{\partial X} \qquad \textit{Eq. 11}$$

In that case, it is possible to draw a tangent line between the two curves of free enthalpy at X_1 and X_2 (Figure 7). Outside of those compositions, the system follows the free energy minimization rule. Between those compositions, the free energy of the system follows this tangent line and the two phases are in equilibrium. This is the *tangent rule* that can be encountered for higher order systems. Biphasic domains correspond in fact to *tie-lines* on which the two phases in equilibrium are represented by the extremities. The equilibrium condition imposed that tie-lines are isobaric and isothermal. Usual "biphasic domain" refers to the juxtaposition of infinite discrete tie-lines between the same phases (states are constant but compositions may vary) (Figure 5 & 6). For the sake of clarity, those discrete tie-lines are not represented (Figure 7) except when it is necessary (e.g solid solutions).

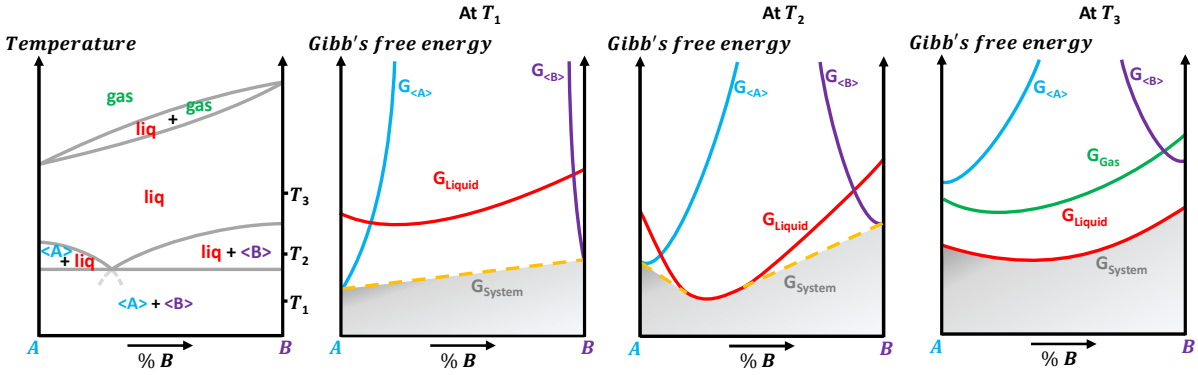

Figure 7. Binary phase diagram (left) and corresponding (G, %B) diagrams for three different temperatures.

A large number of equilibria can be encountered between two components since an "infinity" of pair of components can be established. Here below are listed the most common and useful, in this work, kind of binary phase diagrams:

- *Eutectic invariants* (Figure 7) correspond to the reaction:

$$< A > + < B > \overset{\Delta G=0}{\Longleftrightarrow} Liq$$

  Where two solids have a depression in their melting points. Eutectic invariants are defined by the eutectic point (composition and temperature) and by the compositions limits of the invariant.

- *Stoichiometric compounds* (or *defined compound*) (Figure 8.a) are new solid phases formed by the crystallization of different components together (cf. Part.II.I.2.4). The case presented here has a *congruent melting*: the molten state has the same composition as that of the compound.

- *Peritectic invariants* (Figure 8.b) correspond to the *incongruent melting* of a defined compound according to the reaction:

$$< C > \overset{\Delta G=0}{\Longleftrightarrow} Liq + < B >$$

  The peritectic invariant (temperature and composition) and the compositions limits of the invariant define this three phases domain at a fixed temperature.

- *Eutectoid invariants* (Figure 8.c) are the equivalence of the eutectic invariant but only with solid phases (ΔH>0 from left to right):

$$< A > + < B > \overset{\Delta G=0}{\Longleftrightarrow} < C >$$

- The same equivalence is found between p*eritectoid* and *peritectic* invariants (Figure 8.d (ΔH>0 from left to right):

$$< \boldsymbol{C} > \overset{\boldsymbol{\Delta G=0}}{\Longleftrightarrow} < \boldsymbol{A} > + < \boldsymbol{B} >$$

- Enantiotropy also affects phase diagrams in different way. In the case presented in Figure 8.e, it induces an invariant with the reaction (ΔH>0 from left to right):

$$< \boldsymbol{B} >_{\boldsymbol{LT}} \overset{\boldsymbol{\Delta G=0}}{\Longleftrightarrow} < \boldsymbol{B} >_{\boldsymbol{HT}}$$

- *Complete solid solutions* or *Solid Solution by means of Substitutions* (cf. Part.II.I.2.4) reflect in phase diagram by monophasic solid domains whatever the composition (Figure 8.f). The case represented here is a solid solution with a simple loop for melting. Nevertheless, the loop can present maximum or minimum melting(s).
- When the free energy curve of a phase has two inflection points, the tangent rule can be applied resulting in a biphasic domain. This phenomenon is called *demixion* or *miscibility gap* (Figure 8.g). It involves solid or liquid phases and appears in phase diagram by a biphasic domain surrounded by a monophasic one.
- If the miscibility gap is large enough to reach the fusion loop, it creates a eutectic invariant whose limits are not the pure components (Figure 8.h). The domain between this limit and the pure component corresponds to a *partial solid solution*.

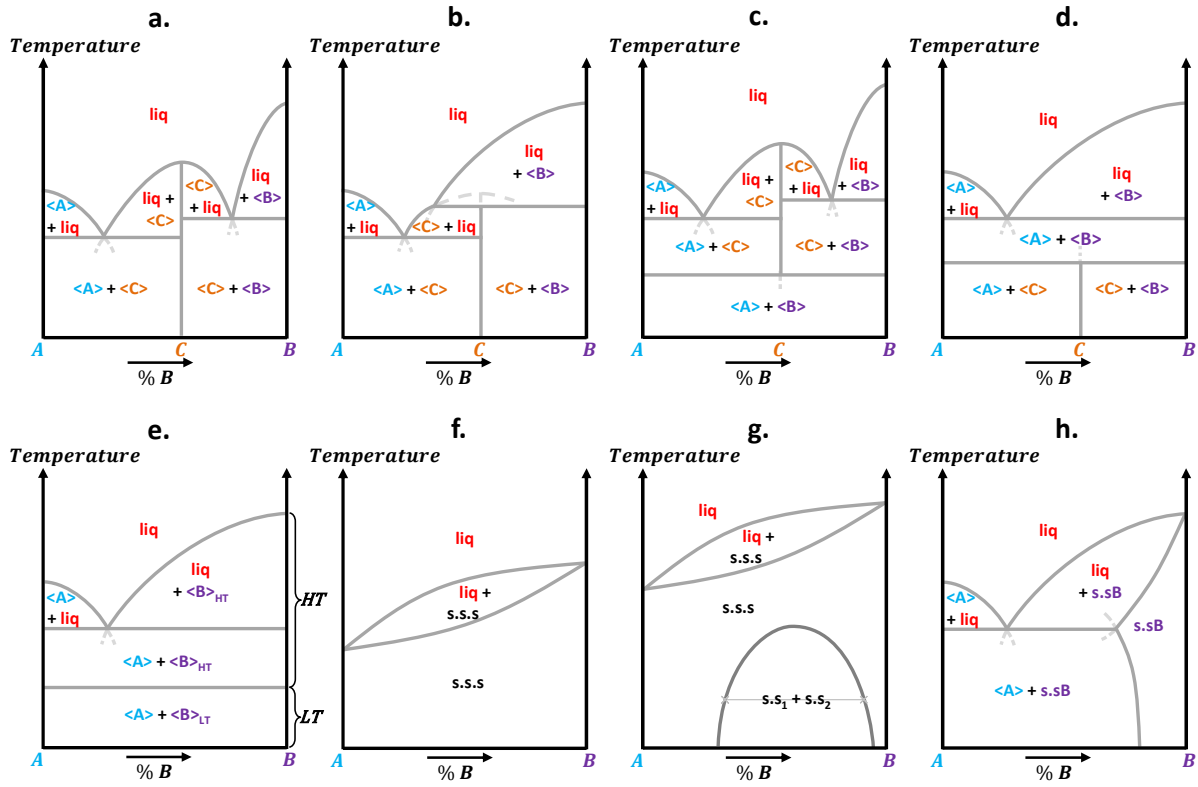

Figure 8. Binary phase diagrams with (a) a stoichiometric compound with congruent melting, (b) a stoichiometric compound with incongruent melting, (c) a eutectoid phase transition, (d) a peritectoid phase transition, (e) an enantiotropic behavior for one component, (f) a complete miscibility between the solid phases, (g) a miscibility gap and (h) a partial miscibility for one component.

In addition to those cases, other equilibria can be found.[14] To finish, metastable equilibria (monotectic, monotectoid, metatectic, syntectic, …) also enrich the possible landscape of binary phase diagrams.

When a mixture, of given composition and temperature, is in a biphasic domain, the two phases in equilibrium (nature and composition) are given by the tie-line at this temperature. Thus, in the Figure 9 mixture m is composed of a solid phase <B> at $x_{m''}$ composition and a liquid phase liq at $x_{m'}$.

Moreover, it is often useful to know the proportion between those two phases. This proportion can be deduced from the *lever rule*:

$$f_{liq}^{m} = \frac{mm''}{m'm''} = \frac{x_{m''} - x_m}{x_{m''} - x_{m'}} \quad \text{and} \quad f_{<B>}^{m} = \frac{m'm}{m'm''} = \frac{x_m - x_{m'}}{x_{m''} - x_{m'}} \quad \text{with} \quad f_{liq}^{m} + f_{<B>}^{m} = 1 \qquad \text{Eq. 12}$$

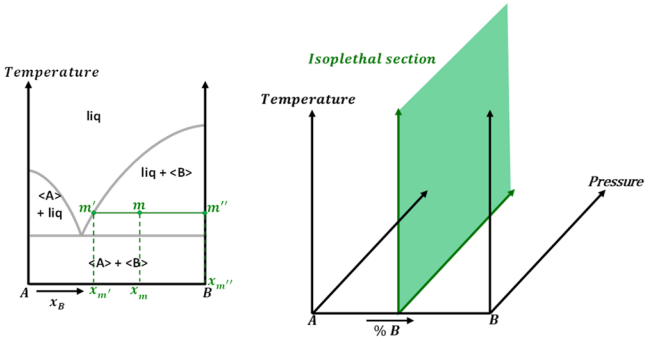

Figure 9. Lever rule applied in biphasic domain (left) and the $\%A = \%B = 50\%$ isoplethal section (right).

Isoplethal sections correspond to parts of phase diagram respecting fixed composition(s) ratio. In a binary diagram, to fix a composition impose to fix the other one. Isoplethal sections have so unary shape (Figure 9): dimensions are reduced from 3 (***T***, ***P*** and %***B***) to 2 (***T*** and ***P***).

III.3 Ternary phase diagram

Ternary is an adjective applied to system containing three components. For a mixture of those components, the compositions of each one are given by Eq. 8. The third composition being deduced from the two other, a complete ternary phase diagram is a 5-order system represented in four dimensions: ***T***, ***P***, %***A*** and %***B***. A visual representation of such system is impossible in our 3D space, therefore the pressure is usually fixed to reduce to a 4-order system represented in 3D: ***T***, %***A*** and %***B*** (Figure 10).

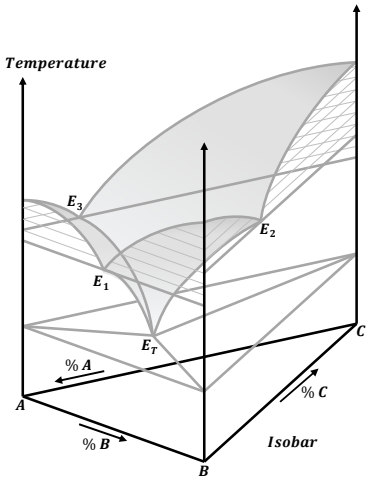

Figure 10. Isobaric representation of a ternary phase diagram with a ternary eutectic invariant at E_T. Domains boundaries are in bold line, tie-lines are in thin lines.

Phase repartition is possible in such representation but the shape and boundaries between each domain is difficult to visualize (Figure 11). This is why, as for binary system, a 2D

representation is preferred: the temperature is also fixed and the isobaric isotherm adopts the *Gibbs' composition triangle*[4] (Figure 11). In theory, the composition triangle can adopt any shape but in practice, the equilateral triangle and isosceles rectangular triangle (not represented here) are used.

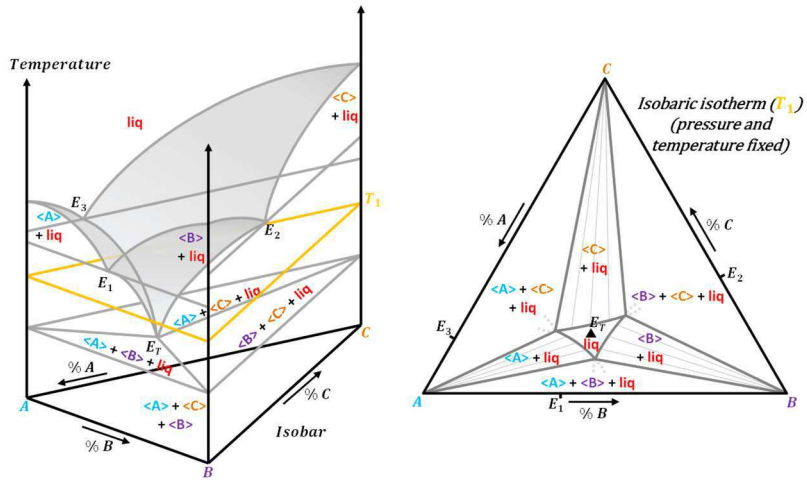

Figure 11. Repartition of the phases in Figure 10 ternary phase diagram (left) and T_1 isothermal and isobaric ternary section.

According to the representation used, the variance evolves:

- For the complete system:

$$\boldsymbol{v = 5 - \varphi} \qquad \textit{Eq. 13}$$

- Isobaric representation:

$$\boldsymbol{v' = 4 - \varphi} \qquad \textit{Eq. 14}$$

- Isobaric isotherms:

$$\boldsymbol{v'' = 3 - \varphi} \qquad \textit{Eq. 15}$$

Shapes of the different domains according to the representation and the variance are listed in Table 3. For the isobaric and isothermal 2D representation, those shapes are easily visible (Figure 11 & 13). For the isobaric 3D representation, the visualization is more difficult (Figure 12) since the boundaries between the domains are often curved surfaces.

As for previous systems, the minimization of **G** and the tangent rule give the stable state of the system. Note that ternary domains correspond to a tangent line between three different phases (Figure 12).

Table 3. Domains shape for ternary phase diagram.

Type of domain	Isobaric and isothermal $(\%A,\%B)$ representation		Isobaric $(T,\%A,\%B)$ representation	
	Variance $v'' = 3 - \varphi$	Domain's shape	Variance $v' = 4 - \varphi$	Domain's shape
Monophasic $(\varphi = 1)$	2	Free surface	3	Free volume
Biphasic $(\varphi = 2)$	1	2D bundle of tie-lines	2	3D bundle of tie-lines
Triphasic $(\varphi = 3)$	0	Tie-triangles	1	3D bundles of tie-triangles
Quadriphasic $(\varphi = 4)$	-1	Point	0	Point

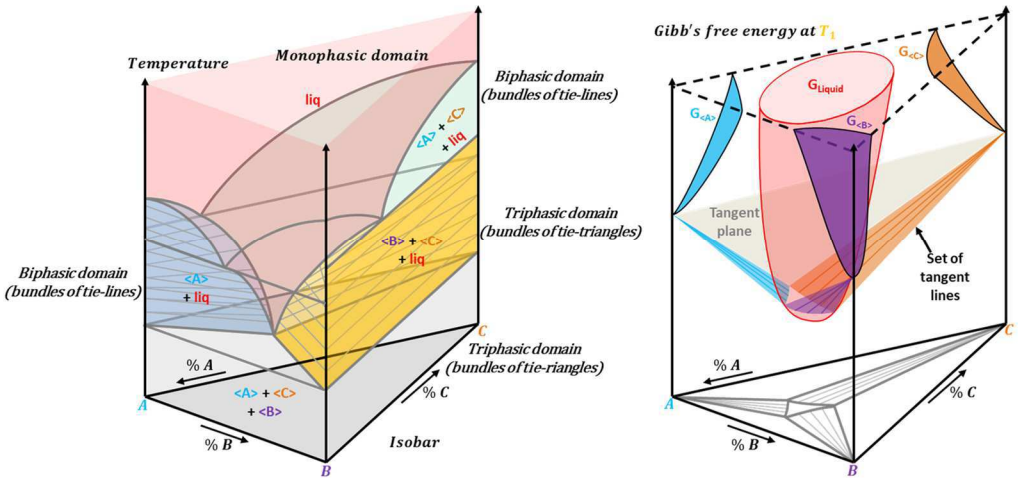

Figure 12. Shape of the different domains (left) and free energy versus composition diagram at T_1 (right) for the Figure 10.

Different usual cases of ternary isotherms are presented in Figure 13. Note that they are represented with the third component as a solvent and for temperatures inferior at the melting point of the two other components. Consequently, the liquid phase can be call a *solution* that can be *undersaturated* (**U.S.S**), *saturated* (**sat. sol.**) or even multiple saturated (**d.s.s** for doubly saturated) (cf. Part.II.II.1.1). The cases presented below are:

- isotherm between two non-miscible solids (*top left*).
- isotherm with a partial miscibility of ***B*** (*middle top*).
- isotherm for a complete miscibility binary system (*top right*).
- isotherm with a defined binary compound with congruent solubility (*bottom left*).
- defined binary compound with non-congruent solubility (*middle bottom*).

- isotherm with a defined ternary compound (*bottom right*).

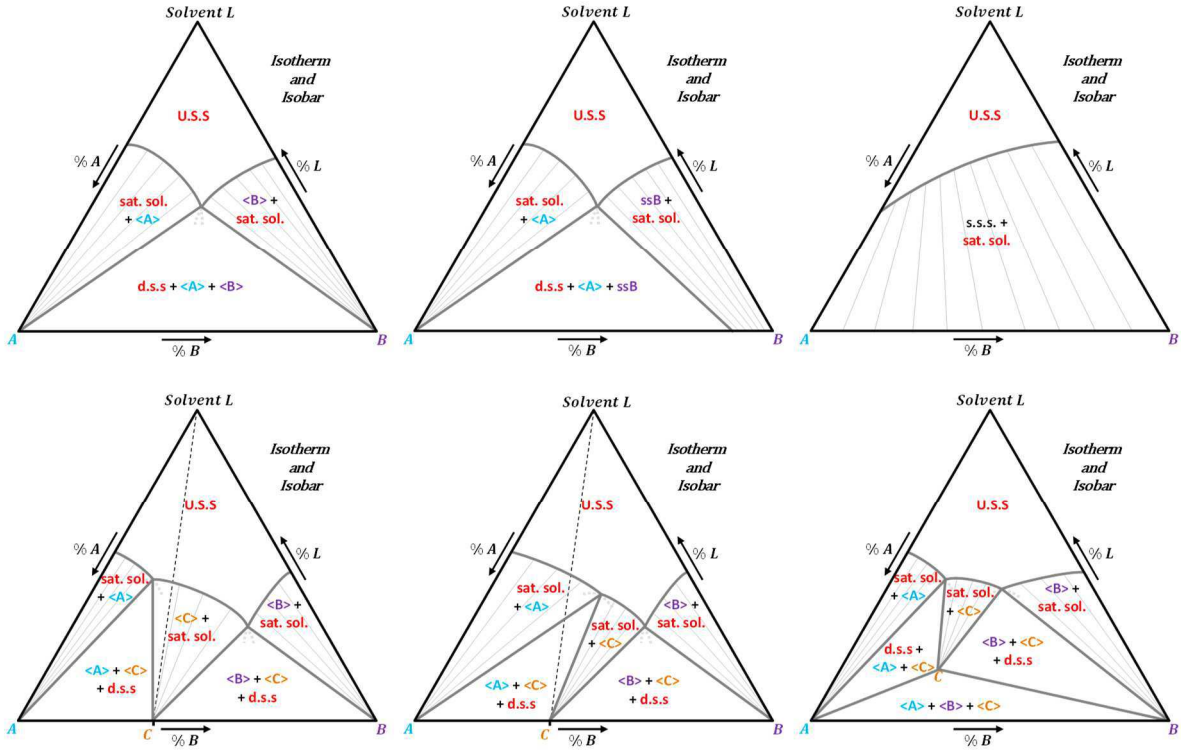

Figure 13. Classical ternary isotherms between: a solvent and (i) two non-miscible solids (top left), (ii) two solids with one partial miscibility (middle top), (iii) two totally miscible solids (top right), a system with a binary compound ($C = A_xB_y$) with (iv) congruent solubility (bottom left) and (v) incongruent solubility (middle bottom) and (vi) a system with a ternary compound ($C = A_xB_yL_y$) (bottom right).

As for binary system, metastability and other behaviors enlarge the landscape of ternary phase diagrams.

The analogy with binary system also fits for determination of the nature and proportion of the phases in a biphasic domain: compositions are the limits of the tie-line and the proportions are given by the lever rule (Figure 14). The same logics is applied in triphasic domains: nature of the three phases are given by the three apexes of the triangle (*tie-triangle*) and the proportion of each phase by a ratio of distances.

Example is given by point $\boldsymbol{M}$ in Figure 14 for which:

- Global composition in component $\boldsymbol{C}$ is given by:

$$\%\boldsymbol{C} = \frac{\boldsymbol{C'_M M}}{\boldsymbol{C'_M C}} * \boldsymbol{100} = \frac{\boldsymbol{c}}{\boldsymbol{BC}} * \boldsymbol{100} \qquad \textit{Eq. 16}$$

- Global composition in component B is:

$$\%\boldsymbol{B} = \frac{\boldsymbol{B'_M M}}{\boldsymbol{B'_M B}} * \mathbf{100} \qquad \textit{Eq. 17}$$

Whereas the proportion of phase **<B>** at this point is:

$$\boldsymbol{f^{M}_{<B>}} = \frac{\boldsymbol{m'_M M}}{\boldsymbol{m'_M B}} = \frac{\boldsymbol{b}}{\boldsymbol{SB}} \qquad \textit{Eq. 18}$$

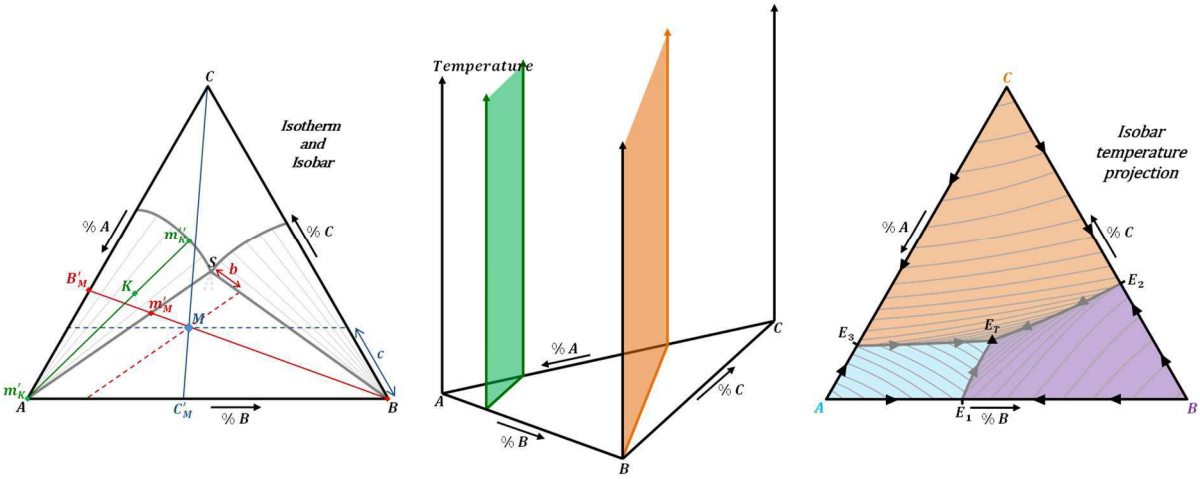

Figure 14. Compositions and phases proportions in a ternary isotherm (left), polythermal projection of Figure 10 ternary phase diagram (right) and different isoplethal sections in a ternary diagram (middle): green $\%A = 75\%$ *binary isoplethal section and orange* $\%A = 3 * \%C$ *binary isopleth.*

Middle picture of Figure 14 presents two binary isoplethal sections extracted from ternary phase diagram. The two isopleths are governed by different kinds of rule: the green one is obtained by fixing one composition constant (%***A*** here) whereas the orange section is obtained by fixing the ratio between two compositions constant (ratio %***A*** and %***C*** here).

Last representation in Figure 14 is the *polythermal projection*. This representation is useful when there is an interest on invariants (here ternary eutectic $\boldsymbol{E_T}$) and in invariant valleys.

III.4 Quaternary phase diagram

With another dimension to deal with, phase diagrams with 4 components cannot be fully represented in 3D. Therefore, quaternary systems are represented as isothermal and isobaric tetrahedron with each component on the apexes (Figure 15).

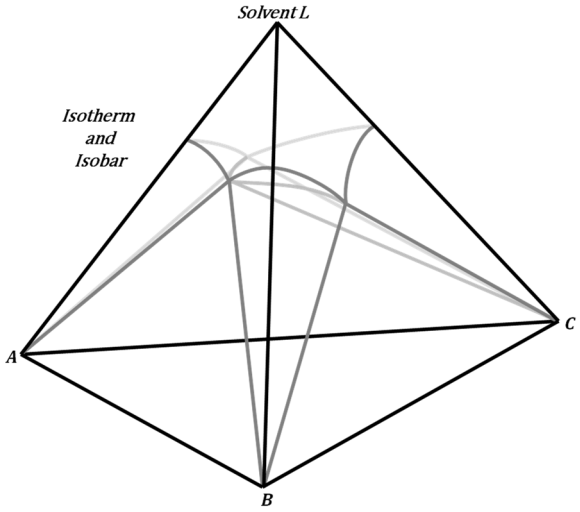

Figure 15. Isothermal and isobaric regular tetrahedron representation of a quaternary diagram.

The initial variance is:

$$\boldsymbol{v = 6 - \varphi} \qquad \textit{Eq. 19}$$

The isothermal and isobaric tetrahedron permits to modify the variance to:

$$\boldsymbol{v' = 4 - \varphi} \qquad \textit{Eq. 20}$$

The shape of the different domains according to this new expression are listed in Table 4:

Table 4. Domains shape for quaternary phase diagram.

Type of domain	Isobar and isotherm ($\%A$,$\%B$,$\%C$) representation	
	Variance $v' = 4 - \varphi$	Domain's shape
Monophasic ($\varphi = 1$)	3	Free volume
Biphasic ($\varphi = 2$)	2	3D bundle of tie-lines
Triphasic ($\varphi = 3$)	1	2D bundle of tie-triangles
Quadriphasic ($\varphi = 4$)	0	Tetrahedron
Pentaphasic ($\varphi = 5$)	-1	Point

Those shapes are highlighted in Figure 16. The case represented concerns a solvent and three different solids.

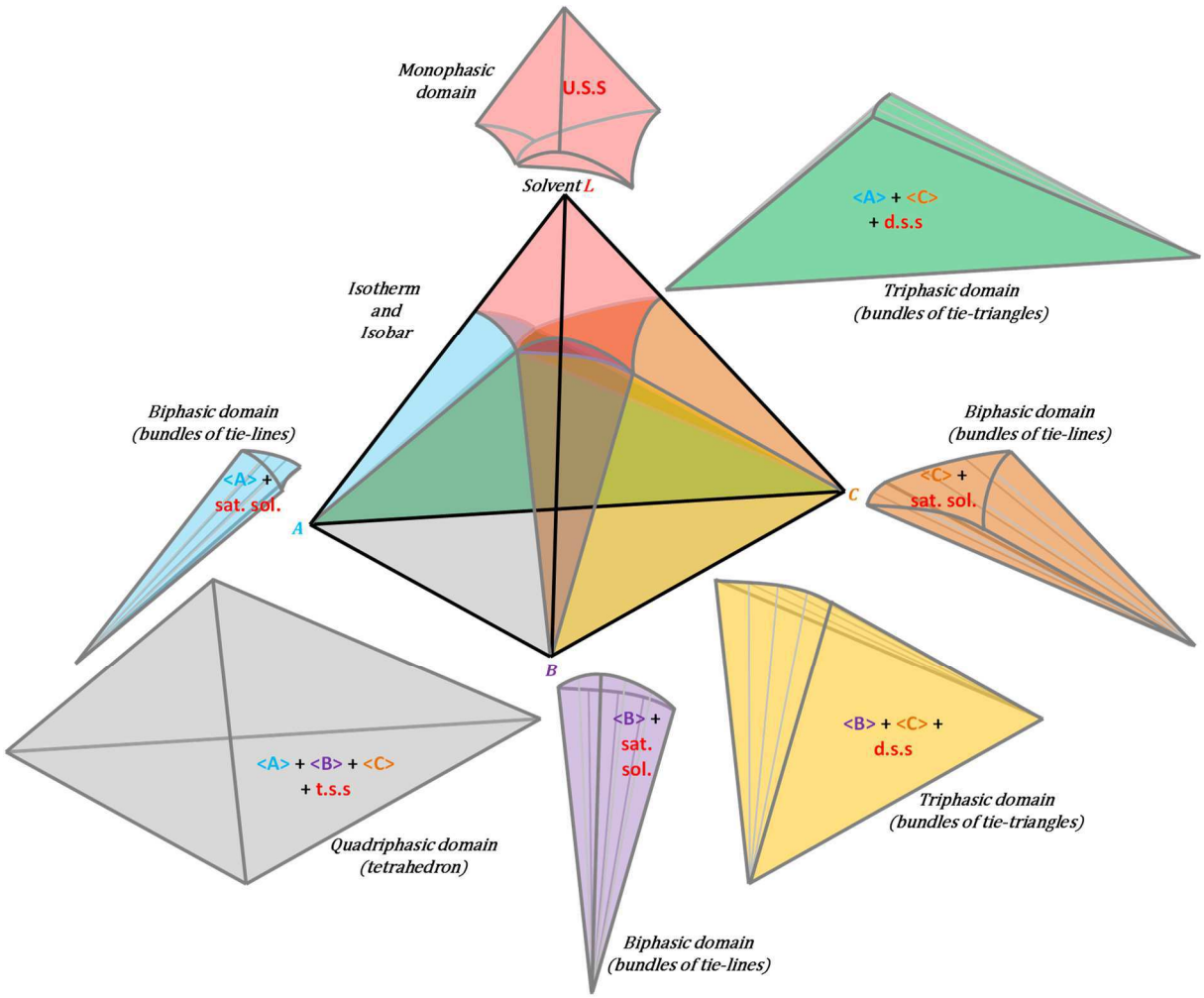

Figure 16. Different phase-domains and phase repartition for the Figure 15 quaternary system.

Two kinds of isopleths can be isolated from a quaternary system (Figure 17):

- Ternary isopleths can be isolated fixing one composition rule such as one composition constant (green triangular plane) or one compositions ratio constant (orange triangular plane)
- Binary isopleths are isolated combining two composition rules: two constant concentrations (violet line), two constant ratios (red line) or one ratio and one composition constant (blue line).

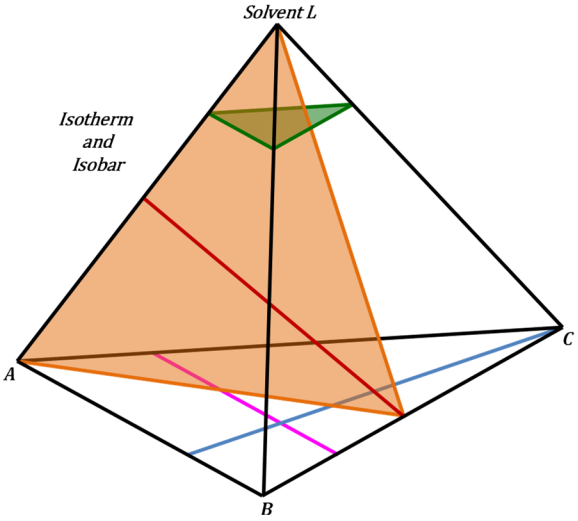

Figure 17. Different isoplethal sections in a quaternary diagram: (i) $\frac{\%B}{\%C} = \frac{\%A}{\%L} = 1$ *binary isopleth (red), (ii)* $\%A = 3 * \%B$ *and* $\%L = 0\%$ *binary isoplethal section (blue), (iii)* $\%C = 25\%$ *and* $\%L = 0\%$ *binary isoplethal section (pink), (iv)* $\%L = 75\%$ *ternary isopleth (green) and (v)* $\frac{\%B}{\%C} = 1$ *ternary isopleth (brown).*

III.5 Hereafter

Systems with higher orders exist, but their study is reduced to the study of binary or ternary section. Even quaternary systems are not often study as such and isopleths are mainly used.

Part.II Crystals

The word *crystal* comes from the Ancient Greek "*crytallos*" (κρνσταλλοσ) which means "*cold drop*" or "*frozen drop*", chosen term after the observation of the hardness of stalactites. Two domains can be distinguished about crystal science. *Crystallography* is the part of science that interests in the structure of crystals, meaning how the particles are arranged in the three dimensions. *Crystallogenesis* interests on crystallization, *i.e* how crystals appear from disorganized states of the matter (gas, solution or amorphous mater).

I Crystallography

Modern crystallography results from the work of mathematicians of the group theory who conceptualized geometrical and analytical properties of crystals.[15] As for all research domain, it was a step by step conceptualization. The first mention of periodicity was made by Romé de l'Isle[16] and René J. Haüy[17] based on macroscopic observations of calcite in 1784. Based on this theory, several other notions such as the "*Miller indices*"[18] or the "*unit cell*"[2] have been

proposed but without evidence. Crystallography finally passed from this hypothetical view of periodic elements to a physical reality thanks to the discovery of the X-ray diffraction phenomenon by crystalline matter.[19]

I.1 The group theory

I.1.1 Repetition motif

The *repetition motif* is the entity the crystal is composed of. Its nature (atom(s), ions and/or molecule(s)) and shape obviously control the interactions that insure the crystalline cohesion.

I.1.2 Asymmetric unit

The *asymmetric unit* is the smallest unit of repetition motif necessary to build the whole crystal using the symmetry operations. This unit can incorporate several repetition motifs ($Z' > 1$) or only part of it ($Z' = ½ , ¼ , \ldots$).

Thus, crystallographers defined as Z' the number of repetition motif included in the asymmetric unit and as Z the number of repetition motifs in the unit cell.

I.1.3 Point Group

When a set of *symmetry elements* is structured into a *Group* (mathematical sense), the operations of that group generate equivalent of the initial object (Figure 18).

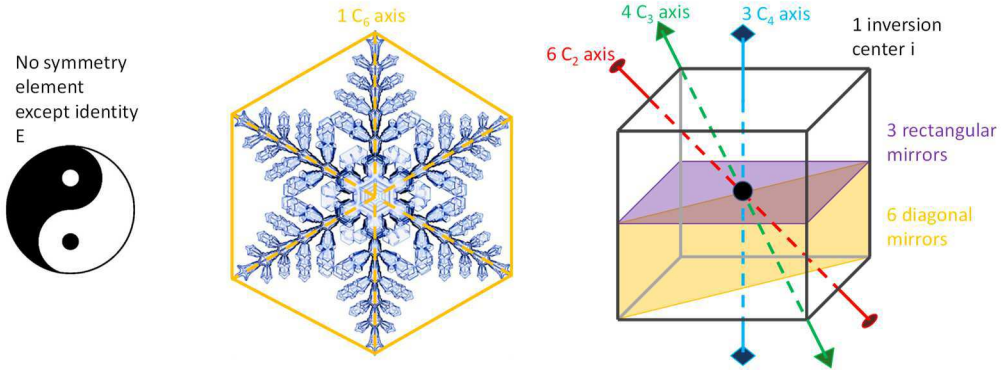

Figure 18. Symmetry elements for: a Ying and Yang symbol (left), a snowflake (middle) and a cube (right).

Among all the possible macroscopic symmetry elements, only ten are available to describe crystalline structures:

- The *proper rotation* x, that rotate the crystalline structure around a x-fold axis (x rotations of $2\pi/x$). Five different can be encountered: $1, 2, 3, 4$ and 6.

- The *improper rotation* $\bar{x}$, that is a *proper rotation* x followed by an inversion i. Five of them can also be find: $\bar{1} = i, \bar{2} = m, \bar{3}, \bar{4}$ and $\bar{6}$.

Combining those different elements, 32 *Point Groups*, or *Crystal Classes*, can be encountered in crystallography (Table 5). Those PG can be used to describe the morphology of the crystals and the macroscopic properties. They can be classified according to their dominant symmetry element in the *7 Crystal Systems* and 11 of them present the *inverse center i* symmetry element.

I.1.4 The unit cell

Let us define a *Multiple Unit Cell* as a volume that permits to rebuild all the crystal lattice by simple translation of it. In this purpose, such a volume must adapt a parallelepipedic form defined by three basic vectors. The corners of the unit cell are the *lattice points* (or *node*).

We can define the *Unit Cell* as the one exhibiting the smallest volume and the highest symmetry. This Unit Cell is defined by the lattice parameters: a, b and c (the lengths of the basic vectors) and α, β and γ (the angles between the edges) (Figure 19).

The planes exhibiting a high motif density are called *reticular planes*. They are defined by their *miller indices* h, k and l ((hkl) plane) and their *reticular distance* d_{hkl} corresponding to the distance between two planes of the same family (parallel planes).

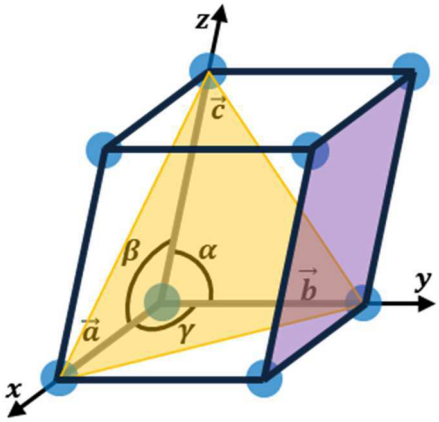

Figure 19. Representation of a unit cell defined by the lattice parameters a, b, c, α, β and γ. Lattice points are represented by blue circles, reticular planes (111) in yellow and (010) in violet.

All the structural information is contained in the unit cell which can be used to rebuild the entire crystal by translation $\vec{r} = u.\vec{a} + v.\vec{b} + w.\vec{c}$ (with u, v and w integers). Note that this translation can also be applied to the lattice point of the network.

I.1.5 Modes

When the unit cell only contains one lattice point (the 8 corner ones being share with 8 unit cells generated by translation), this unit cell is called primitive.

Nevertheless, this one lattice point per unit cell condition is not always respected. Indeed, unit cells can contains 1, 2 or 4 nodes.[20] So Bravais[21] introduced the *4 lattice modes*:

- ***P*** *primitive* or *simple mode*.
- ***A***, ***B*** or ***C*** *base-centered*: nodes are also present on the middle of the faces described, respectively, by the $\vec{a}$, $\vec{b}$ or $\vec{c}$ vector (2 nodes per unit cell).
- ***I*** *body-centered*: a node at the middle of the unit cell (2 nodes per unit cell).
- ***F*** *face-centered*: nodes are present in each faces of the unit cell (4 nodes per unit cell).

Thus, modes also correspond to a translational symmetry $\vec{t} = u.\vec{a} + v.\vec{b} + w.\vec{c}$ (with u, v and w equal to 0 or ½).

Combination of the 4 different modes and of the 7 crystal systems leads to the *14 Bravais Lattices*.

Table 5. The seven crystal systems and their associated point groups and modes.

Crystal System	Dominant Symmetry	Point Group	Cell Parameters	14 Bravais Lattice			
				Primitive *P*	Base Centered *C*	Body Centered *I*	Face Centered *F*
Triclinic	**1** (identity)	**1** and $\bar{1}$	$a \neq b \neq c$ $\alpha \neq \beta \neq \gamma$				
Monoclinic	**2** along $\vec{b}$	**2**, **m** and $2/m$	$a \neq b \neq c$ $\alpha = \beta = \frac{\pi}{2} \neq \gamma$				
Orthorhombic	**2** along $\vec{a}$, $\vec{b}$ and $\vec{c}$	**222**, **mm2** and $2/m2/m2/m$	$a \neq b \neq c$ $\alpha = \beta = \gamma = \frac{\pi}{2}$				
Trigonal	**3** along $\vec{c}$	**3**, $\bar{3}$, **32**, **3m** and $\bar{3}m$	$a = b = c$ $\alpha = \beta = \gamma \neq \frac{\pi}{2}$				
Tetragonal (quadratic)	**4** along $\vec{c}$	**4**, $\bar{4}$, **422**, **4mm**, $\bar{4}$**m2**, $4/m$ and $4/m2/m2/m$	$a = b \neq c$ $\alpha = \beta = \gamma = \frac{\pi}{2}$				
Hexagonal	**6** along $\vec{c}$	**6**, $\bar{6}$, **622**, **6mm**, $\bar{6}$**m2**, $6/m$ and $6/m2/m2/m$	$a = b \neq c$ $\alpha = \beta = \frac{\pi}{2} \neq \gamma = \frac{2\pi}{3}$				
Cubic	**3** along the space diagonal	**23**, **m3**, **432**, $\bar{4}$**3m** and **m3m**	$a = b = c$ $\alpha = \beta = \gamma = \frac{\pi}{2}$				

I.1.6 Space Group

In addition to the symmetry operations of the PG, other symmetries may exist in the description of a crystal structure. Those new operations combine microscopic translation and rotation.

Two kinds can be extracted:

- *Screw Axes*: rotation followed by a translation along the axis of the rotation. One can list: 2_1, 3_1, 3_2, 4_1, 4_2, 4_3, 6_1, 6_2, 6_3, 6_4 and 6_5 (e.g $\mathbf{6_5}$ corresponds to a rotation of $2\pi/\mathbf{6}$ followed by a translation of $\mathbf{5}/\mathbf{6}$ of the shortest translation vector along this axis).
- *Glide Planes*: combination of a mirror and a translation parallel with this mirror. Five different exist: a, b, c, n and d (e.g $\boldsymbol{a}$ corresponds to a reflexion of a $\boldsymbol{m}$ mirror followed by a translation of $\vec{\boldsymbol{a}}/2$ with $\vec{\boldsymbol{a}}$ // $\boldsymbol{m}$).

The combination of all those elements (point group, lattice mode and translational symmetry operation) leads to the 230 *Space Group* (SG).[20] According to their characteristics, they can be divided in several sub-categories. One interesting sub-category in this work is the *centrosymmetric/non-centrosymmetric* space group repartition. *Centrosymmetric* refers to space groups containing the inverse center operation $\boldsymbol{i}$, thus, *non-centrosymmetric* refers to space groups without the $\boldsymbol{i}$ operation.

I.2 Organic crystals

According to the nature of the motif and of the bonds in the crystal edifice, one can classify crystals as ionic (e.g. $NaCl$, ZnS, etc), metallic (e.g. metals and their alloys), covalent (e.g. C diamond, SiO_2, etc) or molecular (e.g. H_2O, $Fe(C_5H_5)_2$, etc).

Among those last, we can distinguish organometallic crystals and organic crystals which are the investigated class of components in this work.

I.2.1 Crystallographic data

As already mentioned, inner symmetry of the chemical motif influences the symmetry elements of the crystal packing.

Indeed, if the motif has an high symmetry, it has a propensity to crystallize in one of the high symmetry crystal systems (tetragonal, hexagonal or cubic).[7]

By contrast, asymmetric motifs would crystallize in the low symmetry systems (triclinic, monoclinic, orthorhombic and sometimes tetragonal).[22]

Organic molecules belong to the 2nd category because their irregular shapes and electronic densities (various chemical functions) make the vast majority of them very "unsymmetrical". Consequently, when there is no orientational disorder (e.g plastic crystal), *Cambridge Structural Database* (CSD) shows that 70% of the organic crystals crystalize in only 10 space groups (more than ⅓ for $P2_1/c$ only).

Table 6. Space group repartition for organic crystals.

Space Group	CSD entries	CSD proportions
$P2_1/c$	131 222	34.29%
$P2_12_12_1$	44 631	11.66%
$P2_1$	32 446	8.48%
$C2/c$	24 252	6.34%
$Pbca$	14 044	3.67%
$Pna2_1$	5969	1.56%
$P1$	5 160	1.35%
$C2$	4 610	1.20%
$Pnma$	3 063	0.80%
$Pbcn$	2 668	0.70%
Other 220 space groups	114 572	29.95%
Total	382 637	100%

I.2.2 Interactions in organic crystals

Different interactions insure the crystal cohesion of organic molecules. Those interactions can be *intra-molecular* (different parts of the same molecule linked) or *inter-molecular* (different molecules linked). Most of the time, several kinds of interactions contribute to the crystal cohesion, forming a bonds network. One can list: *van der Waals interactions*,[23] *π-stacking*,[24] *hydrogen bonds*,[25,26] *coulombic interactions*, etc.

I.2.3 Polymorphism of organic compounds

As for other crystals, organic crystals exhibit polymorphism. Nevertheless, in addition of the strict definition of packing polymorphism, molecular crystal, and so on, organic ones, can exhibit another kind of polymorphism called *conformational polymorphism.*[12,27,28] There, it is the conformation of the molecule itself which varies from one polymorph to the other to accommodate to the different bonds networks.

Nevertheless, different conformations can exist in the same crystal (roughly ⅓ of the cases when $Z' > 1$)

I.2.4 Nomenclature of organic crystals

Different names are used to designate the organic crystals: *salt* designates crystal in which constituent(s) are charged, *cocrystal* for neutral multi-constituents crystal, *solvate* for neutral multi-constituents crystal in which at least one constituent is a solvent, *host-guest associations,* etc (no particular word is used to designate crystals of pure neutral constituent).

II Crystal genesis

Crystallization refers to a first-order transition from a disordered state to a crystalline one. Variant names can be found according to the initial disordered state: *solidification* from vapor state, *recrystallization* from amorphous solid, *melt crystallization*, *precipitation* from solution, etc.

In this work, precipitation, melt crystallization and recrystallization from amorphous have been used. If the details of the mechanisms differ according to the method, global procedures are similar.

II.1 Precipitation[29]

II.1.1 Supersaturation

The *solubility* S is the maximum quantity of a compound (the *solute*) that can be dissolved in a solvent for given temperature and pressure. The resulting solution is so *saturated*. If the concentration is lower than that value, it is said *undersaturated*.

Saturation corresponds to a thermodynamic equilibrium. Nevertheless, it is possible to reach higher concentrations. It is the *supersaturation* which is the driving force of crystallization. To quantify it, several formulas are available: *absolute supersaturation* (ΔC), *relative supersaturation* (σ) or the *supersaturation ratio* (β).[30]

$$\Delta C = C - S \qquad \sigma = \frac{\Delta C}{S} \qquad \beta = \frac{C}{S} \qquad \text{Eq. 21}$$

Supersaturation can be obtained *via* different ways: solvent can be evaporated or the solubility decreases by temperature variation (most of the time by cooling). Solubility can also vary by anti-solvent addition, pH variation, etc. Pressure variations are also used for recrystallization of biologic samples like viruses or proteins.

A supersaturation higher than 1 is theoretically sufficient to induce the crystallization. In practice, supersaturation must be over a certain limit called *Ostwald metastable limit*[8] (Figure 20) to induce a *spontaneous nucleation* and crystallization. Otherwise, the system is out of equilibrium: thermodynamics states that the system should nucleate but *nuclei* cannot reach the critical size. Seeding is the best way to obtain a fast crystallization in this zone.

The width of the metastable zone depends on kinetic factors: the cooling rate and/or the evaporation rate, the solubility, the stirring mode and rate, time, impurities, etc.

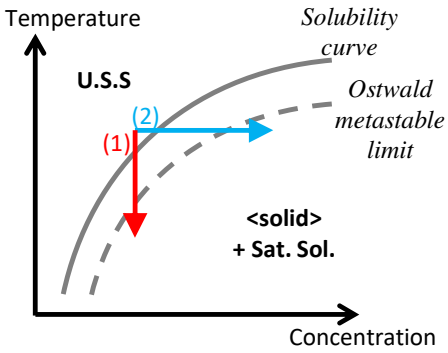

Figure 20. Solubility curve (solid line) and Ostwald metastable limit (dashed line). Crystallization pathway by (1) cooling or (2) solvent evaporation.

II.1.2 Nucleation

The first step of crystallization is the *nucleation* which is the first appearance in the medium of groups of particles, the *nuclei,* respecting the crystal packing and having the possibility to grow into crystals.

II.1.2.1 Primary nucleation & CNT

Primary nucleation corresponds to the development of nanocrystals from the medium without any nuclei. It can be homogeneous if nucleus appears inside the solution,[31] or heterogeneous when nucleus appears on solid interface (impurities, reactor wall, stirrer, etc).[32]

The *Classical Nucleation Theory* (CNT) is an attempt to conceptualize homogeneous nucleation from an energetic point of view.[33,34] Assuming that nuclei adopt a spherical shape of r radius, the free enthalpy variation $\boldsymbol{\Delta G_{nucleation}}$ related to those nuclei is given by:

$$\boldsymbol{\Delta G_{nucleation} = \frac{4}{3}\pi r^3 \Delta g_v + 4\pi r^2 \gamma} \qquad \textit{Eq. 22}$$

With $\boldsymbol{\Delta g_v}$ the Gibbs free energy variation per unit of volume and $\boldsymbol{\gamma}$ the surface tension.

The equation includes two contributions:[35]

- The first term is a stabilizing one and corresponds to the creation of solute/solute interactions. It is directly related to the volume of the nucleus.
- The second term corresponds to solute/solution interactions that destabilize the system and is directly related to the surface of the nuclei.

The sum of those two contributions results on a free energy evolution as presented in Figure 21.

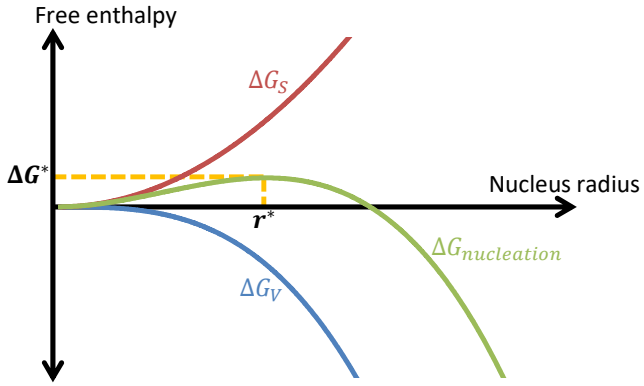

Figure 21. Stabilizing volume contribution (red curve) and destabilizing surface contribution (blue curve) of the free energy evolution of a spherical nucleus according to its radius (green curve).

The evolution of free energy passes *via* a maximum:

$$r^* = \frac{2\gamma}{\Delta g_v} \quad \text{and} \quad \Delta G^* = \frac{16\pi\gamma^3}{3(\Delta g_v)^2} \qquad \textit{Eq. 23}$$

- For $r < r^*$, the *surface contribution* prevails and the formation of the nucleus is energetically unfavorable. Nuclei of those sizes will preferably re-dissolve but they can also grow.
- For $r = r^*$, nuclei reach the critical radius r^*corresponding to the energy barrier ΔG^*. At this size, nuclei can either grow or reduce.
- For $r > r^*$, nuclei are stable and will grow to decrease their free energy.

To conclude, nucleation is a stochastic process also driven by kinetics.

Heterogeneous nucleation occurs for lower energy barrier since the destabilizing crystal/solution surface is reduced for the benefit of solute/foreign surface interface (foreign surface being impurity, reactor wall, …).

II.1.2.2 Secondary nucleation

During crystallization processes, crystals are often submitted to intense mechanical stress like shear stress or collisions with other crystals or reactor walls. In such conditions, small parts of the crystals can be wrenched out of it, and so generate new nuclei.[36]

II.1.3 Growth

Once a nucleus reached the critical radius, it will grow absorbing molecules in the neighborhood. Solvated molecules will dock to the surfaces and will be incorporated into the crystal. This process continues until the system goes back to crystal/saturated solution equilibrium ($\Delta G = 0$). Chemical motif would be incorporated by several ways. The two majors are:

- *Spiral growth:*[37] screw dislocation provides large preferential sites where chemical motifs can dock on. Layer by layer the spiral is regenerated and provides a more regular development than the 2D nucleation at low supersaturation.
- *Two dimensional nucleation:*[38] chemical motif cannot be adsorb on a perfectly flat surface since molecules cannot find any preferential sites. A chemical motif can migrate on the surface by diffusion and be the starting point of a 2D nucleus on this surface. This growth is favored for supersaturation higher than spiral growth.

Final morphology of crystals depends on growth rates of the different faces. Faces with the lowest growth rates will be the prevalent ones (Figure 22). Growth rates are influenced by the crystalline structure and the interactions at the crystal/solution interface and impurities.

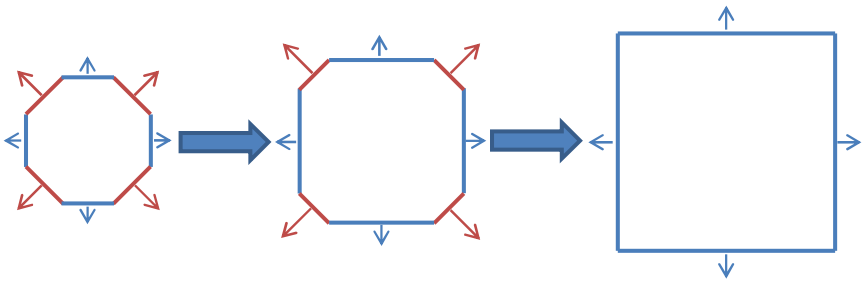

Figure 22. Schematic representation of the crystal growth. Blue arrows symbolize lower growth rates than red ones and controlled the final morphology.

Different theoretical models have been established to predict crystals morphology. The two majors are: the *Bravais-Friedel-Donnay-Harker* (DFDH)[21,39] (the higher the d_{hkl}, the lower the growth rate, and so the larger the morphological index of the (hkl) face) and the *Periodic Bond Chains* (PBC)[40] model (based on the interactions between the chemical motifs and associated energies: crystals will grow favoring the formation of the strongest interactions).

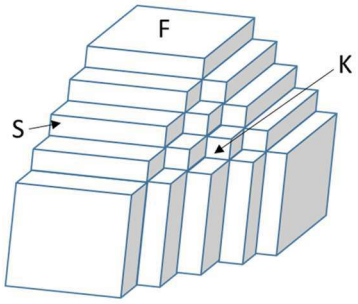

Figure 23. Distinction of the different kinds of crystal faces mentioned in the PBC model:[29] flat F, step S and kink K.

II.1.4 Ostwald ripening[41]

As soon as several crystals are present in suspension, the smaller ones will be dissolved to the profit of larger crystals. The explanation is that larger crystals are more thermodynamically favored than smaller due to more favorable volume over surface ratio.

Ostwald ripening also occurs as soon as there is a contact between crystals but it is faster for a crystal/saturated solution system due to the substantial interactions at the interface and fast diffusion in solution.

II.2 Defects in crystals

Extreme Oswald ripening should lead to a 'perfect' single crystal. This perfect single crystal should be composed of perfect repetitions of the unit cell and should adopt a morphology related to the specific reticular plans of the structure.[19] In practice, 'perfect' crystals do not exist and crystals present defects at least in conformity with thermodynamics for $T \neq 0$ K.

Defects can be:

- *Punctual* (0D):[42] local perturbation of the crystal periodicity. They can be a vacancy (absence of a part of the motif) on a molecular site, a substitution on a molecular site (by another component or a part of the motif) or an insertion on an interstitial site (by another component or a part of the motif). If another component is introduced in the crystal lattice, it is a solid solution. It is S*olid solution by mean of insertion* if the extra-component is incorporated in interstitial sites or *solid solution by mean of substitution* if the constituent occupies molecular sites of the major component.
- *Dislocations* (1D)[43] are linear defects of the crystal lattice along a reticular direction. Two types can be encountered: *edge dislocation* (disruption of a single

molecular plane that results in a local compression of the system) and *screw dislocation* (screw disposition of molecular plane along a reticular direction).

- *Grain boundaries*, *stacking faults* and *twin crystals* (2D) are surface defects and concern "polycrystalline crystals".[44] Grain boundaries appear at an abrupt change of direction of the crystal lattice, stacking faults consist of an error on the repetition of the pattern and twin crystals are composed of crystals sharing a special reticular plane.
- *Inclusions* (3D) correspond to solid, liquid, gas or fluid (gaseous bubble surrounded by a liquid) trapped in a single crystal.[45]

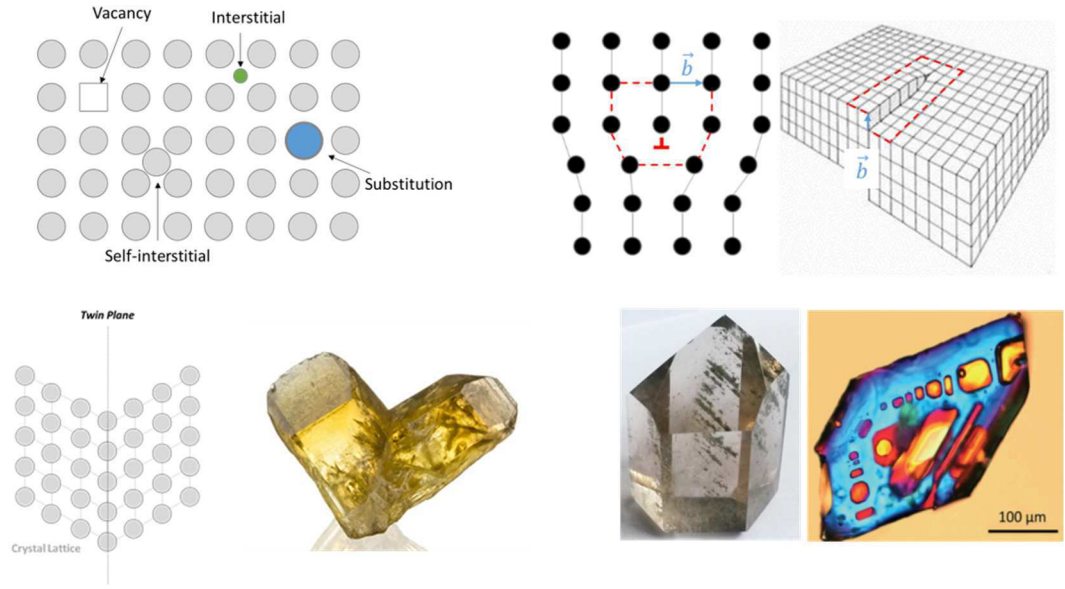

Figure 24. Top left: Different punctual defects in crystals. Top right Edge and screw dislocations. Bottom left: twin crystals. Bottom right: solid inclusions in quartz and fluid inclusions in ammonium perchlorate (Dr. Emilie Bobo credit).

II.2.1 Powdered sample

A powdered sample can be described as a set of randomly oriented small crystalline particles. This set of particles containing single crystals, polycrystalline crystals and damaged crystals.

II.2.2 Single crystal

When the suitable conditions are fulfilled, one can extract from a batch a crystal of sufficient quality (low density of defects) for structural analysis, seeding, etc.

Part.III Chirality

I Definition

I.1 History

The French mineralogist René-Just Haüy first observed, in 1801, that quartz crystals can be divided in two families image of the other through a mirror. He called those families "plagièdre droit" and "plagièdre gauche".

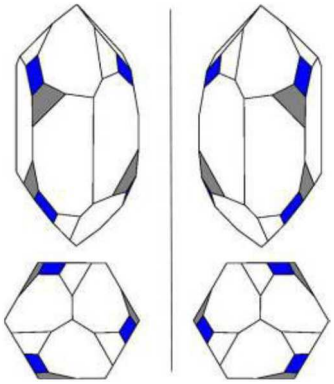

Figure 25. Morphology of quartz "plagièdre gauche" and "plagièdre droit"

In 1815, Jean-Baptiste Biot observed that some compounds (solid, liquid or in solution), like sucrose or tartaric acid, rotated the polarized light (clockwise or anticlockwise).[47]

In 1820, the industrial researcher Charles Kestner synthesized a new compound presenting the same composition than tartaric acid. Nevertheless, this new compound did not deviate polarized light,[48] contrary to conventional tartaric acid extracted from wine. This compound was named "*racemic acid*" (from the Latin "*racemus*" meanings "*grapes*").[49]

In 1848, Kestner gave some of this racemic acid to Louis Pasteur who recrystallized the sodium ammonium tartrate tetrahydrate salt. Disappointed when he realized that the salt did not rotate the polarized light, he also noticed that crystals presented two mirror image shapes.[50] He separated manually the two families and determined their optical rotation of polarized light. Both deviated polarized light with the same intensity but with the exact opposite angle. Based on that fact, he deduced that the crystals were composed of the same molecules themselves image one of the other in a mirror.[51] Pasteur just has established the bases of chirality and achieved the first chiral separation.

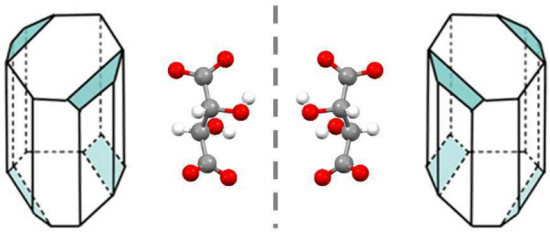

Figure 26. Dextrorotatory (left) and levorotatory (right) sodium ammonium tartrate tetrahydrate crystals and respective tartrate configurations.

In 1874, Jacobus Henricus van't Hoff[52] and Joseph Achille Le Bel[53] simultaneously proposed the spatial arrangement of the asymmetric carbon as an explanation to the chirality (tetrahedral carbon linked with 4 four substituents).

Ten years later, Lord Kelvin first introduced the word *chiral*: "*I call any geometrical figure, or group of points, chiral, and say that it has chirality, if its image in a plane mirror, ideally realized, cannot be brought to coincide with itself.*"[54] Chiral coming from the Greek "*cheir*" (χείρ) means "hand".

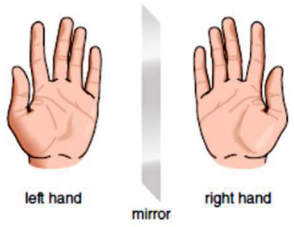

Figure 27. Chiral objects: hands.

The term *enantiomorph* was introduced by Pierre Curie[55] in 1894. It comes from Ancient Greek "*enantios*" (ἐναντίος) and "*morphḗ*" (μορφή), respectively meaning "opposed" and "form".

I.2 Chirality around us

Chirality can be found everywhere. Macroscopic effect can be observed, of course, in objects like crystals or even shoes, but it can be also observed in the livings: hands and other parts of human body are chiral, but also numerous shells and some plants (hops always grow with a left rotation).

Figure 28. Chiral shells (left) and left handed growing hops (right).

Over those macroscopic considerations, the living organisms are highly impacted by chirality at the molecular level, even more, we spoke about the homochirality of life. For instance, human chiral proteinogenic amino acids are ***L*** homochiral and sugars building blocks of DNA and RNA are ***D*** homochiral. The origin of the homochirality of life remains unknown, researches are conducted on amino acids present in meteorites[56,57] or slight energy differences between enantiomers at very low temperatures.[58]

II Properties of chiral system

II.1 Properties

Two enantiomers have exactly same *scalar properties* such as solubility, density, melting temperature, associated enthalpies, etc. But their *vector properties* are exactly opposite. This concerns optical rotation of polarized light, crystal packing, etc.

As illustrated in Figure 29, two enantiomers do not behave the same with another chiral compound. The majority of chiral molecules have different biological activities depending on their handedness (e.g. (R)-limonene smells like oranges whereas (S)-limonene smells like piney-turpentine odor[59]).

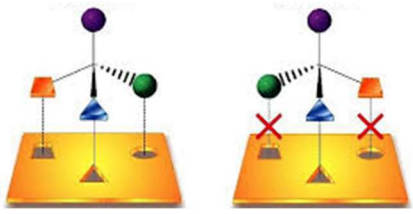

Figure 29. Illustration of the difference of compatibility between a chiral medium and a pair of enantiomers.

Concerning API (*Active Pharmaceutical Ingredient*), this effect is far more crucial. Indeed, the difference of activities can be insignificant, or totally disastrous. Enantiomers can have:

- the same effect (e.g. cocaine).
- less active or inactive effect (e.g. adrenaline and ibuprofen).
- other effects like different therapeutic effects (e.g. levothyroxine used to cure different diseases) or secondary effects. One can cited the case of thalidomide used against morning sickness pregnancy in the 50s. Whereas therapeutic studies has been performed on (R) enantiomer, the racemic prescribed composition caused deformities on 10,000 infants.[60]

Everhardus Jacobus Ariëns was one of the first to denounce what he called "a *highly sophisticated scientific nonsense*".[61] He stated that the undesirable enantiomer, the *distomer*,

should be treated as an impurity (which give for a racemic mixture, 50% of impurity) and removed for the benefit of the active enantiomer, the *eutomer*. In 1992, the FDA (Food and Drug Administration) imposed new drastic rules for chiral substances:[62] industrials have to report pharmacological, pharmaceutical and toxicological data for each enantiomers and the racemic composition.[60,63,64]

II.2 Nomenclature & types of chirality

Chiral refers to systems or objects that differ from their mirror image. *A contrario*, *achiral* refers to systems or objects that are unchanged by mirror symmetry. Enantiomer was introduced by P. Curie to differentiate the two different images and racemic refers to mixture of equal proportion between enantiomers.

Nowadays, enantiomer is also used to describe the specific kind of chirality involving asymmetric atom(s). In this work, we will prefer the use of *optical antipode* or simply *antipode* to differentiate the different optical forms of chiral systems.

II.2.1 Polarimetry

Opposite optical properties were first used to differentiate enantiomers. When deviate light to the right (clockwise), they are called *dextrogyre* and noted (**+**) (and rarely *d*). When deviate to the left (anticlockwise), they are *levogyre* and noted (**-**) (and rarely *l*). This notation is always used but does not give any information on the structure.

II.2.2 Asymmetric atom & Enantiomery

The most common cases of chirality are *asymmetric atoms*, generally asymmetric carbons which are tetrahedral carbons linked with 4 four different substituents (Figure 30). Those atoms can also be called *stereocenter* or *stereogeneric center*.

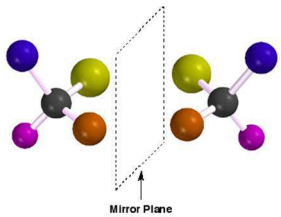

Figure 30. Chirality of asymmetric carbon.

In this case, the word "*enantiomer*" is universally used to differentiate the two optical antipodes.

To describe the chirality of enantiomers, several notations can be used (Figure 31):

- The *absolute configuration* of a stereocenter can be established following the rules edited by Cahn, Ingold and Prelog.[65,66] Enantiomers are either ***R*** (*Rectus*) or ***S*** (*Sinister*).
- *Fischer projections* are used to describe chirality of sugars and amino-acids. Depending on the position of the substituent with the highest priority, enantiomers are noted ***D*** or ***L***.[67]

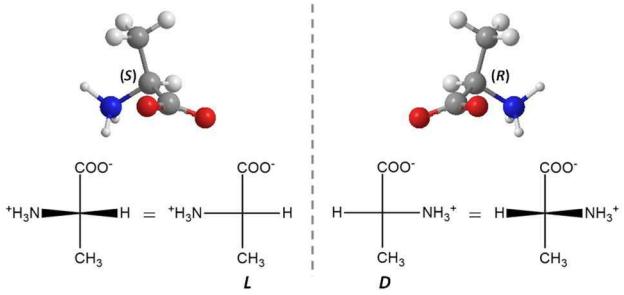

Figure 31. Absolute configuration (top) and Fischer projection (down) of L-(S)-alanine (left) and D-(R)-alanine.

II.2.3 Several asymmetric atoms & Diasteromery

Molecules can have more than one stereocenters. If a molecule has $\boldsymbol{n}$ stereocenters, $\mathbf{2}^{\boldsymbol{n}}$ stereoisomers exist. They are two by two enantiomers, otherwise they are *diastereomers* (Figure 32).

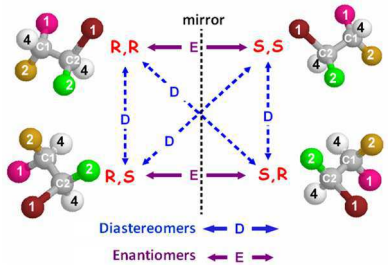

Figure 32. Relations between the four stereoisomers of a molecule with two stereocenters.

II.2.4 Blocked configuration & Atropisomery

Vladimir Prelog defined *atropisomers* as stereoisomers "*due to the so-called secondary structure, i.e. hindered rotation around single bonds*".[68] The chirality is not up to the conformation of the molecule but up to its configuration.

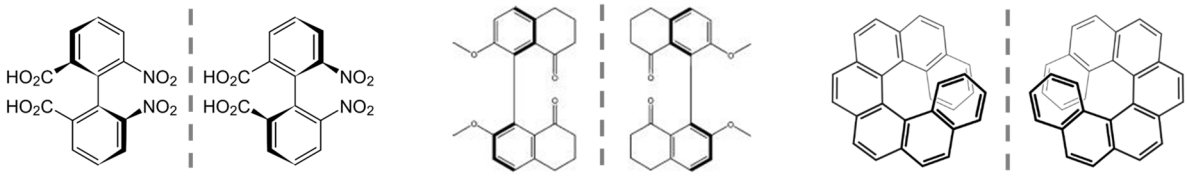

Figure 33. 6,6'-Dinitro-2,2'-dicarboxybiphenyl (left), bis-tetralone (middle) and heptahelicene (right) atropisomers.

II.2.5 Spatial arrangement & Supramolecular chirality

In 1898, Kipping & Pope published that "*ENANTIOMORPHOUS substances are naturally divisible into two classes: (a) consisting of those compounds in which the enantiomorphism is determined by the structure of the chemical molecule, and (b) consisting of those crystalline substances of which the enantiomorphism is not inherent in the molecules, but is determined solely by their arrangement.*"[69] Molecules arrange themselves in a non-symmetrical way , most of the time due to related screw axes. Quartz is a very good example of this since its both polymorphs exhibit that chirality. In quartz β, SiO_4 tetrahedron can arrange in left or right screw axes resulting in both mirror image $P6_421$ and $P6_221$ space groups. The same occurs with Quartz α with $P3_221$ and $P3_121$ space groups.

III Thermodynamic of chiral system[70]

Due to their symmetrical properties, heterogeneous equilibria involving a couple of enantiomers are themselves submit to a symmetrical law centered on the racemic composition.

Consequently, properties (transition temperatures, nature of the phases, structures, etc) observed for a certain composition are also valid for the opposite composition. *Enantiomeric Excess*[71] ($\boldsymbol{e.e}$) is a common way to quantify the proportion between the two enantiomers. A $0\% e.e$ corresponds to the racemic composition whereas a $100\% e.e$ refers to pure enantiomers. Pure definition of $e.e$ does not include any sign and predominant enantiomer must be precise:

$$\%\boldsymbol{e.e} = \left|\frac{R-S}{R+S}\right| * \mathbf{100} = \left|\frac{n_R-n_S}{n_R+n_S}\right| * \mathbf{100} = \left|\frac{m_R-m_S}{m_R+m_S}\right| * \mathbf{100} \qquad \textit{Eq. 24}$$

For a daily use, "modify" the $e.e$ equation to include a sign is relevant:

$$\%\boldsymbol{e.e} = \frac{R-S}{R+S} * \mathbf{100} \qquad \textit{Eq. 25}$$

Here, when (R) enantiomer predominates $e.e$ is positive. If the (S) one is predominant, the $e.e$ is negative.

When two phases are mirror image one of the other, the use of the *Gibbs-Scott phase rule*[72–74] (Eq. 26) is more relevant than the classical Gibbs' phase rule (Part.I.II.3):

$$v = C_{Achi} + \frac{C_{Chi}}{2} + N - \varphi_{Achi} - \frac{\varphi_{Chi}}{2} \qquad Eq.\ 26$$

Where C_{Achi} is the number of achiral independent component(s) (e.g a solvent), C_{Chi} the number of chiral independent component(s) (e.g $C_{Chi} = 2$ for the two related enantiomers), N the number of extensive variable(s), φ_{Achi} the number of achiral phase(s) (e.g racemic liquid or compound) and φ_{Chi} the number of chiral phase(s) (e.g $\varphi_{Chi} = 2$ for two mirror image solid phases).

III.1 The 3 extreme cases

When talking about phase diagram of chiral system, it is accepted to describe them in only three different phase equilibria.

III.1.1 Racemic compound

The most common (90-95% of the cases) example of chiral system forms a defined compound at the racemic composition called *racemic compound* or sometime *racemate*. Crystals of such phase are ordered assemblies of the two enantiomers in equal proportion (Figure 34-middle). Racemic compounds have congruent melting and solubility (Figure 34-left & right) that can be higher or lower than that of the enantiomers.

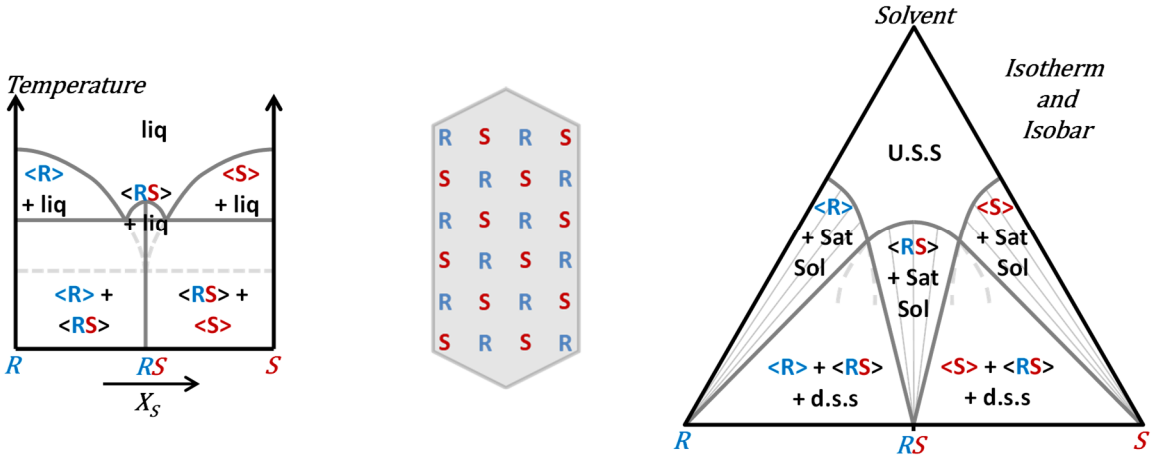

Figure 34. Binary phase diagram (left), racemic composition crystal (middle) and ternary section (right) of a racemic compound forming system.

III.1.2 Conglomerate

When the enantiomers crystallize separately (into *enantiopure* crystals) (Figure 35-middle), they form *conglomerate* (5-10% of the cases). Whatever the composition, enantiomers are *discriminated* and form a eutectic invariant (Figure 35-left). At the racemic composition, ideal conglomerate should present a molar solubility twice as that of the pure enantiomer ($S_{Rac} = S_R + S_S = 2S_R$) (Figure 35-right).

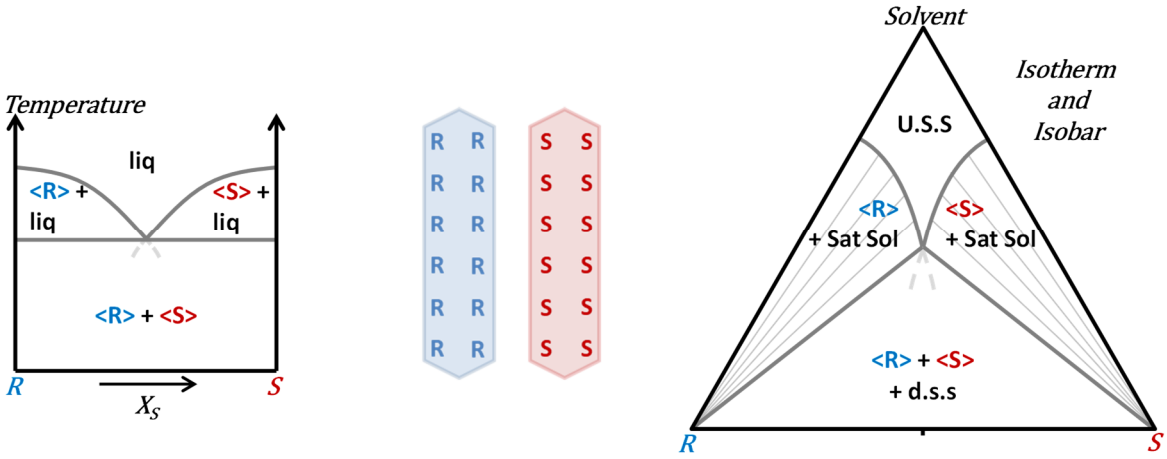

Figure 35. Binary phase diagram (left), racemic composition crystals (middle) and ternary section (right) of a conglomerate forming system.

III.1.3 Solid Solution

In less than 1% of the cases, enantiomers can form *complete solid solution*, also known as *mixed crystal* or *pseudoracemate*. Enantiomers are randomly distributed inside the crystal whose composition equals the composition of the system (Figure 36-middle). In Figure 36-left are represented minimum, ideal and maximum solid solutions. A ternary section of the latest case is also represented (Figure 36-right).

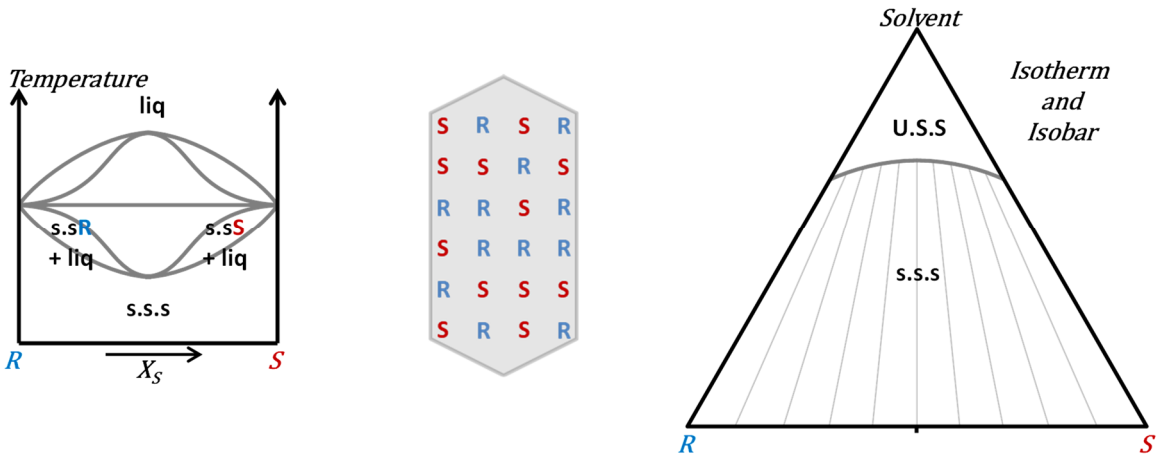

Figure 36. Binary phase diagram (left), racemic composition crystals (middle) and ternary section (maximum(right) of a solid solution forming system.

III.2 Intermediate cases[74,75]

In addition of the three classical systems, other behaviors can be found. Figure 37 presents some cases where polymorphism, phase transition or partial solid solutions occur in a chiral system.

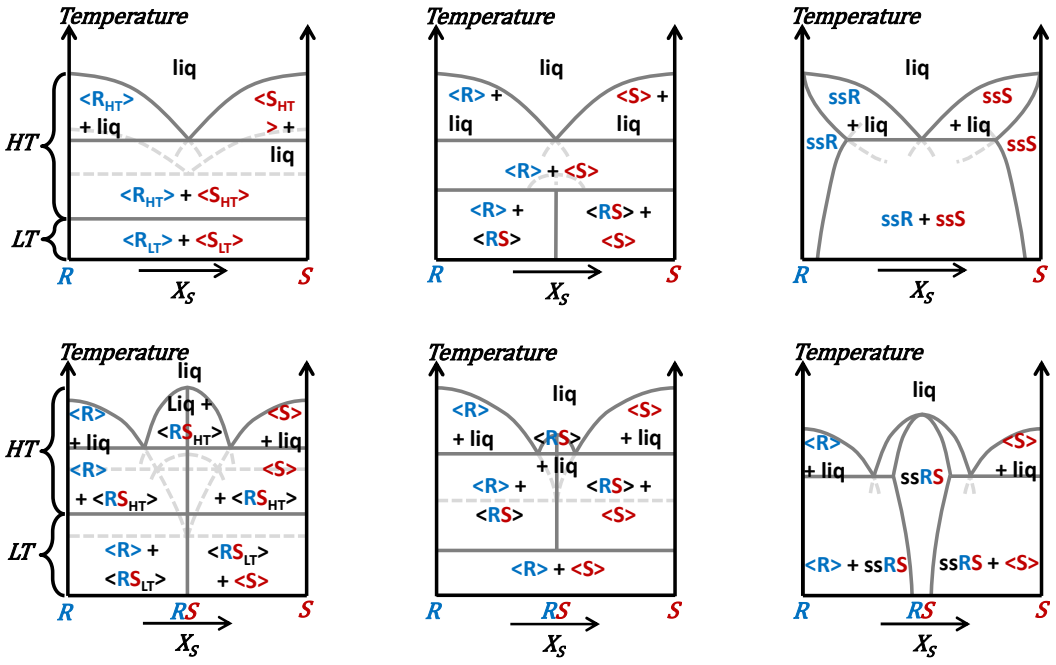

Figure 37.Chiral systems presenting polymorphism of enantiomers (top left) and racemic compound (bottom left), peritectoid (middle top) and eutectoid (middle bottom) and partial solid solution of enantiomers (top right) and racemic compound (bottom right).

The addition of a third component (solvent, coformer, etc) to a chiral system modifies its phase equilibrium and can induces the formation of new compounds with their own behaviors (Figure 38).

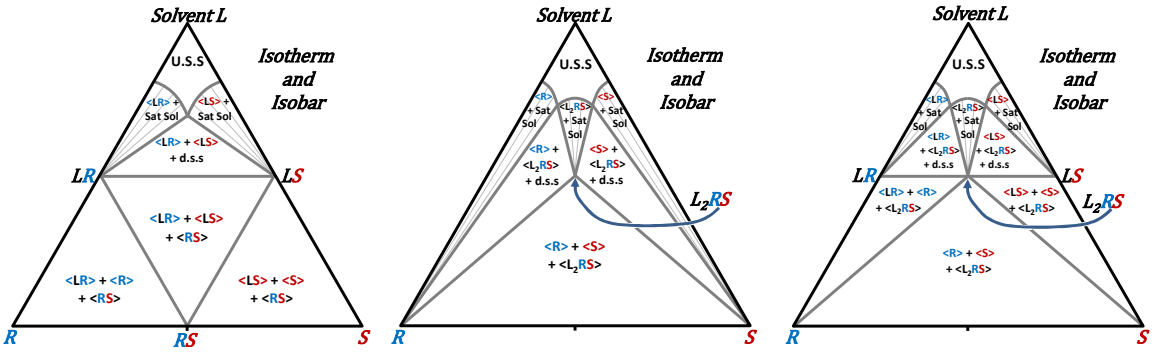

Figure 38. Racemic compound and solvated conglomerate (left), conglomerate and solvated racemic compound (middle) and conglomerate and solvated racemic compound and enantiomers (right) ternary sections.

Other behaviors can also be found.[74–76]

III.3 Crystallography of chiral compounds

In Part.III.I.3.5 we have already discussed about crystal structure of both chiral and achiral molecules. In this part, attention is focused on the distinction between the chirality of the molecule itself and the chirality of the crystalline structure in which the molecule crystallizes. Point groups can so be divided in three classes:[77–79]

- *Centrosymmetric Achiral structure* (CA): $\bar{1}$, $2/m$, mmm, $4/m$, $4/mmm$, $\bar{3}$, $\bar{3}m$, $6/m$, $6/mmm$, $m3$ and $m3m$.
- *Non-centrosymmetric Achiral structure* (NA): m, $mm2$, $\bar{4}$, $4mm$, $\bar{4}2m$, $3m$, $\bar{6}$, $6mm$, $\bar{6}m2$ and $\bar{4}3m$.
- *Non-centrosymmetric Chiral structure* (NC) : 1, 2, 222, 4, 422, 3, 32, 6, 622, 23 and 432.

Enantiomers (and so, conglomerates[80]) can only crystalize in a NC space groups (otherwise, the other enantiomer should be generated by symmetry). 95% of the enantiomers crystallize in only four space group: $P2_12_12_1$, $P2_1$, $C2$ and $P1$.

Racemic compounds[81] can crystallize in any space group but with a huge preference for CA space group (95% of them) of which 95% in $P2_1/c$, $C2/c$, $Pbca$ and $P\bar{1}$ space groups. Other 5% racemic compounds crystallize in NA space groups mainly in $Pna2_1$, $Pca2_1$, Cc and Pc. Last kind of racemic compounds crystallize in NC space groups and are also known as *kryptoracemate*.[82]

Theoretically solid solution can crystallize in all space groups but only few cases were reported.[83]

Table 7. Crystallographic data for racemic mixture.

		Achiral structure		Chiral structure
		CA	NA	NC
Racemic compound (90-95%)	Proportion	≈ 95%	≈ 5%	≈ 0.02%
	Dominant SG	$P2_1/c$, $C2/c$, $Pbca$ and $P\bar{1}$	$Pna2_1$, $Pca2_1$, Cc and Pc	$P2_12_12_1$ and $P2_1$
Conglomerate (5-10%)	Proportion	Forbiden	Forbiden	100%
	Dominant SG	/	/	$P2_12_12_1$, $P2_1$, $C2$ and $P1$
Solid Solution (<1%)	Proportion	No data	No data	No data
	Dominant SG	No data	No data	No data

IV Access to pure enantiomer

IV.1 Overview

Since the new regulation issued by the FDA in 1992, the use of racemic drugs has been vanishing in favor of enantiopure ones (Figure 39).

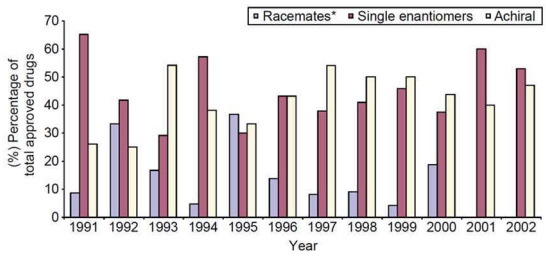

*Figure 39. Annual distribution of FDA-approved drugs (NMEs) according to chirality in the period 1991-2002. * Including diastereomeric mixtures.*[84]

Enantiopure drugs can be obtained from:[84]

- Synthesis from the chiral pool (45%).
- Enantioselective synthesis (9%).
- Resolution from racemic mixture (46%).

To control the enantiopurity of samples two main analysis methods are used:

- The historical one (related to the discovery of chirality)[50,51] is the polarimetry. The optical rotation $\boldsymbol{\alpha}$ of the sample, generally dissolved, depends on its concentration $\boldsymbol{c}$, the length of the measurement cell $\boldsymbol{l}$ (generally 10cm) and of the specific optical rotation $[\boldsymbol{\alpha}]_{\boldsymbol{\lambda}}^{\boldsymbol{t}}$ itself dependent on the sample, the solvent, the temperature and the wavelength of the polarized light (Eq. 27).[71] The deviation varies from maximum,

and opposite, for the enantiomers, to zero for the racemic mixture. Enantiomeric excess (actually the so-called optical purity) is calculated from the ratio of the sample deviation over the deviation of the pure enantiomer (if the analyses are performed in same conditions) (Eq. 28).

$$\alpha = l * c * [\alpha]_{\lambda}^{t} \qquad \textit{Eq. 27}$$

$$e.e = \frac{[\alpha]_{\lambda}^{t}}{[\alpha_0]_{\lambda}^{t}} = \frac{\alpha_{\lambda}^{t}}{\alpha_{0\lambda}^{t}} \qquad \textit{Eq. 28}$$

- Chiral chromatography[85] is based on the different interactions between the enantiomers and the chiral stationary phase. Enantiomers are so eluted at different times and the areas of the peaks can be directly introduced in the equation for enantiomeric excess (Eq. 25 & 26).

If chiral chromatography gives more accurate analyses, polarimetry has the advantage to be quasi-immediate measurements. Therefore, polarimetry can be used for on-line measurements and chromatography to analyze final samples.

In the frame of this work, only few resolution processes *via* crystallization would be presented. Concerning other processes to obtain pure enantiomers without crystallization, one can list: synthesis from chiral pool, asymmetric synthesis,[86] preparative chiral chromatography,[85] biocatalysis,[87] etc.

IV.2 Resolution *via* crystallization

IV.2.1 Pasteurian resolution

As early as 1853, Pasteur[88,89] already performed several chiral resolution exploiting the difference of properties between the two components of a diastereomeric pair.[70] As diastereomers are not mirror images and have so different physical and chemical properties, they can be "easily" separated. Starting from a racemic mixture of enantiomers, another enantiopure component is added (*chiral agent*) to induce a symmetry breaking between the two enantiomers. The two diastereomers formed can then be separated by exploiting their differences in solubility (Figure 40). *Pasteurian resolution*, and its variations,[90–94] are often used at the industrial scale but they need investigations to find the suitable chiral agent combining low cost production and best resolution efficiency.

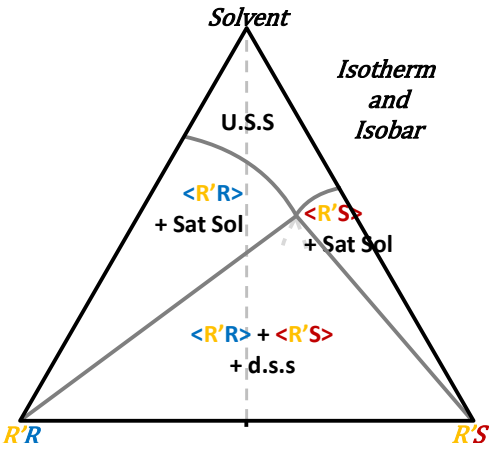

Figure 40. Ternary section representing the difference of solubility used in Pasteurian resolution.

IV.2.2 Preferential Crystallization[95]

Preferential crystallization (PC) processes are *stereoselective* crystallizations of a single enantiomer at a time. It means that, by means of a suitable control of several parameters, only one enantiomer crystallizes whereas thermodynamics predicts the crystallization of the two simultaneously. First preferential crystallization recorded was performed by Désiré Gernez[96] in 1866 who obtained only one morphology of the sodium ammonium tartrate tetrahydrate (cf. Part.III.I.1) by seeding the racemic supersaturated solution with crystals of the same handedness. Since the publications of Secor[97] and Jacques[98] in the middle of the 20th century, preferential crystallization becomes far more interesting for both academic and industrial researchers.

As for other methods, several variations, based on same principle, exist for preferential crystallization. Postulate is made that PC is only applicable to conglomerate forming systems (few examples are known on metastable conglomerate).[99,86,100–104] The true major condition is in fact that the system must present a genuine chiral discrimination in the solid state. The extreme chiral discrimination is conglomerate but it can be mirror image partial solid solutions.[105,106]

The major advantage of PC is that by means of recycles of the mother liquor, the yield in the two enantiomers can be quantitative.

IV.2.2.1 Seeded Isothermal Preferential Crystallization

The Seeded Isothermal Preferential Crystallization (SIPC) is the oldest method of preferential crystallization. A solution of racemic or slightly enriched ($e.e_{ini}$) mixture is cooled down to make it supersaturated. Seeds of one enantiomer (the one initially in excess) are then added at this metastable homogeneous doubly saturated solution to skip the primary nucleation

of this enantiomer and to speed up its selective crystallization. Filtration is performed before the nucleation of the counter-enantiomer.

IV.2.2.2 Seeded Polythermal Programmed Preferential Crystallization

The same logics takes place for the Seeded Polythermal Programmed Preferential Crystallization (S3PC) except that once the seeding is performed, the temperature continues to decrease to increase the crystallizing enantiomer quantity.

IV.2.2.3 Auto-Seeded Polythermal Programmed Preferential Crystallization

The Auto-Seeded Polythermal Programmed Preferential Crystallization process (AS3PC) was developed by Coquerel & al. in 1995.[107] Below is presented its mechanism (Figure 41):[102,108]

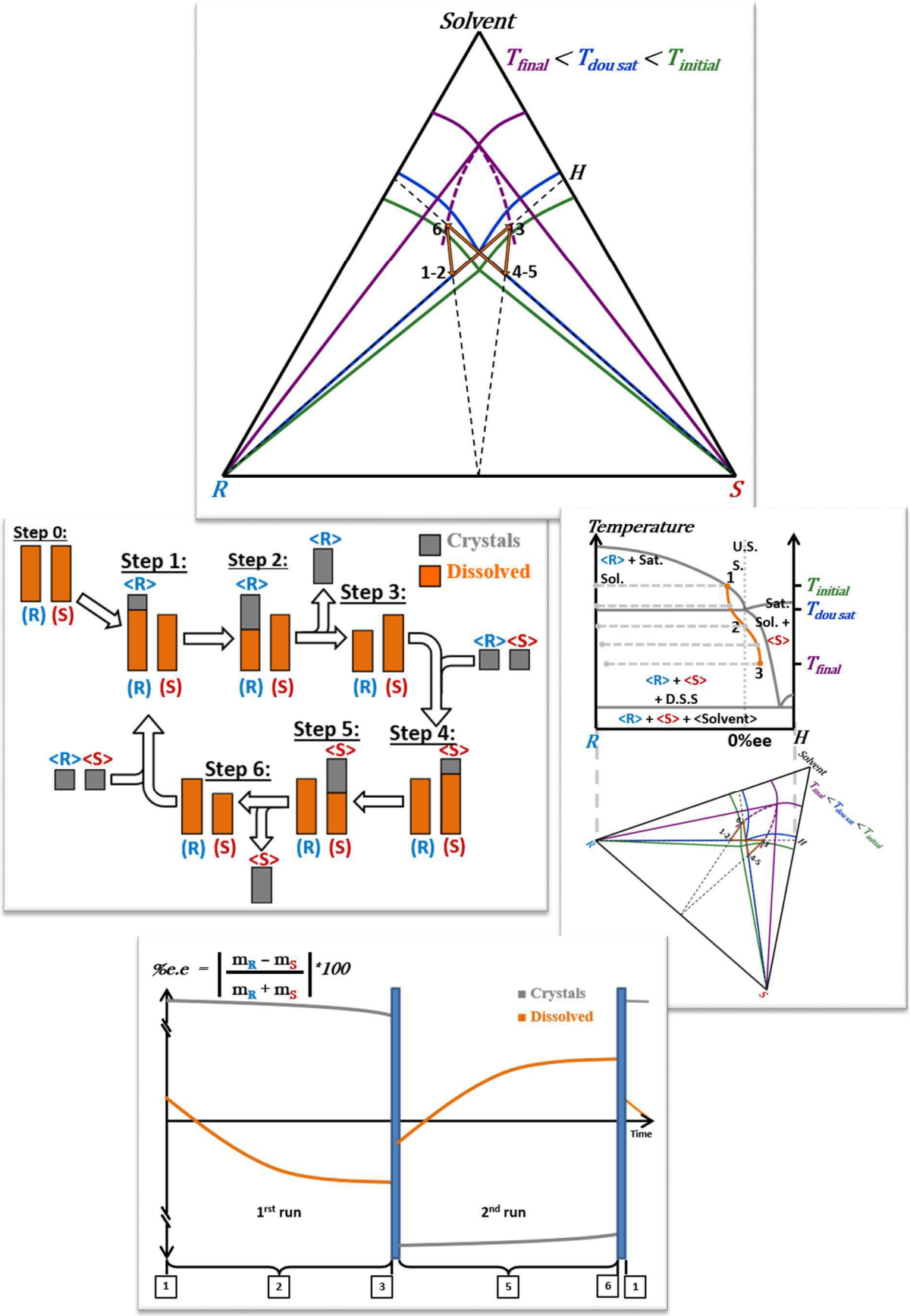

Figure 41. System pathway (i) in the ternary section (top) and (ii) in [RH] isoplethal section (middle right), (iii) e.e of the solution and the suspension (bottom) and classical basic description (middle left) of the AS3PC process.

- Step 0: a doubly saturated solution is prepared at temperature $\boldsymbol{T_{dou\ sat}}$.
- Step 1: seeds of $\boldsymbol{R}$ enantiomer are added and the system heated to temperature $\boldsymbol{T_{initial} > T_{dou\ sat}}$ to obtain a suspension of $\boldsymbol{R}$ enantiomer in a solution lightly enriched with the same enantiomer. At this step the system is on a stable tie-line (biphasic domain) and the solution is saturated in $\boldsymbol{R}$ enantiomers.
- Step 2: the system is cooled down from $\boldsymbol{T_{initial}}$ to $\boldsymbol{T_{final}}$. Solubility decreases which induces crystal growth and secondary nucleation of the $\boldsymbol{R}$ enantiomer while the solution becomes enriched in enantiomer $\boldsymbol{S}$. Mother liquor moves along a metastable tie-line between $\boldsymbol{R}$ and a solution saturated in $\boldsymbol{R}$ and supersaturated in $\boldsymbol{S}$. In theory, PC could be continued until the system reaches the metastable solubility of $\boldsymbol{R}$ enantiomer.
- Step 3: the system is filtrated before the stabilizing nucleation and crystal growth of $\boldsymbol{S}$ enantiomer. The crop of $\boldsymbol{R}$ crystals is weighed and the solution moves toward the metastable tie-line to the metastable solubility. The first run is completed.
- Step 4: The system is heated back to $\boldsymbol{T_{initial}}$ and a mass of racemic mixture, equal to the mass of the crop of $\boldsymbol{R}$ crystals in step 3, is added to the system. After equilibration, the solution is at the symmetrical state as in step 1 with a suspension of $\boldsymbol{S}$ enantiomer in a solution lightly enriched in the same enantiomer.
- Step 5: Symmetrical of step 2: the system is cooled down from $\boldsymbol{T_{initial}}$ to $\boldsymbol{T_{final}}$. Solubility decreases which induces crystal growth and secondary nucleation of the $\boldsymbol{S}$ enantiomer while the solution becomes enriched in enantiomer $\boldsymbol{R}$. The mother liquor moves along the metastable tie-line between $\boldsymbol{S}$ and a solution saturated in $\boldsymbol{S}$ and supersaturated in $\boldsymbol{R}$. In theory, PC could be continued until the system reaches the metastable solubility of $\boldsymbol{S}$ enantiomer.
- Step 6: Symmetrical of step 3. The system is filtrated before the stabilizing nucleation and crystal growth of $\boldsymbol{R}$ enantiomer. The crop of $\boldsymbol{S}$ crystals is weighed and the solution moves along the metastable tie-line to the metastable solubility. The second run is completed.
- Final step: By heating back the system to $\boldsymbol{T_{initial}}$ and compensating the harvest by the same mass of racemic mixture, the system is moved back to the initial step 1. The first cycle is completed.

The AS3PC usually gives better results than SIPC or S3PC methods due to the auto-seeding. It allows a better management of the supersaturation: one enantiomer crystallizes all along the cooling, the system is thus only supersaturated in one enantiomer whereas it is supersaturated in both enantiomers before the seeding for the other methods. Following a more favorable metastable equilibrium, crystal growth and secondary nucleation are favored at the expense of uncontrolled primary nucleation.

Different parameters influence the yield of AS3PC process:

- Parameters inherent to the solvent such as good solubility, good variation of solubility with temperature, or good chiral discrimination (no undesirable racemic solvate for instance).
- Initial temperature and composition: the higher the initial concentration, the better the yield. Moreover, temperature must be adjusted to dissolve a significant part but not all of the initial enantiomeric excess so that the system is auto-seeded. Crystal size distribution and morphology of seeds have, usually, limited effects during AS3PC process.
- The cooling and stirring rate: concerning the cooling rate, the higher the better. Indeed, faster cooling rate enlarges the width of Ostwald metastable zone delaying further the nucleation of the counter-enantiomer. Another effect is to accelerate the crystallization and to promote secondary nucleation and more centered crystal size distribution. But conversely, high cooling rate induces less control of the stereoselective crystallization.

  Stirring is essential to homogenize the temperature and concentration of the system but it is also responsible of secondary nucleation that can lead to undesirable heteronucleation of the counter-enantiomer.
- The final temperature: more important than the cooling and stirring rate is the final temperature. It is connected to the possibility to crystallize the counter-enantiomer. This temperature is usually the last parameter to be set and is determined following the e.e of the solution during a PC run test.

IV.2.2.4 Auto-Seeded Preferential Crystallization Induced by Solvent Evaporation

In 2011, a new process of preferential crystallization has been developed by the SMS laboratory: the Auto-Seeded Preferential Crystallization Induced by Solvent Evaporation

(ASPreCISE).[108,109] The principle is the same except that the supersaturation is induced by solvent evaporation (the composition of the system changes).

IV.2.3 Deracemization

Preferential crystallization consists on successive crystallizations of each enantiomers. Most of the time, only one enantiomer presents an industrial and pharmaceutical interest, this is why PC can be described as a 50% yield process. To go further that 50% yield, a new process has to be designed. Racemization of the distomer can be achieved separately but there is also a process, called *deracemization*, that combines both stereoselective crystallization and in-situ racemization. Starting from a racemic or lightly enriched suspension, the enantiomer in default would be converted into the other one leading to an enantiopure suspension (Figure 42) and the theoretical 100% yield.

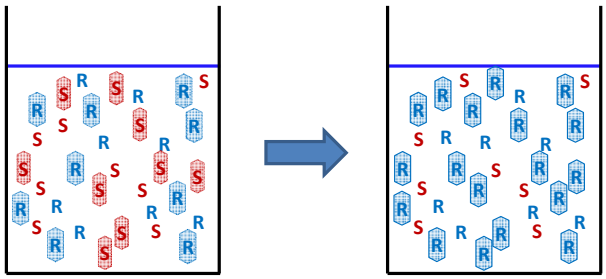

Figure 42. Schematic representation of the deracemization process.

Two conditions must be fulfilled by a system to candidate for deracemization: a rapid racemization in solution and a chiral discrimination at the solid state (as for PC, a conglomerate is the best). Racemization is the transformation of a sample at a scalemic composition toward the racemic composition. Racemization can be instantaneous (e.g supra-molecular chirality) or through a chemical reaction needing a *racemizing agent*[110,111] (i.e a catalyst).

Two main processes, with their own mechanisms, have been established until now:

- *Viedma ripening*[112–119], also known as *attrition-enhanced deracemization*, is the first deracemization process highlighted. Several hypotheses concerning its mechanism have been proposed and refuted. The last version includes the combination of "*four processes: 1) racemization in the solution (not needed for achiral systems), 2) Ostwald ripening; that is, large crystals growing at the expense of smaller crystals, 3) enantioselective (partial) incorporation of clusters, and 4) attrition.*"[116]
- *Temperature cycle enhanced deracemization*[120–124] can be divided into two steps: during cooling there is a stereoselective crystallization of the excess enantiomer

concomitant to a racemization, resulting in 0%*ee* in the solution. During heating, a part of the crystals, preferentially the smaller ones, are dissolved. Successive temperature cycles result in the complete deracemization without need for work up.

IV.2.4 Preferential Enrichment

The last resolution process presented is the *preferential enrichment*.[125–129] It is an unusual process since, contrary to previous processes, it is the solution that is highly enriched in one enantiomer and the crystals that are poorly enriched (Figure 43). Mechanism has not been fully established but an industrial application of this process seems improbable considering the conditions needed: very high supersaturation, long time experiment, stagnant conditions, etc.

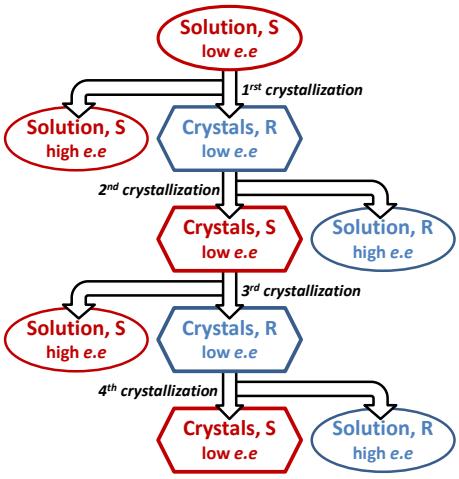

Figure 43. Phases obtained by consecutive preferential enrichments.

Bibliography

(1) Tschoegl, N. W. *Fundamentals of Equilibrium and Steady-State Thermodynamics*; Elsevier, 2000.

(2) Findlay, A. 1874-. *The Phase Rule and Its Applications*; WENTWORTH Press, 2016.

(3) Ediger, M. D.; Angell, C. A.; Nagel, S. R. Supercooled Liquids and Glasses. *J. Phys. Chem.* **1996**, *100* (31), 13200–13212.

(4) Gibbs, J. W. *On the Equilibrium of Heterogeneous Substances*; Connecticut Academy of Arts and Sciences, 1874.

(5) Boltzmann, L. Ueber Die Natur Der Gasmoleküle. *Ann. Phys.* **1877**, *236* (1), 175–176.

(6) Oonk, H. A. J.; Calvet, M. T. *Equilibrium between Phases of Matter. 1: Phenomenology and Thermodynamics*; Springer: Dordrecht, 2008.

(7) Porter, D. A.; Easterling, K. E.; Sherif, M. *Phase Transformations in Metals and Alloys*; CRC Press, 2009.

(8) Ostwald, W. Studien Über Die Bildung Und Umwandlung Fester Körper. *Z. Für Phys. Chem.* **1897**, *22U* (1), 289–330.

(9) Nývlt, J. The Ostwald Rule of Stages. *Cryst. Res. Technol.* **1995**, *30* (4), 443–449.

(10) Ricci, J. E. *The Phase Rule and Heterogeneous Equilibrium*, Dover publications.; New York, 1966.

(11) McCrone, W. C. Polymorphism. *Phys. Chem. Org. Solid State* **1965**, *2*, 725–767.

(12) Burger, A.; Ramberger, R. On the Polymorphism of Pharmaceuticals and Other Molecular Crystals. I. *Microchim. Acta* **1979**, *72* (3–4), 259–271.

(13) Bernstein, J. Polymorphism − A Perspective. *Cryst. Growth Des.* **2011**, *11* (3), 632–650.

(14) Legendre, B.; Querniard, F. Glossary for Binary Phase Diagram Reactions. *J. Phase Equilibria Diffus.* **2014**, *35* (1), 11–14.

(15) Rousseau, J.-J.; Gibaud, A. *Cristallographie géométrique et radiocristallographie: cours et exercices corrigés*; Dunod: Paris, 2007.

(16) Romé de L'Isle, J.-B. L. de (1736-1790). *Des caractères extérieurs des minéraux*; Chez Barrois: A Paris, 1784.

(17) Haüy, R.-J. (1743-1822). *Essai d'une théorie sur la structure des crystaux, appliquée à plusieurs genres de substances crystallisées / par M. l'abbé Haüy,...*; Gogué et Née de La Rochelle: Paris, 1784.

(18) Miller, W. H. *A Treatise on Crystallography*; J. & J. J. DEIGHTON, TRINITY STREET: Cambridge, 1839.

(19) Dunitz, J. D. *X-Ray Analysis and the Structure of Organic Molecules*; Verlag Helvetica Chimica Acta, 1995.

(20) *International Tables for Crystallography.Pdf*, 5th ed.; Theo Hahn, 2005; Vol. A: Space-Group Symmetry.

(21) Bravais, A. *Études cristallographiques*; Gauthier-Villars, 1866.

(22) Pertsin, A. J.; Kitaigorodsky, A. I. The Atom-Atom Potential Method. In *The Atom-Atom Potential Method*; Springer Series in Chemical Physics; Springer, Berlin, Heidelberg, 1987; pp 69–148.

(23) Parsegian, V. A. *Van Der Waals Forces*; Cambridge University Press, 2006.

(24) Hunter, C. A.; Lawson, K. R.; Perkins, J.; Urch, C. J. Aromatic Interactions. *J. Chem. Soc. Perkin Trans. 2* **2001**, *0* (5), 651–669.

(25) Steiner, T. The Hydrogen Bond in the Solid State. *Angew. Chem. Int. Ed.* **2002**, *41* (1), 48–76.

(26) Gilli, G.; Gilli, P. *The Nature of the Hydrogen Bond: Outline of a Comprehensive Hydrogen Bond Theory*; OUP Oxford, 2009.

(27) Dunitz, J. D. Phase Changes and Chemical Reactions in Molecular Crystals. *Acta Crystallogr. B* **1995**, *51* (4), 619–631.

(28) Bernstein, J.; Hagler, A. T. Conformational Polymorphism. The Influence of Crystal Structure on Molecular Conformation. *J. Am. Chem. Soc.* **1978**, *100* (3), 673–681.

(29) Boistelle, R.; Astier, J. P. Crystallization Mechanisms in Solution. *J. Cryst. Growth* **1988**, *90* (1), 14–30.

(30) Coquerel, G. Crystallization of Molecular Systems from Solution: Phase Diagrams, Supersaturation and Other Basic Concepts. *Chem Soc Rev* **2014**, *43* (7), 2286–2300.

(31) Gibbs, J. W. *The Collected Works of J. Willard Gibbs.*; Yale University Press: New Haven, 1948; Vol. 1.

(32) Söhnel, O.; Garside, J. *Precipitation: Basic Principles and Industrial Applications*; Butterworth-Heinemann, 1992.

(33) Kashchiev, D.; van Rosmalen, G. M. Review: Nucleation in Solutions Revisited. *Cryst. Res. Technol.* **2003**, *38* (7–8), 555–574.

(34) Schmelzer, J. W. P. *Nucleation Theory and Applications*; John Wiley & Sons, 2006.

(35) Mullin, J. W. *Crystallization*, 4ed; Butterworth-Heinemann ed.; Elsevier: Oxford, 2001.

(36) McCabe, W. L.; Smith, J. C.; Harriott, P. *Unit Operations of Chemical Engineering*; McGraw-Hill: New York, 1993.

(37) Bennema, P. Spiral Growth and Surface Roughening: Developments since Burton, Cabrera and Frank. *J. Cryst. Growth* **1984**, *69* (1), 182–197.

(38) Volmer, M. Über gerichtetes Kristallwachstum. *Z. Für Phys.* **1922**, *9* (1), 193–196.

(39) Donnay, J. D. H.; Harker, D. A New Law of Crystal Morphology Extending the Law of Bravais. *J. Mineral. Soc. Am.* **1937**, No. 22 (5), 446–467.

(40) Bennema, P.; Meekes, H.; Boerrigter, S. X. M.; Cuppen, H. M.; Deij, M. A.; van Eupen, J.; Verwer, P.; Vlieg, E. Crystal Growth and Morphology: New Developments in an Integrated Hartman–PerdokConnected NetRoughening Transition Theory, Supported by Computer Simulations. *Cryst. Growth Des.* **2004**, *4* (5), 905–913.

(41) Voorhees, P. W. The Theory of Ostwald Ripening. *J. Stat. Phys.* **1985**, *38* (1–2), 231–252.

(42) Mehrer, H. *Diffusion in Solids: Fundamentals, Methods, Materials, Diffusion-Controlled Processes*; Springer Science & Business Media, 2007.

(43) Vitek, V. Atomic Level Computer Modelling of Crystal Defects with Emphasis on Dislocations: Past, Present and Future. *Prog. Mater. Sci.* **2011**, *56* (6), 577–585.

(44) Bollmann, W. *Crystal Defects and Crystalline Interfaces*; Springer Science & Business Media, 2012.

(45) Bobo, E.; Lefez, B.; Caumon, M.-C.; Petit, S.; Coquerel, G. Evidence of Two Types of Fluid Inclusions in Single Crystals. *CrystEngComm* **2016**, *18* (28), 5287–5295.

(46) Haüy, R. J. *Traité de minéralogie*; Chez Louis, 1801.

(47) Biot, J. B. Phénomènes de Polarisation Successive, Observés Dans Des Fluides Homogènes. *Bull Soc Philomath* **1815**, *190*, 1815.

(48) Gay Lussac, J. L. *Schweiggers J.* **1928**, *48*, 381.

(49) Gay Lussac, J. L.; Arago, F. *Annales de chimie et de physique*; V. Masson: Paris, 1838; Vol. 69.

(50) Pasteur, L. *Comptes Rendus Hebd. Séances L'Académie Sci.* **1848**, *26*, 535–538.

(51) Pasteur, L. *Ann. Chim. Phys.* **1848**, No. 24, 442–459.

(52) van't Hoff, J. H. *Bull. Société Chim. Paris* **1875**, *23*, 295–301.

(53) Le Bel, J. A. *Bull. Société Chim. Paris* **1874**, *22*, 334–347.

(54) Lord Kelvin, W. T. Baltimore Lectures on Molecular Dynamics and the Wave Theory of Light (CJ Clay and Sons, London, 1904). **1884**.

(55) Curie, P. Sur la possibilité d'existence de la conductibilité magnétique et du magnétisme libre. *J. Phys. Théorique Appliquée* **1894**, *3* (1), 415–417.

(56) Pizzarello, S.; Zolensky, M.; Turk, K. A. Nonracemic Isovaline in the Murchison Meteorite: Chiral Distribution and Mineral Association. *Geochim. Cosmochim. Acta* **2003**, *67* (8), 1589–1595.

(57) Pizzarello, S. The Chemistry of Life's Origin: A Carbonaceous Meteorite Perspective. *Acc. Chem. Res.* **2006**, *39* (4), 231–237.

(58) Tranter, G. E. Parity-Violating Energy Differences of Chiral Minerals and the Origin of Biomolecular Homochirality. *Nature* **1985**, *318* (6042), 172.

(59) Friedman, L.; Miller, J. G. Odor Incongruity and Chirality. *Science* **1971**, *172* (3987), 1044–1046.

(60) Reddy, I. K.; Mehvar, R. *Chirality in Drug Design and Development*; CRC Press, 2004.

(61) Ariens, E. J. Stereochemistry, a Basis for Sophisticated Nonsense in Pharmacokinetics and Clinical Pharmacology. *Eur. J. Clin. Pharmacol.* **1984**, *26* (6), 663–668.

(62) Chirality; 1992; Vol. 4, pp 338–340.

(63) Guennec, P. L. Towards a Theory of Molecular Recognition. *Theor. Chem. Acc.* **1999**, *101* (1–3), 151–158.

(64) Testa, B.; Mayer, J. Molecular Toxicology and the Medicinal Chemist1Paper Presented at the First Italian–Swiss Meeting on Medicinal Chemistry, Turin, Italy, 1997.1. *Il Farm.* **1998**, *53* (4), 287–291.

(65) Cahn, R. S.; Ingold, C. K.; Prelog, V. The Specification of Asymmetric Configuration in Organic Chemistry. *Experientia* **1956**, *12* (3), 81–94.

(66) Cahn, R. S.; Ingold, C.; Prelog, V. Specification of Molecular Chirality. *Angew. Chem. Int. Ed. Engl.* **1966**, *5* (4), 385–415.

(67) Moreno, L. F. Understanding Fischer Projection and Angular Line Representation Conversion. *J. Chem. Educ.* **2012**, *89* (1), 175–176.

(68) Prelog, V. Chirality in Chemistry. *Croat. Chem. Acta* **2006**, *79* (3), XLIX–LVII.

(69) Kipping, F. S.; Pope, W. J. LXIII.—Enantiomorphism. *J. Chem. Soc. Trans.* **1898**, *73*, 606–617.

(70) J. Jaques; A. Collet; S. H. Wilen. *Enantiomers, Racemates, and Resolutions*; Krieger Publishing Company: Malabar, 1994; Vol. 86.

(71) Horeau, A. Interactions d'énantiomères En Solution; Influence Sur Le Pouvoir : Pureté Optique et Pureté Énantiomérique. **1969**, 3121–3124.

(72) Scott, R. L. Modification of the Phase Rule for Optical Enantiomers and Other Symmetric Systems. *J. Chem. Soc. Faraday Trans. 2 Mol. Chem. Phys.* **1977**, *73* (3), 356–360.

(73) Wheeler, J. C. On Gibbs Phase Rule for Optical Enantiomers. *J. Chem. Phys.* **1980**, *73* (11), 5771–5777.

(74) Coquerel, G. Solubility of Chiral Species as Function of the Enantiomeric Excess. *J. Pharm. Pharmacol.* **2015**, *67* (6), 869–878.

(75) Coquerel, G. Review on the Heterogeneous Equilibria between Condensed Phases in Binary Systems of Enantiomers. *Enantiomer* **2000**, *5*, 481–498.

(76) Kotelnikova, E. N.; Isakov, A. I.; Lorenz, H. Non-Equimolar Discrete Compounds in Binary Chiral Systems of Organic Substances. *CrystEngComm* **2017**, *19* (14), 1851–1869.

(77) Flack, H. D. Chiral and Achiral Crystal Structures. *Helv. Chim. Acta* **2003**, *86* (4), 905–921.

(78) Galland, A.; Dupray, V.; Berton, B.; Morin-Grognet, S.; Sanselme, M.; Atmani, H.; Coquerel, G. Spotting Conglomerates by Second Harmonic Generation. *Cryst. Growth Des.* **2009**, *9* (6), 2713–2718.

(79) Dupray, V. Recrystallization of Enantiomers from Conglomerates. In *Recrystallization*; InTech, 2012.

(80) Belsky, V. K.; Zorkii, P. M. Distribution of Organic Homomolecular Crystals by Chiral Types and Structural Classes. *Acta Crystallogr. A* **1977**, *33* (6), 1004–1006.

(81) Dalhus, B.; Görbitz, C. H. Non-Centrosymmetric Racemates: Space-Group Frequencies and Conformational Similarities between Crystallographically Independent Molecules. *Acta Crystallogr. B* **2000**, *56* (4), 715–719.

(82) Fábián, L.; Brock, C. P. A List of Organic Kryptoracemates. *Acta Crystallogr. B* **2010**, *66* (1), 94–103.

(83) Brandel, C.; Petit, S.; Cartigny, Y.; Coquerel, G. Structural Aspects of Solid Solutions of Enantiomers. *Curr. Pharm. Des.* **2016**, *22* (32), 4929–4941.

(84) Caner, H.; Groner, E.; Levy, L.; Agranat, I. Trends in the Development of Chiral Drugs. *Drug Discov. Today* **2004**, *9* (3), 105–110.

(85) Beesley, T. E.; Scott, R. P. W. *Chiral Chromatography*; John Wiley & Sons, 1998.

(86) Eliel, E. L.; Wilen, S. H.; Mander, L. N. *Stereochemistry of Organic Compounds*; Wiley & Sons, 1994.

(87) Wohlgemuth, R. Asymmetric Biocatalysis with Microbial Enzymes and Cells. *Curr. Opin. Microbiol.* **2010**, *13* (3), 283–292.

(88) Pasteur, L. **1853**, *37*, 162–166.

(89) Pasteur, L. **1853**, *38*, 437–483.

(90) Marckwald, W. Ueber Ein Bequemes Verfahren Zur Gewinnung Der Linksweinsäure. *Berichte Dtsch. Chem. Ges.* **1896**, *29* (1), 42–43.

(91) Pope, W. J.; Peachey, S. J. CVIII.—The Application of Powerful Optically Active Acids to the Resolution of Externally Compensated Basic Substances. Resolution of Tetrahydroquinaldine. *J. Chem. Soc. Trans.* **1899**, *75* (0), 1066–1093.

(92) Marchand, P.; Lefèbvre, L.; Querniard, F.; Cardinaël, P.; Perez, G.; Counioux, J.-J.; Coquerel, G. Diastereomeric Resolution Rationalized by Phase Diagrams under the Actual Conditions of the Experimental Process. *Tetrahedron Asymmetry* **2004**, *15* (16), 2455–2465.

(93) Kellogg, R. M.; Kaptein, B.; Vries, T. R. Dutch Resolution of Racemates and the Roles of Solid Solution Formation and Nucleation Inhibition. In *Novel Optical Resolution Technologies*; Sakai, K., Hirayama, N., Tamura, R., Eds.; Topics in Current Chemistry; Springer Berlin Heidelberg, 2007; pp 159–197.

(94) Sakai, K.; Sakurai, R.; Nohira, H. 6 New Resolution Technologies Controlled by Chiral Discrimination Mechanisms. In *Novel Optical Resolution Technologies*; Sakai, K., Hirayama, N., Tamura, R., Eds.; Topics in Current Chemistry; Springer Berlin Heidelberg, 2006; pp 199–231.

(95) Coquerel, G. 1 Preferential Crystallization. In *Novel Optical Resolution Technologies*; Sakai, K., Hirayama, N., Tamura, R., Eds.; Topics in Current Chemistry; Springer Berlin Heidelberg, 2006; pp 1–51.

(96) Gernez, D. **1866**, *63*, 843.

(97) Secor, R. M. Resolution of Optical Isomers by Crystallization Procedures. *Chem. Rev.* **1963**, *63* (3), 297–309.

(98) Collet, A.; Brienne, M. J.; Jacques, J. Optical Resolution by Direct Crystallization of Enantiomer Mixtures. *Chem. Rev.* **1980**, *80* (3), 215–230.

(99) Inagaki, M. Some Aspects on the Optical Resolution by Preferential Crystallization Based on Phase Equilibrium. *Chem. Pharm. Bull. (Tokyo)* **1977**, *25* (10), 2497–2503.

(100) Lorenz, H.; Polenske, D.; Seidel-Morgenstern, A. Application of Preferential Crystallization to Resolve Racemic Compounds in a Hybrid Process. *Chirality* **2006**, *18* (10), 828–840.

(101) Kaemmerer, H.; Lorenz, H.; Black, S. N.; Seidel-Morgenstern, A. Study of System Thermodynamics and the Feasibility of Chiral Resolution of the Polymorphic System of Malic Acid Enantiomers and Its Partial Solid Solutions. *Cryst. Growth Des.* **2009**, *9* (4), 1851–1862.

(102) Levilain, G.; Coquerel, G. Pitfalls and Rewards of Preferential Crystallization. *CrystEngComm* **2010**, *12* (7), 1983.

(103) Gilks, S. E.; Davey, R. J.; Mughal, R. K.; Sadiq, G.; Black, L. Crystallization of 2-Chloromandelic Acid: Solubility, Formation of the Metastable Conglomerate, and Use of a Nonaqueous Emulsion To Prepare an Enantiomerically Enriched Product. *Cryst. Growth Des.* **2013**, *13* (10), 4323–4329.

(104) Brandel, C.; Amharar, Y.; Rollinger, J. M.; Griesser, U. J.; Cartigny, Y.; Petit, S.; Coquerel, G. Impact of Molecular Flexibility on Double Polymorphism, Solid Solutions and Chiral Discrimination during Crystallization of Diprophylline Enantiomers. *Mol. Pharm.* **2013**, *10* (10), 3850–3861.

(105) Renou, L.; Morelli, T.; Coste, S.; Petit, M.-N.; Berton, B.; Malandain, J.-J.; Coquerel, G. Chiral Discrimination at the Solid State of Methyl 2-(Diphenylmethylsulfinyl)Acetate. *Cryst. Growth Des.* **2007**, *7* (9), 1599–1607.

(106) Wermester, N.; Aubin, E.; Pauchet, M.; Coste, S.; Coquerel, G. Preferential Crystallization in an Unusual Case of Conglomerate with Partial Solid Solutions. *Tetrahedron Asymmetry* **2007**, *18* (7), 821–831.

(107) Coquerel, G.; Petit, M.-N.; Bouaziz, R. Procede De Dedoublement De Deux Antipodes Optiques Par Cristallisation. WO/1995/008522, March 31, 1995.

(108) Coquerel, G.; Levilain, G. Process for the Resolution of Enantiomers by Preferential Evaporative Crystallization. WO2011/073300, December 16, 2010.

(109) Mahieux, J.; Sanselme, M.; Harthong, S.; Melan, C.; Aronica, C.; Guy, L.; Coquerel, G. Preparative Resolution of (±)-Bis-Tetralone by Means of Autoseeded Preferential Crystallization Induced by Solvent Evaporation (ASPreCISE). *Cryst. Growth Des.* **2013**, *13* (8), 3621–3631.

(110) Yamada, S.; Hongo, C.; Yoshioka, R.; Chibata, I. Method for the Racemization of Optically Active Amino Acids. *J. Org. Chem.* **1983**, *48* (6), 843–846.

(111) Yoshioka, R. 3 Racemization, Optical Resolution and Crystallization-Induced Asymmetric Transformation of Amino Acids and Pharmaceutical Intermediates. In *Novel Optical Resolution Technologies*; Sakai, K., Hirayama, N., Tamura, R., Eds.; Topics in Current Chemistry; Springer Berlin Heidelberg, 2007; pp 83–132.

(112) Viedma, C. Experimental Evidence of Chiral Symmetry Breaking in Crystallization from Primary Nucleation. *J. Cryst. Growth* **2004**, *261* (1), 118–121.

(113) Viedma, C. Chiral Symmetry Breaking During Crystallization: Complete Chiral Purity Induced by Nonlinear Autocatalysis and Recycling. *Phys. Rev. Lett.* **2005**, *94* (6), 065504.

(114) Viedma, C. Selective Chiral Symmetry Breaking during Crystallization: Parity Violation or Cryptochiral Environment in Control? *Cryst. Growth Des.* **2007**, *7* (3), 553–556.

(115) Noorduin, W. L.; Vlieg, E.; Kellogg, R. M.; Kaptein, B. From Ostwald Ripening to Single Chirality. *Angew. Chem. Int. Ed.* **2009**, *48* (51), 9600–9606.

(116) Noorduin, W. L.; van Enckevort, W. J. P.; Meekes, H.; Kaptein, B.; Kellogg, R. M.; Tully, J. C.; McBride, J. M.; Vlieg, E. The Driving Mechanism Behind Attrition-Enhanced Deracemization. *Angew. Chem. Int. Ed.* **2010**, *49* (45), 8435–8438.

(117) Spix, L.; Alfring, A.; Meekes, H.; van Enckevort, W. J. P.; Vlieg, E. Formation of a Salt Enables Complete Deracemization of a Racemic Compound through Viedma Ripening. *Cryst. Growth Des.* **2014**, *14* (4), 1744–1748.

(118) Rougeot, C.; Guillen, F.; Plaquevent, J.-C.; Coquerel, G. Ultrasound-Enhanced Deracemization: Toward the Existence of Agonist Effects in the Interpretation of Spontaneous Symmetry Breaking. *Cryst. Growth Des.* **2015**, *15* (5), 2151–2155.

(119) Steendam, R. R. E.; Dickhout, J.; van Enckevort, W. J. P.; Meekes, H.; Raap, J.; Rutjes, F. P. J. T.; Vlieg, E. Linear Deracemization Kinetics during Viedma Ripening: Autocatalysis Overruled by Chiral Additives. *Cryst. Growth Des.* **2015**, *15* (4), 1975–1982.

(120) Suwannasang, K.; Flood, A. E.; Rougeot, C.; Coquerel, G. Using Programmed Heating–Cooling Cycles with Racemization in Solution for Complete Symmetry Breaking of a Conglomerate Forming System. *Cryst. Growth Des.* **2013**, *13* (8), 3498–3504.

(121) Suwannasang, K.; Coquerel, G.; Rougeot, C.; Flood, A. E. Mathematical Modeling of Chiral Symmetry Breaking Due to Differences in Crystal Growth Kinetics. *Chem. Eng. Technol.* **2014**, *37* (8), 1329–1339.

(122) Suwannasang, K.; Flood, A. E.; Coquerel, G. A Novel Design Approach To Scale Up the Temperature Cycle Enhanced Deracemization Process: Coupled Mixed-Suspension Vessels. *Cryst. Growth Des.* **2016**, *16* (11), 6461–6467.

(123) Li, W. W.; Spix, L.; de Reus, S. C. A.; Meekes, H.; Kramer, H. J. M.; Vlieg, E.; ter Horst, J. H. Deracemization of a Racemic Compound via Its Conglomerate-Forming Salt Using Temperature Cycling. *Cryst. Growth Des.* **2016**, *16* (9), 5563–5570.

(124) Katsuno, H.; Uwaha, M. Mechanism of Chirality Conversion by Periodic Change of Temperature: Role of Chiral Clusters. *Phys. Rev. E* **2016**, *93* (1).

(125) Ushio, T.; Tamura, R.; Takahashi, H.; Azuma, N.; Yamamoto, K. Unusual Enantiomeric Resolution Phenomenon Observed upon Recrystallization of a Racemic Compound. *Angew. Chem. Int. Ed. Engl.* **1996**, *35* (20), 2372–2374.

(126) Tamura, R.; Fujimoto, D.; Lepp, Z.; Misaki, K.; Miura, H.; Takahashi, H.; Ushio, T.; Nakai, T.; Hirotsu, K. Mechanism of Preferential Enrichment, an Unusual Enantiomeric Resolution Phenomenon Caused by Polymorphic Transition during Crystallization of Mixed Crystals Composed of Two Enantiomers. *J. Am. Chem. Soc.* **2002**, *124* (44), 13139–13153.

(127) Iwama, S.; Horiguchi, M.; Sato, H.; Uchida, Y.; Takahashi, H.; Tsue, H.; Tamura, R. Observation of the Preferential Enrichment Phenomenon for Essential α-Amino Acids with a Racemic Crystal Structure. *Cryst. Growth Des.* **2010**, *10* (6), 2668–2675.

(128) Gonnade, R. G.; Iwama, S.; Mori, Y.; Takahashi, H.; Tsue, H.; Tamura, R. Observation of Efficient Preferential Enrichment Phenomenon for a Cocrystal of (Dl)-Phenylalanine and Fumaric Acid under Nonequilibrium Crystallization Conditions. *Cryst. Growth Des.* **2011**, *11* (2), 607–615.

(129) Uchida, Y.; Iwama, S.; Coquerel, G.; Tamura, R. A Kinetic/Thermodynamic Origin of Regular Chiral Fluctuation or Symmetry Breaking Unique to Preferential Enrichment. *Chem. - Eur. J.* **2016**, *22* (33), 11660–11666.

Contribution to Chiral Discrimination in the Solid State & Access to Pure Enantiomer via Crystallization

Chapter 2 - Preferential Crystallization of a solid/solid demixing system

Laboratoire SMS, Université de Rouen Normandie

François-Xavier Gendron

29/06/2018

Introduction

The 4-amino-3-(4-chlorophenyl)-butanoic acid, known as *baclofen* and distributed as *liorésal*, is a chiral *Active Pharmaceutical Ingredient* (API) (Figure 1). It is a γ-Amino-Butyric Acid (GABA)[1] agonist used as muscle relaxant in treatments of cerebral palsy,[2] specific types of neuralgia,[3] spinal cord injuries[4] and addictive behaviors.[5–7] In March 2014, the French *Agence Nationale de Sécurité des Médicaments et des produits de santé* (ANSM) issued a *Temporary Recommendation for Use* (TRU)[8] to suppress alcohol dependence based on self-medication of a French physician.[9,10] The TRU has been officially recommended by the French Alcohol Society in 2015.[7–9,11–13]

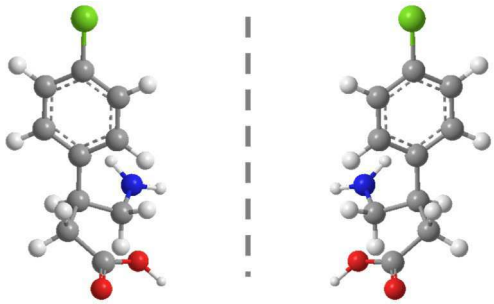

Figure 1. (S)-(+)-baclofen (left) and (R)-(-)-baclofen (right).

In the current prescriptions and pharmaceutical studies, baclofen is used at the racemic mixture. Nevertheless, it is known that the (R)-(-)-baclofen enantiomer is thrice more active than the (S)-(+)-baclofen.[14] The prescription of (R) enantiomer only seems preferable to reduce ingested quantities for the same therapeutic activity. This would be particularly interesting against alcohol addiction for which high-doses seem necessary.

To achieve this enantiopure composition, several ways have been developed.

For example, (R)-(-)-baclofen can be produce using enzymatic catalysts like *rhodoccocus sp. Bacterium*[15] (Figure 2).

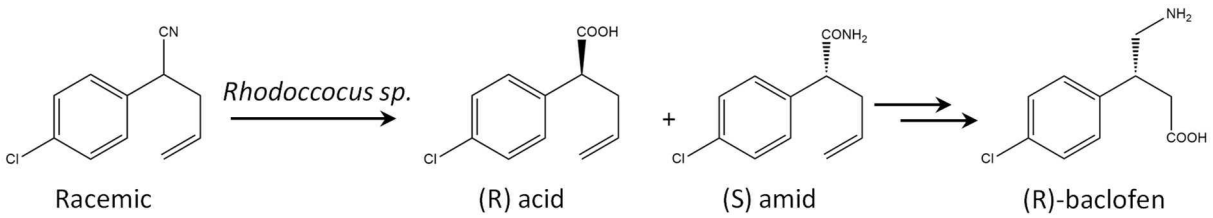

Figure 2. Schematic way of synthesis of (R)-(-)-baclofen using rhodoccocus sp. Bacterium.

Another way of synthesis has been presented by R. Chebenert & M. Desjardins[16] using asymmetric synthesis from a prochiral glutarate (Figure 3).

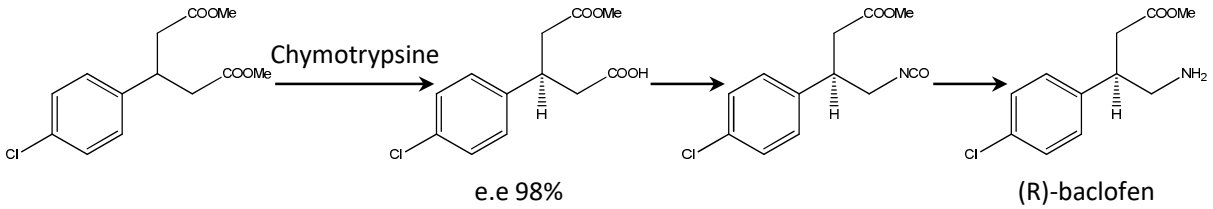

Figure 3. Schematic way of synthesis of (R)-(-)-baclofen via dissymmetric synthesis from prochiral glutarate.

(R)-(-)-baclofen can also be obtained *via* asymmetric synthesis from (S)-pyroglutamic acid[17,18] (Figure 4).

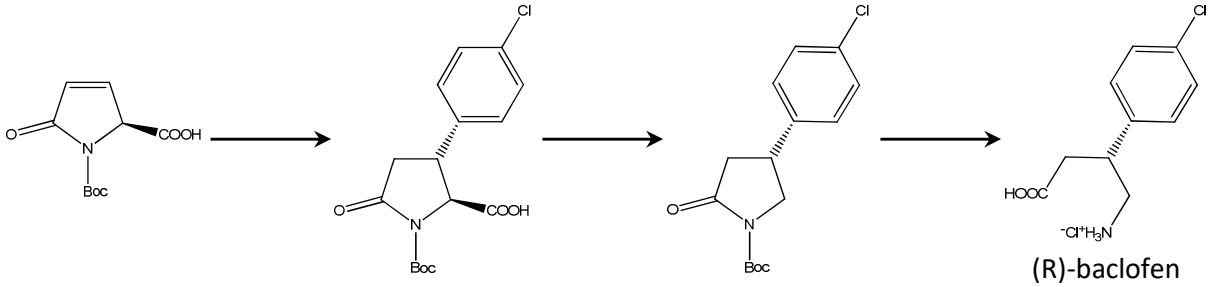

Figure 4. Schematic way of synthesis of (R)-(-)-baclofen from (S)-pyroglutamic acid.

Finally, one can achieve the enantiopure composition *via* the diastereomeric resolution between (S)-α-phenylethylamine and a baclofen intermediate of synthesis[19] (Figure 5).

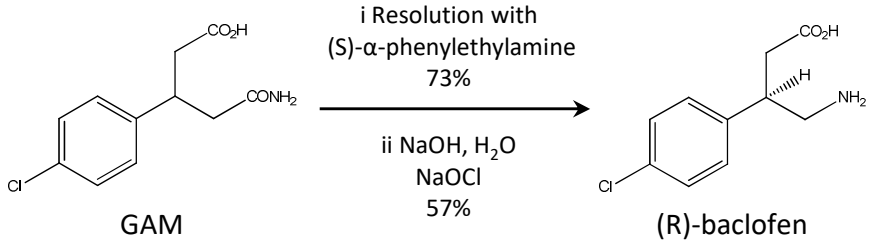

Figure 5. Schematic diastereomeric resolution leading to the resolution of enantiopure (R)-(-)-baclofen.

However, those processes could be hardly applicable at the industrial scale for several different reasons. They can involve low yields production, expensive reagents, additional impurities to remove for therapeutic used, etc.

With the aim of developing a low-cost process to obtain enantiopure (R)-(-)-baclofen, preferential crystallization processes have been investigated. Those processes, in particular the auto-seeded ones, are interesting because they can be easily scale up for industrial applications,

they do not require any expensive chiral derivative agent and they permit successive recycles of materials.[20,21] In the literature, numerous cases are known of preferential crystallization performed on conglomerate forming systems and only few examples have been published on systems presenting partial solid solutions.[22,23] The phase equilibria of the system presented here is another example of such a deviation from classical PC and is, to our knowledge, the first experimental example of complete solid solution close to fusion.

Part.I Screen of conglomerate

It is usually accepted that, in order to achieve preferential crystallization, system must present a full chiral discrimination in the solid state i.e a conglomerate forming system. This assumption is not totally true since only a chiral discrimination is necessary. Moreover, if spotting a conglomerate is not sufficient to insure the application of preferential crystallization, it is almost an inherent condition to achieve it.[24]

In 95% of the cases, the systems form racemic compounds. Conglomerate is thus searched with crystallization partners: counter ions (salts), solvent molecules (solvates) and/or co-crystal formers (cocrystals). The formation of a stable conglomerate is an essential preliminary step, but it has also a drawback by adding step(s) in the process (formation of the conglomerate and return to the initial system) and bringing new impurities.

I Baclofen system

Unfortunately, baclofen forms a racemic compound, as illustrated in Figure 6 where different diffractograms have been recorded for racemic and enantiopure baclofen.

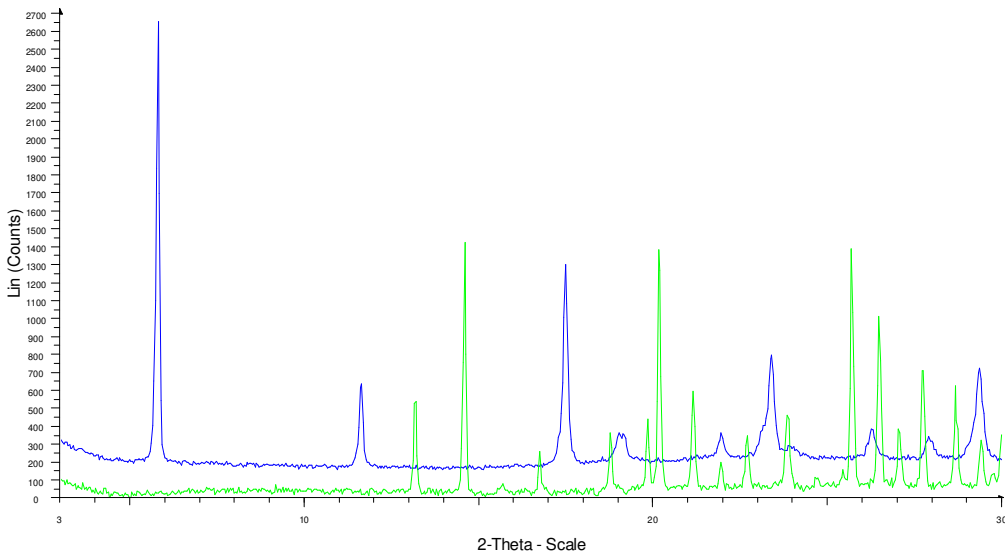

Figure 6. Diffractograms of baclofen racemic compound (blue) and baclofen enantiomer (green).

II Conglomerate screening

Since pure baclofen alone does not form a stable conglomerate, a screen of conglomerate has been performed.

II.1 Workflow of the screen

Workflow to optimize screen of conglomerate has been proposed by Gonella & al.[24] combining SHG and XRPD measurements (Figure 7). Nevertheless, a more general workflow can be proposed with an additional step (Figure 8).

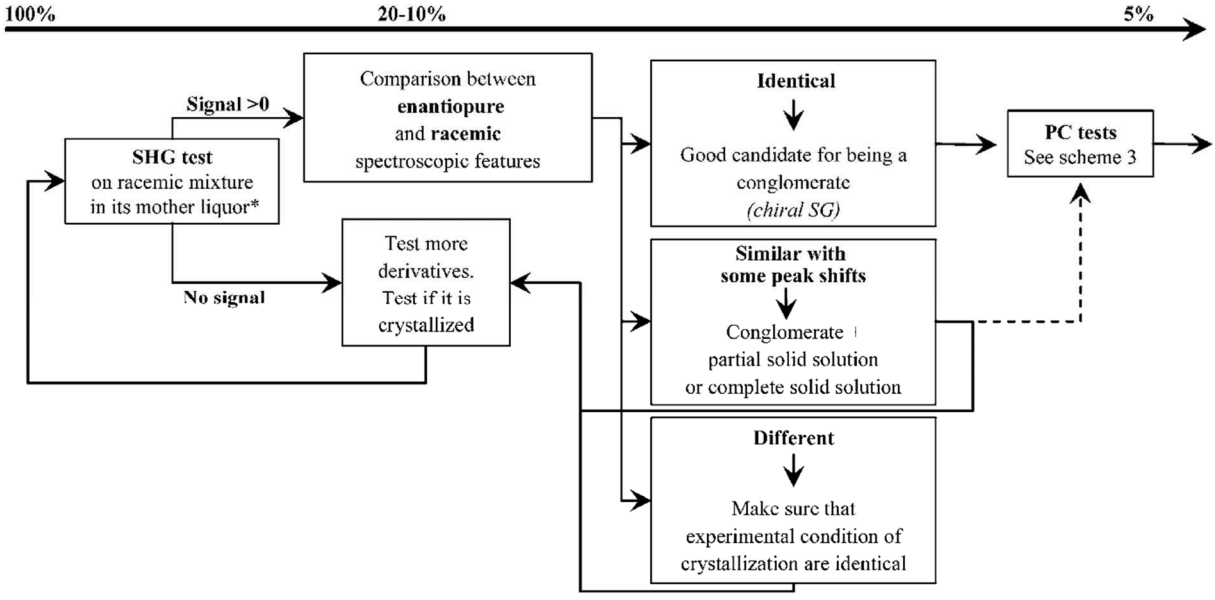

Figure 7. Workflow to spot a conglomerate proposed by Gonella & al. [24]

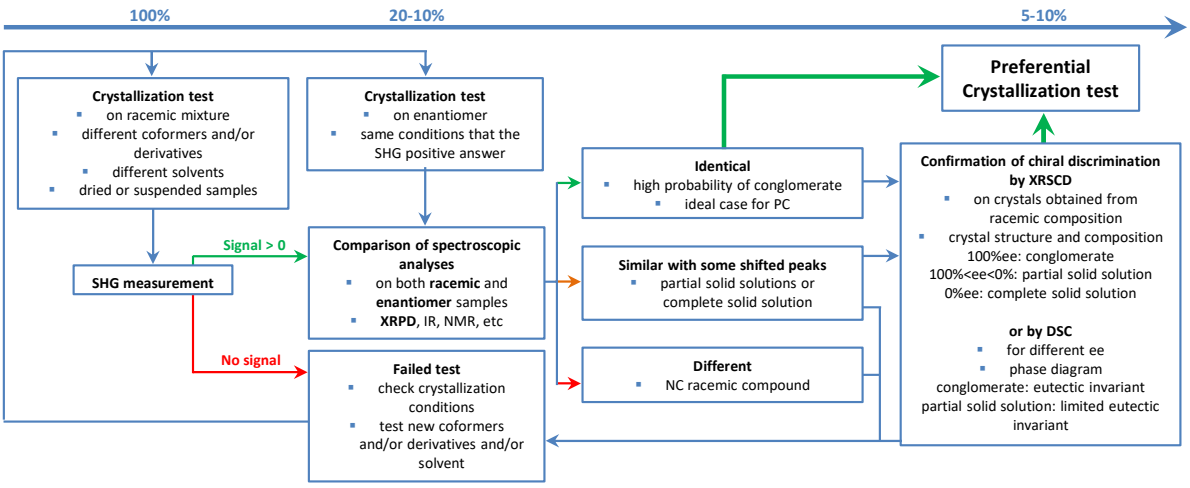

Figure 8. Modified workflow to spot a conglomerate.

- Crystallization test: tests of crystallization of racemic derivatives or racemic "cocrystals" (salt, solvate or cocrystal) are performed in different solvents. Preferably, both "dried" and "in suspension" samples should be analyzed. The higher the number of candidates (derivatives, cocrystals and solvents), the higher the chance to spot conglomerate(s).
- *Second Harmonic Generation* (SHG) prescreening:[25,26] SHG is a nonlinear optic process permitting to differentiate non-centrosymmetric (SHG positive) and centrosymmetric (SHG negative) materials. Conglomerates are necessarily SHG positive whereas the vast majority of the racemic compounds are SHG negative because of their centrosymmetric space groups. However, SHG cannot be used to differentiate between conglomerates and non-centrosymmetric racemic compounds (e.g kryptoracemates). If SHG alone is not sufficient to spot conglomerate(s), this prescreening serves to eliminate a majority of candidates and presents the advantage to be a faster (4s for each candidate) and a cheaper method (only racemic mixtures, generally cheaper than enantiopure, are necessarily).
- *X-ray powder diffraction* (XRPD): as soon that a suitable candidate has been detected by SHG, differentiation between conglomerate and racemic compound systems are performed by comparing their spectroscopic properties. Basically, diffractograms between enantiopure and racemic compositions obtained under the same conditions are compared. In case of a conglomerate, a perfect match is expected, whereas diffractograms of racemic compound forming system would be different. Shifts on the peak positions can be indicative of a complete solid solution or of mirror image partial solid solutions. The later presents the chiral discrimination necessary for PC, even if it is less suitable than a conglomerate. If

other solid state spectroscopic analyses can be performed (IR, NMR, etc) the use of XRPD would give the most accurate results.

- *X-ray single crystal diffraction*: this last verification can be concomitant with first PC tests once suitable system(s) has(ve) been highlighted. Single crystals are grown from racemic mixtures and then analyzed by XRD. Besides the determination of the crystal structure (space group, cell parameters, etc), this analysis would also provide the information on the composition of the single crystal. Helpful information such as the ratio between the API and coformer(s) but most important of all, the actual composition between the two enantiomers. In the case of conglomerate, only one enantiomer would be present. Racemic compound and complete solid solution systems would present racemic single crystals. For mirror image partial solid solution, both enantiomer would be present but in different proportions. In fact, compositions of single crystals would be the miscibility limits at the temperature of the crystal growth.

II.2 Screen of baclofen conglomerate

The screen of conglomerate on which this study is based has been performed by Dr. Julien Mahieux. Both carboxylic acid and amine functions are present in baclofen molecule ($pKa_1 = 3.87$ and $pKa_2 = 9.62$ respectively[27]). Thus, the screen has been performed by cocrystallization of baclofen with different acids and bases to form a salt (in 1:1 stoichiometry). The advantage of a salt conglomerate is twice: the ionic bond would favor a good crystallinity of the salt and the return to the free API is normally possible by a simple salting out.

More than one hundred different acids, bases and alkaline metals (Table 1) have been tested. Four different solvents (water, acetone, methanol and ethanol) have been used and analyses have been performed in suspension and on dried samples.

Table 1. List of tested partners. Four kinds of samples have been encountered: ***Bolded partners*** *are the new phases detected by XRPD but SHG negative. Underlined partners are SHG positive but patterns are juxtaposition of the initial components.* ***Underlined and bolded partners*** *have both SHG positive answers and new XRD patterns. Otherwise, tested partners did not give any SHG positive answer nor any new XRD pattern.*

Hydrochloric acid	Perchloric acid	Hydrobromic acid
Sebacic acid	Sulfuric acid	Sulfamic acid
Nitric acid	Citric acid	Adipic acid
Glutaric acid	Citraconic acid	Fumaric acid
Oxalic acid	Malonic acid	**Maleic acid**
Stearic acid	Succinic acid	Mucic acid

Itaconic acid	cis,cis-muconic acid	Subaric acid
Uric acid	Boric acid	Hydroiodic acid
Cholic acid	**Glycolic acid**	Isophtalic acid
Pimelic acid	Methylsulfamic acid	**1-hydroxy-2-naphtoic acid**
2-tetrahydrofuoric acid	Acetic acid	**Chloroacetic acid**
Bromoacetic acid	Iodoacetic acid	**Methoxyacetic acid**
p-tolylacetic acid	Dichloroacetic acid	**1,2-phenylenediacetic acid**
Trifluoroacetic acid	**Trichloroacetic acid**	3-nitrobenzoic acid
4-nitrobenzoic acid	4-hydroxybenzoic acid	2,4-dihydroxybenzoic acid
2,5-dichlorobenzoic acid	2,5-dinitrobenzoic acid	3,4-dichlorobenzoic acid
3,4-dinitrobenzoic acid	**3,5-dinitrobenzoic acid**	2-chloro-4-nitrobenzoic acid
3-methyl-4-nitrobenzoic acid	3-methoxy-4-nitrobenzoic acid	3-fluoro-4-nitrobenzoic acid
3-bromo-4-nitrobenzoic acid	3-bromo-5-nitrobenzoic acid	4-methyl-3-nitrobenzoic acid
3-nitro-5-(triluoromethyl)benzoic acid	4-fluoro-3-nitrobenzoic acid	4-chloro-3-nitrobenzoic acid
5-chloro-2-nitrobenzoic acid	2-methyl-3,5-dinitrobenzoic acid	2-chloro-3,5-dinitrobenzoic acid
4-chloro-3,5-dinitrobenzoic acid	**Methanesulfonic acid**	Ethanesulfonic acid
1-propansulfonic acid	**Benzenesulfonic acid**	4-hydroxybenzenesulfonic acid
4-chlorobenzenesulfonic acid	4-nitrobenzenesulfonic acid	1-naphtalene-sulfonic acid
3-pyridinesulfonic acid	**1H-benzimidazol-2-sulfonic acid**	2,4-diaminobenzenesulfonic acid
2,5-diaminobenzenesulfonic acid	Trifluoromethanesulfonic acid	**p-toluenesulfonic acid monohydrated**
3,5-diamino-2,4,6-trimethylbenzenesulfonic acid	Propionic acid	Butyl-éthyl-hydroxy-propionic acid
n-butyric acid	2-phenylbutyric acid	3-phenylbutyric acid
Undecanedioic acid	Dodecanedioic acid	Tetradecanedioic acid
o-toluic acid	3,5-dinitro-4-toluic acid	Phosphoric acid
Pyrophosphoric acid	Salicylic acid	3,5-dinitrosalicylic acid
Hydrocinnamic acid	Trans-cinnamic acid	Trans-3,4-dimethoxycinnamic acid
Methanesulfamic acid	Tetrafluroboric acid	Ethanolamine
Benzylamine	Diphenylamine	n-butylamine
Ethylenediamine	Tert-butylamine	Hexamethylenetetramine
Tetrahydrofurfurylamine	N,N'-dibenzylethylenediamine	Triethanolamine
Ammoniac	Sodium hydroxide	Potassium hydroxide
Calcium hydroxide	Magnesium hydroxide	Aluminum hydroxide
Strontium hydroxide	Lithium hydroxide monohydrated	Rubidium formiate hydrated

Table 1 collects crystallization partners tested. Among the 49 SHG positive tests, comparison between diffractograms of racemic and enantiopure cocrystals highlighted that only the cocrystallization of baclofen with the maleic acid formed a "conglomerate" (Figure 9) in the four different solvents tested.

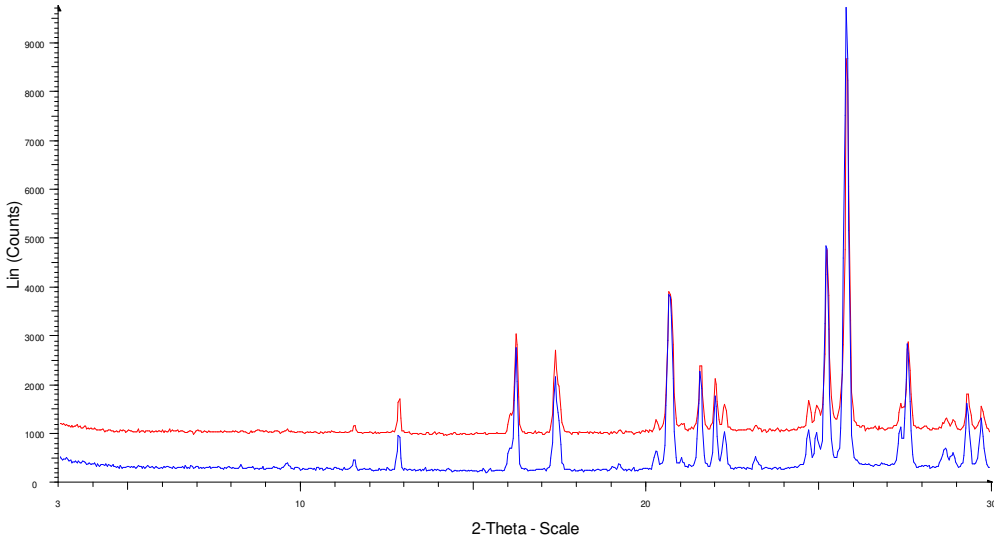

Figure 9. Diffractograms of racemic (red) and enantiopure (blue) baclofen/maleic acid "cocrystal".

The low occurrence of "conglomerate" for this system (only 1 over 117 tested partners) seems an unusual behavior. Actually, only twenty new phases have been highlighted (Table 1), twelve seem to be centrosymmetric racemic compounds (SHG negative), seven non-centrosymmetric racemic compounds (SHG positive) and only one a "conglomerate". So, the only conglomerate detected has to be compared with the limited occurrence of crystallized mixtures, i.e $^{1}/_{20}$.

Part.II Baclofen/maleic acid system

The use of maleic acid (Figure 10) in this process presents different advantages. Beside the chiral discrimination that the cocrystal between baclofen and maleic acid provides, maleic acid is rather cheap[28] and is pharmaceutically acceptable.[29]

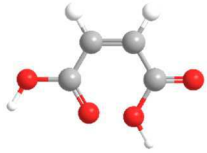

Figure 10. Maleic acid molecule.

Various solvents can be used to form this “conglomerate” (water, alcohols, acetone, diethyl ether, dichloromethane, ethyl acetate, acetonitrile, mixture of them, etc). In other words, no solvate has been spotted for that salt. In the following, crystallization of racemic and enantiopure composition of the salt have been carried out by evaporation at room temperature of a suspension in acetone. Several solvents gave rise to single crystals, especially water and the water/propan-1-ol azeotropic mixture.

I Structure

Single crystals suitable for crystal structure determination by X-ray diffraction analyses were crystallized by slow evaporation of solutions. It is interesting to observe that some crystals present hemihedral faces (Figure 11).

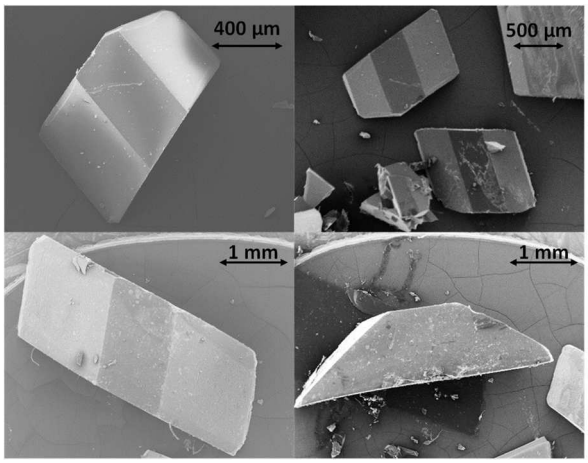

Figure 11. SEM pictures of Baclofen hydrogenomaleate. Top left and bottom left present crystal of opposite hemihedral faces.

The resolution data for one single crystal obtained at 20°C from a racemic solution (Figure 12) are presented below (Table 2). Interestingly, the single crystals display a total reflexion for certain faces.

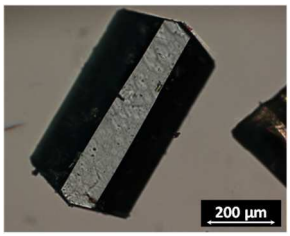

Figure 12. Optical microscopic view of a 20°C single crystal obtained from racemic solution.

Table 2. Crystal data of the baclofen hydrogenomaleate.

Empirical formula	$C_{10}H_{13}ClNO_2^+, C_4H_3O_4^-$
Formula weight	329.73 $g.mol^{-1}$
Temperature	*293.15 K*
Crystal system	*Monoclinic*
Space group	$P2_1$ ($n°4$)
Z, Z'	2, 1
a/Å	5.728 (1)
b/Å	13.774 (1)
c/Å	9.618 (9)
α/°	90
β/°	106.628 (1)
γ/°	90
Volume/Å^3	727.2 (2)
Final R_1 ($I > 2\sigma(I)$)	0.0287
Final $wR(F^2)$ ($I > 2\sigma(I)$)	0.0812
Final R_1	0.0294
Final $wR(F^2)$	0.0817
Flack parameter	$-0.02(5)$
$R_1 = \Sigma (\|\|F_O\|-\|F_C\|\|) / \Sigma \|F_O\|$ $wR_2 = [\ \Sigma [\ w (F_O^2 - F_C^2)^2] / \Sigma [\ w (F_O^2)^2\ ]\ ]^{1/2}$	

The asymmetric unit is represented in Figure 13 and is composed of a single molecule of baclofen with the protonated amine (ammonium) and of one deprotonated maleic acid molecule (hydrogenomaleate). Thus, the baclofen hydrogenomaleate salt has been formed and would be noted BaHMa hereafter.

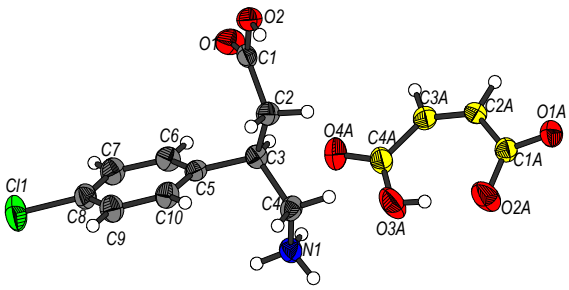

Figure 13. Asymmetric unit of baclofen hydrogenomaleate (atoms are represented by their anisotropic movement).

One can observe an intramolecular bond between the two carboxylic functions of the hydrogenomaleate (one of this function being unprotonated). These intramolecular bonds do not largely impact the cohesion. Intermolecular hydrogen bonds ensure the cohesion inside the crystalline structure. They are strong (d<2Å) hydrogen bonds (Table 3 & Figure 14) and exist

between baclofen cations and maleate anions: the ammonium group of baclofen is involved in two hydrogen bonds with two different maleate anions (Figure 14-pink) and its carboxylic acid moiety with a third hydrogenomaleate (Figure 14-blue).

Table 3. Strong hydrogen bonds data in baclofen hydrogenomaleate crystalline structure.

D-H...A	d(D-H) en Å	d(H...A) Å	d(D...A) Å
Intramolecular (yellow)			
O(3A)-H(3A1)...O(2A)	0.82	1.59	2.40 (2)
intermolecular			
N(1)-H(1A)...O(1A)#1 (pink)	0.89	2.07	2.87 (2)
N(1)-H(1B)...O(4A)#2 (pink)	0.89	2.04	2.84 (2)
O(2)-H(2)...O(1A)#3 (blue)	0.82	1.83	2.64 (2)

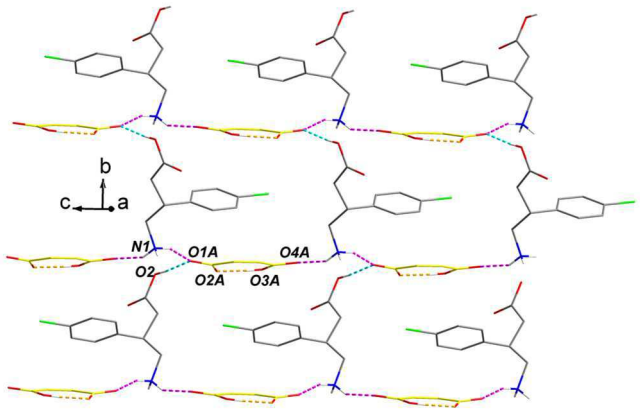

Figure 14. Strong hydrogen bonds scheme. Hydrogenomaleate intramolecular hydrogen bonds are represented in yellow. Intermolecular hydrogen bonds involving the ammonium functions of baclofen are represented in pink whereas those involving only carboxylic functions are in blue.

This network of strong hydrogen bonds leads to the formation of corrugated sheets perpendicular to ***a*** axis (Figure 15). Weak hydrogen bonds (d~2.5Å) exist between those pleated sheets (Figure 15-right)

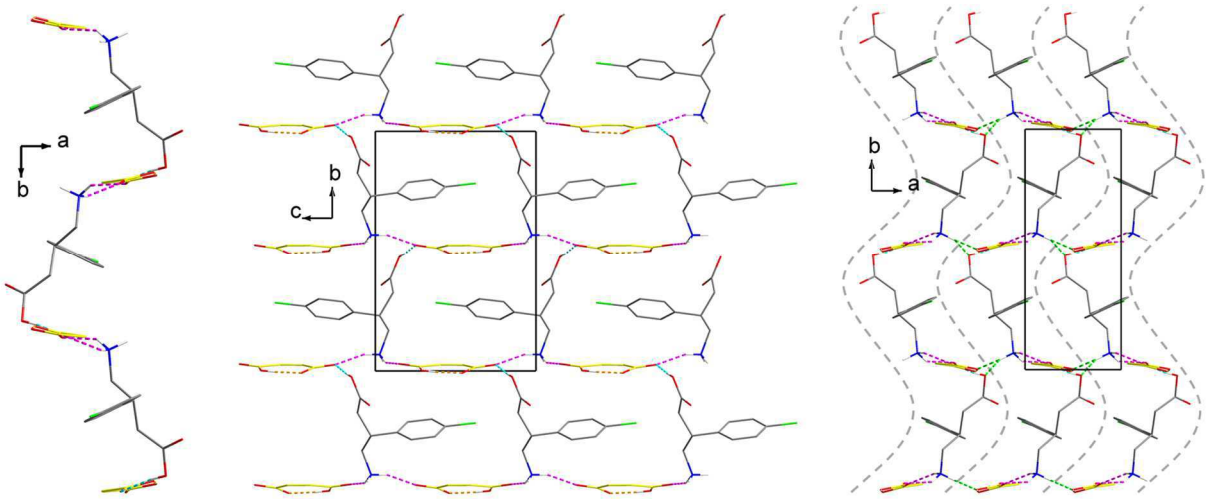

Figure 15. (a) Side (left) and planar (middle) views of a corrugated sheet and corrugated sheets juxtaposition (right) (weak hydrogen bonds are represented in green).

As illustrated in Figure 16, both calculated and experimental diffractograms match together.

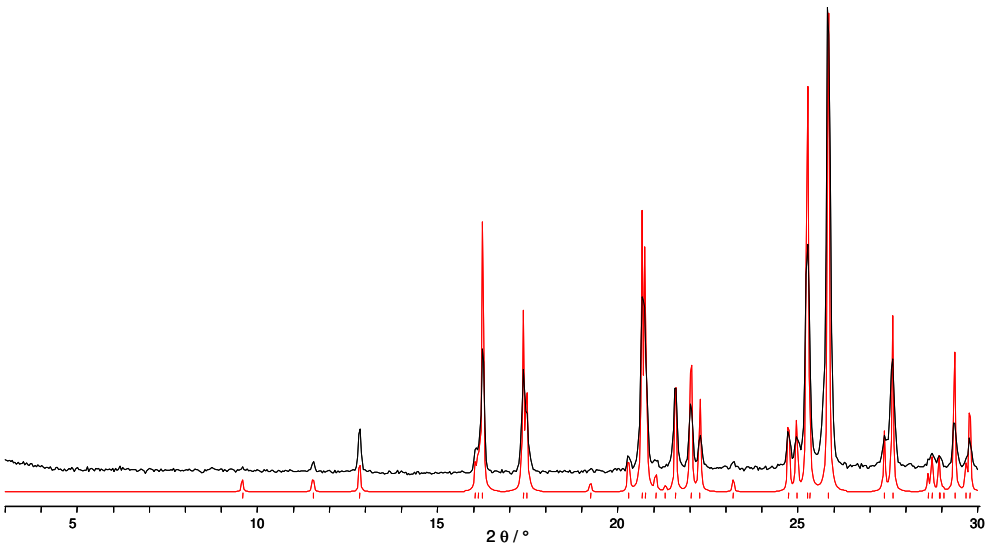

Figure 16. Calculated (red) and experimental (black) diffractogram of BaHMa salt.

In the frame of this work, in addition to single crystals obtained from enantiopure composition, single crystals grown from racemic mixture at different temperature were particularly of interest. Here below are compared the crystallographic data of single crystals grown from racemic composition at 20°C, 50°C and 70°C (Figure 17) in the azeotrope water/propan-1-ol.

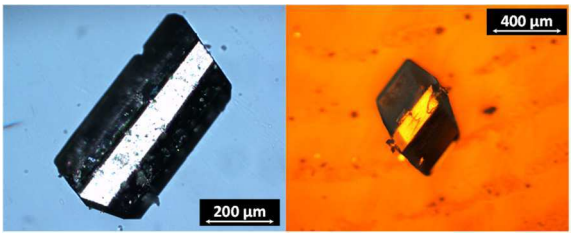

Figure 17. 50°C (left) and 70°C (right) single crystals obtained from racemic solution.

Table 4. Crystallographic data for single crystal grown at 20°C, 50°C and 70°C.

	20°C single crystal	*50°C single crystal*	*70°C single crystal*
Empirical formula	$C_{10}H_{13}ClNO_2^+, C_4H_3O_4^-$	$C_{10}H_{13}ClNO_2^+, C_4H_3O_4^-$	$C_{10}H_{13}ClNO_2^+, C_4H_3O_4^-$
Formula weight	329.73 $g.mol^{-1}$	329.73 $g.mol^{-1}$	329.73 $g.mol^{-1}$
Temperature	*293.15 K*	*293.15 K*	*293.15 K*
Crystal system	*Monoclinic*	*Monoclinic*	*Monoclinic*
Space group	$P2_1$ (n°4)	$P2_1$ (n°4)	$P2_1$ (n°4)
Z, Z'	2, 1	2, 1	2, 1
a/Å	5.728 (1)	5.7359 (6)	5.7360 (6)
b/Å	13.774 (1)	13.793 (15)	13.7855 (15)
c/Å	9.618 (9)	9.622 (10)	9.6252 (10)
α/°	90	90	90
β/°	106.628 (1)	106.600 (2)	106.667 (2)
γ/°	90	90	90
Volume/Å^3	727.2 (2)	729.56 (13)	729.12 (13)
Final R_1 (I > 2σ(I))	0.0287	0.0305	0.0299
Final $wR(F^2)$ ($I > 2\sigma(I)$)	0.0812	0.0776	0.0830
Final R_1	0.0294	0.0308	0.0302
Final $wR(F^2)$	0.0817	0.0779	0.0834
Flack parameter	−0.02 (5)	0.01 (5)	0.05 (5)
$R_1 = \Sigma (\|\|F_O\|-\|F_C\|\|) / \Sigma \|F_O\|$ $wR_2 = [\ \Sigma [\ w (F_O^2 - F_C^2)^2\ ] / \Sigma [\ w (F_O^2)^2\ ]\ ]^{1/2}$			

The lack of disorder and the low value of Flack parameter together point out a quasi-total chiral discrimination of the baclofen hydrogenomaleate single crystals. This feature seems to be valid for temperatures at least below 70°C.

This information is important since, despite the thermodynamic behavior of this system (a high temperature complete solid solution), application of preferential crystallization makes sense for temperatures inferior to 70°C.

II Chemical stability

On heating, maleic acid loses a water molecule to form the maleic anhydride (Figure 18) as does baclofen through the formation of its lactam[27] (Figure 19).

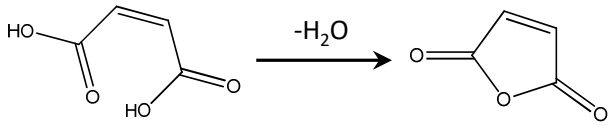

Figure 18. Maleic acid degradation in its anhydride form.

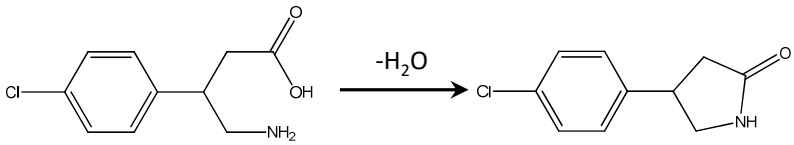

Figure 19. Baclofen degradation in its Lactam.

Logically, baclofen hydrogenomaleate salt also undergoes degradation concomitant with its melting (Figure 20).

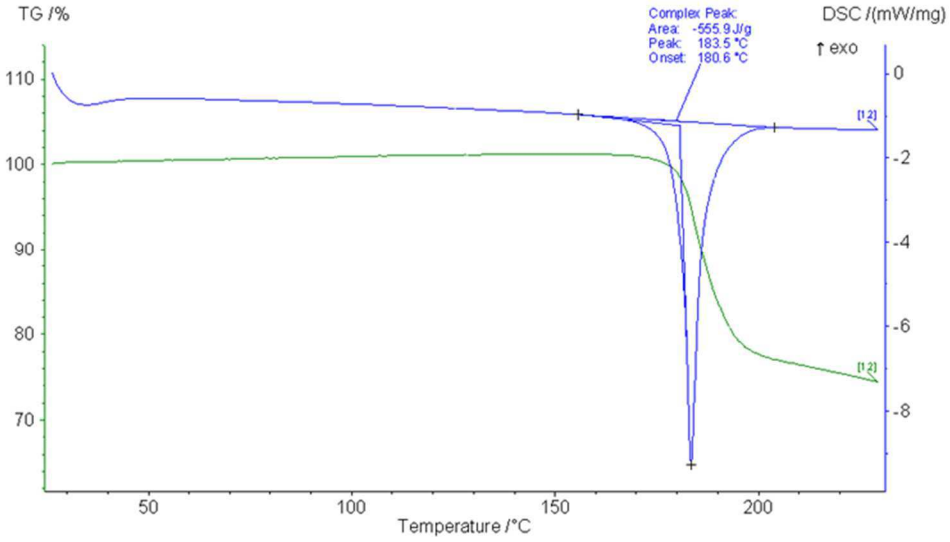

Figure 20. TG-DSC-MS analysis of enantiopure BaHMa. Water departure has been registered concomitantly to mass loss by the MS.

As presented in the next part, the behavior upon heating of the BaHMa salt is totally unusual. In order to correctly describe the heterogeneous equilibria, we needed first to clarify if the degradation occurred after or before the fusion.

In the first hypothesis, thermal events observed on DSC are the melting of the sample which precede the degradation. It corresponds to the thermodynamic heterogeneous equilibrium and can be used to further characterize BaHMa system (invariant phenomenon, solidus shape, etc).

The second hypothesis corresponds to a chemical reaction prior to the melting. Then, the composition of the mixture evolves and another system is obtained. The observed events do not present any interest here.

In an attempt to determine what hypothesis is valid, HS-microscopy (Hot Stage-microscopy) and solid annealings have been performed for different e.e:

- HS-microscopy (Figure 21 & 22) permitted to observe that crystals were not submitted to any degradation before their melting into a clear liquid phase. The coloration of this liquid corresponds to its degradation.
- During the annealings, degradation occurred at different time as a function of the enantiomeric excess. The lower the e.e, the more delayed this degradation (Figure 23). This behavior is opposite than the one observed during heating where the lower the e.e, the lower the thermal events.

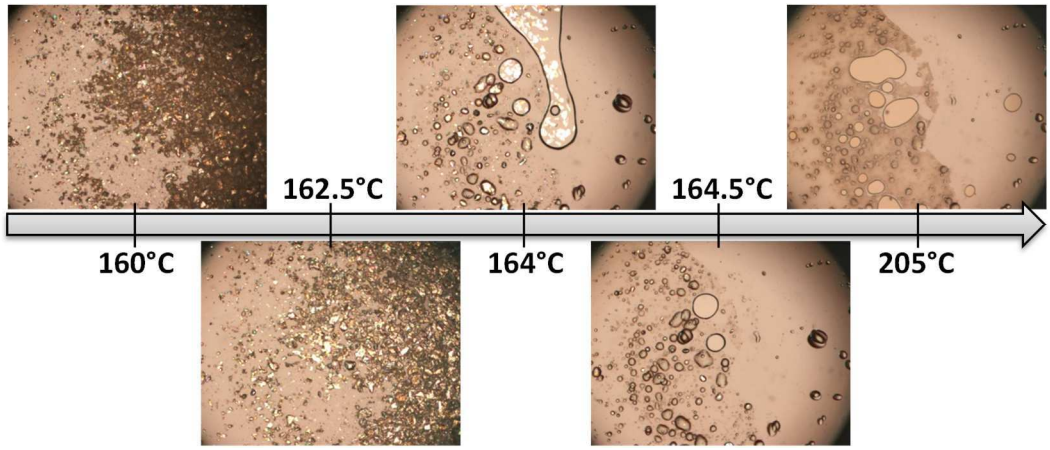

Figure 21. HS-microscopy result of racemic BaHMa heated at 5 K.min^{-1}.

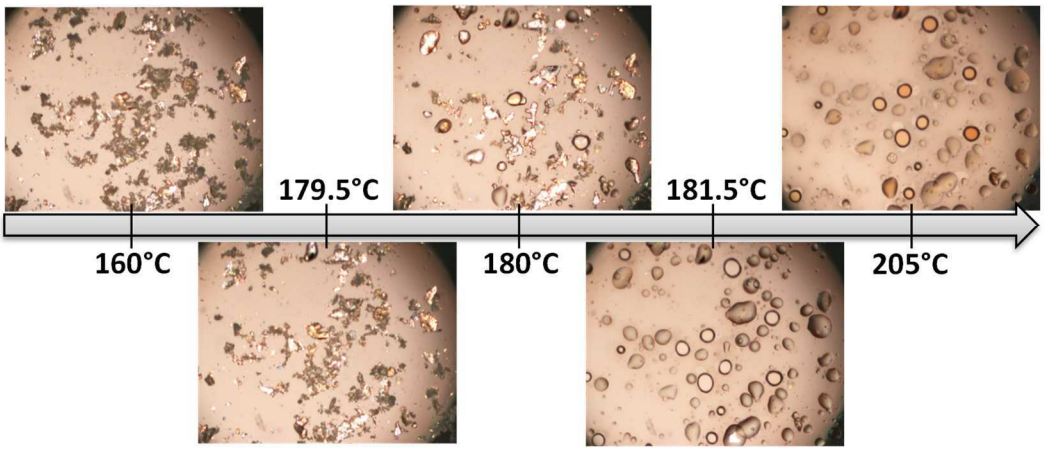

Figure 22. HS-microscopy result of enantiopure BaHMa heated at 5 K.min^{-1}.

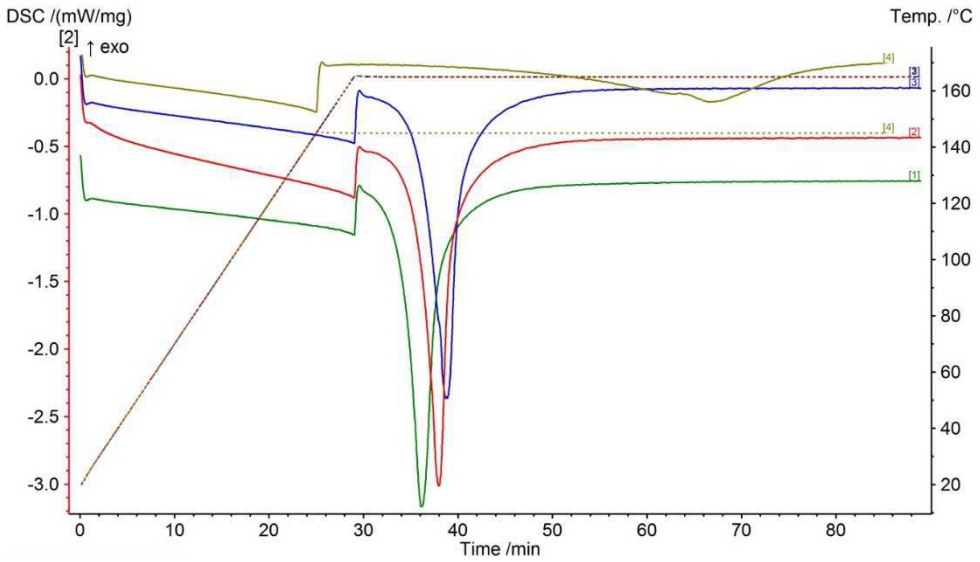

Figure 23. Annealing of different e.e samples, from top to down: racemic, 15%ee, 35%ee and 50%ee.

Thanks to those experiments, we can conclude that the BaHMa melting occurs prior to its degradation, at least when the samples have been submitted to a 5 $K.min^{-1}$ heating rate. Therefore, this system can also be characterized by its melting temperature.

Note that only the first melting event has to been considered since the concomitant degradation modifies the chemical composition. As a consequence, only the solidus curves can be investigated.

III Binary phase diagrams

III.1 Data collection

The phase diagram between the two enantiomers of BaHMa is in fact a binary isoplethal section of the ternary system between (S)-baclofen, (R)-baclofen and maleic acid. This section is characterized by the constant proportion of maleic acid ($X_{maleic\ acid} = 50\%$).

Three set of results have been useful in its determination:

- The first one is the analyses of the different single crystals indicating the quasi total chiral discrimination below 70°C.
- The most useful set of results comes from the exploitation of the DSC experiments. The DSC have been performed on different samples issued from the preferential crystallization, on both solids or evaporated solutions, whatever the entrainment was successful or not. Thus, a range covering all the possible compositions between the (R) and (S)-BaHMa has been analyzed.

  From it, one can clearly observe that the system does not present any eutectic invariant indicative of the formation of a conglomerate (Figure 24).

Instead of an invariant, the melting temperatures of samples of higher compositions than 30%e.e are similar to that of the enantiopure substance. For lower e.e, solidus temperatures quickly decrease to that of the racemic mixture. This evolution of the melting temperature pointed that the system presented a complete solid solution at high temperature.

To fit high temperature complete solid solution and the chiral discrimination below 70°C, the system must present a transition between the two discriminated phases and the total solid solution. Accurate re-exploitation of the DSC highlighted that small phenomena occur before the melting. The lower the e.e, the higher the temperature of those phenomena (Figure 25).

- The last data collected is the limit of the domain of the partial solid solution at room temperature. A single crystal grown from the racemic composition at 20°C has been redissolved and analyzed by chiral chromatography. An enantiomeric excess of +98.51%ee has been recorded.

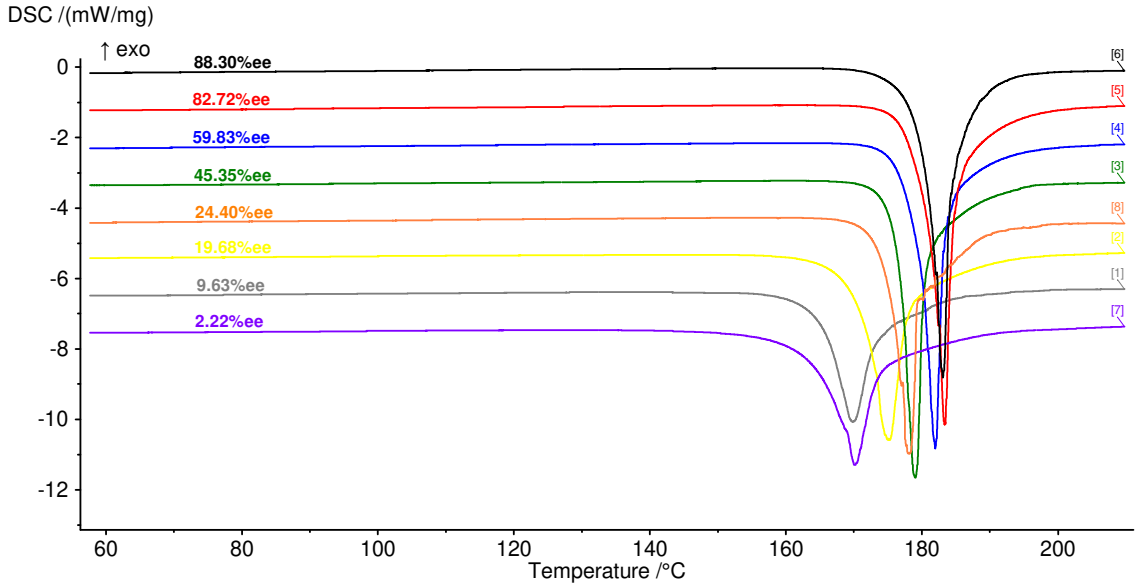

Figure 24. Thermograms of different enantiomeric excess of BaHMa.

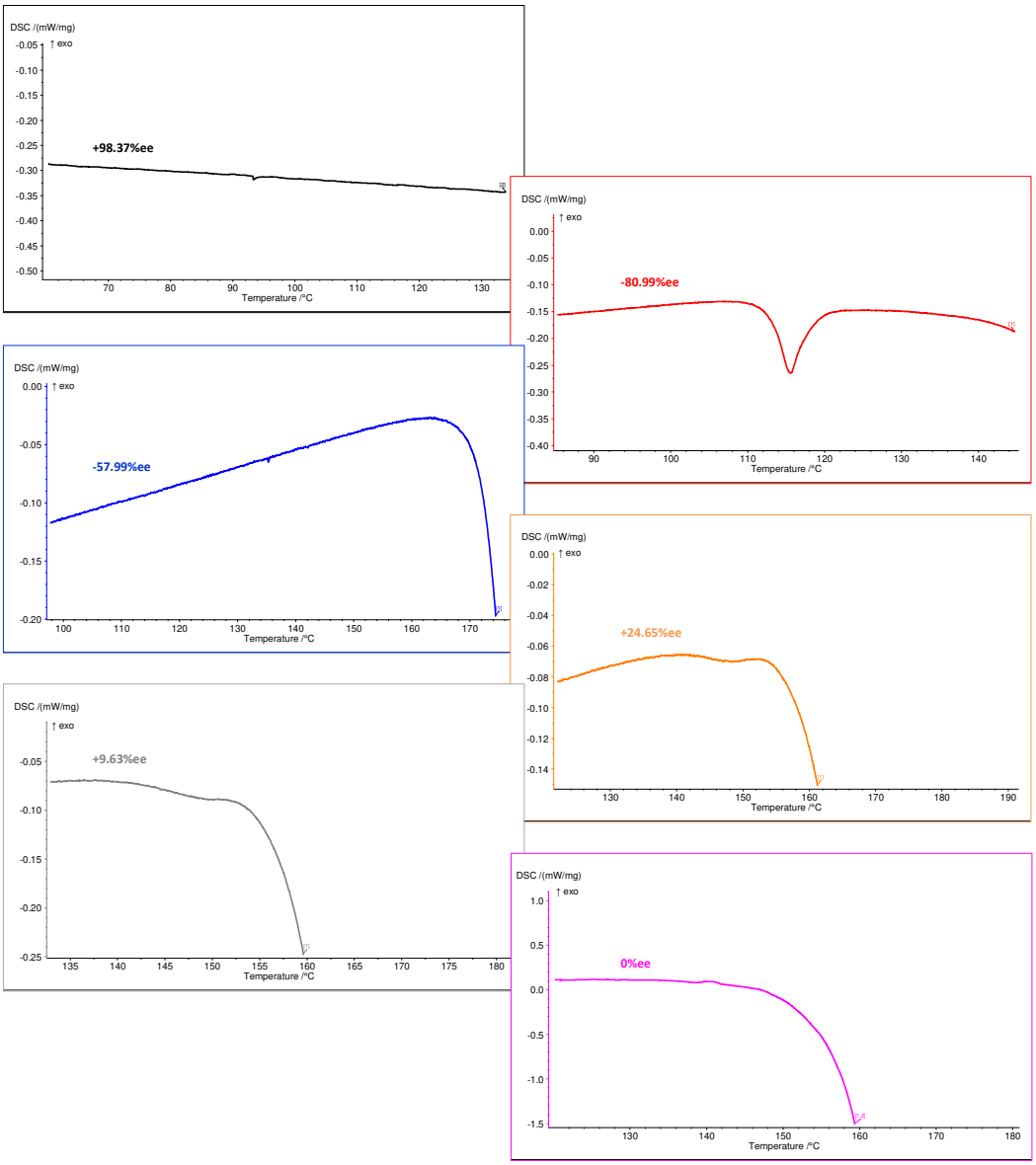

Figure 25. Magnified thermograms at different e.e showing the complete solid solution event.

Other experiments such as TR-XRPD or high temperature annealing have been performed to observe the total solid solution. Unfortunately, none of them were successful, the degradation of BaHMa put a serious limit to the time dedicated for each experiment.

III.2 Construction of the binary phase diagram

The different results have been plotted on the binary isoplethal section. Due to the symmetrical properties of chirality, data collected for a certain enantiomeric excess has been regenerated for the opposite enantiomeric excess to ease the visualization of the different limits between the domains.

The phase diagram is presented in Figure 26. Only the solidus and the demixing curves have been plotted. Without considering the missing liquidus, the phase diagram is divided in two domains (the top part, which is a degraded molten liquid, is excluded):

- Prior melting, a monophasic domain is present. It is a unique isostructural solid phase with the crystal structure previously described (SG = $P2_1$). At high temperature, the structure can incorporate both enantiomers whatever the proportion. It results in the formation of a complete solid solution (**C.S.S**) by means of substitutions of one enantiomer by the other on every crystallographic site.
- The last domain, crucial for the rest of this study, is a biphasic domain which corresponds to the demixion in the solid state of the **C.S.S** into two mirror image partial solid solutions (**ss((R)-BaHMa)** and **ss((S)-BaHMa)**). During heating, the two families of molecules diffuse to give rise to a single solid phase. From quasi totally demixed phases at room temperature, the compositions converge to the racemic composition at 145°C. This discrimination into two chiral partial solid solutions permits the application of processes usually restricted to conglomerate forming systems with eutectic invariants.

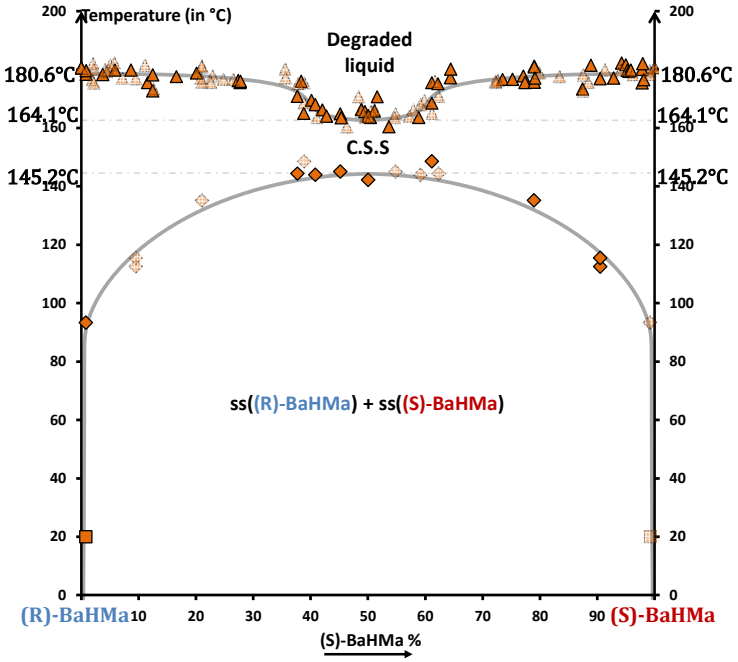

Figure 26. Binary phase diagram for the BaHMa system. Melting behavior has been deduced from DSC data (▲) and the demixion domain combining both DSC data (♦) and the redissolved single crystal composition (■). Experimental points are full and the symmetrical generated points are transparent.

Proposed by Coquerel in 2000,[30] it is the first time that a phase diagram involving a demixion of a complete solid solution of enantiomers has been experimentally observed.

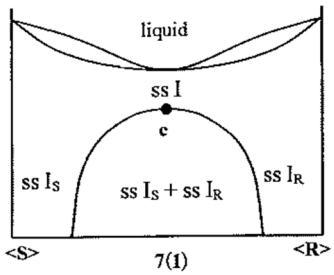

Figure 27. Miscibility gap in the solid state with a maximum critical point.[30]

Part.III Preferential Crystallization, enantiomeric purification & salting out

I Enantiomeric Excess determination

Two techniques have been used to determine the e.e of the samples.

I.1 Polarimetry

Polarimetry has been used between each preferential crystallization run to measure the enantiomeric excess of both solid and solution phases. Even though this technique is less accurate than chiral chromatography, it is much faster and provides reliable information which is essential for the compensation step.

First step was to determine the best wavelength for this system. For this purpose, enantiopure salt has been dissolved in the azeotrope water/propan-1-ol and the optical rotation of the different wavelengths have been measured:

Table 5. Optical rotation of enantiopure BaHMa in azeotrope water/propan-1-ol (22 mg.mL^{-1}) and at 25°C for the different available wavelengths.

Wavelength λ	589 nm	578 nm	546 nm	436 nm	365 nm
Optical rotation α	-0.11°	-0.08°	-0.10°	-0.19°	-0.35°

The selected wavelength for the rest of the study is 365nm since, as usual, the best optical deviation of the polarized light (-0.35°) is observed when there is not excessive adsorption.

Calibration curves for optical rotation at this wavelength and refractive index have been drawn in parallel. For more precise measurements, the refraction can be used to calculate the global composition (i.e $C = C_R + C_S$) which is then used to determine the expected optical rotation for a 100%ee sample.

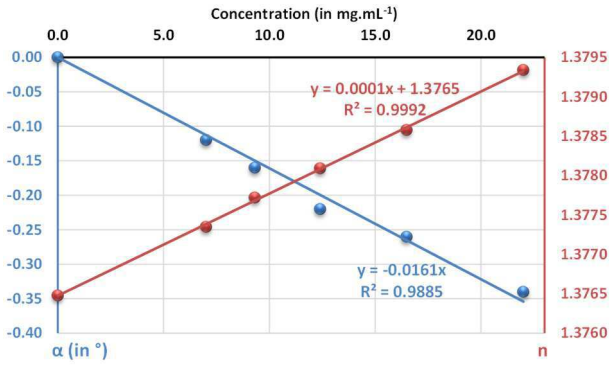

Figure 28. Calibration curves of optical rotation (blue curve) and refractive index (red curve) according to the concentration.

The specific optical rotation can be deduced from the formula:

$$\alpha = [\alpha]_{365nm}^{25°C} * l * C$$

In these conditions, i.e $t = 25°C$, $\lambda = 365nm$, $l = 1dm$ and with the azeotrope water/propan-1-ol as solvent, the specific optical rotation of baclofen hydrogenomaleate equals to $[\alpha]_{365nm}^{25°C} = 16.4°.mL.g^{-1}.dm^{-1}$.

Even if the 365nm wavelength was the best available, BaHMa had a low optical deviation compared to other chiral compounds. Thus, precise e.e determinations using this technique were not effective (as indicated by the relatively poor coefficient r^2 of the calibration curve).

I.2 Chiral chromatography

The chiral chromatography method used in this work is based on the publication of Hefnawy & Aboul-Enein[31] who developed an analytical HPLC method for the separation of the enantiomers.

The experimental conditions used here were:

- Column: Chirobiotic T (15cm*4.6mm*5µm)
- Mobile phase: isocratic mixture of methanol, water, acetic acid and triethylamine in those proportions: 98:2:0.1:0.1
- Flow rate: 1mL.min^{-1}
- Detection: UV detector set on 226nm
- Injected volume: 10µL per analysis

Those conditions combine a good separation of the enantiomers and an acceptable time for analyses (Figure 29):

$$\alpha_{S,R} = \frac{k_R}{k_S} = 1.459 \qquad \text{with} \qquad k_i = \frac{t_i - t_m}{t_m} \qquad \text{and} \qquad R = 1.18\frac{t_S - t_m}{\omega_S + \omega_R} = 2.55$$

With: - $\alpha_{S,R}$: selectivity between (S) and (R)-BaHMa peaks

- k_i: retention factor of the component i ((S) or (R)-BaHMa here)
- t_i: retention time of the component i
- t_m: hold-up time
- R: resolution factor
- ω_S: full width at half maximum

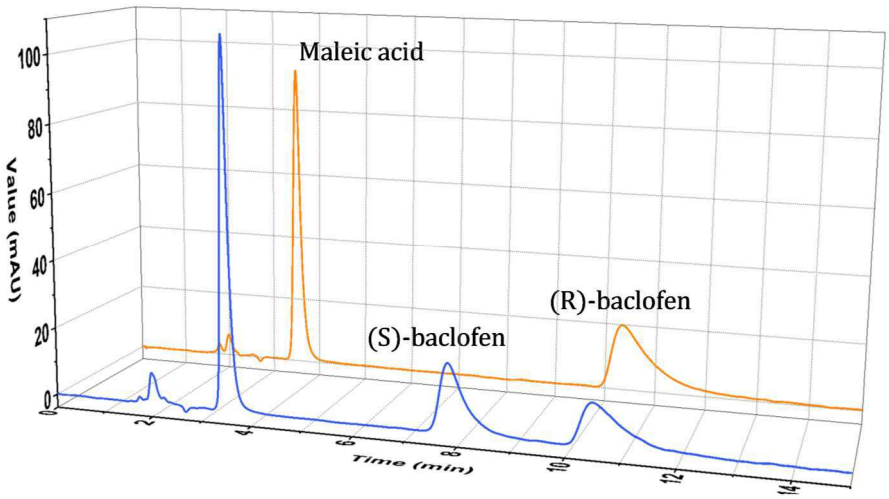

Figure 29. HPLC chromatograms of racemic BaHMa (blue) and (R)-BaHMa (orange).

II Preferential crystallization

Baclofen hydrogenomaleate salt has been spotted to be a very good candidate for chiral resolution since it has a quasi-total chiral discrimination below 70°C. The next step was to find the adequate experimental conditions for a preparative resolution by using Preferential Crystallization.

First conditions to be set were the choice of the solvent and of the PC method that would be applied.

As discussed in the first chapter, AS3PC[21,32] (Auto-Seeded Polythermal Programmed Preferential Crystallization) usually gives better results than SIPC (Seeded Isothermal Preferential Crystallization) and S3PC (Seeded Polythermal Programmed Preferential Crystallization) variants. Lack of data are available to compare with ASPreCISE[33,34] (Auto Seeded Preferential Crystallization Induced by Solvent Evaporation). First applications results

are comparable to those performed by AS3PC method. Nonetheless, the set-up to perform ASPreCISE being more constraining (vacuum, distilled solvent management, etc), AS3PC has been preferred over all other methods, and ASPreCISE was kept in mind as an alternative to unsuccessful AS3PC (unfavorable variation of solubility versus temperature and/or if chemical degradation of the chiral solute on heating exists).

For AS3PC application, the solvent must fulfill some conditions: it should not trigger chemical decomposition, it must give a good solubility at a reasonable temperature, it has to exhibit a good variation of solubility versus temperature. Moreover, no epitaxy nor undesirable racemic solvate nor any undesirable metastable equilibria should interfere in the stereoselective self-assembling process.

In addition to the screen of conglomerates, solvent and solubility screens on the BaHMa salt have been performed. Twelve different solvents and eight different hydrochloride acid concentrations have been tested. We focused our screen of solvents on mixtures of solvents, particularly azeotropes for their interesting properties. Nineteen azeotropic mixtures have been tested.

If all the "solvents" tested led to the recrystallization of the BaHMa salt from clear solution, none of them presented interesting solubility except for hydrochloride acid solutions.

II.1 Preferential Crystallization process

Once the suitable conditions have been established, cycles of preferential crystallizations have been conducted following those steps:

a. A volume V (40mL) of racemic BaHMa saturated solution (doubly saturated solution) has been prepared at $T_{dou\,sat}$. The solution has been placed in a closed cylindric tube (3cm diameter*9cm length) (the reactor) with a cross-shaped magnetic stirring bar to ensure agitation.
b. A certain mass of (R)-BaHMa corresponding to at least 2.2% of the racemic BaHMa mass has been introduced in the reactor.
c. The suspension has been heating up to a temperature $T_{initial} = T_{dou\,sat} + \Delta T$, ΔT being chosen to ensure a partial dissolution of the excess (R)-BaHMa. The system was now a light suspension of (R)-BaHMa and a (S)-BaHMa undersaturated solution (saturated in (R)-BaHMa).
d. A temperature program has been applied to the system to cool it down from $T_{initial}$ to T_{final} with a controlled cooling ramp dT/dt. With temperature decreasing, (R)-

BaHMa crystallized (the system stayed lightly supersaturated in (R)-BaHMa), and the nucleation of the (S)-BaHMa was avoided.

e. At T_{final}, the suspension has been filtrated as fast as possible. Liquid phase has been put back in the reactor and temperature set to $T_{initial}$. Meanwhile the solid has been dried, weighed (m_{crop}) and a part has been redissolved in the azeotrope water/propan-1-ol (10 mg.mL^{-1}) to determine its optical rotation (OP_{crop}). The first PC run was completed.
f. The same mass of racemic BaHMa as the mass of the crude crops has been introduced in the reactor (m_{rac}) and solvent could also be compensated to V.
g. Once the compensation was completed, $T_{initial}$ has been maintained (during t) to obtain the thermodynamic equilibrium (light suspension of (S)-BaHMa). This thermodynamic equilibrium is the opposite than the one reached in step **c**.
h. The same temperature program as that used in step **d.** has been applied. (S)-BaHMa crystallized while (R)-BaHMa remained in solution.
i. At T_{final}, the suspension has been filtrated as fast as possible. Solid has been dried, weighed (m_{crop}) and its OP_{crop} has been measured while the liquid was set to $T_{initial}$. The second run was completed.
j. The system has been compensated in racemic BaHMa and solvent to obtain a light suspension or (R)-BaHMa.
k. After t time at $T_{initial}$ temperature, the system has gone back to a thermodynamic equilibrium.
l. Steps **d.** to **k.** were repeated all over again to successively preferentially crystallize (R)-BaHMa during odd runs and (S)-BaHMa during even runs.

Prior to perform cycles of preferential crystallization, several tests must be carried out.

The protocol of the first one follows the steps **a.** to **d.** previously described. The only difference is the cooling step which is carried out on a larger temperature range. Liquid samplings are performed all along this cooling. The expected enantiomeric excess vs. time curve of the mother liquor during an effective preferential crystallization run is presented in Figure 30. First part corresponds to the preferential crystallization of the enantiomer initially in excess whose concentration decreases in solution. At a moment, when passing through a 50-50 composition, it results in the *change of the sign* of the mother liquor. The second part is the *filtration window* in which the best results can be obtained (best mass and e.e of the crop). The

third part corresponds to the return to equilibrium for the system due to the crystallization of the counter enantiomer.

Once a similar experimental curve is obtained, a validation test is performed under the same conditions but with a filtration carried out inside the filtration window. If the crop presents both good mass and e.e, preferential crystallization worked. Conditions (cooling rate, ΔT, stirring, etc) can be tuned or complete PC cycles can be tested.

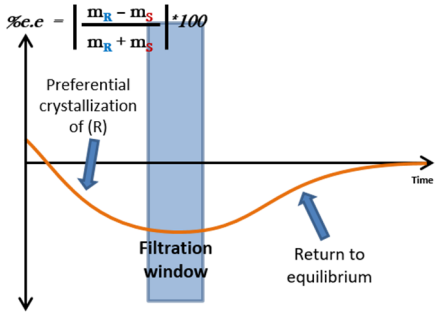

Figure 30. Enantiomeric excess over time during test run of AS3PC.

During preferential crystallization, 10µL liquid samplings have been performed to measure enantiomeric excess versus time by means of HPLC. Moreover, enantiomeric excess of the solid has been also measured by HPLC to obtain a more accurate value.

II.2 Preferential Crystallization performed in azeotrope water/propan-1-ol

II.2.1 Advantages of azeotropic mixture

First solvent in which AS3PC has been tested is the one used to prepare BaHMa salt: the azeotropic mixture between water and propan-1-ol.

Azeotrope mixtures behave as pure solvents. Indeed, they are mixtures of two or more solvents whose proportions do not changed when passed to the gas state. The use of azeotropic mixture or pure solvent is not essential to perform preferential crystallization, but azeotropes are interesting alternatives.

Indeed, the major advantage of preferential crystallization processes is the continuous recycling of the mother liquors, even more for the Auto-Seeded methods which permit fast sequence of runs. Pure solvents and azeotropes fit with this idea of “fast sequence” since the experimenter would just need to compensate with the “solvent” in case of need.

A contrario, compensation of non-azeotropic mixture could be more tricky. If necessary, the manipulator must first determine the actual composition and volume of the solution before compensation (with pure solvent(s), pH adjustment, etc).

II.2.2 First attempt of Preferential Crystallization

The choice of the azeotropic mixture between water and propan-1-ol results from different attempts to grow single crystals at different temperatures, notably from the crystal growth at 50°C and 70°C.

The ability of this "solvent" to give rise to single crystals at those temperatures illustrates the very good chiral discrimination of BaHMa enantiomers in this mixture. Of course, this ability is essential to any Preferential Crystallization application, thereby this solvent has been chosen for the first attempts to performed PC *via* the AS3PC method.

The azeotrope water/propan-1-ol is a minimum azeotrope as illustrated by the work of Murti & van Winkle[35] (Figure 31) and present properties recapped in Table 6.[36]

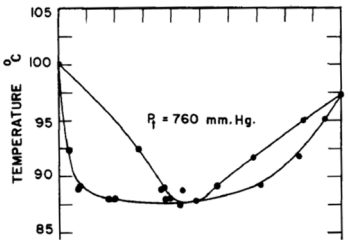

Figure 31. T-X-Y diagram for 1-propanol-water.[35]

Table 6. Data of the azeotropic mixture water/propan-1-ol.[36]

1st solvent	%mol	2nd solvent	%mol	$T_{boiling}$	Density
propan-1-ol	43.29%	water	56.71%	88.1°C	0.870g.mL^{-1} at 25°C

The solubility of the racemic BaHMa at different temperatures has been determined (Table 7). A significant variation over temperature is observed (solubility at 50°C is thrice that at 20°C). Even if the solubility seems quiet too low for of an industrial application, preferential crystallization has been tested.

Table 7. Solubility of racemic BaHMa in azeotrope water/propan-1-ol.

Temperature (in °C)	Solubility (in %mass)
20°C	1.49%
35°C	2.80%
50°C	4.81%

Conditions and results for the Test run and the Validation run are presented in Table 8 and Figure 32. A (R)-BaHMa suspension has been prepared at 51°C and the system has been cooled at 0.5 K.min^{-1}. Starting from negative, the enantiomeric excess of the solution changed of sign after 10 min before reaching a maximum at 36 min ($e.e_{max}$) and decreasing back to 0%. Filtration window has been determined to be between 30 and 40 minutes.

Validation test filtrating at 37 min demonstrates a very good e.e of the crop (-95.92%ee) for a final mass of 0.4731g. Thus, 0.4634g of (R)-BaHMa has been recovered corresponding to an increase of 67% of the seed mass.

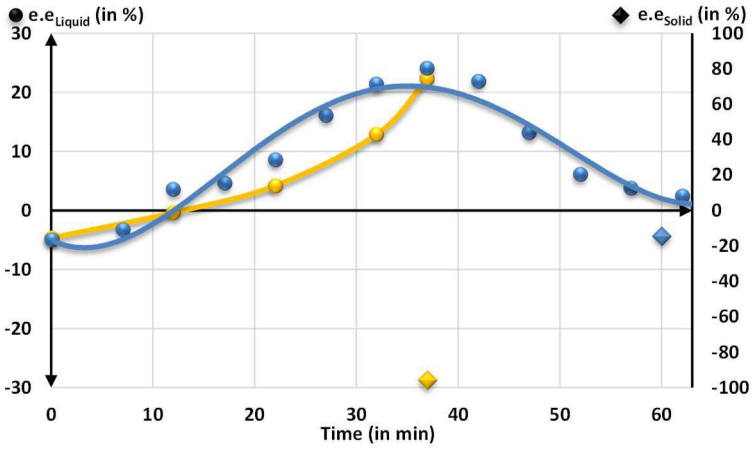

Figure 32. Enantiomeric excess of the liquid (●) and solid (♦) over time during Test run (blue) and Validation run (yellow) of AS3PC in azeotrope water/propan-1-ol.

Table 8. Result of the Test run and Validation run of AS3PC in azeotrope water/propan-1-ol. $e.e_{max}$ has been bolded.

	Parameters		Solution		Solid		
	Temperature (in °C)	Time (in min)	Mass (in g)	e.e (in %ee)	Mass (in g)	e.e (in %ee)	Enantiomer Mass (in g)
Test run	■ 40mL of doubly saturated solution at 50°C (1.7583g of racemic BaHMa in 34.796g of solvent) ■ 0.2778g of (R)-BaHMa suspended at 51°C						
	51°C	0 min		-4.98%			
	47.5°C	7 min		-3.28%			

	45°C	12 min		+3.56%			
	42.5°C	17 min		+4.64%			
	40°C	22 min		+8.58%			
	37.5°C	27 min		+16.06%			
	35°C	32 min		+21.36%			
	32.5°C	37 min		**+24.06%**			
	30°C	42 min		+21.88%			
	27.5°C	47 min		+13.14%			
	25°C	52 min		+6.10%			
	22.5°C	57 min		+3.78%			
	20°C	62 min		+2.42%	1.0543g	-14.62%	0.6042g
Validation run	▪ **40mL of doubly saturated solution at 50°C (1.7583g of racemic BaHMa in 34.796g of solvent)** ▪ **0.2775g of (R)-BaHMa suspended at 51°C**						
	51°C	0 min		-4.68%			
	45°C	12 min		-0.38%			
	40°C	22 min		+4.16%			
	35°C	32 min		+12.86%			
	32.5°C	37 min		**+22.28%**	**0.4731g**	**-95.92%**	**0.4634g**

II.2.3 Cyclisation of the PC runs

As Preferential Crystallization has been proved to be effective in this solvent, the next step was to perform cycles of PC.

The solubility being poor in this solvent, the compensation step could have been problematic. Indeed, an excessive addition of racemic BaHMa and an unnoticed partial solvent evaporation could lead to a suspension of both BaHMa enantiomers, cancelling the preferential crystallization.

To prevent this advert effect, $T_{initial}$ has been risen from 51°C to 53°C. At this temperature, the solution is no more doubly saturated: one of the BaHMa enantiomers forms a very light suspension. Nevertheless, a new test run (Figure 33) had to be performed to identify the new filtration windows (the identical cooling rate has been applied). It appeared that the $e.e_{max}$ of the mother liquor has been obtained after 46 min of cooling (30°C).

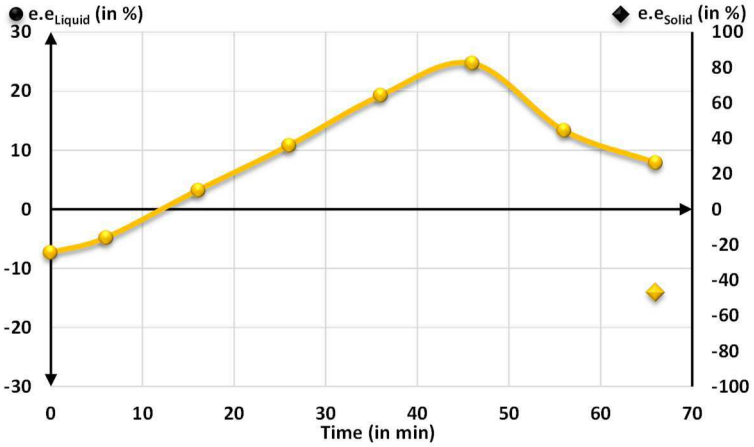

Figure 33. Enantiomeric excess of the liquid (●) and solid (♦) over time during Test run and Validation run of AS3PC in azeotrope water/propan-1-ol started from 53°C.

Table 9. Result of the Test run of AS3PC in azeotrope water/propan-1-ol started from 53°C. $e.e_{max}$ has been bolded.

	Parameters		Solution		Solid		
	Temperature (in °C)	Time (in min)	Mass (in g)	e.e (in %ee)	Mass (in g)	e.e (in %ee)	Enantiomer Mass (in g)
Test run	■ 40mL of doubly saturated solution at 50°C (1.7583g of racemic BaHMa in 34.796g of solvent) ■ 0.2574g of (R)-BaHMa suspended at 53°C						
	53°C	0 min		-7.33%			
	50°C	6 min		-4.81%			
	45°C	16 min		+3.19%			
	40°C	26 min		+10.81%			
	35°C	36 min		+19.27%			
	30°C	46 min		**+24.73%**			
	25°C	56 min		+13.35%			
	20°C	66 min		+7.90%	0.9650g	-46.98%	0.7092g

In Figure 34 and Table 10 are summarized the results of a six-consecutive PC runs (three-consecutive cycles). These cycles permitted to obtain information concerning the equilibration time between each run and about the compensation in racemic BaHMa and solvent.

Each run was successful: the liquid phases changed of sign and the solids were highly enriched. The first run resulted in 0.6682g of crop at -91.08%ee corresponding to an augmentation of 155% of the initial seed mass.

The equilibration time between each run has been gradually decreased from 4h to 30min. Indeed, 30min of equilibration appeared sufficient to produce a suspension of a single enantiomer.

Too much solvent added during compensation led to a decrease of the mass of the crops like for Runs 3 & 4. By the way, the system could be sent back to a more effective state by either stopping the compensation in solvent or by compensating with a bigger mass of racemic BaHMa (e.g Run 5).

This cyclisation also highlighted the need for a fast e.e analysis method to control the enantiopurity of the crop: unusual low value should lead to a partial compensation of the mass collected or to a higher compensation of solvent.

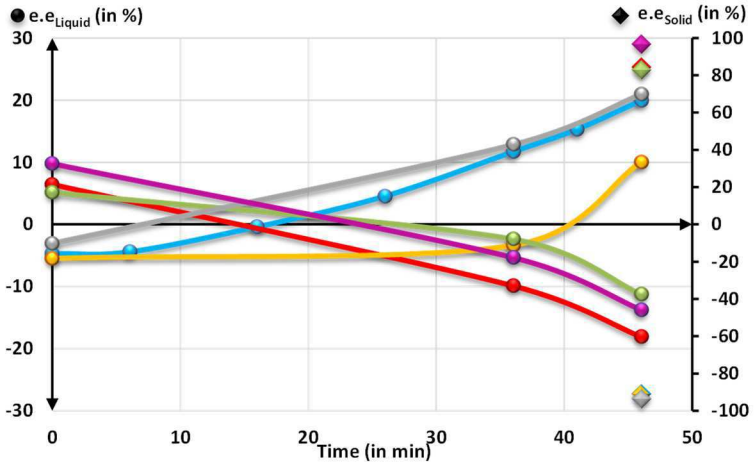

Figure 34. Enantiomeric excess of the liquid (●) and solid (♦) over time during PC runs: Run 1 (blue), Run 2 (red), Run 3 (yellow), Run 4 (green), Run 5 (grey) and Run 6 (violet).

Table 10. Results of consecutive runs of AS3PC in azeotrope water/propan-1-ol with decreasing time of equilibration between each run. $e.e_{max}$ has been bolded.

	Parameters		Solution		Solid		
	Temperature (in °C)	Time (in min)	Mass (in g)	e.e (in %ee)	Mass (in g)	e.e (in %ee)	Enantiomer Mass (in g)
Initial state	■ 40mL of doubly saturated solution at 50°C (1.7583g of racemic BaHMa in 34.796g of solvent) ■ 0.2505g of (R)-BaHMa suspended at 53°C						
Run 1	53°C	0 min		-4.71%			
	50°C	6 min		-4.44%			
	45°C	16 min		-0.40%			
	40°C	26 min		+4.54%			
	35°C	36 min		+11.69%			
	32.5°C	41 min		+15.30%			
	30°C	46 min		**+19.92%**	**0.6682g**	**-91.08%**	**0.6383g**
Compensation	■ 0.6895g of racemic BaHMa and 2mL of solvent ■ 4H at 53°C						
Run 2	53°C	0 min		+6.43%			
	35°C	36 min		-9.89%			

	30°C	46 min		-18.08%	0.6587g	+84.29%	0.6070g
Compensation	■ 0.6718g of racemic BaHMa and 2mL of solvent ■ 12H at 53°C						
Run 3	53°C	0 min		-5.47%			
	35°C	36 min		-3.37%			
	30°C	46 min		+10.02%	0.4971g	-91.03%	0.4748g
Compensation	■ 0.4955g of racemic BaHMa and 2mL of solvent ■ 2H at 53°C						
Run 4	53°C	0 min		+5.14%			
	35°C	36 min		-2.38%			
	30°C	46 min		-11.27%	0.4156g	+82.72%	0.3797g
Compensation	■ 0.4153g of racemic BaHMa ■ 1H at 53°C						
Run 5	53°C	0 min		-3.07%			
	35°C	36 min		+12.84%			
	30°C	46 min		+20.93%	0.5608g	-93.78%	0.5434g
Compensation	■ 0.5550g of racemic BaHMa and 1.5mL of solvent ■ 30min at 53°C						
Run 6	53°C	0 min		+9.76%			
	35°C	36 min		-5.35%			
	30°C	46 min		-13.76%	0.5339g	+96.59%	0.5248g

Once a certain level of control has been found (concerning the compensation/equilibration step), a new set of PC cycles has been performed with 30min between each run.

The results of the different runs are presented in Figure 35 and Table 11. Ten consecutive successful runs have been performed.

In Runs 4, 5 & 6 the masses collected were higher than previous runs. Despite their good optical purity, the entire masses have not been compensated. The reason was the high uncertainty of polarimetry for this system and the unusual mass filtrated.

Nonetheless, it is known that the mass of the crops increases after few PC runs. As chiral chromatography analyses confirmed the good enantiomeric excess, a complete compensation could be considered for future tests.

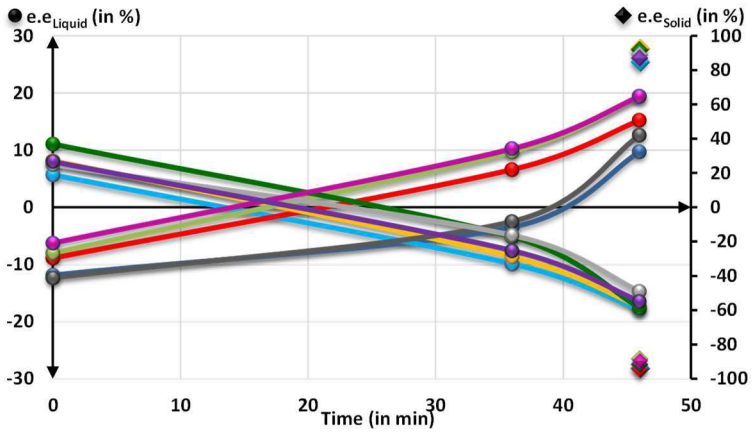

Figure 35. Enantiomeric excess of the liquid (●) and solid (♦) over time during PC runs: Run 1 (dark blue), Run 2 (light blue), Run 3 (red), Run 4 (yellow), Run 5 (light green), Run 6 (dark green), Run 7 (dark grey), Run 8 (light grey), Run 9 (light violet) and Run 10 (dark violet).

Table 11. Results of consecutive runs of AS3PC in azeotrope water/propan-1-ol. $e.e_{max}$ has been bolded.

	Parameters		Solution		Solid		
	Temperature (in °C)	Time (in min)	Mass (in g)	e.e (in %ee)	Mass (in g)	e.e (in %ee)	Enantiomer Mass (in g)
Initial state	■ 40mL of doubly saturated solution at 50°C (1.7583g of racemic BaHMa in 34.796g of solvent) ■ 0.2445g of (R)-BaHMa suspended at 53°C						
Run 1	53°C	0 min		-11.88%			
	35°C	36 min		-3.47%			
	30°C	46 min		**+9.75%**	**0.5012g**	**-94.04%**	**0.4862g**
Compensation	■ 0.5120g of racemic BaHMa and 1.2mL of solvent ■ 30min at 53°C						
Run 2	53°C	0 min		+5.70%			
	35°C	36 min		-9.90%			
	30°C	46 min		**-17.87%**	**0.4679g**	**+84.61%**	**0.4319g**
Compensation	■ 0.4621g of racemic BaHMa and 1mL of solvent ■ 30min at 53°C						
Run 3	53°C	0 min		-8.86%			
	35°C	36 min		+6.62%			
	30°C	46 min		**+15.26%**	**0.5496g**	**-95.07%**	**0.5361g**
Compensation	■ 0.5469g of racemic BaHMa and 2mL of solvent ■ 30min at 53°C						
Run 4	53°C	0 min		+8.16%			
	35°C	36 min		-8.64%			
	30°C	46 min		**-17.34%**	**0.6465g**	**+92.52%**	**0.6223g**
Compensation	■ 0.5122g of racemic BaHMa						

	■ 30min at 53°C						
Run 5	53°C	0 min		-8.02%			
	35°C	36 min		+9.69%			
	30°C	46 min		**+19.47%**	**0.6463g**	**-88.51%**	**0.6092g**
Compensation	■ 0.5136g of racemic BaHMa and 1.5mL of solvent ■ 30min at 53°C						
Run 6	53°C	0 min		+11.09%			
	35°C	36 min		-5.15%			
	30°C	46 min		**-17.59%**	**0.6124g**	**+91.71%**	**0.5870g**
Compensation	■ 0.4975g of racemic BaHMa and 1.5mL of solvent ■ 30min at 53°C						
Run 7	53°C	0 min		-12.35%			
	35°C	36 min		-2.47%			
	30°C	46 min		**+12.65%**	**0.5378g**	**-91.71%**	**0.5155g**
Compensation	■ 0.5306g of racemic BaHMa and 1.5mL of solvent ■ 30min at 53°C						
Run 8	53°C	0 min		+7.46%			
	35°C	36 min		-4.89%			
	30°C	46 min		**-14.73%**	**0.5254g**	**+88.90%**	**0.4962g**
Compensation	■ 0.5238g of racemic BaHMa and 1.5mL of solvent ■ 30min at 53°C						
Run 9	53°C	0 min		-6.25%			
	35°C	36 min		+10.26%			
	30°C	46 min		**+19.42%**	**0.6444g**	**-89.51%**	**0.6106g**
Compensation	■ 0.5183g of racemic BaHMa and 1.5mL of solvent ■ 30min at 53°C						
Run 10	53°C	0 min		+8.00%			
	35°C	36 min		-7.59%			
	30°C	46 min		**-16.49%**	**0.7194g**	**+87.05%**	**0.6728g**

Despite the very good feasibility of the BaHMa resolution by means of the auto-seeded preferential crystallization, the solubility, and consequently the production rate, are too low for any industrial application. This production rate has been calculated dividing the total mass of pure enantiomer by the volume of the solution and the duration of the experiment. Thus, BaHMa enantiomers has been obtained with a 11.4 $g.L^{-1}.H^{-1}$ productivity.

In order to improve the productivity of this resolution, it has to be conducted in "solvents" presenting higher solubility. Among the large range of solvents tested (polar and apolar, protic and aprotic), only the acidic solutions, particularly with hydrochloride acid, have presented interesting solubility. Even if less easy to compensate after every run than the azeotrope mixtures, those "solvents" lead to a more productive preferential crystallization conducted by cooling.

II.3 Preferential Crystallization performed in water and hydrochloride solutions

Solubility of racemic BaHMa for different concentrations of hydrochloride acid (0M, 1M and 2M) and different temperatures (20°C, 35°C and 50°C) are presented in Table 12. Solubility in water (0M) is lower than that in the azeotrope but the solubility properties become more interesting when the solution is acidified:

- The more acidic the solution, the higher the solubility: At 20°C, the value of solubility in HCl 1M is six time higher than that in water. In HCl 2M, it is eight time.
- The more acidic the solution, the higher the solubility variation vs. temperature: From 20 to 50°C, solubility increases by twice in water whereas in HCl 1M it increases by almost thrice. The variation is higher than thrice and a half in HCl 2M.

Nonetheless, experiments cannot be carried out in higher concentrations of hydrochloride acid. Indeed, the use of higher concentrations could lead to the formation of the hydrochloride salt of baclofen (incongruent solubility behavior of BaHMa). Equally, higher temperatures must be avoided due to chemical degradation of BaHMa salt that would be enhanced in those conditions.

Table 12. Solubility of racemic BaHMa in water and 1M and 2M hydrochloride acid solution.

Temperature (in °C)	Solubility in water (in %mass)	Solubility in HCl 1M (in %mass)	Solubility in HCl 2M (in %mass)
20°C	0.75%	4.51%	6.48%
35°C	1.00%	6.86%	11.44%
50°C	1.78%	12.54%	22.24%

II.3.1 Preferential Crystallization in water

Even if the solubility in water are not interesting, PC has been performed in it to prove its feasibility. The conditions and the results for the Test and the Validation runs are presented in

Figure 36 and Table 13. Conditions are similar as those described earlier: the starting point is a suspension at 53°C in a 40mL vessel prepared by mixing a doubly saturated solution at 50°C with an excess of (R)-BaHMa and the cooling rate adjusted at 0.5 $K.min^{-1}$. Test run gave expected results: starting from negative (enriched in (R)-BaHMa) the e.e changed its sign before it decreased. The Validation run confirmed these results with a crop of 0.2704g with -93.77%ee at 46min (corresponding to 0.2698g of pure (R)-BaHMa,).

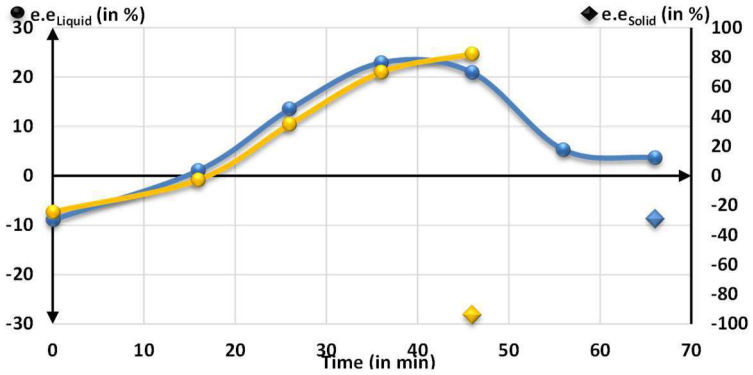

Figure 36. Enantiomeric excess of the liquid (●) and solid (♦) over time during the Test run (blue) and the Validation run (yellow) of AS3PC in water.

Table 13. Result of the Test run and Validation run of AS3PC in water. $e.e_{max}$ has been bolded.

	Parameters		Solution		Solid		
	Temperature (in °C)	Time (in min)	Mass (in g)	e.e (in %ee)	Mass (in g)	e.e (in %ee)	Enantiomer Mass (in g)
Test run	■ 40mL of doubly saturated solution at 50°C (0.7249g of racemic BaHMa in 40g of water) ■ 0.2002g of (R)-BaHMa suspended at 53°C						
	53°C	0 min		-8.94%			
	45°C	16 min		+1.09%			
	40°C	26 min		+13.52%			
	35°C	36 min		**+22.89%**			
	30°C	46 min		+20.89%			
	25°C	56 min		+5.26%			
	20°C	66 min		+3.63%	0.8559g	-28.87%	0.5515g
Validation run	■ 40mL of doubly saturated solution at 50°C (0.7249g of racemic BaHMa in 40g of water) ■ 0.2000g of (R)-BaHMa suspended at 53°C						
	53°C	0 min		-7.33%			
	50°C	16 min		-0.80%			
	45°C	26 min		+10.43%			
	40°C	36 min		+20.95%			
	35°C	46 min		**+24.64%**	**0.2791g**	**-93.77%**	**0.2704g**

II.3.2 Preferential Crystallization in HCl 1M

The same procedure has been applied in HCl 1M. Results are presented in Figure 37 and Table 14.

Since the solubility is higher than in previous solvents, $T_{initial}$ has been dropped to 50.5°C to obtain the suspension. The preferential crystallization is effective but three elements differ from previous tests:

- The maximum enantiomeric excess in the mother liquor is lower (≈10%ee). This decrease can result from two contributions: the solubility is higher, thus, the unbalance of the two enantiomers in solution would be lower. Also, the variation of solubility versus temperature is higher resulting in higher supersaturation which can prompt nucleation of the counter-enantiomer.
- The kinetics is different than previous tests: if the change of sign occurs at similar times (≈15min) the filtration window has shrunk (estimated between 23 and 29min).
- When filtrating at 26 min, 0.8885g at -90.56%ee has been obtained. It corresponds to 0.8466g of (R)-BaHMa and an increase of 412% of the seed mass.

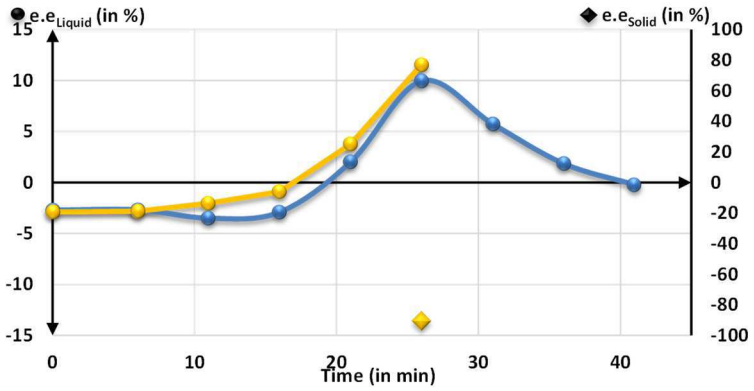

Figure 37. Enantiomeric excess of the liquid (●) and solid (♦) over time during Test run (blue) and Validation run (yellow) of AS3PC in HCl 1M.

Table 14. Result of the Test run and Validation run of AS3PC in HCl 1M. $e.e_{max}$ has been bolded.

	Parameters		Solution		Solid		
	Temperature (in °C)	Time (in min)	Mass (in g)	e.e (in %ee)	Mass (in g)	e.e (in %ee)	Enantiomer Mass (in g)
Test run	■ 40mL of doubly saturated solution at 50°C (5.8326g of racemic BaHMa in 40.68g of HCl 1M) ■ 0.1735g of (R)-BaHMa suspended at 50.5°C						
	50.5°C	0 min		-2.71%			
	47.5°C	6 min		-2.69%			
	45°C	11 min		-3.50%			

	42.5°C	16 min		-2.91%			
	40°C	21 min		+2.02%			
	37.5°C	26 min		**+9.95%**			
	35°C	31 min		+5.75%			
	32.5°C	36 min		+1.85%			
	30°C	41 min		-0.22%			
Validation run	■ **Reset at 50.5°C for 3h**						
	50.5°C	0 min		-2.89%			
	47.5°C	6 min		-2.81%			
	45°C	11 min		-2.03%			
	42.5°C	16 min		-0.90%			
	40°C	21 min		+3.76%			
	37.5°C	26 min		**+11.55%**	**0.8885g**	**-90.56%**	**0.8466g**

No cyclisation experiment has been performed under those conditions. Only based on this run and considering an equilibration time of 15min between each run, the productivity here should be at least of 44 $g.L^{-1}.H^{-1}$.

II.3.3 Preferential crystallization in HCl 2M

Finally, AS3PC has also been tested in HCl 2M which presents the best solubility. Results of the first tests are presented in Figure 38 and Table 15. Due to the high solubility in this solvent, parameters have been adapted to a higher seed mass and a lower initial temperature to ensure the formation of a stable suspension as a starting situation.

The preferential crystallization was effective with the best filtration window at 26min (37.5°C). At this time, the liquid presented a +10.79%e.e and 1.4580g of solid with -81%e.e has been filtrated.

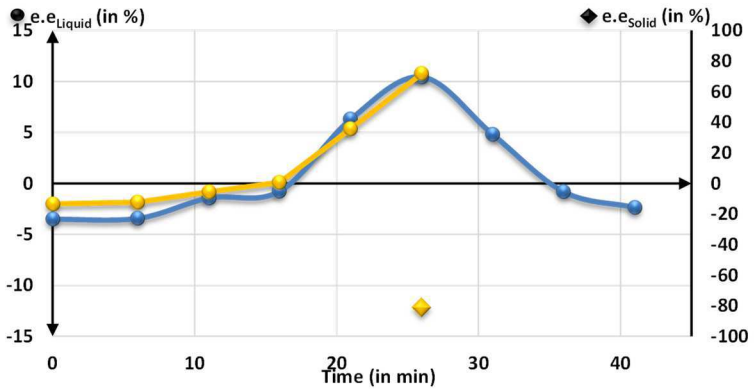

Figure 38. Enantiomeric excess of the liquid (●) and solid (♦) over time during Test run (blue) and Validation run (yellow) of AS3PC in HCl 2M.

Table 15. Result of the Test run and Validation run of AS3PC in HCl 2M. $e.e_{max}$ is bolded.

	Parameters		Solution		Solid		
	Temperature (in °C)	Time (in min)	Mass (in g)	e.e (in %ee)	Mass (in g)	e.e (in %ee)	Enantiomer Mass (in g)
Test run	■ 40mL of doubly saturated solution at 50°C (11.7835g of racemic BaHMa in 41.2g of HCl 2M) ■ 0.2501g of (R)-BaHMa suspended at 50.5°C						
	50.5°C	0 min		-3.50%			
	47.5°C	6 min		-3.42%			
	45°C	11 min		-1.42%			
	42.5°C	16 min		-0.75%			
	40°C	21 min		+6.31%			
	37.5°C	26 min		**+10.46%**			
	35°C	31 min		+4.82%			
	32.5°C	36 min		-0.81%			
	30°C	41 min		-2.34%			
Validation run	■ Reset at 50.5°C for 30min						
	50.5°C	0 min		-2.01%			
	47.5°C	6 min		-1.84%			
	45°C	11 min		-0.83%			
	42.5°C	16 min		+0.11%			
	40°C	21 min		+5.36%			
	37.5°C	26 min		**+10.78%**	**1.4580g**	**-80.99%**	**1.3194g**

Based on this test, consecutive preferential crystallizations have been performed. As presented in Figure 39 and Table 16, five consecutive successful runs have been achieved with only 10min of equilibration. Compensation in solvent seemed not to be always necessary but a complete dissolution of the BaHMa and a brown color has been observed after the fifth run.

The coloration of the solution revealed the degradation of the BaHMa under those conditions. A controlled atmosphere might be enough to resolve that problem. With this process, the productivity has reached 72 $g.L^{-1}.H^{-1}$.

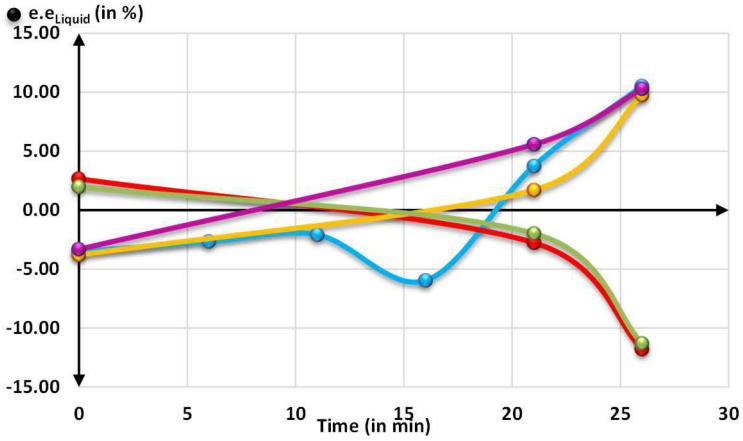

Figure 39. Enantiomeric excess of the liquid (●) and solid (♦) over time during PC runs: Run 1 (blue), Run 2 (red), Run 3 (yellow), Run 4 (green) and Run 5 (violet).

Table 16. Results of consecutive runs of AS3PC in HCl 2M. $e.e_{max}$ is bolded.

	Parameters		Solution		Solid		
	Temperature (in °C)	Time (in min)	Mass (in g)	e.e (in %ee)	Mass (in g)	e.e (in %ee)	Enantiomer Mass (in g)
Initial state	■ 40mL of doubly saturated solution at 50°C (1.7583g of racemic BaHMa in 34.796g of HCl 2M) ■ 0.2505g of (R)-BaHMa suspended at 50.5°C						
Run 1	50.5°C	0 min		-3.53%			
	47.5°C	6 min		-2.66%			
	45°C	11 min		-2.09%			
	42.5°C	16 min		-5.98%			
	40°C	21 min		+3.74%			
	37.5°C	26 min		**+10.52%**	**1.7437g**	**-89.94%**	**1.6560g**
Compensation	■ 1.7457g of racemic BaHMa ■ 10min at 50.5°C						
Run 2	50.5°C	0 min		+2.66%			
	40°C	21 min		-2.77%			
	37.5°C	66 min		**-11.80%**	**2.1713g**	**+98.37%**	**2.1536g**
Compensation	■ 2.1404g of racemic BaHMa and 2mL of HCl 2M ■ 10min at 50.5°C						
Run 3	50.5°C	0 min		-3.82%			
	40°C	21 min		+1.70%			
	37.5°C	66 min		**+9.73%**	**1.2724g**	**-96.25%**	**1.2485g**

Compensation	■ 1.7853g of racemic BaHMa ■ 10min at 50.5°C					
Run 4	50.5°C	0 min		+1.97%		
	40°C	21 min		-1.99%		
	37.5°C	66 min		**-11.32%**	**1.7507g**	**+75.10%**	**1.5327g**
Compensation	■ 1.7508g of racemic BaHMa ■ 10min at 50.5°C					
Run 5	50.5°C	0 min		-3.33%		
	40°C	21 min		+5.56%		
	37.5°C	66 min		**+10.27%**	**1.6133g**	**-95.68%**	**1.5784g**
Compensation	■ 1.7508g of racemic BaHMa ■ 10min at 50.5°C					

III Enantiomeric purification

This step, called *enantiomeric purification*, is simply a partial redissolution of the BaHMa salt in a solvent. This solvent can be any previous mentioned "solvent" allowing the formation of the baclofen hydrogenomaleate salt.

The process is based on the ternary section between BaHMa enantiomers and the "solvent". Nonetheless, the most important data are the solubility of the racemic mixture and the width of the partial solid solutions domains (Figure 40).

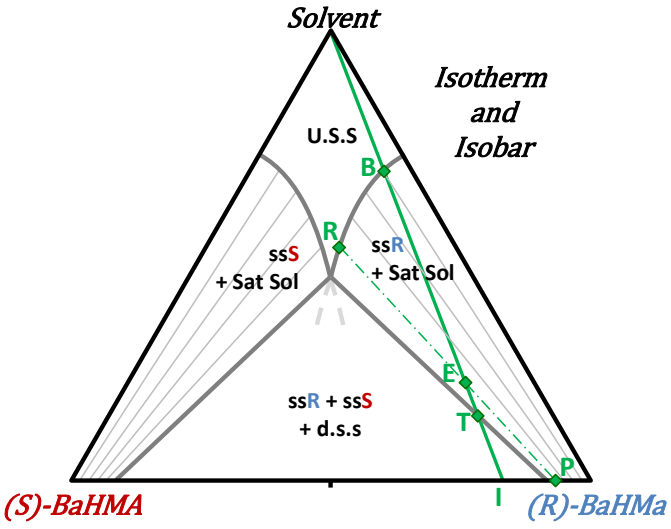

*Figure 40. Schematic BaHMa enantiomers and solvent ternary section. System pathway during the enantiomeric purification from solid **I** to solid **P** is highlighted in green.*

Starting from a mixture of both BaHMa enantiomers (point **I**), the system will follow the green line when solvent is added to the system. Thus, the system passes through different domains but only one of them permits the enantiomeric purification:

- From **I** to **T**, it is a triphasic domain where the two BaHMa partial solid solutions are in equilibrium with their doubly saturated solution. If the suspension is filtrated, a better e.e would be reached but the solid would be composed of the two partial solid solutions.
- At point **T** the system is at the limiting tie-line between the triphasic and biphasic domains. In the case of true conglomerate, it is theoretically the best spot to filtrate and to recover the maximum mass of pure enantiomer. In the case presented here, filtration at **T** point will permit to recover the maximum mass of the partial solid solution.
- From **T** to **B**, adding more solvent decreases the collected mass of solid but its enantiomeric excess increases. This is highlighted by point **E** where the cropped solid is of **P** composition and the remaining liquid is **R**. Best e.e and lowest mass would be obtained at point **B**. Thus, a compromise must be found between the mass recovered and the final enantiomeric excess.
- Exceeding point **B** will lead to undersaturated system.

One example has been carrying out to illustrate this process: 0.4239g of BaHMa at -50.43%ee (i.e 0.3189g of (R)-BaHMa and 0.1050g of (S)-BaHMa) has been suspended under agitation in 27.0787g of water for 12 hours at 20°C.

The suspension has then been filtrated and washed twice with water. 0.1905g of solid has been recovered whose e.e was -98.59%ee whereas the remaining liquid phase presenting an enantiomeric excess of -11.56%ee.

IV Salting out

Salting out processes are based on the incongruent solubility of salts under certain conditions, especially varying the pH of the system.

Moreover, we can expect that the return to pure baclofen would be concomitant with an enantiomeric purification better than the previous one performed on crude BaHMa, since not limited by the partial solid solution.

Figure 41 illustrates this fact. Baclofen hydrogenomaleate has an incongruent solubility (yellow domains). Salting out consists in, starting from baclofen hydrogenomaleate, to place

the system in the biphasic blue domains where enantiopure baclofen equilibrates with its saturated solution along the tie-lines. Then, the system is filtrated to only recover baclofen in the solid state.

Intuitively, starting with enantiopure baclofen hydrogenomaleate leads to enantiopure baclofen (orange lines). But, the same result can be obtained for scalemic compositions (violet line and tie-line) for which the pathway to pure solvent also passes in the biphasic blue domain. As the final e.e is higher than the initial one, both enantiomeric purification and salting out should happen at the time.

In the case represented below, this enantiomeric purification takes place whatever the scalemic composition since baclofen racemic compound has been represented in a domain (green) that does not exceed the 1:1 baclofen/maleic acid stoichiometry. Nonetheless, if this domain is large enough, salting out can lead to the racemic baclofen for near racemic BaHMa samples.

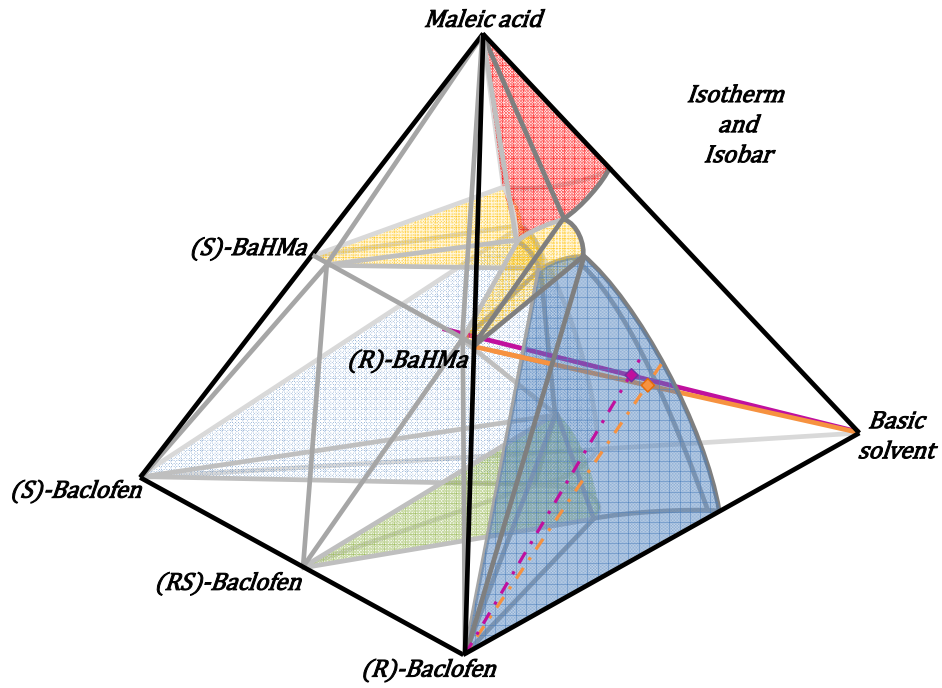

Figure 41. Schematic possible 4-order phase diagram between baclofen enantiomers, maleic acid and a basic solvent (or basic solution). Colored domains correspond to bundles of tie-line for baclofen enantiomers (blue), baclofen racemic compound (green), baclofen hydrogenomaleate enantiomers (yellow) and maleic acid (red). Orange and violet lines correspond to incongruent solubility of enantiopure and high e.e of BaHMa. Dashed lines are corresponding of tie-lines permitting to obtain enantiopure baclofen from the two previous cases.

Starting with almost 1g of enantiopure baclofen hydrogenomaleate (corresponding to 0.6480g of baclofen and 0.3520g of maleic acid), a clear solution has been obtained by dissolution in 10mL of NaOH 1M at 25°C and under agitation.

The pH of the solution has been adjusted by adding a certain volume of concentrated hydrochloric acid (37% in mass). Temperature has also been controlled. Additions of the acidic solution led to the precipitation of the baclofen. The suspension has then been filtrated, dried, weighted and analyzed by X-ray powder diffraction and NMR.

Three tests have been conducted to verify the feasibility of this process for different values of pH and temperatures.

Table 17. Salting out results.

	37% HCl volume added	Final temperature	Final pH	Cropped mass
Test 1	230µL	25°C	9.02	0.5485g
Test 2	320µL	25°C	7.90	0.5546g
Test 3	240µL	10°C	9.29	0.5786g

The NMR analysis (Figure 42) confirmed that the filtrated samples were mainly composed of pure baclofen with some possible residual maleic acid (6 ppm peak), nevertheless, none other impurities have been revealed by the NMR analyses. XRPD measurements also confirmed that the solids recrystallized and filtered were enantiopure baclofen under its B polymorphic form.

To conclude, the mass cropped and the purity indicate a good yield of the process (≈85% of the baclofen has been recovered after the salting out). Moreover, Test 2 & 3 indicate that the salting out process can be optimized by varying temperature and pH to increase the mass of the crop without affecting the chemical, enantiomeric and structural purity. A priori, adjusting the pH at the baclofen pHi and at low temperature (e.g. 0°C for instance) should be the optimum process in view to maximize the yield. Nevertheless, the process should also lead to the pure form B which is the only one in the public domain so far.

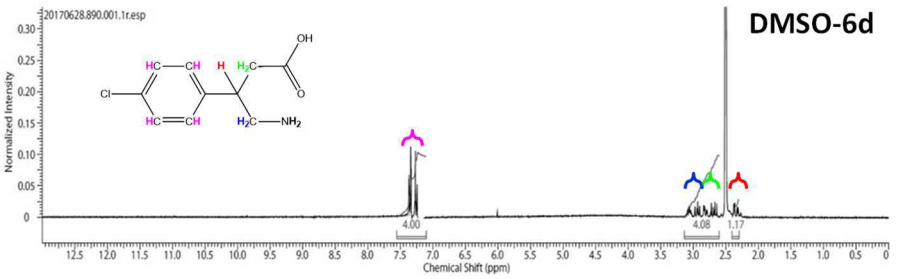

Figure 42. NMR ^{1}H of salting out test in deuteride DMSO.

Part.IV Discussion on preferential crystallization carried out on non-conglomerate forming systems

If a conglomerate forming system is the ideal case to perform preferential crystallization, the process is also applicable on other equilibria.

I Preferential crystallization for racemic compounds

Lorenz & al. performed the preferential crystallization of one enantiomer and of the racemic compound of mandelic acid.[37] Principle is similar as that in classical preferential crystallization except that only one enantiomer can be resolved successively and that the compensation between the runs is ensured with a mixture of solid phases at the eutectic composition (Figure 43). If the theory is valid to all racemic compound forming systems, the large tendency of the nature to crystallize rapidly in racemic compound prevents its application. Indeed, only two examples are known: mandelic acid[37] and malic acid.[38]

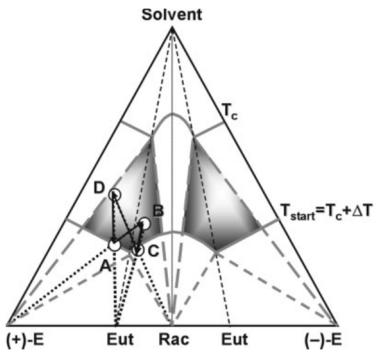

Figure 43. Preferential crystallization performed in a cyclic operation mode for a racemic compound.[37]

The process implemented corresponds to the SIPC process for conglomerate with a seeding of a supersaturated solution. However, auto-seeded process seems also possible.

II Preferential Crystallization on metastable conglomerate

When low nucleation rate of stable racemic compound is observed, it is possible to apply the preferential crystallization on a metastable conglomerate. During the entrainment, both crystallizations of the counter-enantiomer and of the racemic compound are avoided (Figure 44 & 45). Contrary to the previous case for which auto-seeded processes seem applicable, in this case a total redissolution between the runs is necessary to avoid any undesirable crystallization of the stable racemic compound.[21,39,40]

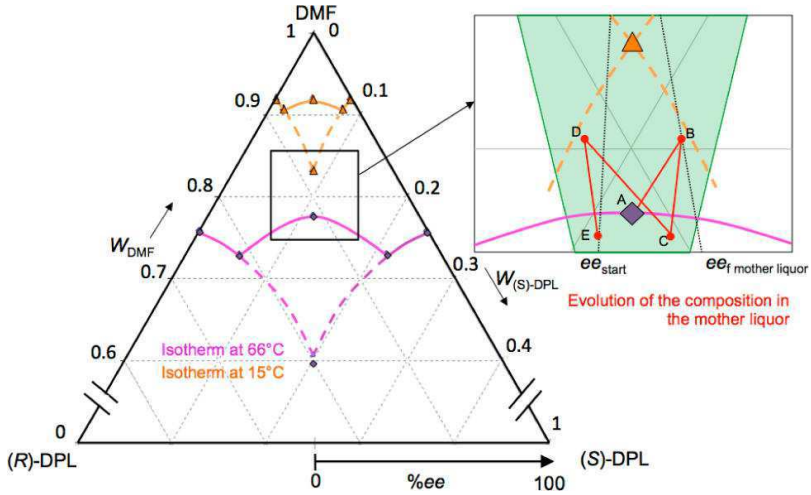

Figure 44. Isothermal sections at 66 and 15 °C in the DMF-rich part of the ternary solubility diagram (DMF−(R)-DPL−(S)-DPL). Dashed lines correspond to metastable solubility lines. Error bars are smaller than the dots representing experimental data points.[39]

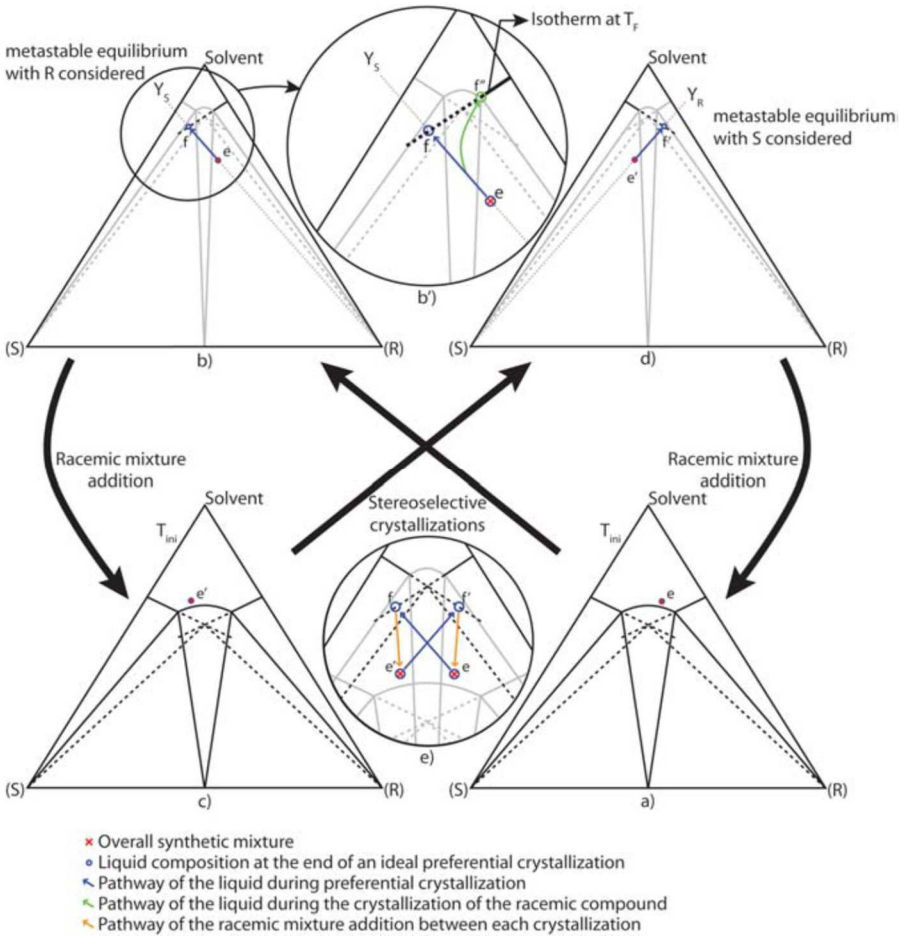

Figure 45. Description of preferential crystallization via the metastable conglomerate.[21]

III Preferential Crystallization on mirror image partial solid solutions

More relevant studies, to the case presented in this work, have been depicted where preferential crystallization has been performed on mirror image solid solutions.

III.1 Comparison of cases collated

Only few examples are known,[41,22,23] which is consistent to the low occurrence of such equilibria. But we can assume that, as for true conglomerate, spotting a system presenting the chiral discrimination in the form of mirror image partial solid solutions *"is just halfway to achieving a preparative resolution by preferential crystallization."*[24]

Among the few examples known (Figure 46 & 47), the BaHMa system is the first one presenting a demixion of a complete solid solution and permitting an efficient preferential crystallization of its partial solid solutions.

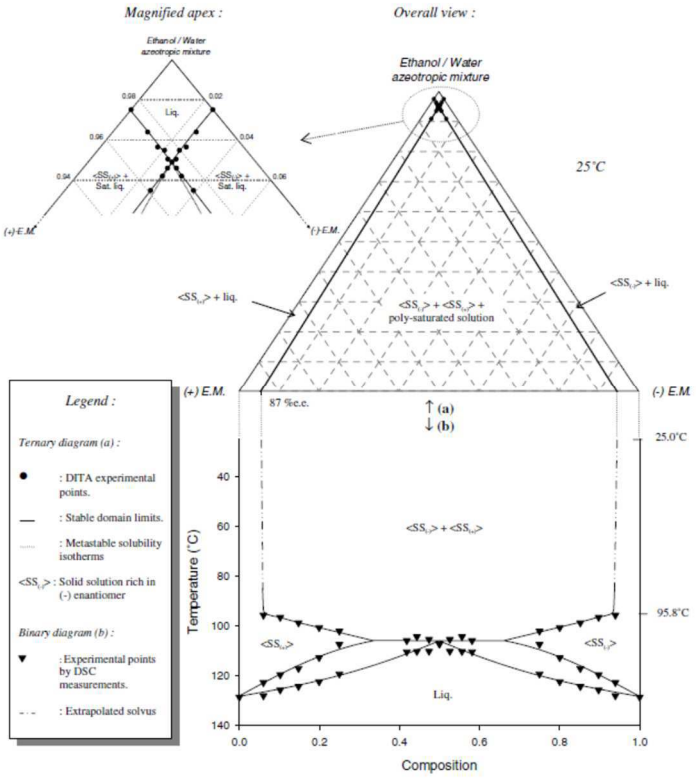

Figure 46. Isothermal section of the ternary phase diagram [(+)-E.M.–(-)-E.M.–(ethanol–water azeotropic mixture)] at 25°C (a) and binary phase diagram of [(+)-E.M.–(-)-E.M.] (b).[41]

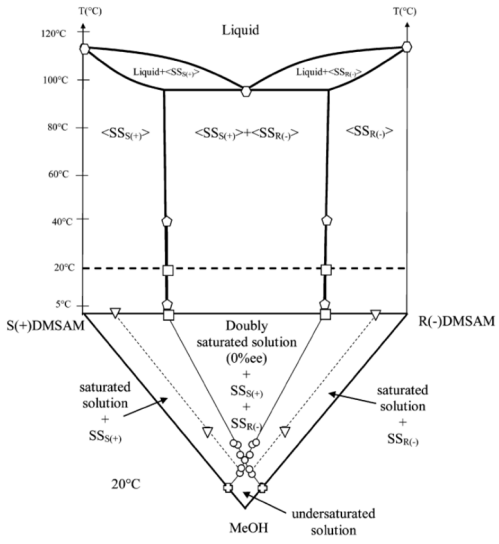

Figure 47. Up: binary phase diagram S(+)DMSAM/R(-)DMSAM in the temperature range 120 °C to 5 °C. The upper part of this diagram is mostly extrapolated from DSC measurements and consistent with HPLC measurements and the ternary isotherm. Down: ternary isotherm S(+)-DMSAM/R(-)DMSAM/MeOH determined at 20 °C; this isotherm is represented under the binary diagram. Caption used to differentiate the experiments: solubility measurements (open cross), DITA (O), complementary experiments leading to a tie-line (Δ), HPLC measurements at 20 °C (□), 5 °C and 40 °C (⌂), DSC measurements (octagon). The metastable solubility curves are not represented.[40]

Logically, the thinner the partial solid solution domain, the better the final enantiomeric excess of the crops (Table 17). In the three collated cases, limits of the monophasic domain do not evolve versus temperature in the range used for PC.

Table 18. Partial solid solutions limits and PC results for the three known cases.

System	Partial solid solution domain	e.e of the crude crops via AS3PC
E.M[23,41]	87%e.e	54%e.e
DMSAM[40]	48%e.e	46%e.e
BaHMa	>99%e.e	91%e.e

III.2 Mechanism

A mechanism derived to the one valid for true conglomerate is presented below. The partial solid solutions, and their consequences, have been taking into consideration (Figure 48 & 49).

- Step 0: a doubly saturated solution is prepared at temperature $\boldsymbol{T_{dou\ sat}}$.
- Step 1: seeds of $\boldsymbol{R}$ enantiomer are added and the system is heated up to temperature $\boldsymbol{T_{initial} > T_{dou\ sat}}$. Mother liquor moves along the tie-line between the $\boldsymbol{ssR}$ and a solution lightly enriched in $\boldsymbol{R}$ enantiomer. If enough time is given to the system, it is the stable green tie-line $\boldsymbol{ssR_I}$. Otherwise, it is a metastable intermediate tie-line.
- Step 2: the system is cooled down from $\boldsymbol{T_{initial}}$ to $\boldsymbol{T_{final}}$. Solubility decreases which induces crystal growth and secondary nucleations of the seeds while the solution becomes enriched in enantiomer $\boldsymbol{S}$. Solution moves now along metastable tie-line between $\boldsymbol{ssR_F}$ and a solution saturated in $\boldsymbol{R}$ and supersaturated in $\boldsymbol{S}$. In theory, PC could be continued until the system reaches the metastable solubility of $\boldsymbol{ssR_F}$. Two behaviors seem plausible. The first one, which has been observed by Renou & al.[40] and Wermester & al.,[40] presents a lower e.e for $\boldsymbol{ssR_F}$ than for $\boldsymbol{ssR_I}$. The second case is the reverse and would lead to better results (Figure 48).
- Step 3: The system is filtrated before the nucleation and crystal growth of $\boldsymbol{ssS}$ enantiomer. The crop of $\boldsymbol{ssR_F}$ crystals is weighed and the mother liquor moves toward the metastable tie-line to the metastable solubility.
- Step 4: The system is heated back to $\boldsymbol{T_{initial}}$ and a mass of racemic mixture, corresponding to the cropped $\boldsymbol{ssR_F}$ crystals in step 3, is added to the solution. After

equilibration, the system is in the symmetrical state as that in step 1 with a suspension of $\boldsymbol{ssS}$ ($\boldsymbol{ssS_I}$ if stable tie-line) in a solution lightly enriched in the same enantiomer.

- Step 5: Symmetrical of step 2: the system is cooled down from $\boldsymbol{T_{initial}}$ to $\boldsymbol{T_{final}}$. Solubility decreases which induces crystal growth and secondary nucleation of the seeds while the solution becomes enriched in enantiomer $\boldsymbol{R}$. Mother liquor moves along a metastable tie-line between $\boldsymbol{ssS_F}$ and a solution saturated in $\boldsymbol{S}$ and supersaturated in $\boldsymbol{R}$. In theory, PC could be continued until the mother liquor reaches the metastable solubility of $\boldsymbol{ssS_F}$.
- Step 6: Symmetrical of step 3. The system is filtrated before the stabilizing nucleation and crystal growth of $\boldsymbol{R}$ enantiomer. The crop of $\boldsymbol{ssS_F}$ crystals is weighed and the solution moves along the metastable tie-line to the metastable solubility.
- Final step: By heating back the system to $\boldsymbol{T_{initial}}$ and compensating the mass of the crop by racemic mixture, the system goes back to the initial step 1.

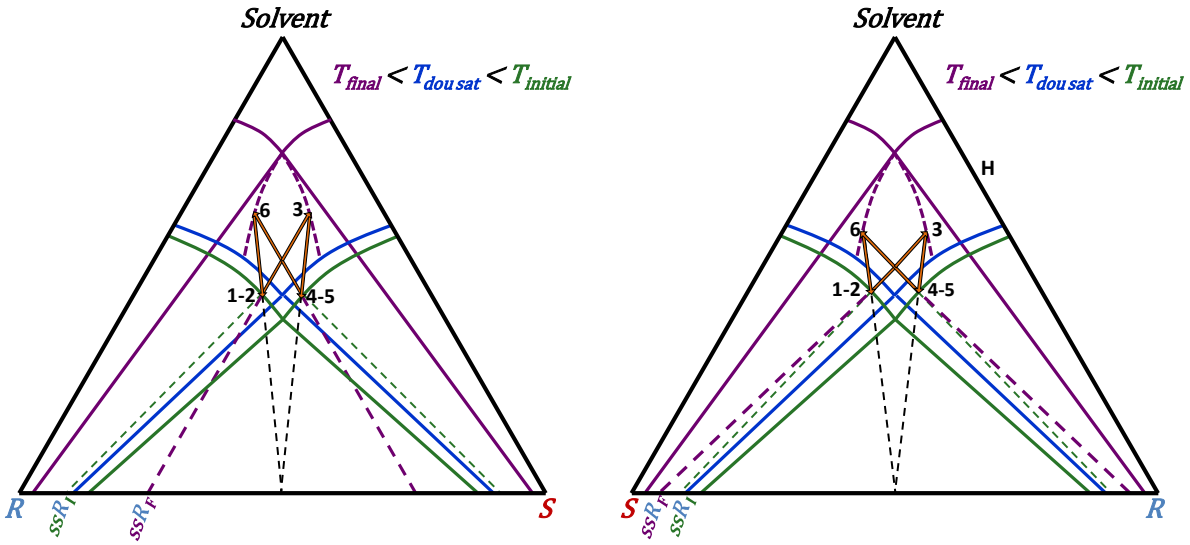

Figure 48. Schematic pathway during AS3PC process with metastable tie-line (dashed violet line) outer (left) or inner (right) the partial solid solutions (green domains). Dashed green line corresponds to the stable tie-line of the system at $T_{initial}$.

To finish, two additional considerations must be taken into account:

- The first one is that the solid does not directly pass from the tie-line at $\boldsymbol{ssR_I}$ to that at $\boldsymbol{ssR_F}$ but explores all the intermediate partial solid solutions between those values. As a result, crystals would grow in layers respecting those partial solid solutions with a core of $\boldsymbol{ssR_I}$, a shell of $\boldsymbol{ssR_F}$ and a continuum between them (Figure 49).
- The second is that PC is an out of equilibrium process, there is no time for diffusion of the molecules in the matrix of the major antipode. In other words,

homogenization of the solid phase is very unlikely and a centripetal gradient in e.e should exist for every particle (Figure 49).

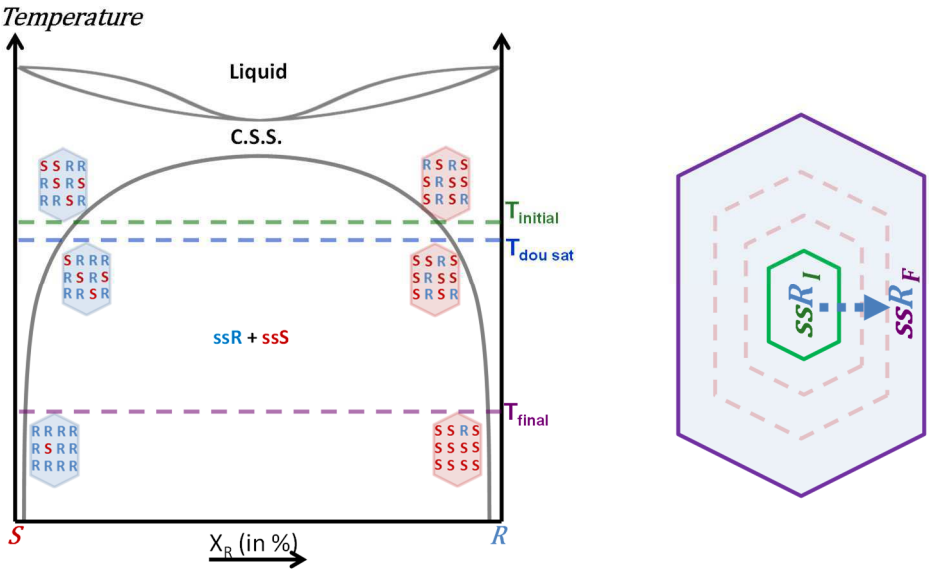

Figure 49. Schematic evolution of the crystal compositions with the temperature (left) and shcematic layer reparation of a crystal along its crystallization (right)..

Conclusion

In this chapter, two major parts have been distinguished and discussed.

The first part has only fundamental interest. Indeed, the experimental proof of a new kind of chiral binary system, so far predicted only, has been detailed. Even though this first case has been blurred by the chemical degradation close to fusion, the clear evidence of a chiral system presenting a solid/solid demixion of a complete solid solution has been presented. By considering:

(i) the clear difference in the four substituents of the stereogeneric center,

(ii) the number and the nature of H-bonds in the crystal structure,

this result was not anticipated at all.

The second part has more some application interests. It is a good example of preferential crystallization process applied to a solid/solid demixing system. Rationales have been presented about the mechanism taking place during the AS3PC process of partial solid solutions and about the enantio-purification of salting out process. The results obtained are promising in the perspective of a low cost and effective preparative resolution at industrial scale.

Bibliography

(1) Dario, A.; Pisani, R.; Sangiorgi, S.; Soragna, A.; Reguzzoni, M.; Protasoni, M.; Pessina, F.; Fesce, R.; Peres, A.; Tomei, G. Baclofen and Potential Therapeutic Use: Studies of Neuronal Survival. *Eur. J. Pharmacol.* **2006**, *550* (1), 33–38.

(2) Albright, A. L. Topical Review: Baclofen in the Treatment of Cerebral Palsy. *J. Child Neurol.* **1996**, *11* (2), 77–83.

(3) Fromm, G. H.; Terrence, C. F.; Chattha, A. S. Baclofen in the Treatment of Trigeminal Neuralgia: Double-Blind Study and Long-Term Follow-Up. *Ann. Neurol.* **1984**, *15* (3), 240–245.

(4) Dario, A.; Tomei, G. A Benefit-Risk Assessment of Baclofen in Severe Spinal Spasticity. *Drug Saf.* **2004**, *27* (11), 799–818.

(5) Assadi, S. M.; Radgoodarzi, R.; Ahmadi-Abhari, S. A. Baclofen for Maintenance Treatment of Opioid Dependence: A Randomized Double-Blind Placebo-Controlled Clinical Trial [ISRCTN32121581]. *BMC Psychiatry* **2003**, *3*, 16.

(6) Corwin, R. L.; Boan, J.; Peters, K. F.; Ulbrecht, J. S. Baclofen Reduces Binge Eating in a Double-Blind, Placebo-Controlled, Crossover Study: *Behav. Pharmacol.* **2012**, *23* (5 and 6), 616–625.

(7) Addolorato, G.; Caputo, F.; Capristo, E.; Domenicali, M.; Bernardi, M.; Janiri, L.; Agabio, R.; Colombo, G.; Gessa, G. L.; Gasbarrini, G. Baclofen Efficacy in Reducing Alcohol Craving and Intake: A Preliminary Double-Blind Randomized Controlled Study. *Alcohol Alcohol* **2002**, *37* (5), 504–508.

(8) Simioni, N.; Preda, C.; Deken, V.; Bence, C.; Cottencin, O.; Rolland, B. Characteristics of Patients with Alcohol Dependence Seeking Baclofen Treatment in France: A Two-Centre Comparative Cohort Study. *Alcohol Alcohol* **2016**, *51* (6), 664–669.

(9) Ameisen, O. Complete and Prolongated Supression of Symptoms and Consequences of Alcohol-Dependence Using High-Dose Baclofen: A Self-Case Report of a Physician. *Alcohol Alcohol* **2005**, *40* (2), 147–150.

(10) Ameisen, O. *Le dernier verre*; Denoël, 2008.

(11) Morley, K. C.; Baillie, A.; Leung, S.; Addolorato, G.; Leggio, L.; Haber, P. S. Baclofen for the Treatment of Alcohol Dependence and Possible Role of Comorbid Anxiety. *Alcohol Alcohol* **2014**, *49* (6), 654–660.

(12) Rolland, B.; Paille, F.; Gillet, C.; Rigaud, A.; Moirand, R.; Dano, C.; Dematteis, M.; Mann, K.; Aubin, H.-J. Pharmacotherapy for Alcohol Dependence: The 2015 Recommendations of the French Alcohol Society, Issued in Partnership with the European Federation of Addiction Societies. *CNS Neurosci. Ther.* **2016**, *22* (1), 25–37.

(13) Reynaud, M.; Aubin, H.-J.; Trinquet, F.; Zakine, B.; Dano, C.; Dematteis, M.; Trojak, B.; Paille, F.; Detilleux, M. A Randomized, Placebo-Controlled Study of High-Dose Baclofen in Alcohol-Dependent Patients—The ALPADIR Study. *Alcohol Alcohol* **2017**, *52* (4), 439–446.

(14) Chang, C.-H.; Yang, D. S. C.; Yoo, C. S.; Wang, B.-C.; Pletcher, J.; Sax, M.; Terrence, C. F. Structure and Absolute Configuration of (R)-Baclofen Monohydrochloride. *Acta Crystallogr. B* **1982**, *38* (7), 2065–2067.

(15) Wang, M.-X.; Zhao, S.-M. Highly Enantioselective Biotransformations of 2-Aryl-4-Pentenenitriles, a Novel Chemoenzymatic Approach to (R)-(−)-Baclofen. *Tetrahedron Lett.* **2002**, *43* (37), 6617–6620.

(16) Chenevert, R.; Desjardins, M. Chemoenzymatic Enantioselective Synthesis of Baclofen. *Can. J. Chem.* **1994**, *72* (11), 2312–2317.

(17) Herdeis, C.; Hubmann, H. P. Synthesis of Homochiral R-Baclofen from S-Glutamic Acid. *Tetrahedron Asymmetry* **1992**, *3* (9), 1213–1221.

(18) Chang, M.-Y.; Sun, P.-P.; Chen, S.-T.; Chang, N.-C. A Facile Synthesis of 3-Aryl Pyroglutamic Acid. Facile Synthesis of Baclofen and Chlorpheg. *Tetrahedron Lett.* **2003**, *44* (28), 5271–5273.

(19) Caira, M. R.; Clauss, R.; Nassimbeni, L. R.; Scott, J. L.; Wildervanck, A. F. Optical Resolution of Baclofen via Diastereomeric Saltpair Formation between 3-(p-Chlorophenyl)Glutaramicacid and (S)-(-)-α-Phenylethylamine. *J. Chem. Soc. Perkin Trans. 2* **1997**, *0* (4), 763–768.

(20) Coquerel, G. 1 Preferential Crystallization. In *Novel Optical Resolution Technologies*; Sakai, K., Hirayama, N., Tamura, R., Eds.; Topics in Current Chemistry; Springer Berlin Heidelberg, 2006; pp 1–51.

(21) Levilain, G.; Coquerel, G. Pitfalls and Rewards of Preferential Crystallization. *CrystEngComm* **2010**, *12* (7), 1983.

(22) Renou, L.; Morelli, T.; Coste, S.; Petit, M.-N.; Berton, B.; Malandain, J.-J.; Coquerel, G. Chiral Discrimination at the Solid State of Methyl 2-(Diphenylmethylsulfinyl)Acetate. *Cryst. Growth Des.* **2007**, *7* (9), 1599–1607.

(23) Wermester, N.; Aubin, E.; Pauchet, M.; Coste, S.; Coquerel, G. Preferential Crystallization in an Unusual Case of Conglomerate with Partial Solid Solutions. *Tetrahedron Asymmetry* **2007**, *18* (7), 821–831.

(24) Gonella, S.; Mahieux, J.; Sanselme, M.; Coquerel, G. Spotting a Conglomerate Is Just Halfway to Achieving a Preparative Resolution by Preferential Crystallization. *Org. Process Res. Dev.* **2012**, *16* (2), 286–293.

(25) Galland, A.; Dupray, V.; Berton, B.; Morin-Grognet, S.; Sanselme, M.; Atmani, H.; Coquerel, G. Spotting Conglomerates by Second Harmonic Generation. *Cryst. Growth Des.* **2009**, *9* (6), 2713–2718.

(26) Simon, F.; Clevers, S.; Dupray, V.; Coquerel, G. Relevance of the Second Harmonic Generation to Characterize Crystalline Samples. *Chem. Eng. Technol.* **2015**, *38* (6), 971–983.

(27) Florey, K.; Brittain, H. G. *Analytical Profiles of Drug Substances and Excipients. Vol. 22-29 Vol. 22-29*; Academic: New York, 1972.

(28) Lohbeck, K.; Haferkorn, H.; Fuhrmann, W.; Fedtke, N. Maleic and Fumaric Acids. In *Ullmann's Encyclopedia of Industrial Chemistry*; Wiley-VCH Verlag GmbH & Co. KGaA, Ed.; Wiley-VCH Verlag GmbH & Co. KGaA: Weinheim, Germany, 2000.

(29) Rowe, R. C.; Sheskey, P. J.; Quinn, M. E. *Handbook of Pharmaceutical Excipients*; Pharmaceutical Press, 2009.

(30) Coquerel, G. Review on the Heterogeneous Equilibria between Condensed Phases in Binary Systems of Enantiomers. *Enantiomer* **2000**, *5*, 481–498.

(31) Hefnawy, M. M.; Aboul-Enein, H. Y. Enantioselective High-Performance Liquid Chromatographic Method for the Determination of Baclofen in Human Plasma. *Talanta* **2003**, *61* (5), 667–673.

(32) Coquerel, G.; Petit, M.-N.; Bouaziz, R. Procede De Dedoublement De Deux Antipodes Optiques Par Cristallisation. WO/1995/008522, March 31, 1995.

(33) Coquerel, G.; Levilain, G. Process for the Resolution of Enantiomers by Preferential Evaporative Crystallization. WO2011/073300, December 16, 2010.

(34) Mahieux, J.; Sanselme, M.; Harthong, S.; Melan, C.; Aronica, C.; Guy, L.; Coquerel, G. Preparative Resolution of (±)-Bis-Tetralone by Means of Autoseeded Preferential

Crystallization Induced by Solvent Evaporation (ASPreCISE). *Cryst. Growth Des.* **2013**, *13* (8), 3621–3631.

(35) Murti, P.; Van Winkle, M. Vapor-Liquid Equilibria for Binary Systems of Methanol, Ethyl Alcohol, 1-Propanol, and 2-Propanol with Ethyl Acetate and 1-Propanol-Water. *Ind. Eng. Chem. Chem. Eng. Data Ser.* **1958**, *3* (1), 72–81.

(36) Ponton, J. Azeotrope Databank http://homepages.ed.ac.uk/jwp/Chemeng/Chemeng/azeotrope_bank.html (accessed Mar 28, 2018).

(37) Lorenz, H.; Polenske, D.; Seidel-Morgenstern, A. Application of Preferential Crystallization to Resolve Racemic Compounds in a Hybrid Process. *Chirality* **2006**, *18* (10), 828–840.

(38) Kaemmerer, H.; Lorenz, H.; Black, S. N.; Seidel-Morgenstern, A. Study of System Thermodynamics and the Feasibility of Chiral Resolution of the Polymorphic System of Malic Acid Enantiomers and Its Partial Solid Solutions. *Cryst. Growth Des.* **2009**, *9* (4), 1851–1862.

(39) Brandel, C.; Amharar, Y.; Rollinger, J. M.; Griesser, U. J.; Cartigny, Y.; Petit, S.; Coquerel, G. Impact of Molecular Flexibility on Double Polymorphism, Solid Solutions and Chiral Discrimination during Crystallization of Diprophylline Enantiomers. *Mol. Pharm.* **2013**, *10* (10), 3850–3861.

(40) Gilks, S. E.; Davey, R. J.; Mughal, R. K.; Sadiq, G.; Black, L. Crystallization of 2-Chloromandelic Acid: Solubility, Formation of the Metastable Conglomerate, and Use of a Nonaqueous Emulsion To Prepare an Enantiomerically Enriched Product. *Cryst. Growth Des.* **2013**, *13* (10), 4323–4329.

(41) Aubin, E.; Petit, M. N.; Coquerel, G. Resolution of the Ethanolamine Salt of (±)Mandelic Acid by Using the AS3PC Method: Principle, Application and Results. *J. Phys. IV Proc.* **2004**, *122*, 157–162.

Spontaneous Symmetry Breaking

Chapter 3 - Racemic isoplethal section between two atropisomers & Chirality Induced by Dissymmetric Distribution

Laboratoire SMS, Université de Rouen Normandie

François-Xavier Gendron

29/06/2018

Introduction

This chapter details the study of phase equilibria between two different compounds. Those compounds are 2-phenylthio-3-methyl-cyclohex-2-enone derivatives (Figure 1). Basically, they are composed of a phenyl group (substituted or not) linked via a sulfur atom to a 3-methyl-cyclohexene with a ketone function.

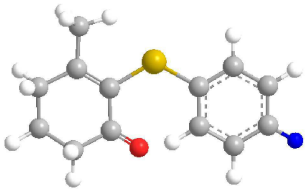

Figure 1. Common features of components studied in this chapter (para derived position highlighted in blue).

More precisely, we studied phase equilibria between two compounds substituted in *para* position of the thiophenyl group (Figure 2): one with a methyl group (*p-Me component*) and the other with a chlorine atom (*p-Cl component*).

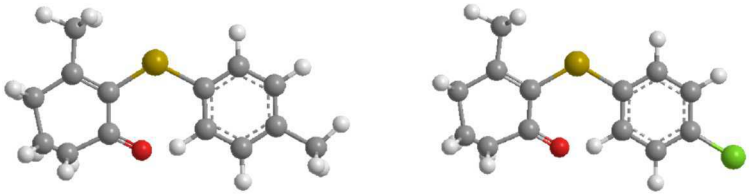

Figure 2. p-Me (left) and p-Cl (right) derivatives.

They present different features making their study complicated, and thereby, interesting. One can list:

- The chirality which is not beared by a stereogeneric center but by atropisomery. Enantiomers, i.e the reverse optical forms, are then mirror images because of two symmetrical wells of energy corresponding to opposite configurations.
- The activation energy to switch from one configuration to the other is too high in the solid state (atropisomery). However, this barrier is low enough in the liquid state (molten or solution) and racemization occurs almost instantaneously.
- The racemization in solution prevent any measure of enantiomeric excess or optical purity by the different technics available in our laboratory.

The initial aim of this study, given by the Pr. Reiko Kuroda from Tokyo University of Science, Japan, was to establish the phase diagram between the racemic composition of the two components.

In this purpose, Pr. Kuroda has first furnished p-Me and p-Cl at the racemic compositions. In the last few months of this thesis, syntheses of the components at a larger scale has been carry out by Ryusei Oketani, another PhD student in the SMS laboratory.

Due to the complexity of the study, all the experimental results would be first presented, then, they would be discussed.

Part.I Context of the study

I Chirality of p-Me and p-Cl

Compounds studied present atropisomery which is a special kind of chirality. Prelog defined atropisomers as stereoisomers "*due to the so-called secondary structure, i.e. hindered rotation around single bonds*".[1] The chirality is not related to the chemical structure of the molecule but to its configuration. Note that if the rotation of a single bond is limited, the atropisomer can adopt several torsion angles.

The two opposite optical forms in atropisomerism would be called antipodes. They are differentiated by their rotations of polarized light in the solid state (likewise quartz): one antipode would be *dextrogyre* (+) and the other one *levogyre* (-).

II Racemization in the liquid

When the molecules are solvated or in the molten state, the configuration is not blocked anymore.

This results in a spontaneous, instantaneous and total racemization in the liquid state (molten phase or solution): **the only liquid that can exist is a racemic liquid**.

The consequence of this racemization on phase diagram is illustrated in Figure 3. In the case of a conglomerate forming system, whatever the optical purity of the solid, it becomes a racemic liquid which is represented by a vertical monophasic line. The same vertical line is present for a racemic compound forming system. In that case, the only possible solid, under normal crystallization conditions, is the racemic compound.

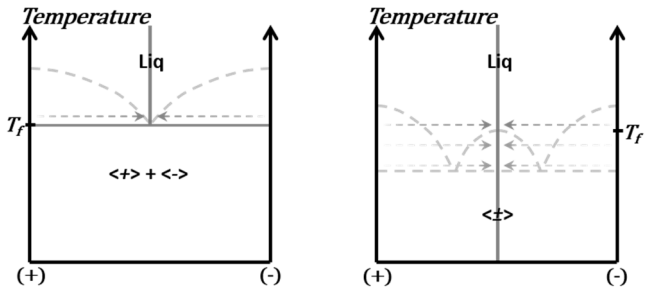

Figure 3. Racemization influence on phase diagram for conglomerate (left) and racemic compound (right) forming systems.

III Deracemization in the solid

Another consequence of the loss of the chirality in the liquid state is the possibility to perform deracemization for conglomerate forming system.

If the recrystallization conditions only give rise to one nucleus, this one would growth preferentially, even after the appearance of other nuclei of same or opposite handedness. As a result, an unbalance between the antipodes can appear.

Otherwise, both antipodes crystallize quasi-concomitantly to give a racemic mixture.

Whatever the optical purity obtained by crystallization or mixing of the two antipodes, the solid would evolve to reach one pure antipode only (the one initially in excess) (Figure 4). This evolution can be accelerated by putting the crystals in suspension (or when they are partially molten) by means of continuous grinding[2–9] or temperature cycling for instance.[10–14]

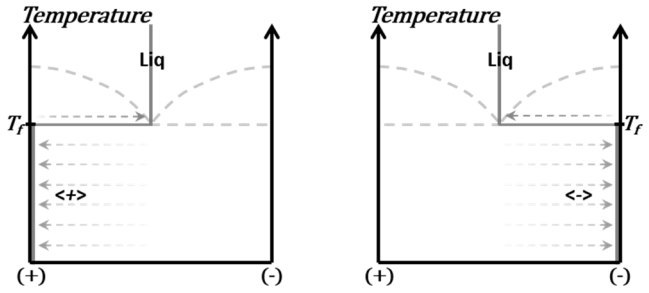

Figure 4. Deracemization of the conglomerate.

IV Application on the system

The hindered rotation responsible of the chirality corresponds to the torsion angles around the sulfur bonds. Thus, the two components exist as two antipodes (Figure 5). They would be labelled: (+)-p-Me, (-)-p-Me, (+)-p-Cl and (-)-p-Cl.

Differentiation between *conformation* and *configuration* would be made in this chapter. Conformation would be used to describe the different torsion angles adopted by one antipode. Configuration can be used to differentiate the two antipodes of opposite conformations.

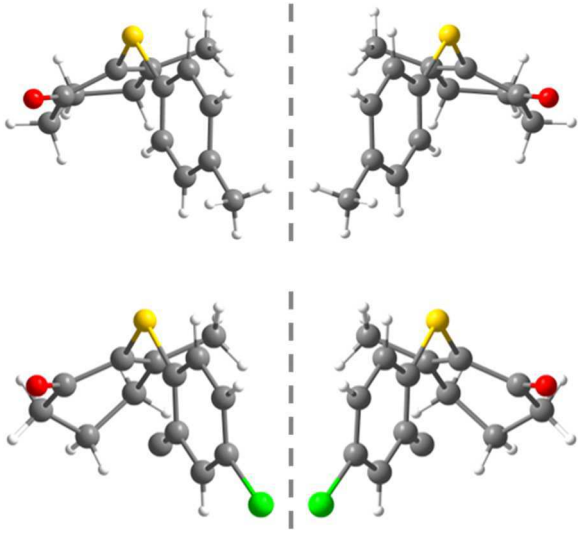

Figure 5. p-Me atropisomers (top) and p-Cl atropisomers (bottom).

An ambiguity exists in the order of the system. According to Ricci[15] "*If two or more homogeneous parts of a heterogeneous system always occur in the same proportions, giving a total mass of constant composition, they constitute together a single phase […]. This is the case, for example, when a solid exists in two optically enantiomorphic forms but is instantaneously and completely racemized in passing through the liquid or dissolved state*". According to this definition, the system is a 2-order system since racemization occurs in the liquid. Nonetheless, as the study involves equilibria in the solid state in which racemization is very slow, we can consider the system as a 4-order system.

Thus, the phase equilibria investigated between the two racemic compositions is a *binary isoplethal section* of a *quaternary system*. To represent this section, there are several ways (Figure 6): the classical isothermal tetrahedral representation, square projections of the tetrahedron, the binary representation and what we called the "extended binary" representation available when no diagonal equilibrium occurs ((+)-p-Me/(-)-p-Cl or (-)-p-Me/(+)-p-Cl).

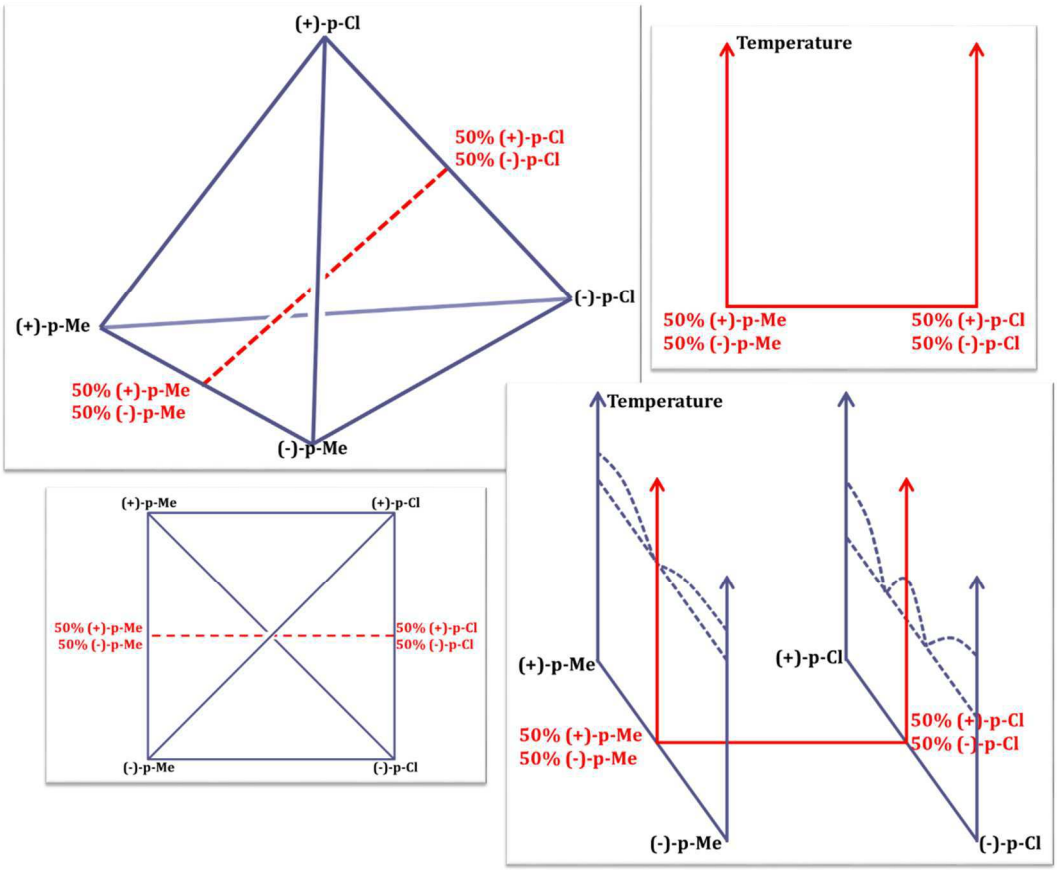

Figure 6. Tetrahedral, one square projection, binary and extended binary representations of the system. Racemic isoplethal section is represented in red.

The racemization of the liquid takes place not only for the pure components but also for all mixtures between the p-Me and the p-Cl components. Thus, there are large composition domains that cannot be explored.

Part.II Results

It has been decided to present the different proportions between the two components in mass fraction of p-Cl (Eq 1.).

$$p - x\%Cl = \frac{m_{p-Cl}}{m_{p-Cl} + m_{p-Me}} * 100 \qquad \text{Eq. 1}$$

Thus, the 1:1 stoichiometry composition between the two components corresponds to *p-51.29%Cl.*

I Initial crystalline structures

I.1 p-Me conglomerate

Several single crystals of p-Me have been easily obtained from solution, by solvent evaporation or by cooling. The use of methanol gave the best crystals but diethyl ether or mixture heptane/dichloromethane can be used as well.

Once the primary nucleation occurs, the compound presents a very good crystallinity and crystals of two morphologies can be obtained (Figure 7). One morphology looks like truncated rods whereas the other presents a more 'contracted' form. In our experiment, rod crystals were the biggest ones with dimensions close to 10mm by 2mm.

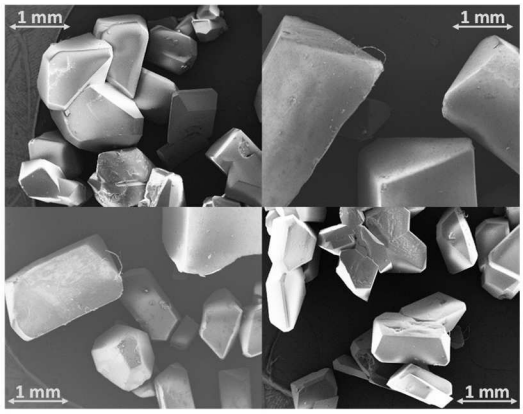

Figure 7. SEM pictures of p-Me crystals.

A single crystal has been isolated and its structure has been determined by X-ray diffraction.

The main crystallographic data are collected in Table 1. The system is orthorhombic with the common chiral space group $P2_12_12_1$ (58% of chiral organic molecules) and the asymmetric unit is $Z' = 1$.

Thus, only one antipode is present in every single crystal and the compound forms a conglomerate noted **O** (**O**rthorhombic). The two mirror image O-p-Me crystals are noted **<O-(+)-p-Me>** and **<O-(-)-p-Me>**.

Table 1. O-p-Me crystallographic data.

Empirical formula	$C_{14}H_{16}OS$
Formula weight	232.33 $g.mol^{-1}$
Temperature	*293.15 K*
Crystal system	*Orthorhombic*
Space group	$P2_12_12_1$ $(n°19)$
Z, Z'	4, 1
a/Å	7.4083 (6)
b/Å	11.4061 (9)
c/Å	14.6281 (11)
α/°	90
β/°	90
γ/°	90
Volume/Å^3	1236.07
d_{calc}/g.cm^{-3}	1.248
F(000) / e$^-$	496
Absorption coefficient μ (MoKα$_1$) / mm^{-1}	0.238
Absolute structure parameter	−0.06 (9)

The molecules establish some interactions from the *para-methyl* moiety toward the centroid of an adjacent phenyl along **a** (≈3.7 Å). These interactions give rise to molecular chains spreading along this direction (Figure 9 & 10). Cohesion between the molecular chains is ensured by mean of weak van der Waals interactions (Figure 10, 11 & 12).

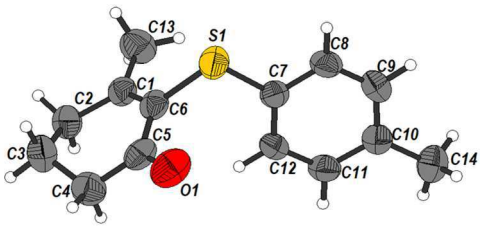

Figure 8. Asymmetric unit in thermal ellipsoidal representation with labelled atoms.

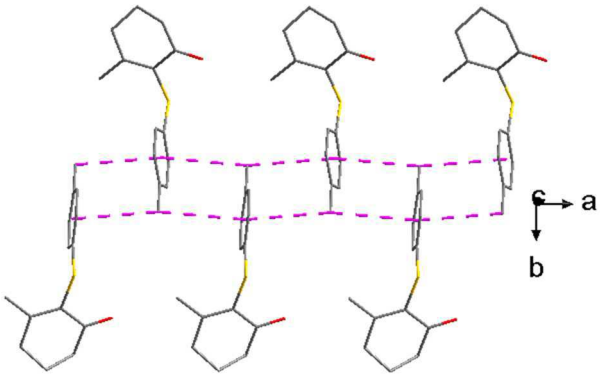

*Figure 9. Interactions (dashed violet) establish from consecutive molecules along **a** leading to molecular chains in this direction.*

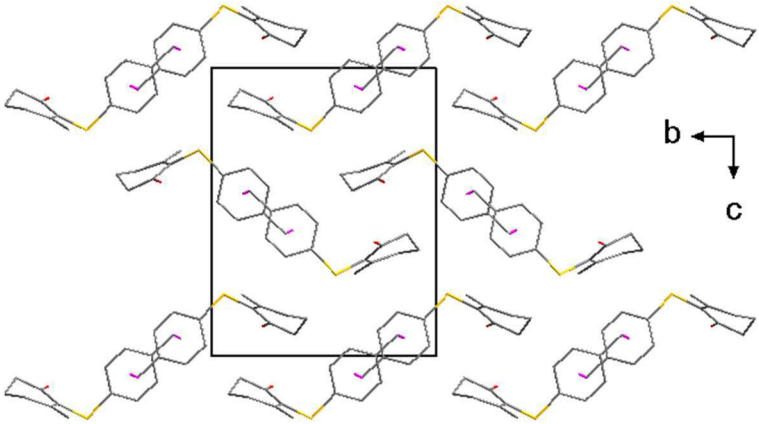

*Figure 10. Projection along **a** direction. Interactions in molecular chains are represented in violet.*

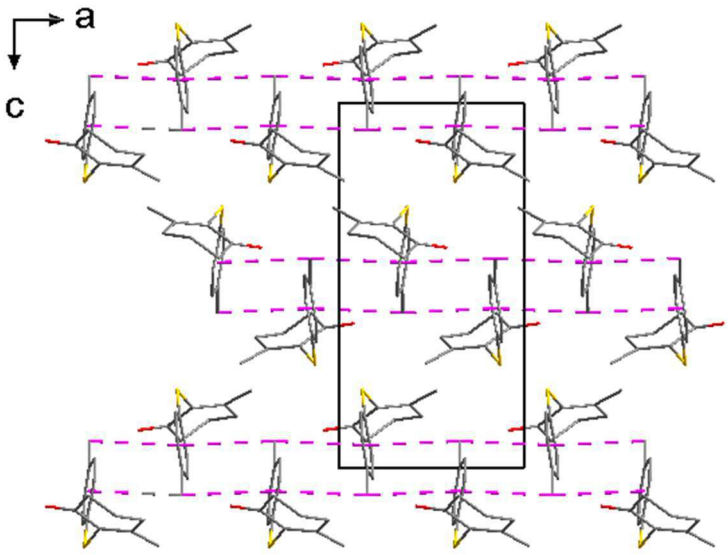

*Figure 11. Projection along **b** direction. Interactions in molecular chains are represented in violet.*

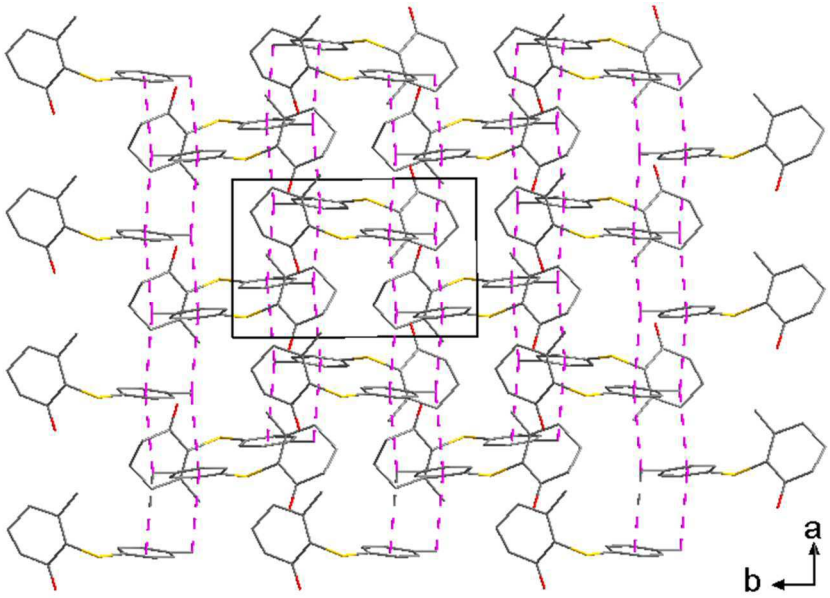

Figure 12. Projection along ***c*** direction*. Interactions in molecular chains are represented in violet.*

The calculated and the experimental diffractograms are given in Figure 13 and match together. It confirms that this crystal structure is representative of the whole batch i.e there is, as far as X-ray diffraction can say, a good structural purity.

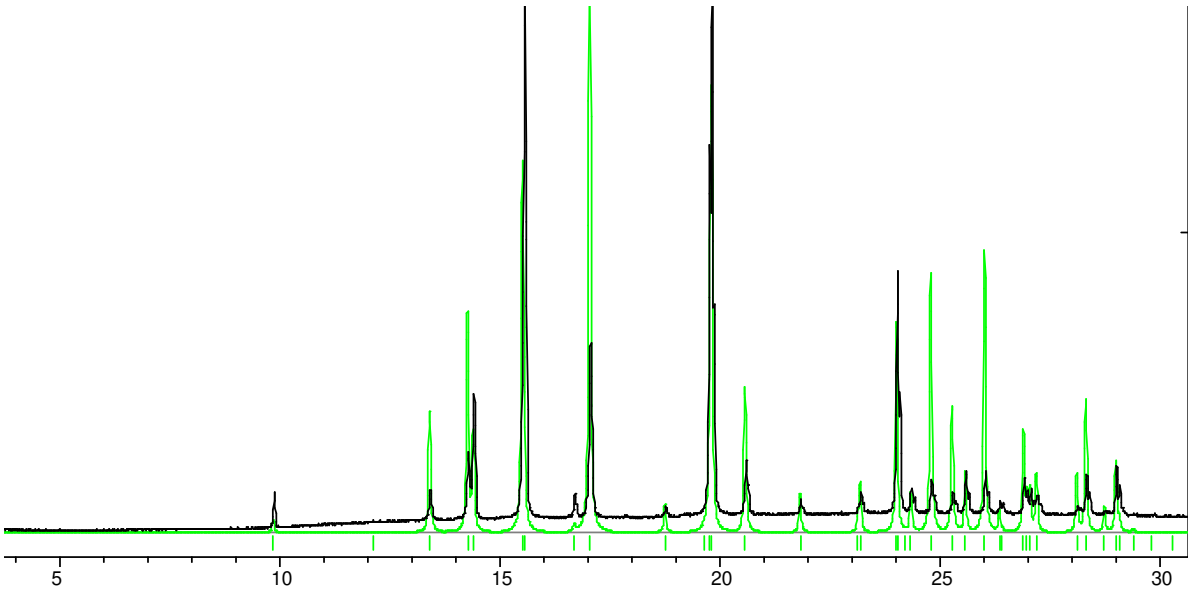

Figure 13. Calculated (green) and experimental (black) diffractograms for O-p-Me.

I.2 p-Cl racemic compound

Likewise, p-Cl single crystals can be easily obtained from methanol solution (evaporation or by cooling) and from other solvents. Two morphologies, one more elongated and the other more contracted, have been observed (Figure 14).

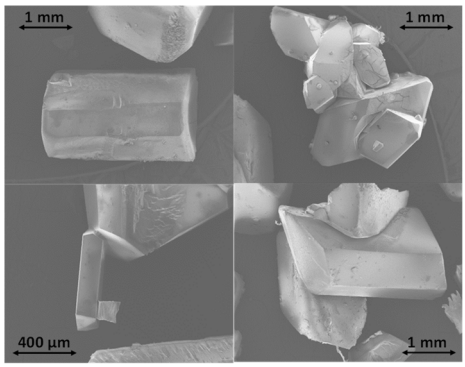

Figure 14. SEM pictures p-Cl crystals.

The structure of p-Cl has been determined from single crystal X-ray diffraction.

The crystallographic data are collected in Table 2. The space group being centro-symmetric, both antipodes are present in equal proportion. As a result, p-Cl crystallizes as a racemic compound noted **T** (**T**riclinic).

The p-Cl crystals are noted **<T-(±)-p-Cl>**.

Table 2. T-(±)-p-Cl crystallographic data

Empirical formula	$C_{13}H_{13}OSCl$
Formula weight	252.74 $g.mol^{-1}$
Temperature	*293.15 K*
Crystal system	*Triclinic*
Space group	$P\bar{1}$ ($n°2$)
Z, Z'	4 , 2
a/Å	7.5800 (10)
b/Å	11.2213 (15)
c/Å	14.975 (2) A
α/°	86.305 (2)
β/°	88.715 (2)
γ/°	75.620 (2)
Volume/Å^3	1231.3 (3)
d_{calc}/g.cm^{-3}	1.363
F(000) / e$^-$	528
Absorption coefficient μ (MoKα_1) / mm^{-1}	0.455
Extinction coefficient	0.232

The asymmetric unit is composed of two molecules of p-Cl noted **MolO** and **MolA** hereafter (Figure 15, 16 & 17). The main difference for these two molecules resides in the torsion angle between the two cycles around the sulfur atom (Figure 17).

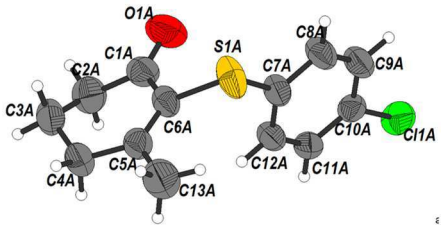

*Figure 15. **MolA** extracted from the asymmetric unit in thermal ellipsoidal representation with labelled atoms. The **MolA** molecules will be display in standard grey in the following figures.*

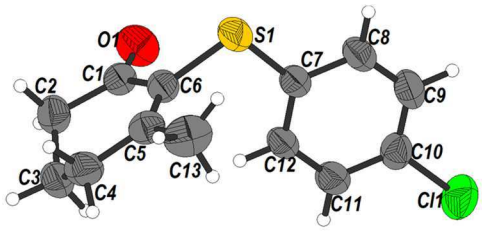

*Figure 16. **MolO** extracted from the asymmetric unit in thermal ellipsoidal representation with labelled atoms. The **MolO** molecules will be display in yellow in the following figures.*

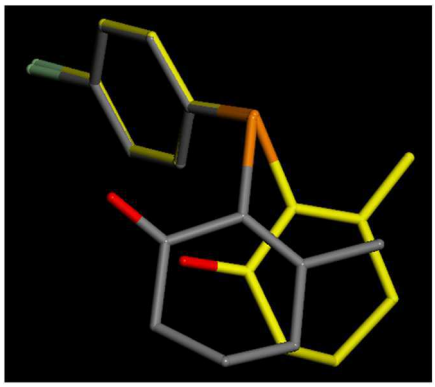

*Figure 17. Superimposition of **MolO** (yellow) and **MolA** (grey).*

The two molecules do not present the same kind of interactions with their neighborhoods. Two adjacent **MolO** along **c** establish ππ interactions (d≈3.8Å) and lead to dimers (Figure 18, 19 & 20). As the **MolA** molecules are intercalated between those dimers, they present weak interactions with their environment (shortest distances are ≈3.7Å but do not involve some ππ or chlorine to π interactions).

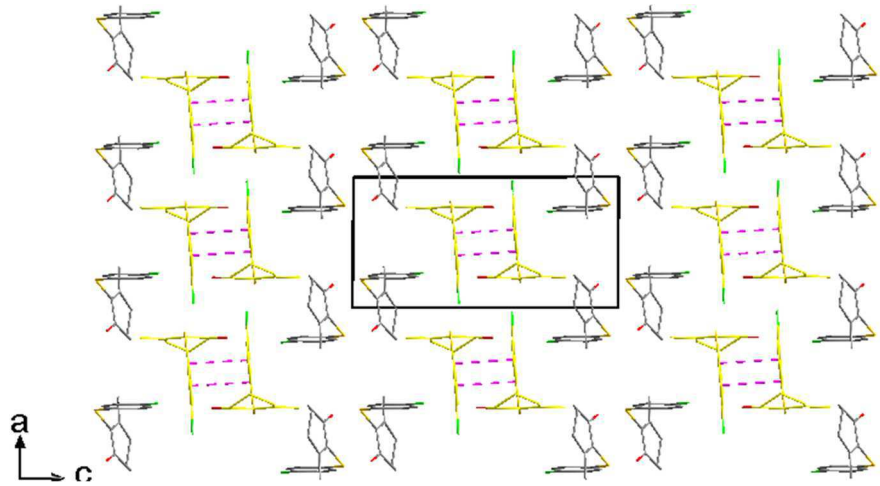

*Figure 18. Projection along **b** axis. The **MolO** molecules establish ππ interactions and give rise to dimers. The **MolA** molecules are intercalated between the dimers.*

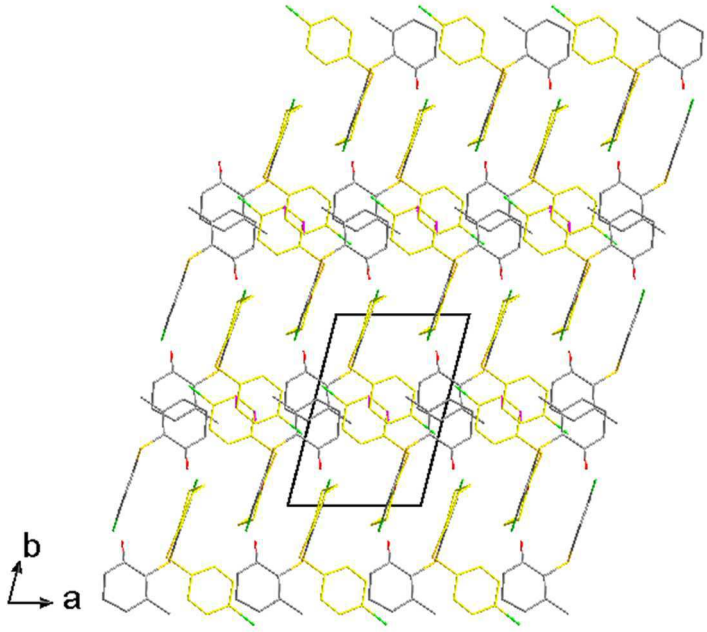

*Figure 19. Projection along **c** axis. The **MolO** molecules establish ππ interactions and give rise to dimers. The **MolA** molecules are intercalated between the dimers.*

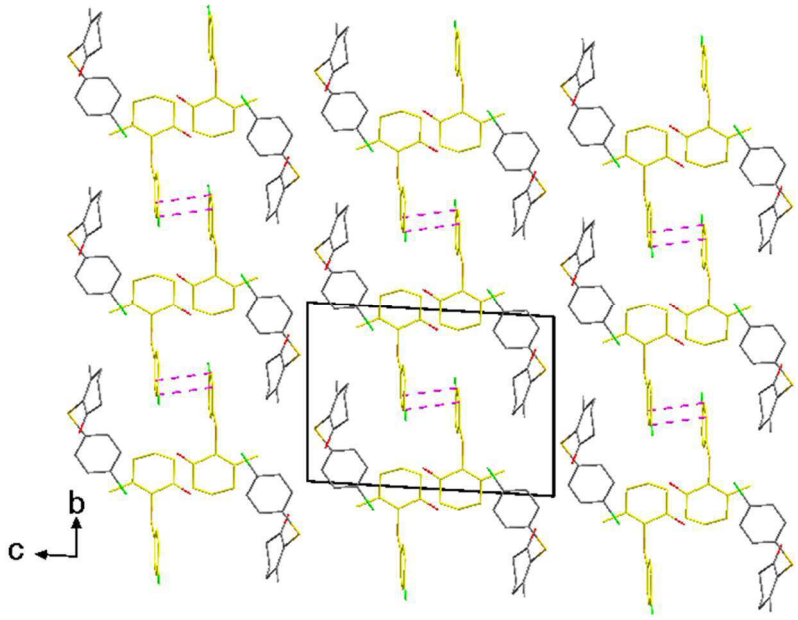

*Figure 20. Projection along **a** axis. The **MolO** molecules establish ππ interactions and give rise to dimers. The **MolA** molecules are intercalated between the dimers.*

The calculated and the experimental powder patterns are given on Figure 21. They match together and confirm the structural purity of the batch.

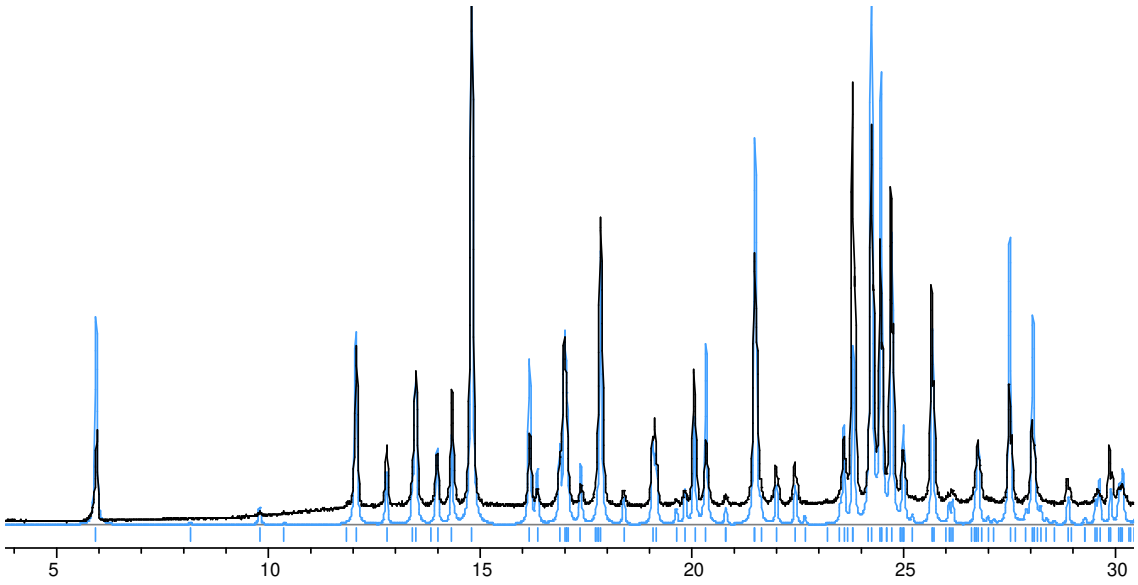

Figure 21. Calculated (blue) and experimental (green) diffractograms of T-(±)-p-Cl.

II Recrystallization issues

It is worth mentioning that in this system, whatever the ratio between p-Me and p-Cl, there is a poor kinetics of recrystallization. This effect has been observed for both the molten state and the dissolved compound, and the higher the p-Cl composition, the slower the recrystallization.

During manipulations performed in solution, a liquid/liquid demixion can be obtained when supersaturation overcomes a certain limit without enhancing the crystallization kinetics (in methanol and mixture heptane/dichloromethane).

By serendipity we observed, in the molten state, that milled glass accelerates by more than two orders of magnitude the nucleation kinetics. Indeed, as illustrated in Figure 22, pure p-Cl samples do not directly recrystallize whatever the cooling rate imposed (2, 5, 10 and 20 K.min^{-1}). Those samples need one or two days at room temperature to ensure the recrystallization.

When glass is added inside the crucible, a complete different behavior is observed since recrystallization occurs during the cooling. Three experiments have been made to characterize this phenomenon. The recrystallization behavior has been tested with: milled sodium borosilicate glass (cover slide), sodium borosilicate glass fragments (three fragments of cover slide) and milled lithium borate glass (Lindemann capillary) in the same mass proportion p-Cl/glass.

According to those tests (Figure 22), the nature of the glass (chemical composition) does not have an impact on the recrystallization kinetics, but the surface area of glass does: recrystallizations occurs at the same point for the two kinds of glass tested but it is slow down when only few fragments are introduced. High surface area of glass (powdered milled glass) and possibly sharp edges prompt primary heterogeneous nucleation.

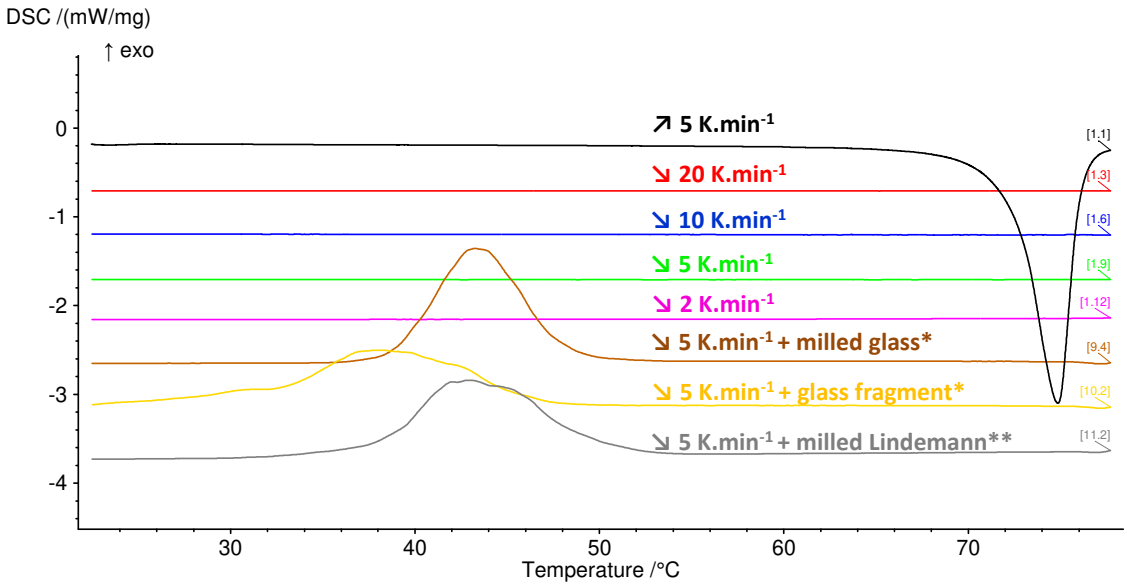

Figure 22. p-Cl first heat and consecutive cooling thermograms at different cooling rates or with glass inside the DSC crucible.

It has also been noticed that the introduction of powdered glass did not change the thermodynamics of the system: the same phase equilibria have been obtained with or without glass inside the system.

III Amorphous behaviors

The temperatures of glass transition have also been determined for both components. An interesting fact is that recrystallization occur after the glass transition with more than 20°C lag.

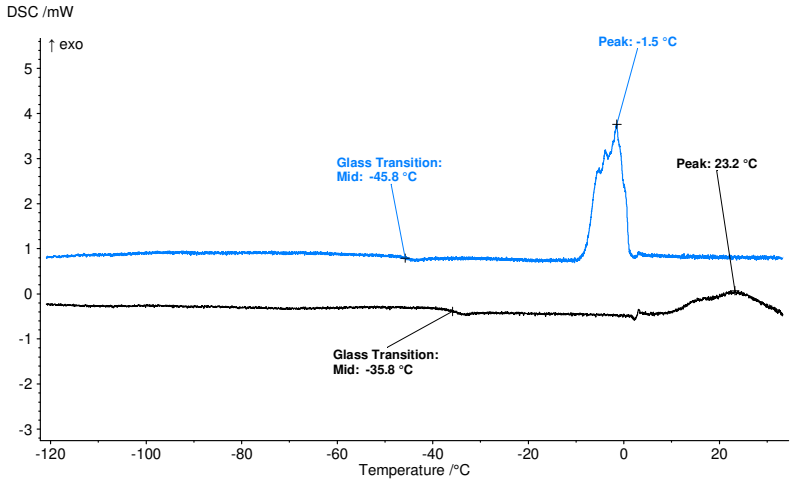

Figure 23. Amorphous p-Me (blue) and p-Cl (black) behaviors.

IV 1st heterogenous equilibrium observed – Simple Eutectic

The first set of thermal and crystallographic analyses were conducted on samples prepared by a manual mixing of different p-Me/p-Cl proportions. After the DSC analyses, samples always recrystallize in another equilibrium and no return to the initial one is possible.

IV.1 X-ray powder diffraction analyses

Diffractograms of the different compositions (Figure 24) are just juxtapositions of T-(±)-p-Cl racemic compound and O-p-Me conglomerate patterns, which was expected according to the way of preparation.

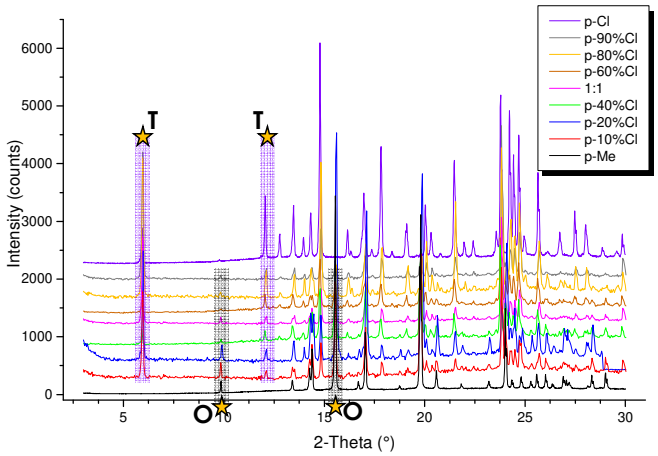

Figure 24. Diffractograms of the different compositions by manual mixing.

IV.2 Differential Scanning Calorimetry analyses

As shown in the Figure 25, thermograms all presented two distinct phenomena (except for the pure components). The first always occurs at 60°C whatever the compositions, even for enriched compositions of p-2.5%Cl and p-97.5%Cl. The second occurs at different temperatures according to the composition: it varies between the two melting points passing through a minimum at around p-60%Cl composition.

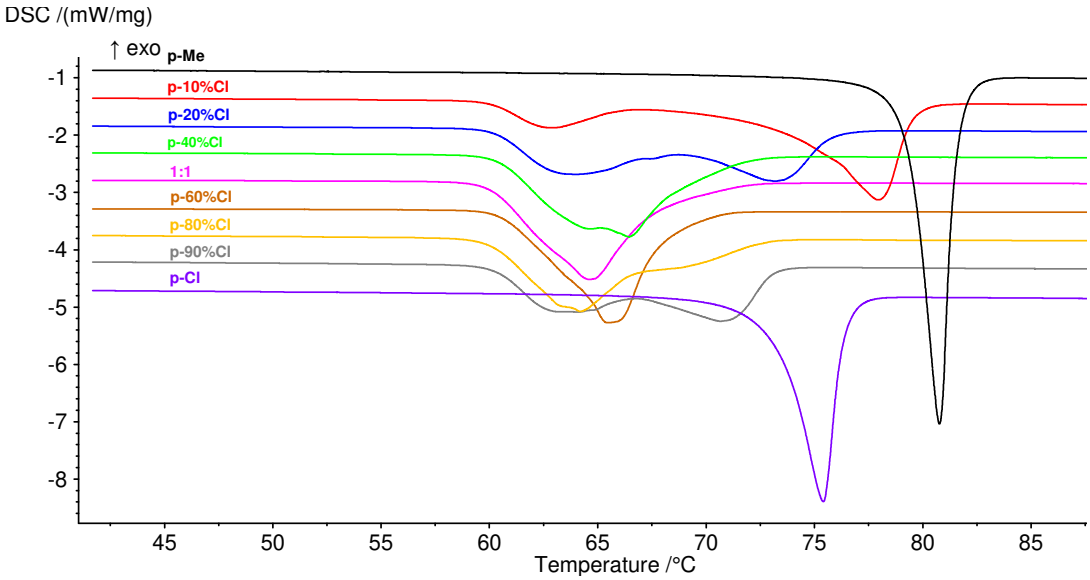

Figure 25. Thermograms of different compositions by manual mixing.

IV.3 Racemic isoplethal section

Plotting the thermal events on the racemic isoplethal section led to the interpretation of a eutectic invariant crossing the whole range of composition (Figure 26).

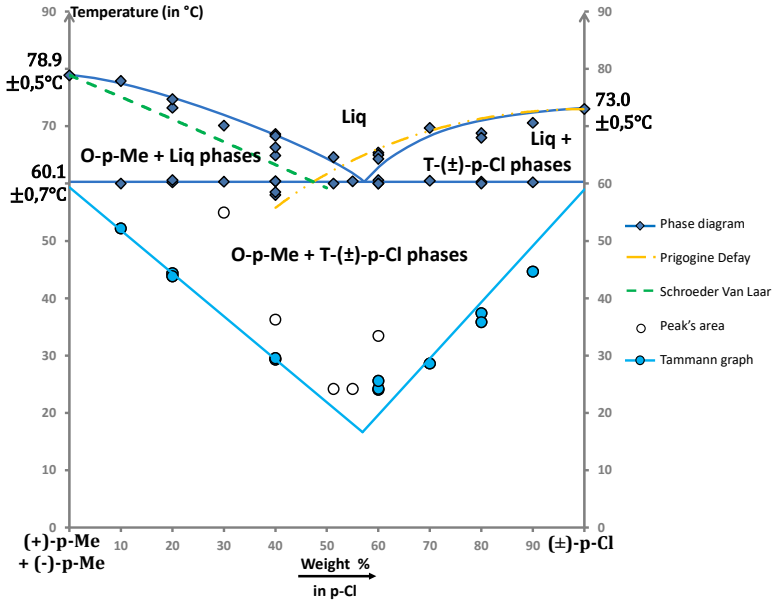

Figure 26. Simple Eutectic equilibrium represented in the racemic isoplethal section. Nature of the phases in equilibrium are indicted only.

The eutectic invariant is at 60.1°C, but the eutectic composition cannot be clearly specified based on the thermograms only. This is why Tammann graph[16,17] and theoretical liquidus curves have been represented. The corresponding models are: Schroeder Van Laar[16–18] simplified equation for **O**-p-Me conglomerate ($T_{fus}^{\boldsymbol{O}-p-Me} = 78.9 \pm 0.5°C$ and $\Delta H_{fus}^{\boldsymbol{O}-p-Me} = +119.3 \pm 0.6\, J/g$) (Eq. 2) and Prigogine Defay[16,17,19] simplified equation adapted to our system ($T_{fus}^{\boldsymbol{T}-p-Cl} = 73.0 \pm 0.5°C$ and $\Delta H_{fus}^{\boldsymbol{T}-p-Cl} = +97.2 \pm 1.5\, J/g$) for T-(±)-p-Cl (Eq 3).

$$ln(X^{O-p-Me}) = \left(\frac{1}{T_{fus}^{O-p-Me}} - \frac{1}{T}\right)\frac{\Delta H_{fus}^{O-p-Me}}{R} \quad \text{Eq. 2}$$

$$ln(4X' * (1 - X')) = \left(\frac{1}{T_{fus}^{T-p-Cl}} - \frac{1}{T}\right)\frac{\Delta H_{fus}^{T-p-Cl}}{R} \text{ with } X' = 100 - 2 * |50 - X^{T-p-Cl}| \quad \text{Eq. 3}$$

We observed that Tammann triangle gives a eutectic composition near 57% and the theoretical liquidus curves partially fit with the experimental ones. Indeed, they intercept at the eutectic temperature (60 ± 0.7°C) but at a lower composition than expected. This difference can be explained by the fact that those equations are usually used for binary systems only and that the $\Delta Cp_{liq-sol}$ have not been considered.

V 2nd heterogeneous equilibrium observed – Partial Solid Solutions

A second type of equilibrium, totally different but repeatable several times, has been obtained with recrystallized samples.

Those samples have been obtained either from previous molten samples or from solvent evaporation (methanol, diethyl ether or dichloromethane/heptane mixture).

V.1 Differential Scanning Calorimetry analyses

In Figure 27 are presented the thermograms for different compositions of recrystallized molten samples. Two thermal events can be easily distinguished for each composition (except for p-65%Cl and the pure components):

- For the first event, one can observe that an invariant at 50°C seems to be reached around the p-55%Cl composition. Otherwise, the temperature of the first event evolves from this invariant to the melting point of the components.
- Second thermal events vary from one melting point to the other *via* a minimum reached around p-55%Cl.

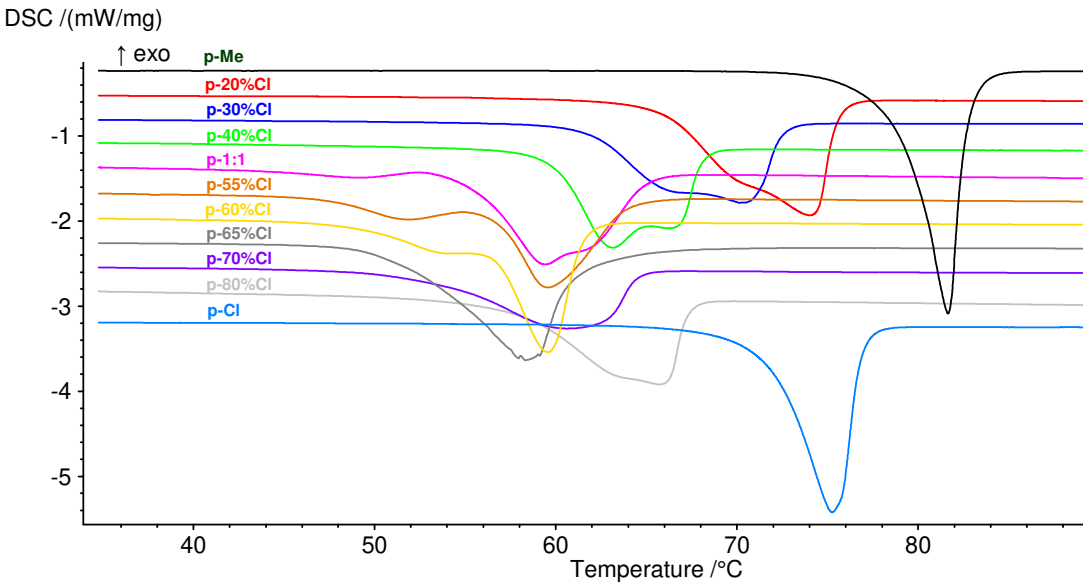

Figure 27. Thermograms of different compositions obtained by recrystallization.

V.2 X-ray powder diffraction analyses

X-ray powder diffraction patterns of those samples are consistent with the DSC measurements.

In Figure 28 where they are represented, two pieces of information can be extracted:

- The first one is the similarity of the patterns with the initial products. Indeed, recrystallized p-Cl presents the exact same pattern as the initial one, i.e T-(±)-p-Cl. The patterns observed for the recrystallized p-Me up to p-40%Cl are the same as the initial p-Me, i.e O-p-Me, except that two peaks disappear (at 10° and 16.7°). It

suggests that this equilibrium involves almost the same T-(±)-p-Cl phase and a very similar O-p-Me phase.

- When the evolution of the XRPD patterns versus composition are compared, it is likely that there are partial solid solutions. Indeed, one can notice that the compositions can be associated with a succession of one pattern/two patterns/one pattern:
  - From pure p-Me up to p-40%Cl, only the similar O-p-Me XRPD pattern (without the 10° and 16.7° peaks) has been obtained.
  - From p-40%Cl to p-70%Cl, a juxtaposition of the similar O-p-Me and of the T-(±)-p-Cl patterns have been obtained. The lower the p-Cl composition, the lower the T-(±)-p-Cl peak intensities and the higher the O-p-Me Bragg peaks.
  - For compositions greater than p-70%Cl, only the XRPD pattern of the T-(±)-p-Cl has been obtained.

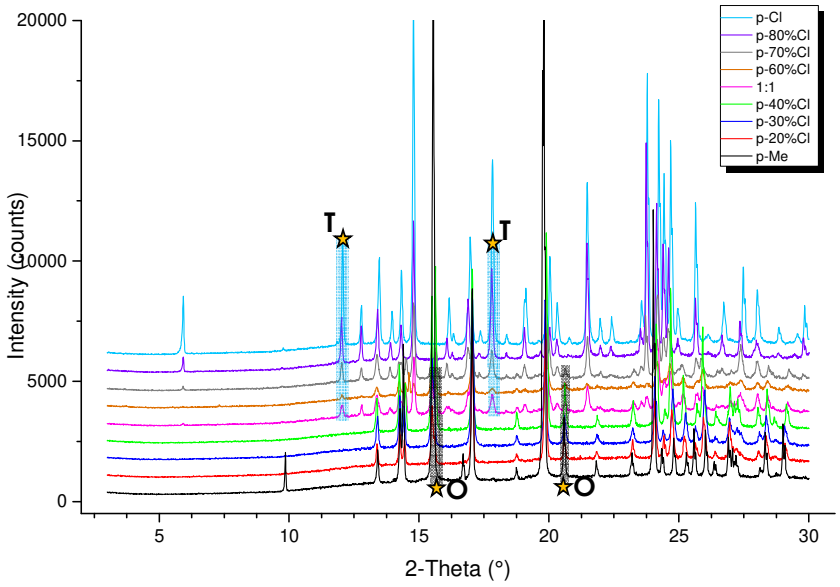

Figure 28. Diffractograms of different compositions obtained by recrystallization.

Combining DSC and XRPD data, partial solid solutions and a eutectic invariant can be proposed.

V.3 Single Crystal X-ray Diffraction

To confirm this interpretation, single crystals grown from different compositions have been analyzed by X-ray diffraction.

The investigated compositions in p-Cl were: 20, 40, 60, 80 and 90%. Among those compositions, different single crystals presenting different structures have been collected, giving the final proof of the formation of two partial solid solutions.

The results for each partial solid solution would be presented separately.

V.3.1 Orthorhombic O-p-Me partial solid solution

From the global p-20, 40 and 60%Cl compositions, single crystals presenting partial solid solutions of the O-p-Me structure have been extracted.

Their crystallographic data are presented in the Table 3:

Table 3. Crystallographic data of O-p-Me partial solid solution single crystals.

Pool composition	Pure p-Me	p-20%Cl	p-40%Cl	p-60%Cl
Crystal composition	**0%Cl**	**≈17%Cl**	**≈40%Cl**	**≈46%Cl**
Crystal system	*Orthorhombic*	*Orthorhombic*	*Orthorhombic*	*Orthorhombic*
Space group	$P2_12_12_1$ ($n°19$)	$P2_12_12_1$ ($n°19$)	$P2_12_12_1$ ($n°19$)	$P2_12_12_1$ ($n°19$)
Z, Z'	4, 1	4, 1	4, 1	4, 1
a/Å	7.4083 (6)	7.426 (1)	7.4444 (7)	7.4634 (6)
b/Å	11.4061 (9)	11.386 (2)	11.364 (1)	11.3498 (9)
c/Å	14.6281 (11)	14.610 (3)	14.571 (2)	14.5526 (11)
Volume/Å^3	1236.07	1235.2 (4)	1232.6 (2)	1232.72 (17)
d_{calc}/g.cm^{-3}	1.248	1.297	1.292	1.306
F(000) / e$^-$	496	513	508	512
Absorption coefficient μ (MoKα_1) / mm^{-1}	0.238	0.293	0.317	0.345
Absolute structure parameter	−0.06 (9)	0.06 (1)	0.05 (10)	-0.05 (11)

The **a** parameter increases with the p-Cl composition, whereas both **b** and **c** parameters decrease. As a result, a contraction of the unit cell is observed.

In those crystals, the asymmetric unit is composed of one molecule with a SOF factor corresponding to the global composition (Figure 29). The carbon **C14** and the chlorine atom share the same fractional coordinates due to the partial substitution of the p-Me molecule by

the p-Cl molecule. Therefore, the p-Cl molecule adopts the conformation of the host molecule: p-Me.

The packing of the molecule within the crystal is also quite similar to O-p-Me (Figure 30). Along **a** axis, π interactions (≈3.7 Å) exist with the neighboring methyl group or the chlorine atom.

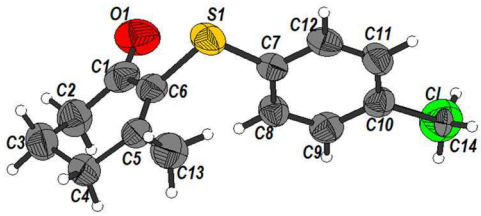

Figure 29. Disordered asymmetric unit in thermal ellipsoidal representation with atom labelled. The para position is occupied with ≈60% of methyl group and ≈40% of chlorine atom (40%Cl crystal).

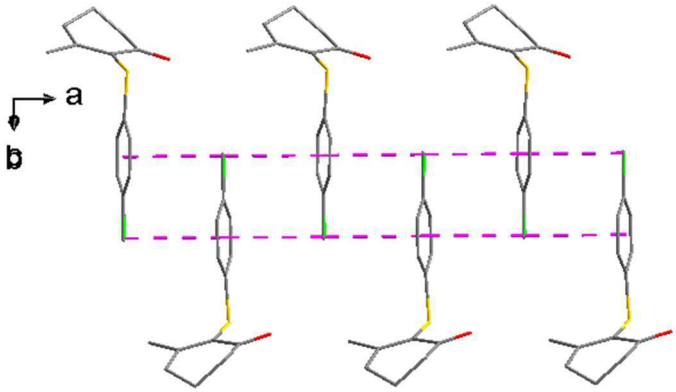

*Figure 30. Molecular chains along **a** in the 40%Cl crystal. Interactions (dashed violet) can be π/methyl or π/chlorine, the last kind enlarge the average length to ≈3.7 Å and might be stronger.*

Concerning the patterns some differences are present, even if the single crystals preserve the same symmetry. Even though the ticks stay present, the peaks at 10° and 16.7° of the pure O-p-Me vanish in the partial solid solution, which agree well with the experimental XRPD patterns.

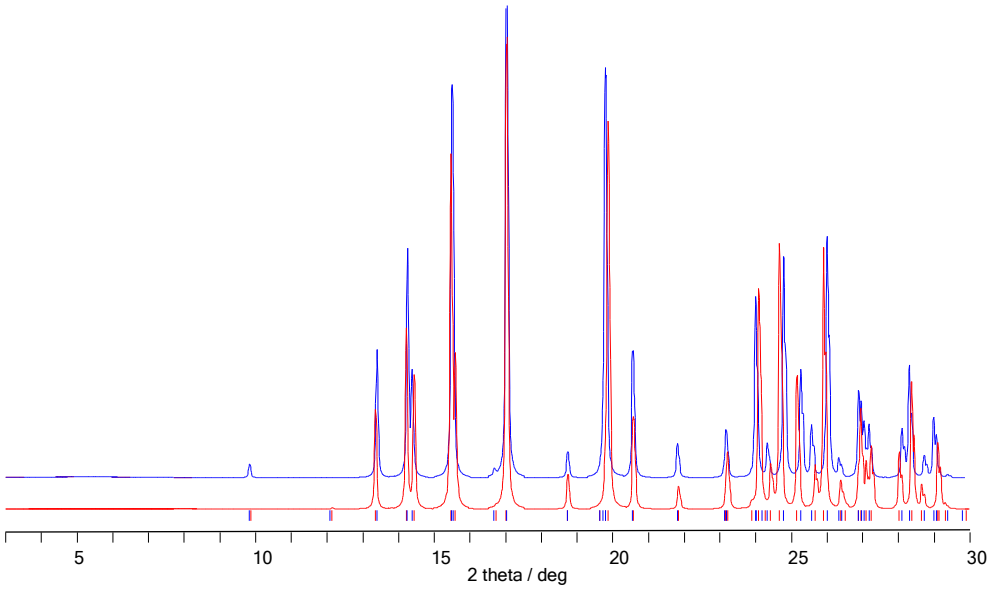

Figure 31. Calculated XRPD pattern for pure O-p-Me (blue) and for ss(O-p-40%Cl) (red).

V.3.2 Triclinic T-p-Cl partial solid solution

Single crystals corresponding to a partial solid solution at enriched p-Cl compositions have also been analyzed. They have grown from p-60, 80 and 90%Cl solutions and their resolutions have been more complex.

During the refinement, both space group $P\bar{1}$ and $P1$ have been tested. The first was chosen due to the similarity with the T-(±)-p-Cl cell parameters but the occupancy factors of the chlorine atoms and methyl group (Z'=2) were difficult to stabilized. *A contrario*, when the crystals have been resolved in $P1$, refinement could be applied molecule by molecule (Z'=4).

To confirm it, SHG measurements of recrystallized p-Cl, p-95%Cl and p-90%Cl have been performed. Whereas p-Cl was, as expected, SHG negative (centrosymmetric space group), recrystallized p-90%Cl and p-95%Cl samples generated second harmonic signals, confirming the $P1$ refinement and the non-centrosymmetry of the partial solid solution.

Below are presented the crystallographic data of single crystals obtained from different compositions:

Table 4. Crystallographic data of T-p-Cl partial solid solution single crystals.

Pool composition	Pure p-Cl	p-90%Cl	p-80%Cl	p-60%Cl
Crystal composition	**100%Cl**	**91%Cl**	**86%Cl**	**79%Cl**
Crystal system	*Triclinic*	*Triclinic*	*Triclinic*	*Triclinic*
Space group	$P\bar{1}$ $(n°2)$	$P1$ $(n°1)$	$P1$ $(n°1)$	$P1$ $(n°1)$
Z, Z'	4 , 2	4 , 4	4 , 4	4 , 4
a/Å	7.580 (1)	7.585 (1)	7.590 (1)	7.5992 (6)
b/Å	11.221 (2)	11.249 (1)	11.252 (2)	11.2677 (10)
c/Å	14.975 (2)	15.005 (2)	15.011 (2)	15.0357 (13)
α/°	86.305 (2)	86.152 (2)	86.201 (3)	86.013 (2)
β/°	88.715 (2)	88.844 (2)	88.768 (3)	89.003 (2)
γ/°	75.620 (2)	75.728 (2)	75.717 (3)	75.859 (2)
Volume/Å^3	1231.3 (3)	1238.0 (2)	1244.1 (3)	1245.41 (18)
d_{calc}/g.cm^{-3}	1.363	1.348	1.333	1.348
F(000) / e$^-$	528	526	523	528
Absorption coefficient μ (MoKα_1) / mm^{-1}	0.455	0.436	0.419	0.450
Absolute structure parameter		-0.05 (15)	-0.07 (13)	0.34 (14)

The asymmetric unit is composed of four molecules (Figure 32). The packing and the different molecular conformations are similar to that of the pure T-(±)-p-Cl.

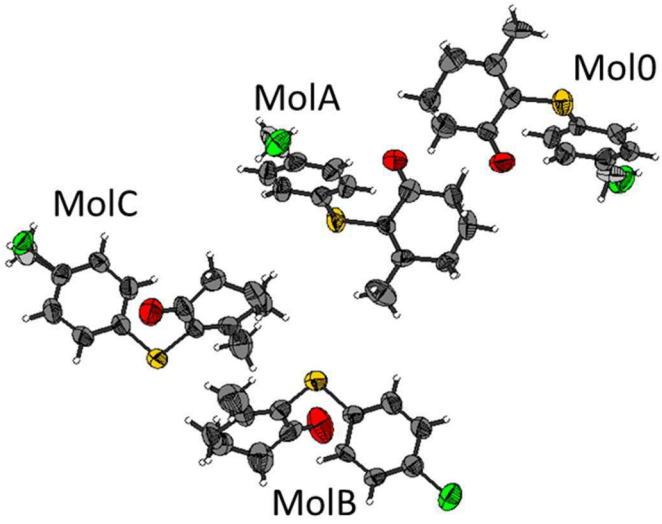

Figure 32. Asymmetric unit of 91%Cl crystal (Z'=4).

The distribution of the methyl group/chlorine atom is specific for the four positions. If three molecules exhibited logical *Statistical Occupancy Factor* (*sof*) lower than 100% for the chlorine atoms, the fourth (fixed as **MolB** here) remained occupied by chlorine atoms only ($sof_{MolB}^{p-Cl} = 100\%$).

According to this dissymmetry of distribution, it appears that the inversion center is lost when a fraction of p-Me molecule substitutes p-Cl molecule in the triclinic T structure. Even though the genuine center of symmetry disappears, a pseudo inversion center stays present in the crystal (Figure 33).

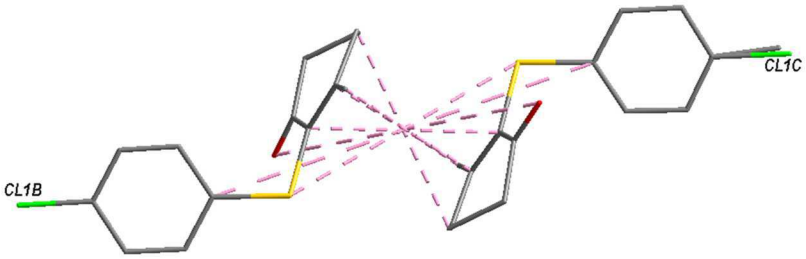

*Figure 33. Representation of the pseudo inversion center (dashed line intersection) existing between **MolB** ($sof_{MolB}^{p-Cl} = 100\%$) and **MolC** ($sof_{MolC}^{p-Cl} = 88\%$).*

The calculated pattern for the partial solid solution perfectly match with the experimental one and the pure T-(±)-p-Cl (Figure 34).

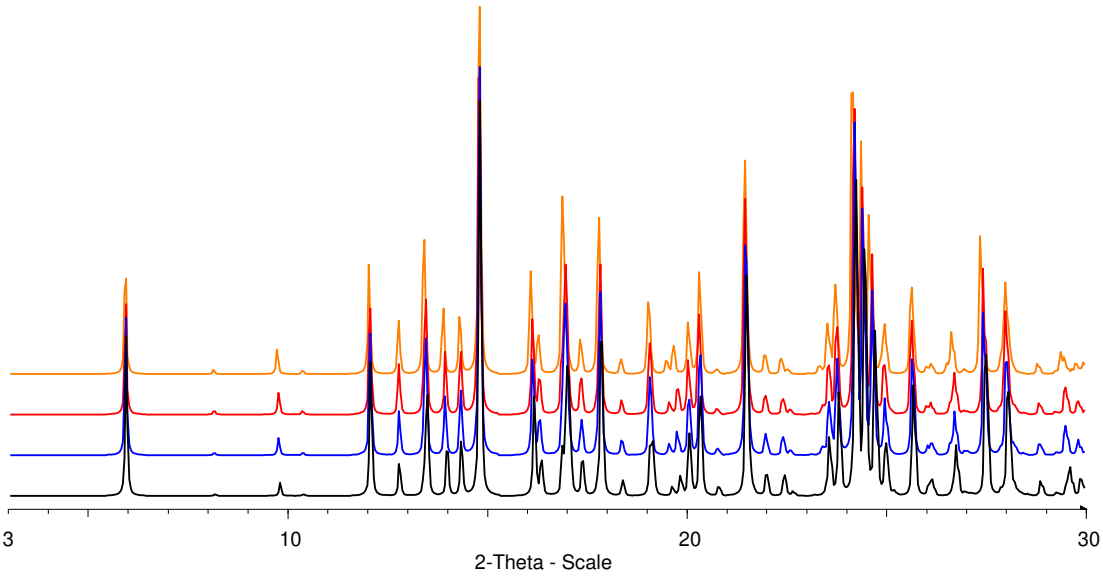

Figure 34. Calculated pattern for T-(±)-p-Cl (black) and the partial solid solution structures obtained from pools at p-90%Cl (blue), p-80%Cl (red) and p-60%Cl (orange).

V.4 Racemic isoplethal section

When the DSC signals are plotted and linked to the different crystallographic data, a racemic isoplethal section can be drawn as in Figure 35.

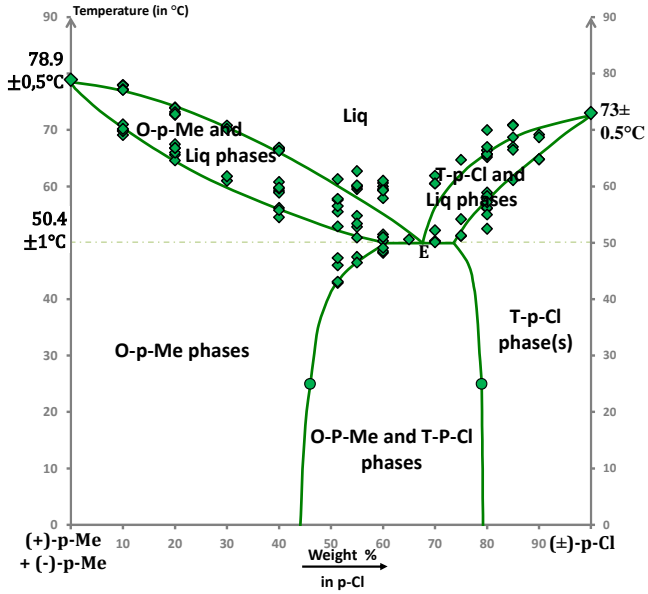

Figure 35. Partial Solid Solution equilibrium represented in the racemic isoplethal section. Nature of phases are indicated only.

The equilibrium observed corresponds to partial solid solutions with a eutectic invariant. The partial solid solutions are present on each side of the section (p-Cl incorporated in O-p-Me and p-Me in T-p-Cl structures) and the eutectic invariant is observed at 50.4°C between 60%

and 74% compositions. The eutectic composition cannot be determined accurately and it is approximated at circa 67% p-Cl composition.

VI 3rd heterogeneous equilibrium observed – Complete Solid Solutions

Another equilibrium has been sometime observed when the molten samples recrystallized. Indeed, molten p-80%Cl, p-85%Cl and p-90%Cl can spontaneously recrystallize adopting the O-p-Me solid solutions.

These solid solutions have also been observed by seeding molten p-Cl with O-p-Me and so belong to the complete solid solutions equilibria.

VI.1 X-ray powder diffraction analyses

As illustrated in the Figure 36, two kinds of samples presenting this complete solid solutions equilibrium have been observed:

- Samples only presenting the orthorhombic O-p-Me pattern.
- Other samples of the same compositions presenting both O-p-Me and T-p-Cl patterns.

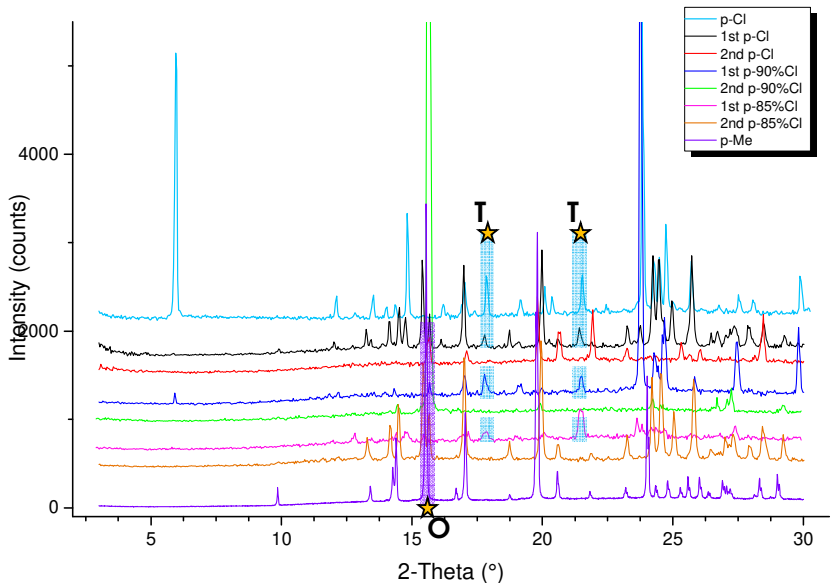

Figure 36. Diffractograms of the samples presenting only the orthorhombic pattern or both orthorhombic/triclinic patterns in the complete solid solutions equilibrium.

VI.2 Differential Scanning Calorimetry analyses

The DSC performed on the previous samples are presented in Figure 37. A first endothermic phenomenon around the 50°C occurs and is directly followed by an exothermic one. Then, the samples finally melt respecting the partial solid solutions equilibrium temperatures.

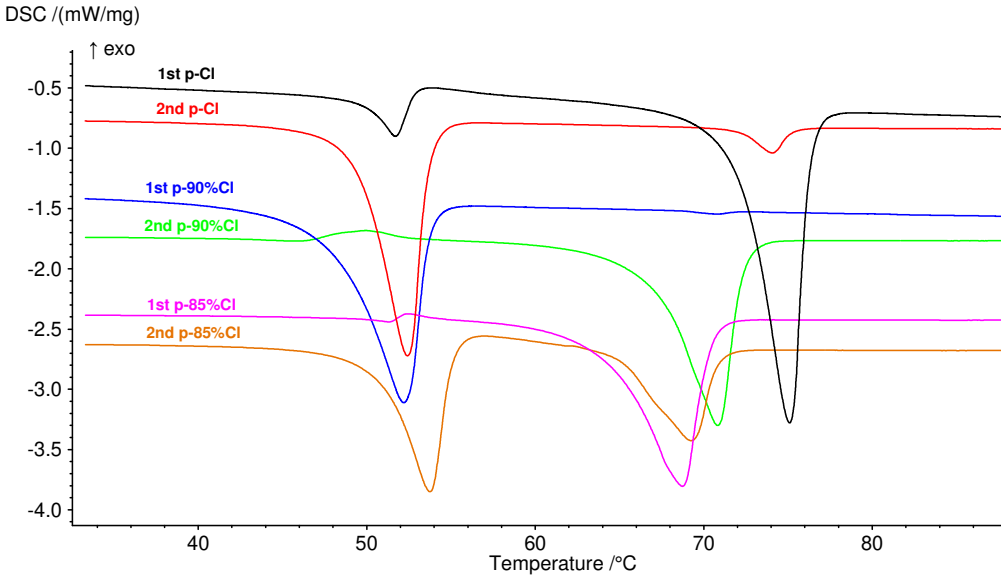

Figure 37. Thermograms of different compositions obtained by recrystallization or O-p-Me seeding.

VI.3 HS-microscopy experiments

One sample presenting this behavior has been analyzed *via* HS-microscopy. Upon the heating (Figure 38), a reorganization of the crystals has been observed at around 50°C. This reorganization is difficult to illustrate with pictures only, but the video clearly showed a partial melt and recrystallization of the sample between 46.5 and 52°C. After that event, the system did not evolve anymore up to its complete melting.

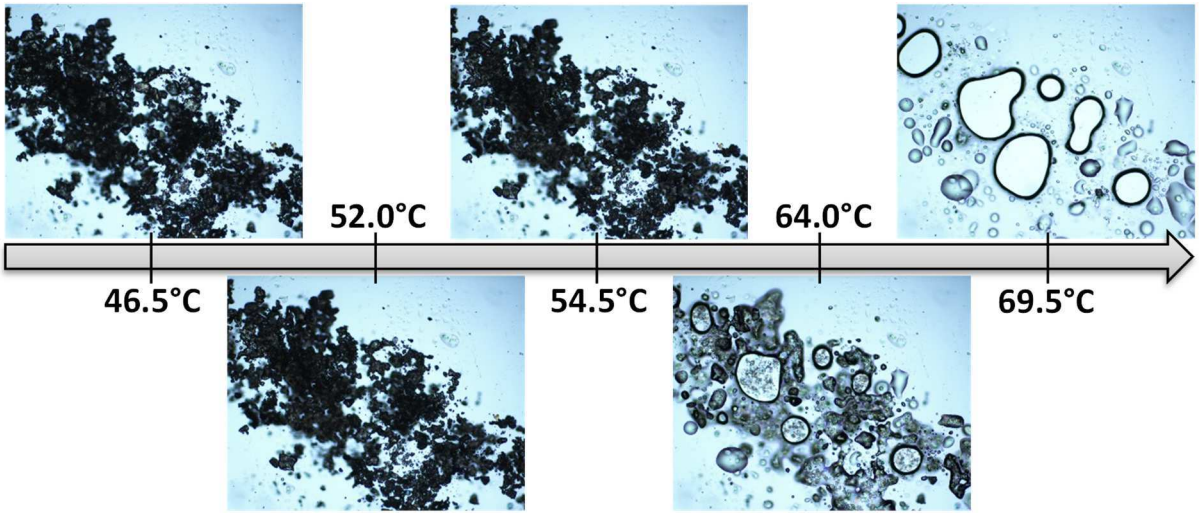

Figure 38. HS-microscopy result of p-80%Cl presenting the Complete Solid Solution behavior heated at 5 K.min^{-1}.

From this experiment, the interpretation of the DSC curves is no longer uncertain: the first endothermic events observed correspond to the melting of the O-p-Me complete solid solutions. Then, the sample recrystallized into the partial solid solutions p-Cl to reach a more stable equilibrium during the exothermic phenomena.[20–22]

VI.4 Racemic isoplethal section

This complete solid solutions equilibrium is represented in the Figure 39. Being metastable and the continuity of the O-p-Me partial solid solutions, its liquidus and solidus have been extrapolated to fit with the additional DSC data.

The melting temperature for the metastable p-Cl orthorhombic phases is 52.4°C and the complete solid solutions present a congruent minimum point **C** at 47.5°C and 77.2% in p-Cl.

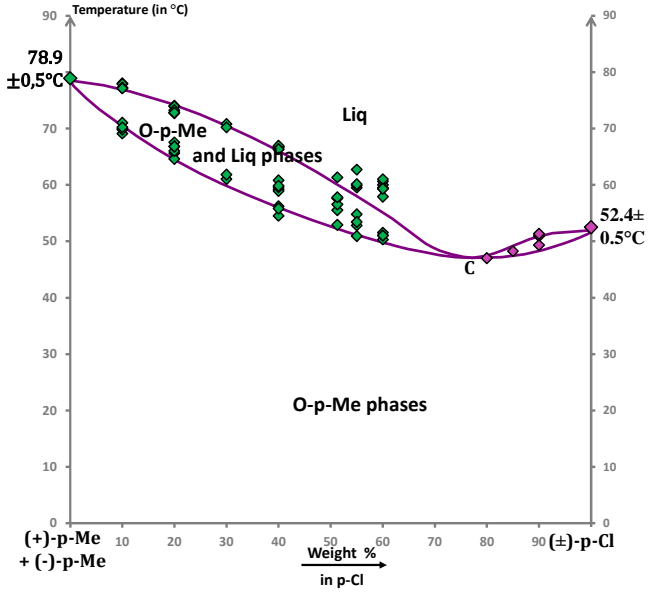

Figure 39. Complete Solid Solutions equilibrium represented in the racemic isoplethal section. Nature of phases are indicated only.

VII Relative stability of the three different equilibria

Three different equilibria can be reached for this system. Except by single crystal X-ray analyses (with significant Flack parameters), we are in the impossibility to check the composition in each atropisomers of the two compounds. Thus, two hypotheses can be proposed to justify their coexistences:

- The first hypothesis that can be proposed is that the system is no longer at the racemic isoplethal section. Indeed, one can argue that a first homochiral cluster can result in the apparition of an enantiomeric excess in the solid state. Thus, the equilibria presenting the solid solutions should be representative of a partial or even full deracemized system. Nonetheless, this hypothesis seems unlikely for two reasons:
    - Single crystals presenting two opposites configurations have been obtained and analyzed from the same sample.

- A phase diagram combining the racemization in solution, a racemic simple eutectic equilibrium and deracemized partial solid solutions equilibria cannot be drawn.

- The other hypothesis is that the equilibria are at three different level of stability.

VII.1 Complete solid solutions equilibrium metastability

In addition to the DSC and HS-microscopy analyses performed on the complete solid solutions equilibrium, Figure 40 presents other observations to conclude on the relative stability of this equilibrium.

Diffraction and thermal analyzes have been performed on a complete solid solutions sample after its melting/recrystallization at 50°C. After this recrystallization, only the triclinic T pattern is observed and the melting respects the same equilibrium.

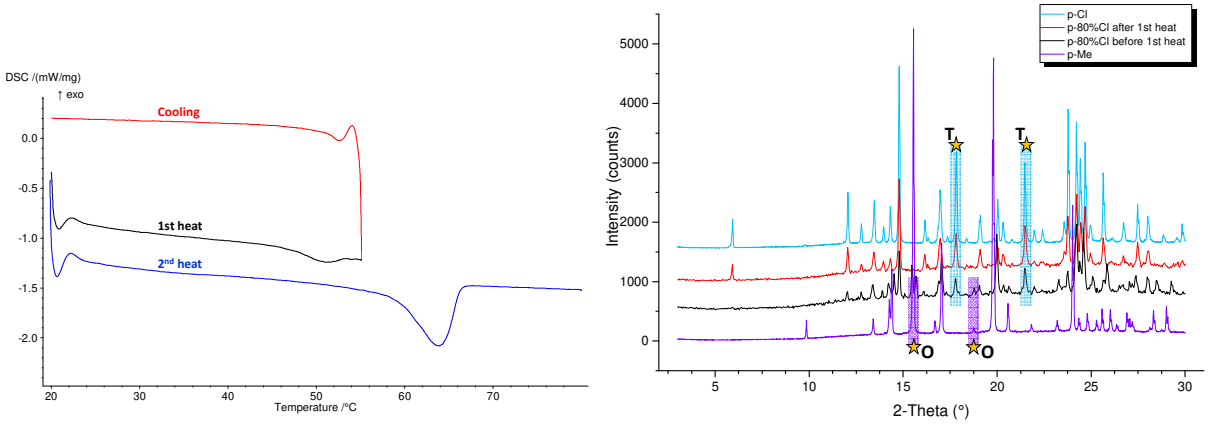

Figure 40. XRPD (right) and DSC (left) analyzes performed on a p-80%Cl complete solid solutions samples.

All those results point out that the complete solid solutions equilibrium is metastable compare to the partial solid solutions equilibrium.

VII.2 Stable partial solid solutions equilibrium

Difficulties have been encountered concerning the relative stabilities of the two other heterogeneous equilibria.

To check their relative stabilities, several annealings have been tested. They have been performed on samples respecting both equilibria, for different compositions, time and temperatures.

All of them but one failed since no transition from one equilibrium to the other has been recorded.

The common point of the failures was that the annealings involved solid phases only, contrary to the successful one in which the transition was accelerated by the partially molten sample.

This annealing has been monitored by Hot Stage-microscopy (Figure 41). A p-20%Cl sample prepared by manual mixing (and so respecting the simple eutectic behavior) has been heated at 62°C. The eutectic invariant being overpassed, the sample was partially molten. Then, the temperature has been kept constant for almost a week. After two days, the sample slowly recrystallized: the liquid disappeared to give rise to crystals of good morphology. The phase transition was completed after 132 hours.

A long XRPD acquisition (12H) confirmed that the samples obtained after this annealing was only composed of the orthorhombic O-p-Me partial solid solutions.

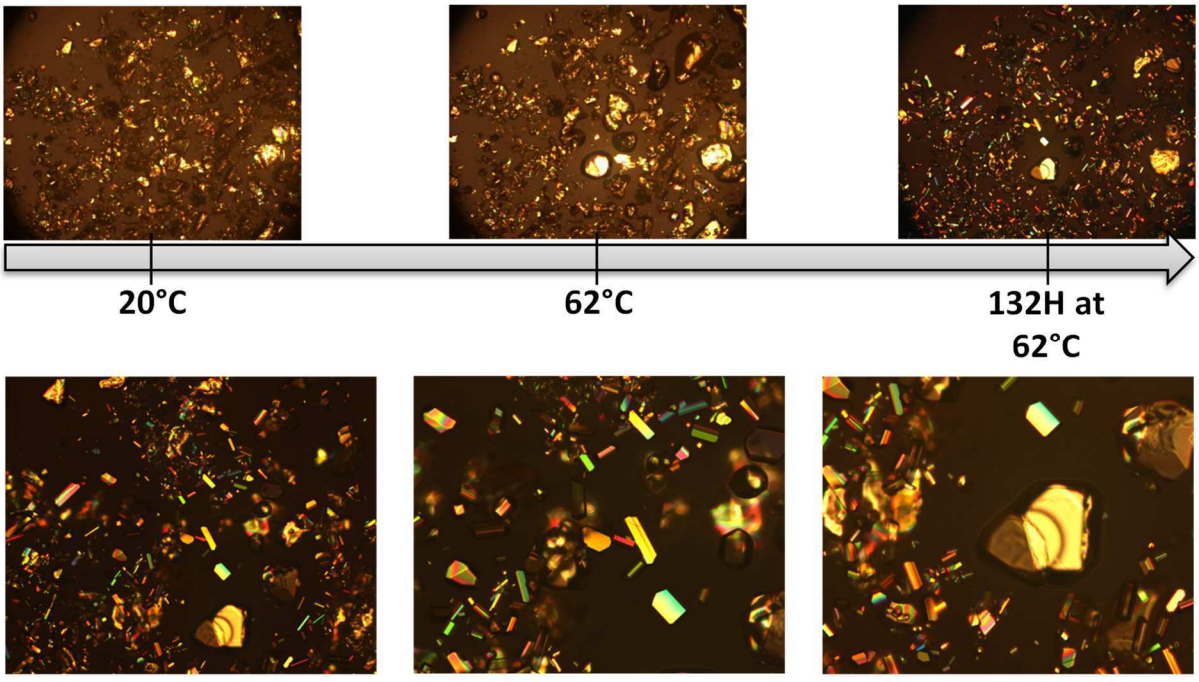

Figure 41. Top: HS-microscopy result of p-20%Cl preparing by manual mixing with annealing at 62°C. Bottom: magnified pictures after the 132H of annealing.

The conclusion of this experiment is that the partial solid solutions equilibrium corresponds to the stable state (Figure 42). This result was unexpected since the temperatures observed for the mirror image partial solid solutions equilibrium are lower than that of the simple eutectic.

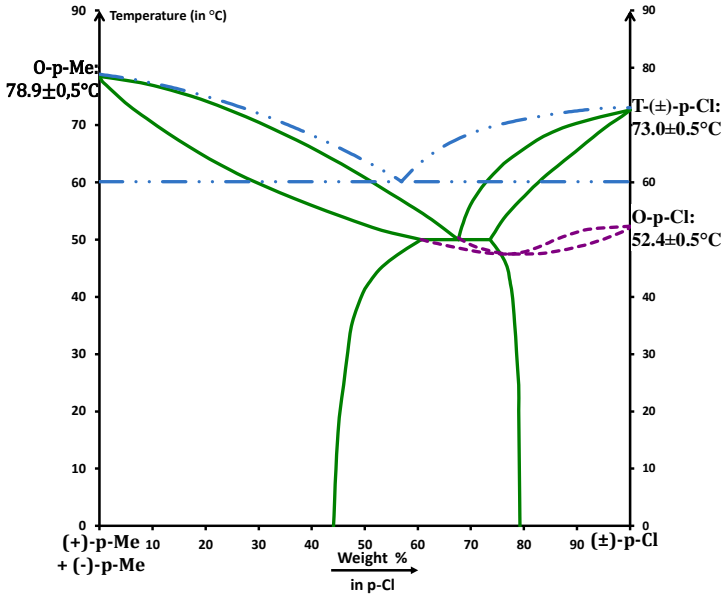

Figure 42. The three different equilibria represented in the racemic isoplethal section.

Part.III Discussion

I Apparent simple eutectic equilibrium

First issue to be discussed is the simple eutectic equilibrium and the thermodynamic impossibility for the same phases to exhibit different liquidus curves.

As presented in Figure 42, different liquidus have been obtained for the two components in the different equilibria. If this difference of liquidus in the p-Cl part could be justified since it present different structure ($P\bar{1}$ or $P1$), the same cannot be applied to the p-Me part. For this one, it is the exact same crystal structure that forms solid solutions and present different liquidus.

In order to reconciliate these two opposite facts, two explanations can be proposed:

- *The two liquidus are in fact one and unique.* Indeed, the two curves are similar, the difference being mainly induced by the eutectic composition deduced from the Tammann graph.
- *The simple eutectic is an apparent equilibrium.* That means that any physical mixture of the pure components is out of equilibrium and will irreversibly evolve to the partials solids solutions just by diffusion in the solid state. Unfortunately, this process is very slow, even if long annealings are applied.

II On the dissymmetry of distribution and a possible new kind of chirality

The loss of symmetry in the triclinic T-p-Cl partial solid solutions has another unexpected effect.

When the p-Me is incorporated inside the triclinic structure, none of p-Me and p-Cl molecules present homogeneous distribution, nor even symmetrical *sof* (Statistical Occupancy Factor) in the different positions. As a result, the inversion center vanishes but a pseudo-inversion center remains since the configurations (***(+)*** or ***(-)***) and the conformations (**Γ** or **γ**) of the four positions are maintained (Figure 43).

The dissymmetry of distribution on the *sof* results in an unbalance of the two configurations for the two components. The Optical Purity (O.P) for each component can be calculated using Eq. 4. The values for the different single crystals are presented in Table 5.

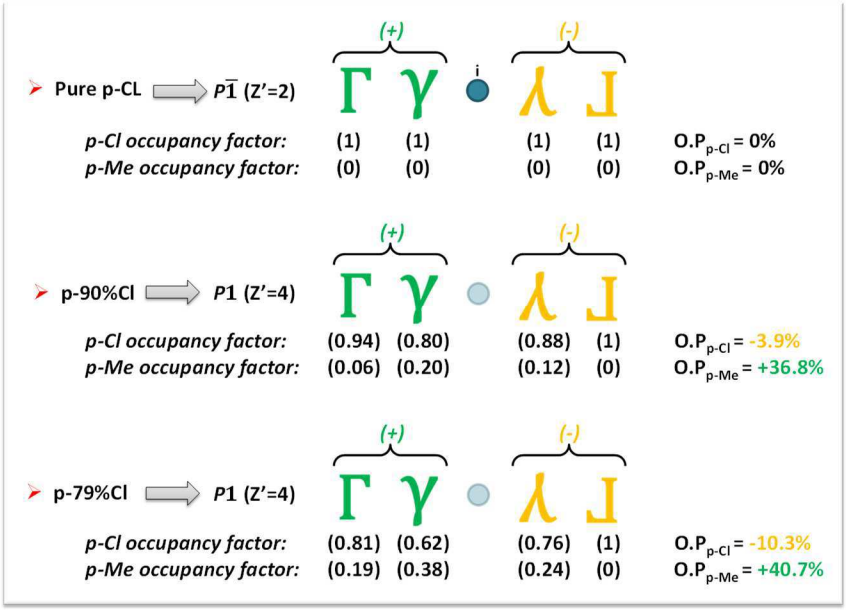

Figure 43. Schematic representation of the dissymmetric distribution on the crystallographic sites and of the chirality induced by dissymmetry of distribution.

$$\boldsymbol{O.P_{p-Cl}} = \frac{sof_{\Gamma}^{p-Cl} + sof_{\gamma}^{p-Cl} - sof_{\Gamma}^{p-Cl} - sof_{\gamma}^{p-Cl}}{sof_{\Gamma}^{p-Cl} + sof_{\gamma}^{p-Cl} + sof_{\Gamma}^{p-Cl} + sof_{\gamma}^{p-Cl}} * \mathbf{100} \qquad \text{Eq. 4}$$

Table 5. sof of the different single crystals analyzed and their respective chirality.

Pool composition	Space Group	Z′	Statistical Occupancy Factor for p-Cl				Crystal composition			
			MolO	MolA	MolC	MolB	%p-Cl	$O.P_{p\text{-}Cl}$	%p-Me	$O.P_{p\text{-}Me}$
p-40%Cl	$P2_12_12_1$	1	0.40				40%	**+100%**	60%	**+100%**
	$P2_12_12_1$	1	0.37				37%	**+100%**	63%	**+100%**
p-60%Cl	$P2_12_12_1$	1	0.46				46%	**+100%**	54%	**+100%**
	$P1$	4	0.81	0.62	0.76	1	79%	**-10.3%**	21%	**+40.7%**
p-90%Cl	$P1$	4	0.94	0.80	0.88	1	90%	**-3.9%**	10%	**+36.8%**
	$P1$	4	0.96	0.80	0.88	1	91%	**+3.3%**	9%	**-33.3%**

Every single crystal belonging to the Triclinic partial solid solution structure is not racemic. In fact, both p-Me and p-Cl components present an unbalance of their configurations, and this unbalance is of opposite sign for the two components (Figure 43). Thus, the domains containing the Triclinic partial solid solutions enumerate two Triclinic phases that are mirror images one to the other: **ss(T-(+)-p-Cl)** and **ss(T-(-)-p-Cl)**.

This chirality is induced by dissymmetric distribution on the crystallographic sites. It is, as far as we know, the first time that this phenomenon is mentioned; we proposed to name it: *Chirality Induced by Dissymmetric Distribution (CIDD).*

III Absence of the triclinic T-p-Cl complete solid solutions

Another unexpected behavior of this system is that the triclinic structure, which is a racemic compound for the pure composition, cannot be obtain for the p-Me, even when inoculation of seeds with T-(±)-p-Cl is performed. By contrast, O-p-Me conglomerate can form a complete solid solution.

According to the statistic about chiral systems, the reverse situation was expected since ≈90-95% of the chiral systems form a racemic compound, whereas ≈5-10% a conglomerate and <1% form solid solution.[16]

Surely, the atypical triclinic partial solid solution, which is not a racemic structure, influences this behavior. But another consideration could be the glass transition temperature.

A rough approximation of the melting temperature of the hypothetical Triclinic p-Me is around -60°C, which is below but close to the glass transition of the molten p-Me (Tg = -45.8°C). Intuitively, it gives the impression that the Triclinic p-Me is less stable than the liquid.

By contrast, p-Cl glass transition is far below the melting of the different phases (Tg = -35.8°C).

IV Beyond the racemic isoplethal section

The equilibria of the racemic isoplethal section have been determined. Nonetheless, the phases of those equilibria being not all racemic, higher order representations than the binary section are necessary. Moreover, the binary representation cannot illustrate the results after deracemizations, which are the ultimate evolutions of the system.

Whatever the representation used, possible domains are the colored ones, uncolored areas represent the domains that cannot be explored.

IV.1 Apparent simple eutectic equilibrium

Because of its nature (apparent equilibrium) and its simplicity compare to the other equilibria, the simple eutectic phase diagram has been represented first.

Different representations can be used (Figure 26, 44 & 45), the most useful one being the "extended binary" representation that allies all the compositions reached by the 'equilibrium' and the temperature (Figure 44).

All the phases being confined in a triangle composed of (+)-p-Me, (-)-p-Me and (±)-p-Cl, the system can be considered as *quasi-ternary*.

The different domains are:

- In grey: a monophasic domain composed of the racemic liquid.
- In orange: biphasic domain (bundle of tie-lines) between the racemic liquid and the T-(±)-p-Cl racemic compound.
- In yellow: triphasic domain (bundle of tie-triangles) between the racemic liquid and the two O-p-Me antipodes (O-(+)-p-Me and O-(-)-p-Me).
- In violet: triphasic domain (bundle of tie-triangles) between the three solid phases (T-(±)-p-Cl, O-(+)-p-Me and O-(-)-p-Me).
- In green: the two eutectic triangles between one antipode of the O-p-Me and the racemic liquid and p-Cl racemic compound.

- At the eutectic point E: four phases equilibrate: racemic liquid, T-(±)-p-Cl, O-(+)-p-Me and O-(-)-p-Me.

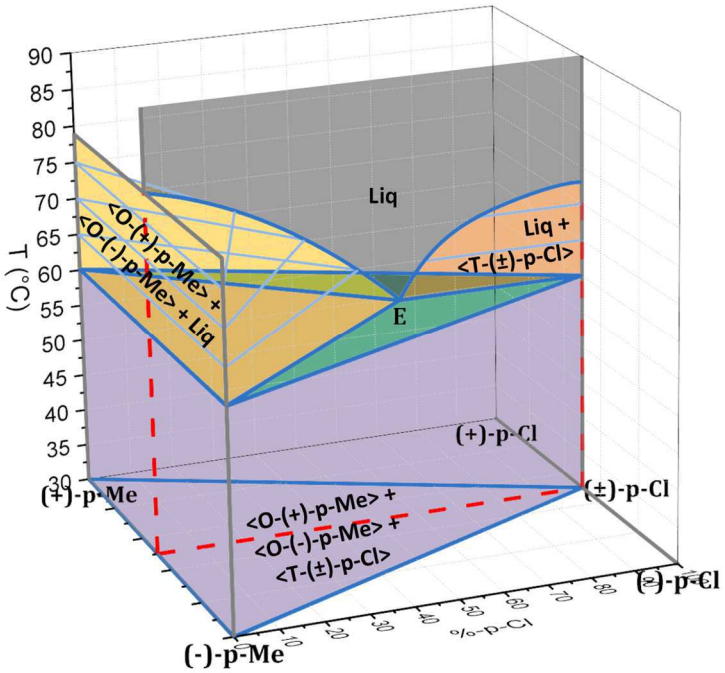

Figure 44. Extended binary representation of the simple eutectic equilibrium.

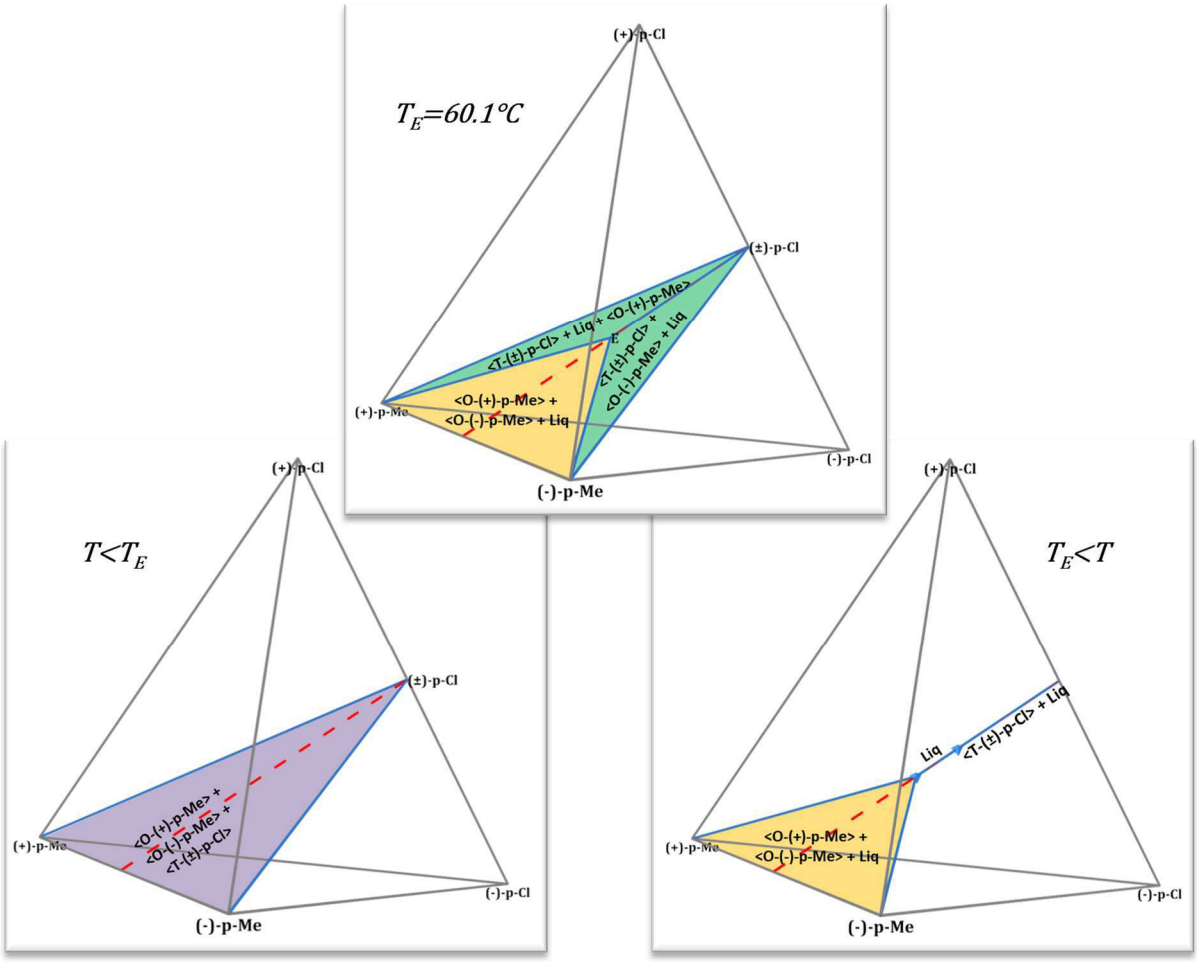

Figure 45. Tetrahedral representations of the simple eutectic equilibrium.

In Figure 46 & 47 are represented the ultimate evolution of the system when deracemization occurred. With one component missing (O-(+)-p-Me here), the domains in which it was involved has disappeared.

In the frame of this work, this behavior should not appear since the deracemization process should lead to the partial solid solution.

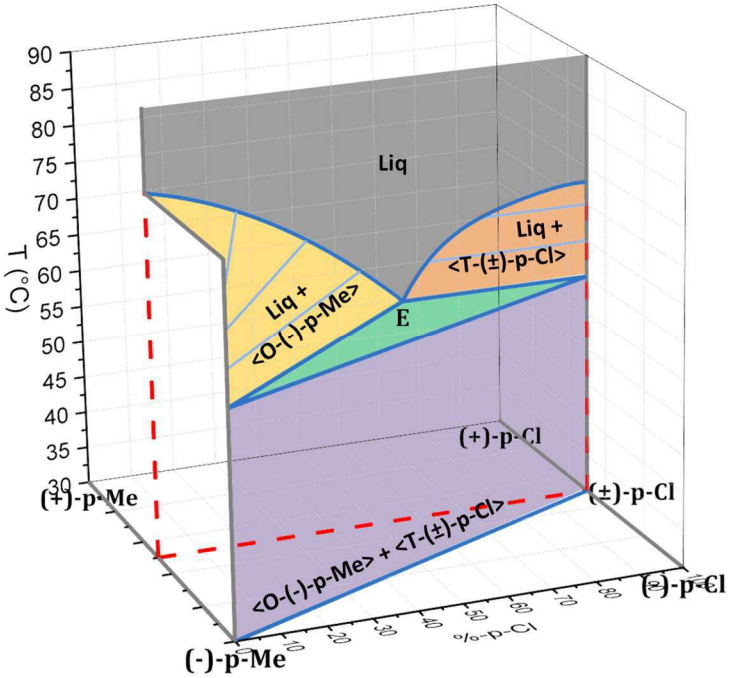

Figure 46. Totally deracemized extended binary representation of the simple eutectic equilibrium.

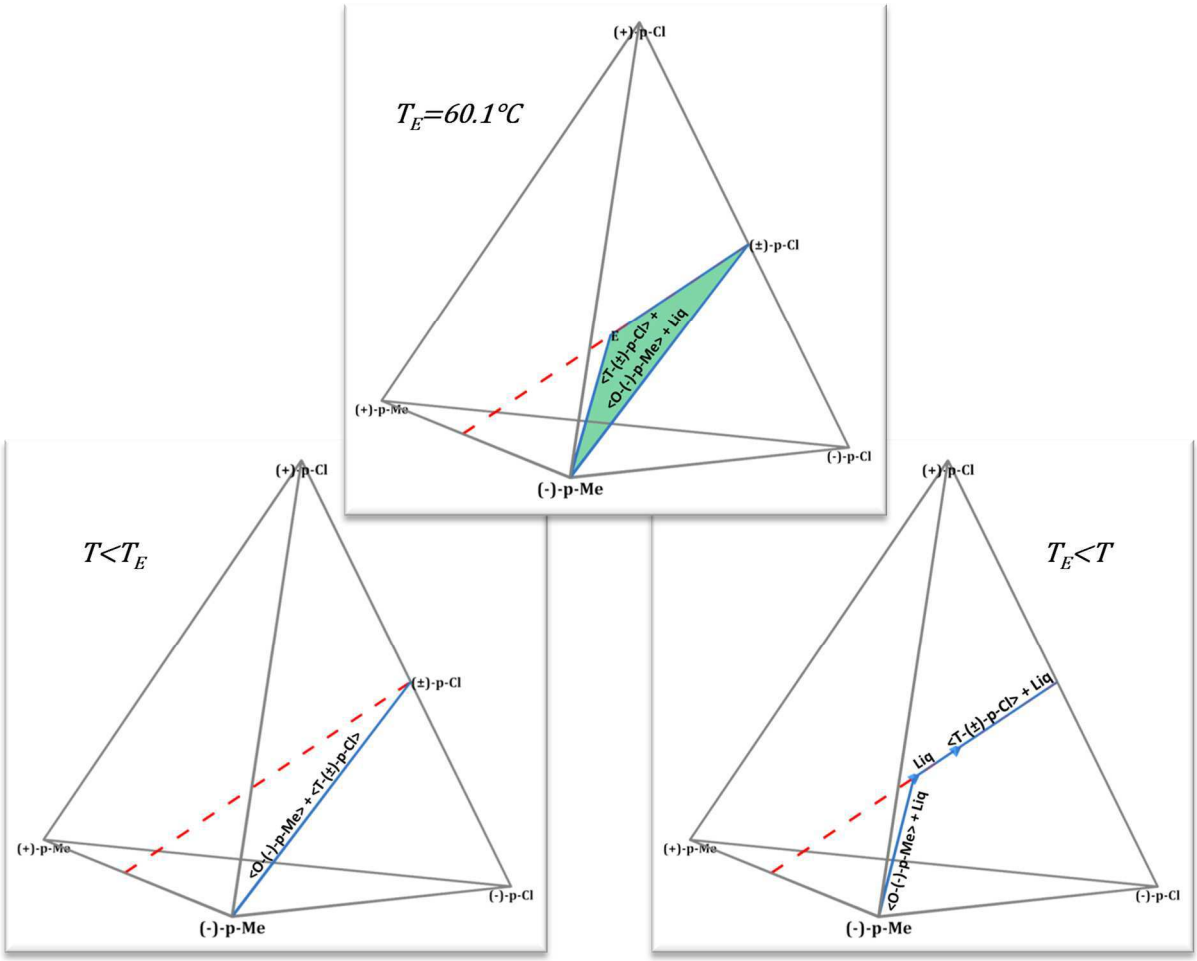

Figure 47. Totally deracemized tetrahedral representations of the simple eutectic equilibrium.

The case presented is the O-(-)-p-Me deracemization, but the O-(+)-p-Me deracemization has the same probability to occur.

IV.2 Metastable Complete Solid Solutions equilibrium

The second equilibrium illustrated with 3D representation is the metastable complete solid solutions. Different representations can be used (Figure 39, 48 & 49).

The complete solid solutions are observed for both Orthorhombic O-p-Me antipodes (from (+)-p-Me to (+)-p-Cl and from (-)-p-Me to (-)-p-Cl). Nonetheless, solid phases do not explore the diagonal compositions ((+)-p-Me/(-)-p-Cl and (-)-p-Me/(+)-p-Cl), therefore extended binary representation can be used.

The different domains are:

- In grey: the racemic liquid monophasic domain.
- In green: triphasic domain (bundle of tie-triangles) between the racemic liquid and the two mirror image solid solutions css(O-(+)-p-Me) and css(O-(-)-p-Me).
- In blue: biphasic domain (bundle of tie-lines) between the two complete mirror image solid solutions css(O-(+)-p-Me) and css(O-(-)-p-Me).
- At the Congruent point C: three phases are in equilibrium: the liquid and the two complete solid solutions.

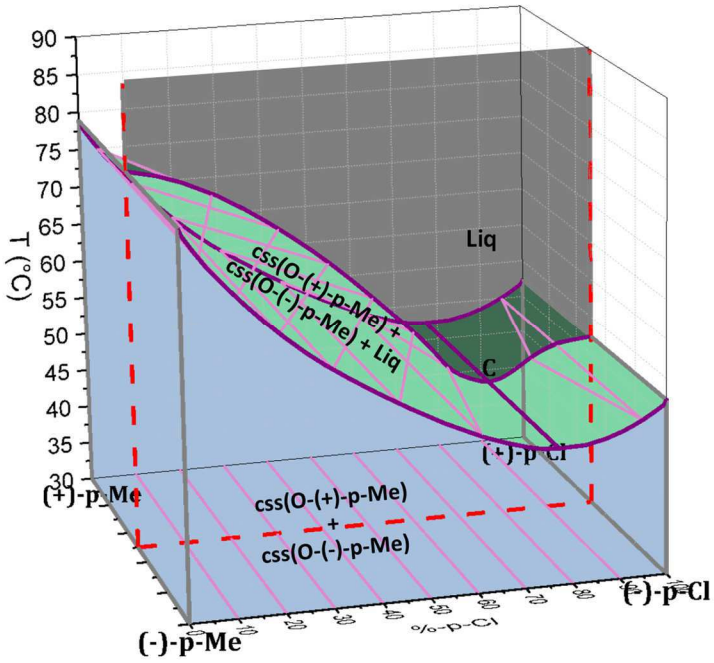

Figure 48. Extended binary representation of the complete solid solutions equilibrium

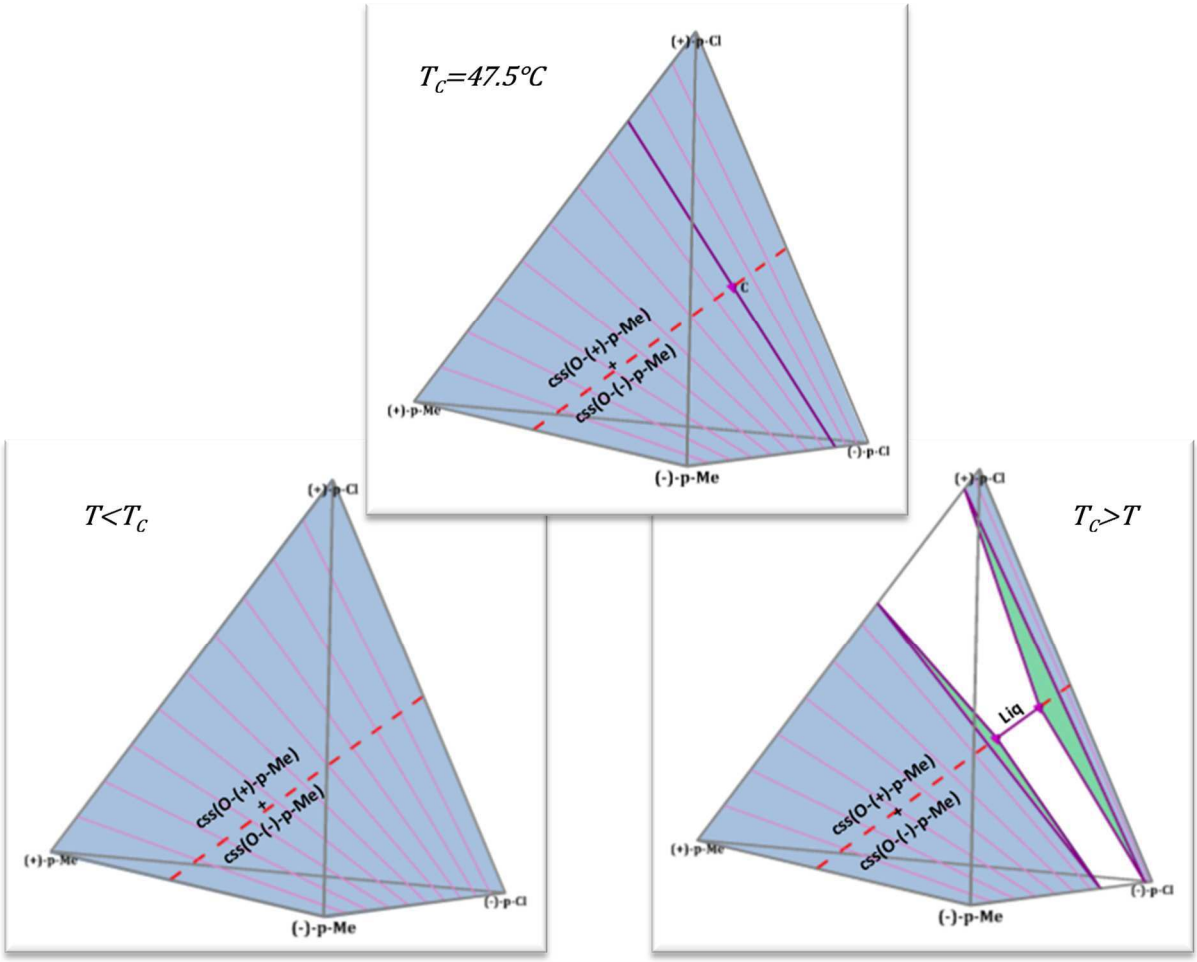

Figure 49. Tetrahedral representations of the complete solid solutions equilibrium.

If deracemization occurs in this system, the solid phase could be deracemized in css(O-(+)-p-Me) or css(O-(-)-p-Me) with an equal probability (Figure 50 & 51). Seeding can trigger the evolution toward the desired enantiomers

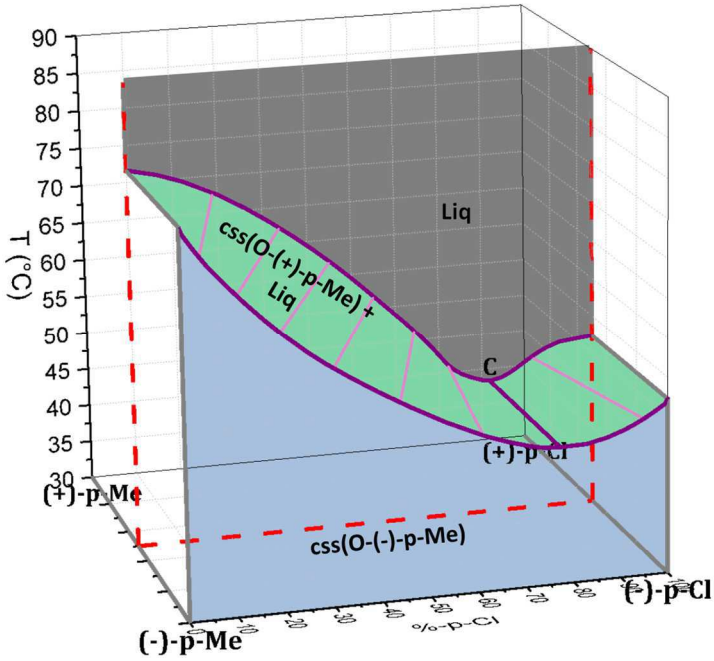

Figure 50. Totally deracemized extended binary representation of the complete solid solutions equilibrium.

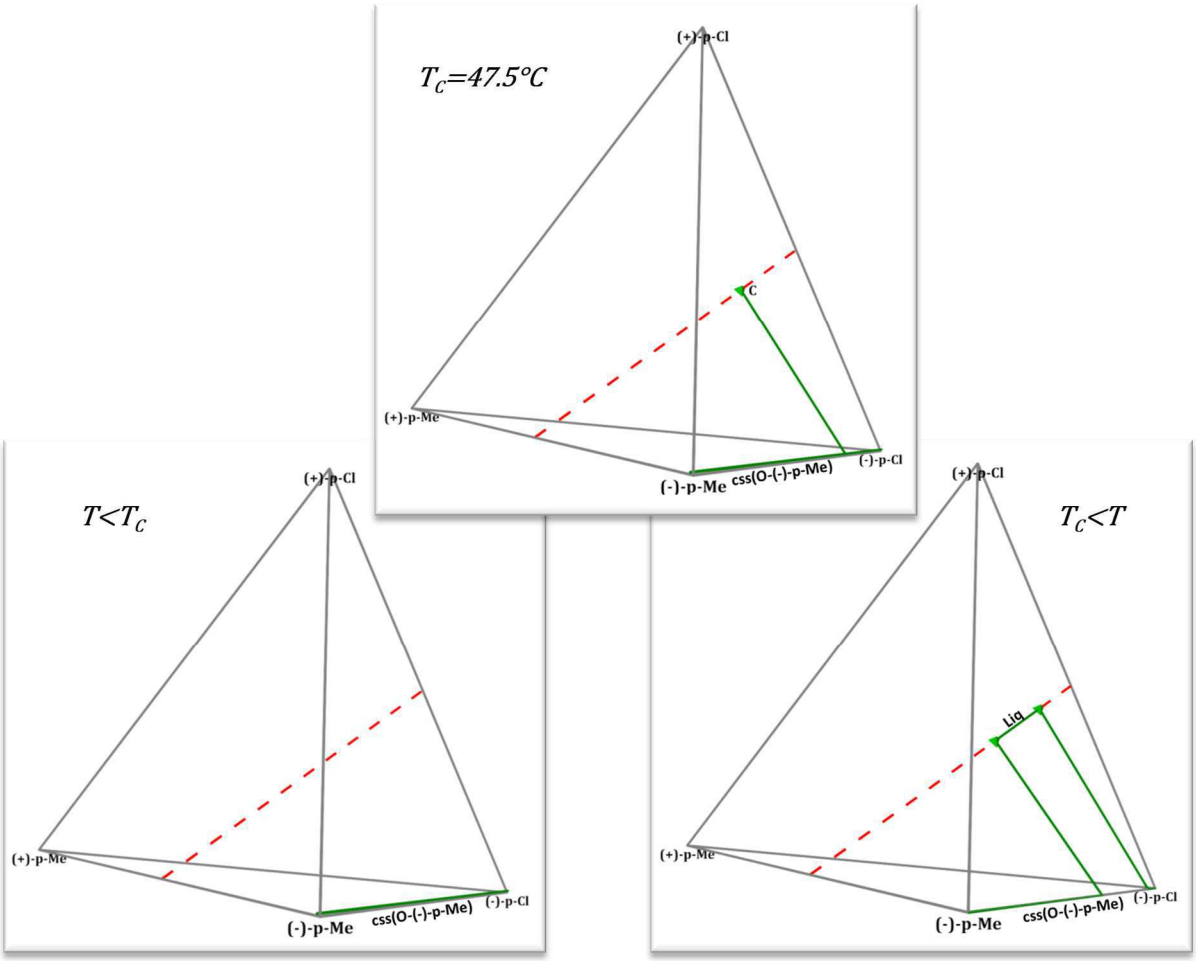

Figure 51. Totally deracemized tetrahedral representations of the complete solid solutions equilibrium.

IV.3 Stable partial solid solutions equilibrium

Concerning the partial solid solutions equilibrium, the extended binary representation can no longer be used. Indeed, crossed phases are in equilibrium: orthorhombic crystals of (+)-p-Me would incorporate (+)-p-Cl antipode whereas triclinic crystals with (+)-p-Cl excess also present an excess of (-)-p-Me. Such a phase cannot be represented in Figure 52.

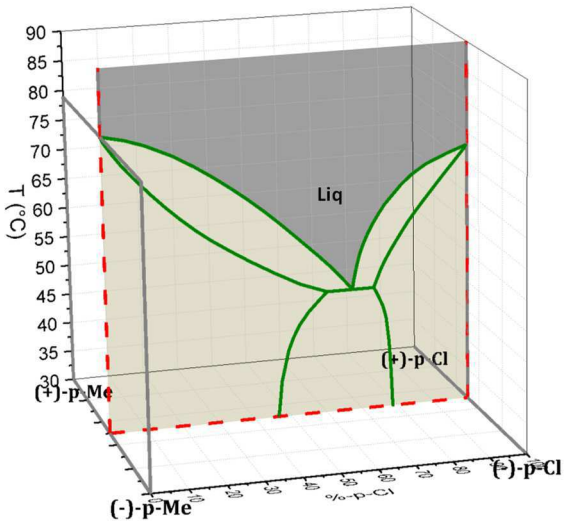

Figure 52. Tentative extended binary representation of the partial solid solutions equilibrium.

If the only interest is on the orthorhombic or the triclinic partial solid solutions, the extended binary representation can be used.

If the interest is in all the range of composition, tetrahedron must be used, completed with the square projection to help the 3D view (Figure 53, 54 & 55).

In those figures, the domains are:

- a monophasic racemic liquid in Figure 55.
- In dark blue: biphasic domain (bundle of tie-lines) between the two partial mirror image solid solutions ss(O-(+)-p-Me) and ss(O-p-(-)-Me) (Figure 53, 54 & 55).
- In violet: biphasic domain (bundle of tie-lines) between the two partial mirror image solid solutions ss(T-(+)-p-Cl) and ss(T-(-)-p-Cl) (Figure 53, 54 & 55).
- In yellow: Quadriphasic domain (tetrahedron) between the four partial solid solutions (ss(O-(+)-p-Me), ss(O-p-(-)-Me), ss(T-(+)-p-Cl) and ss(T-(-)-p-Cl)) (Figure 53).
- In light blue, red and green: the four eutectic tetrahedrons (the fourth being not represented to ease the view) between the racemic liquid and three solid phases (Figure 54)

e.g: ss(O-p-(-)-Me), ss(O-p-(+)-Me), ss(T-(+)-p-Cl) and racemic liquid in the non-represented tetrahedron.

- At the Eutectic point E: a five phase equilibrium occurs between the racemic liquid and the four partial solid solutions (Figure 54).
- In orange: triphasic domain between the two O-p-Me partial solid solutions and the liquid (Figure 55).
- In grey: triphasic domain between the two T-p-Cl partial solid solutions and the liquid (Figure 55).

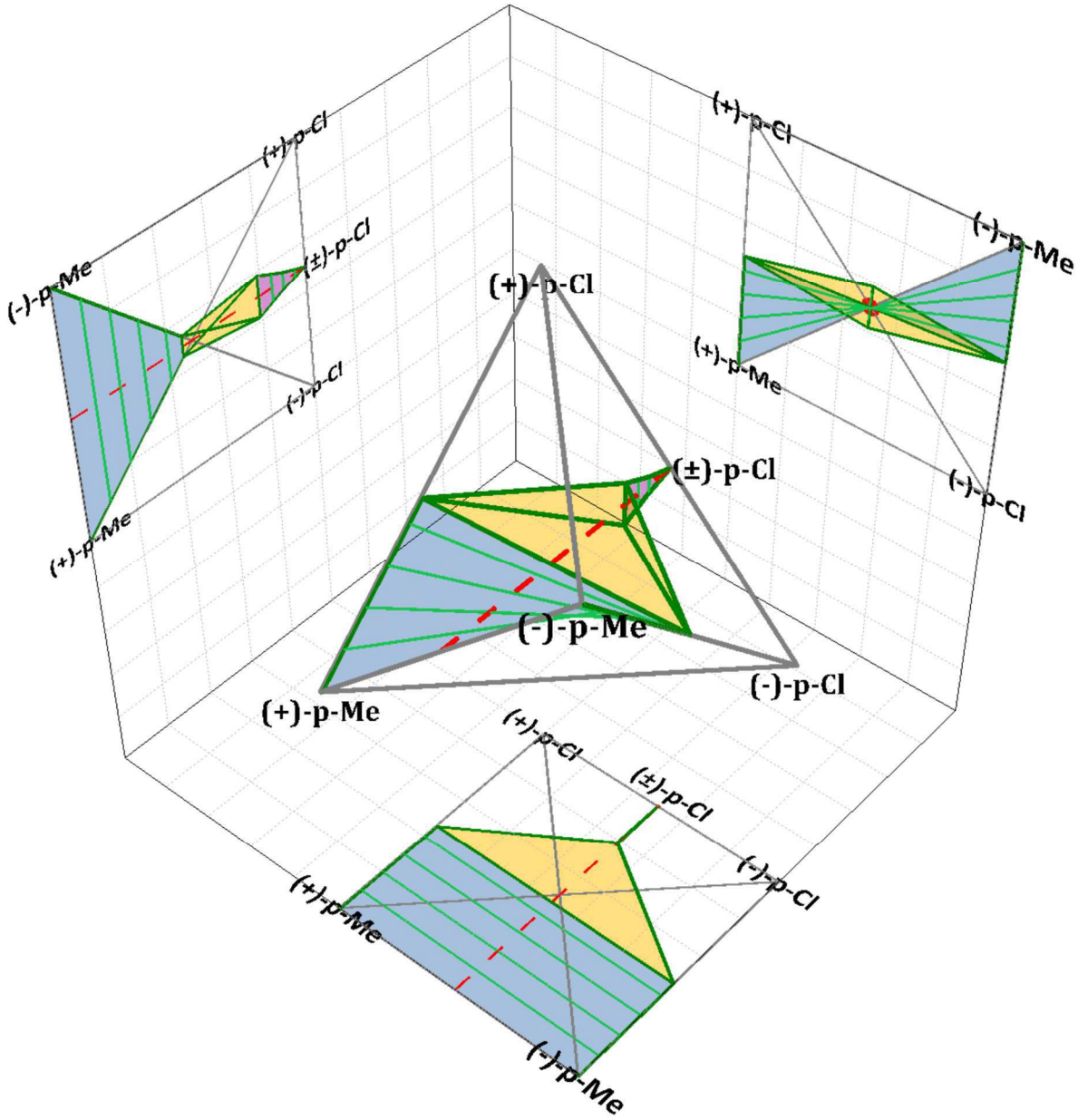

Figure 53. Tetrahedral and related square projection representations of the partial solid solutions equilbrium for $T<T_E$.

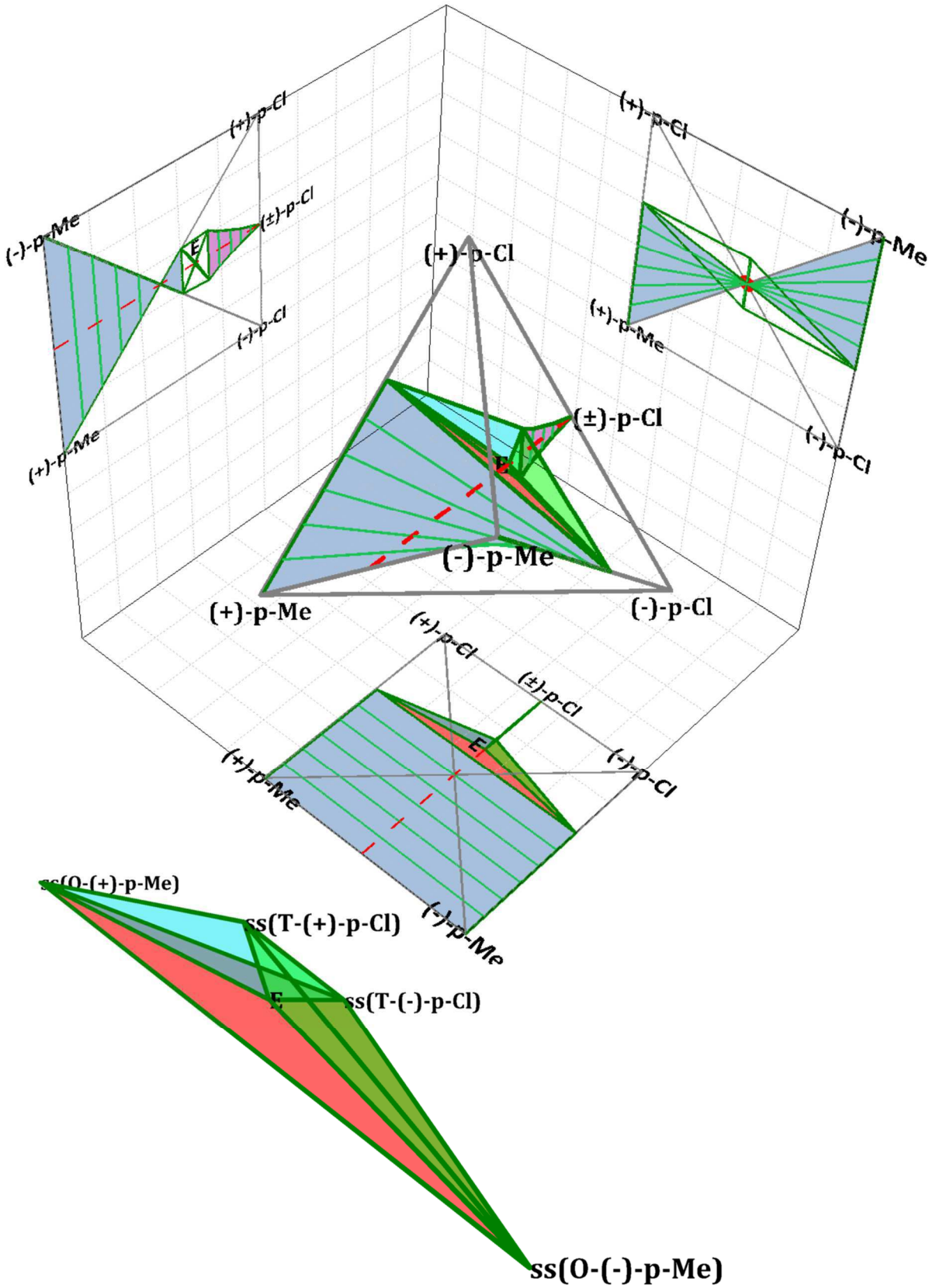

Figure 54. Tetrahedral and related square projection representations of the partial solid solutions equilbrium for $T=T_E$ and magnified eutectic tetrahedron.

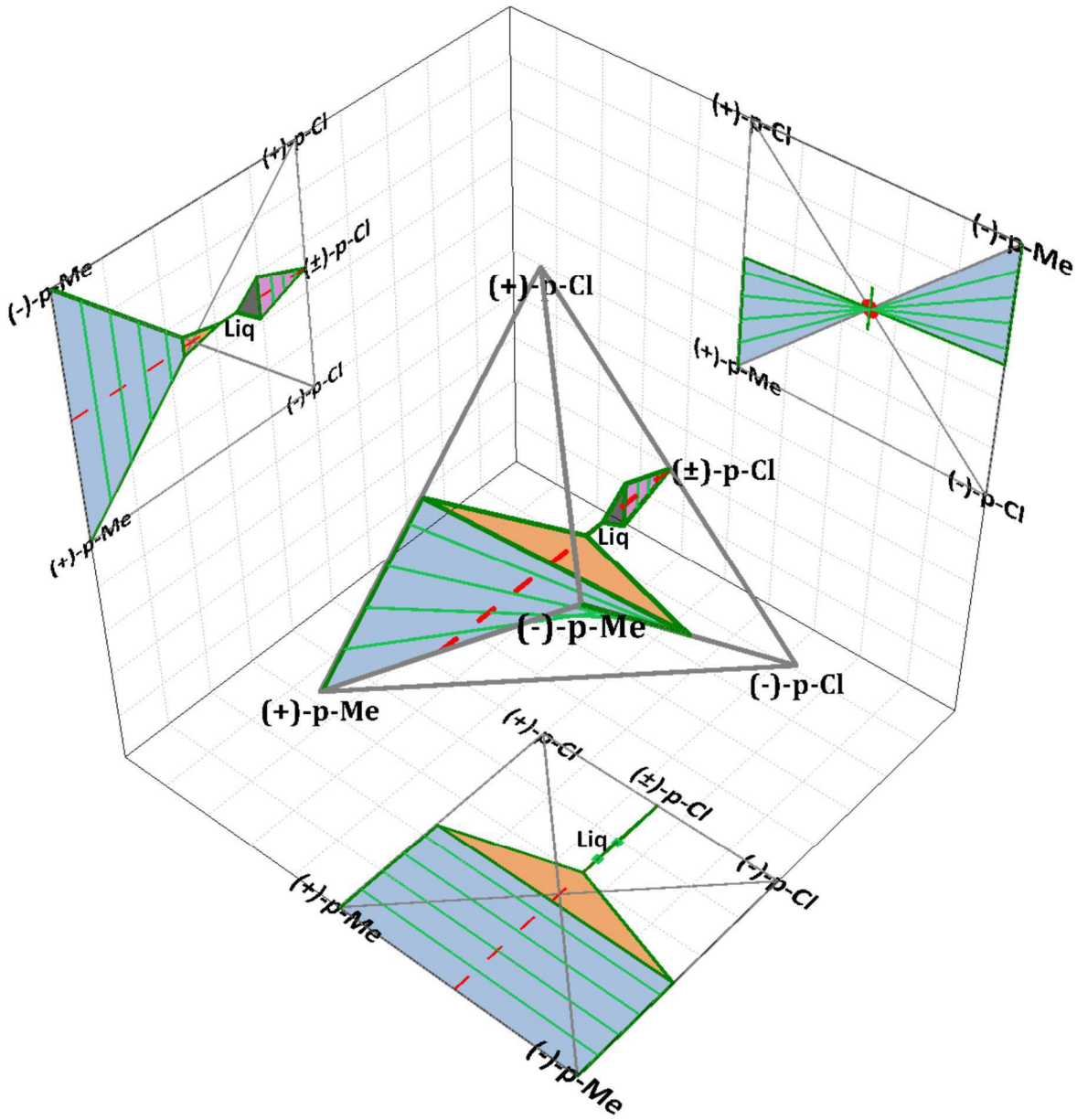

Figure 55 Tetrahedral and related square projection representations of the partial solid solutions equilbrium for $T>T_E$.

In Figure 56 is represented one possibility of deracemization for this equilibrium. The case represented is for deracemized O-(+)-p-Me and deracemized T-(+)-p-Cl. Deracemization is also possible for O-(-)-p-Me/T-(-)-p-Cl, O-(+)-p-Me/T-(-)-p-Cl or O-(-)-p-Me/T-(+)-p-Cl couples.

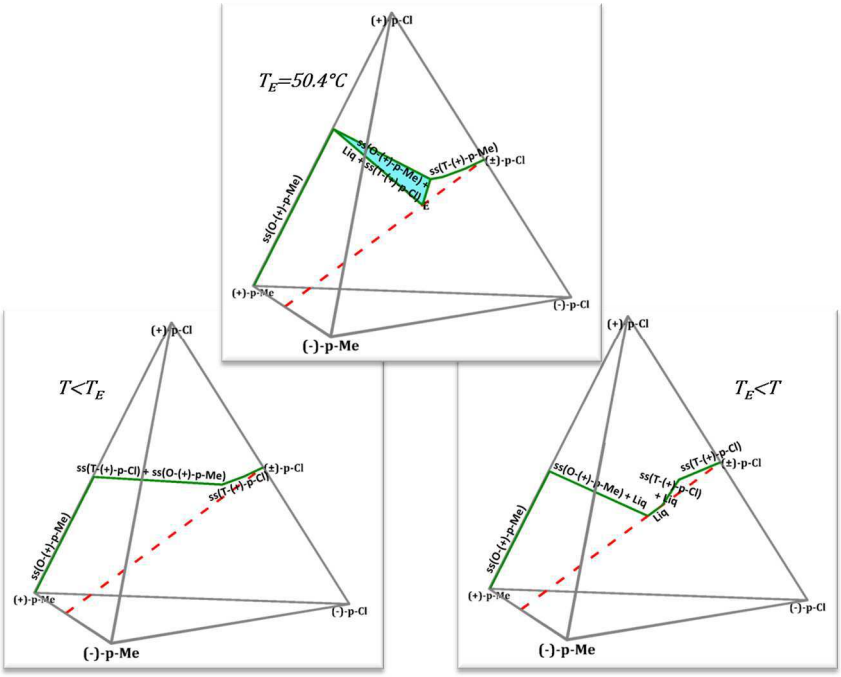

Figure 56. Totally deracemized tetrahedral representations of the partial solid solutions equilibrium.

V Extrapolated case of Chirality Induced by Dissymmetric Distribution

The *CIDD* (Chirality Induced by Dissymmetric Distribution) is a double chirality phenomenon since the two chiral components of the partial solid solutions present this dissymmetry of distribution (with opposite signs).

The reflection on this phenomenon is limited in our study by the limits of the partial solid solutions domain and its $Z' = 4$ ($Z' = 2$ in the racemic compound) which complicate the distribution.

If we consider the following simplest case where (Figure 57):

- Components **A** and **B** are chiral (atropisomery) but form isostructural centrosymmetric racemic compounds with $Z' = 1$.
- Complete solid solutions present the greatest possible *CIDD* between the pure components. For all intermediate compositions, the inversion center vanishes and the highest possible dissymmetric distribution takes place.

Whatever the composition, the minor component occupies only one position. Inside a crystal, the e.e in the minor component is thus 100% and the major component presents an intermediate opposite e.e.

Two families of crystals can be obtained according to which position is occupied. Those families are mirror images.

At the 1:1 stoichiometry (50% composition), each site is only occupied by one component. Thus, only one antipode of each component is present in a crystal. This crystal presents an e.e of +100% in one component and of -100% in the other.

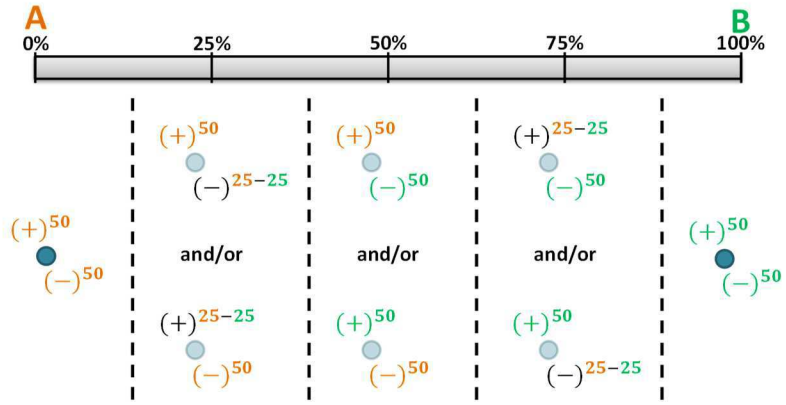

Figure 57. Schematic CIDD phenomenon observed between two isostructural racemic compounds.

Figure 58 represents the tetrahedron of such a system. Starting from the racemic compound, biphasic domain appears up to the 1:1 **(+)-A/(-)-B** and **(-)-A/(+)-B** compositions. Note that in this model, all the mirror image solid solutions are in one plane and connected by tie-lines.

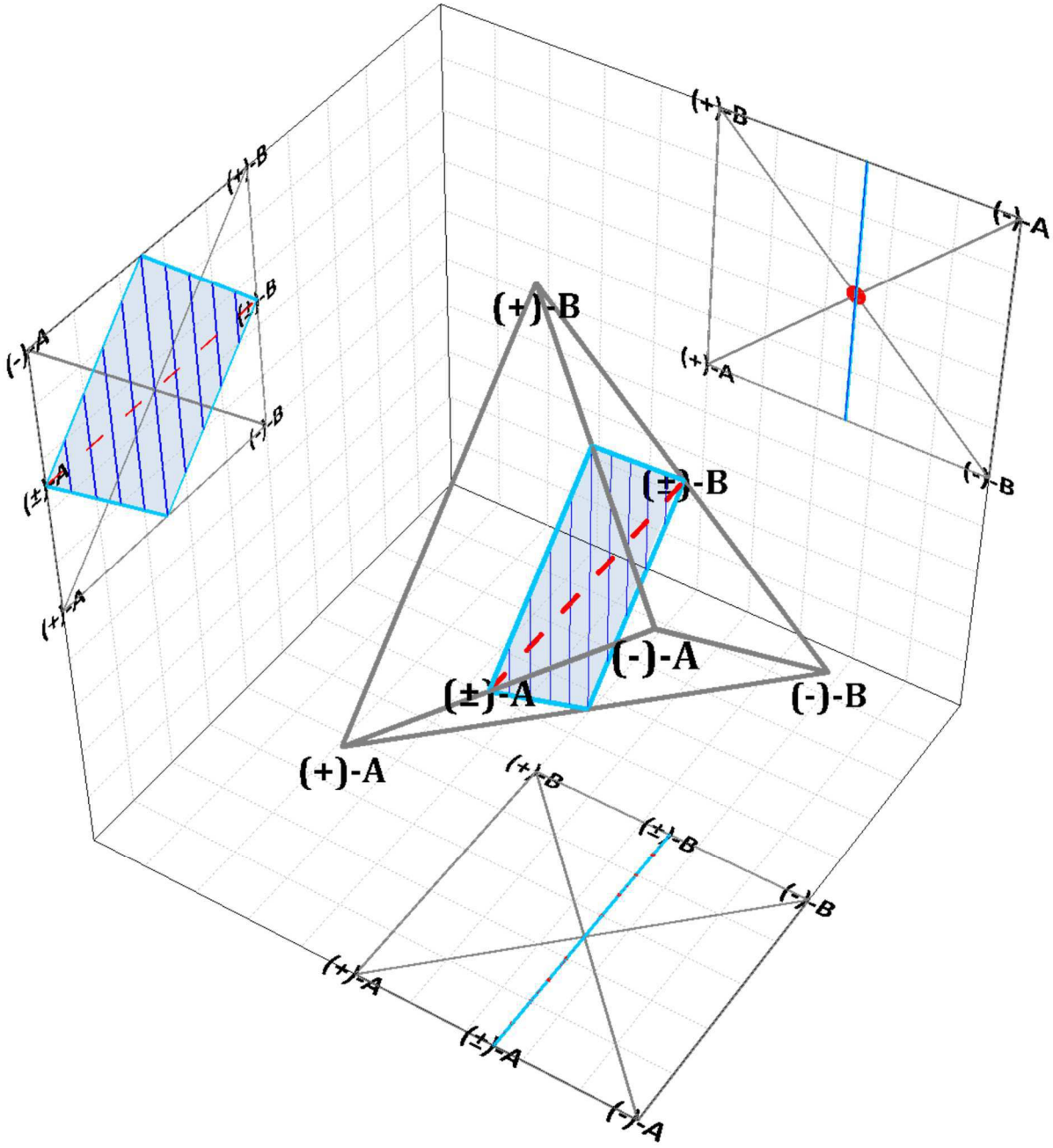

Figure 58. Tetrahedron for CIDD observed between two isostructural racemic compounds.

Deracemization of this model would lead to only one family of crystal, with the best efficacity for the 1:1 stoichiometry because both components should be fully deracemized (Figure 59).

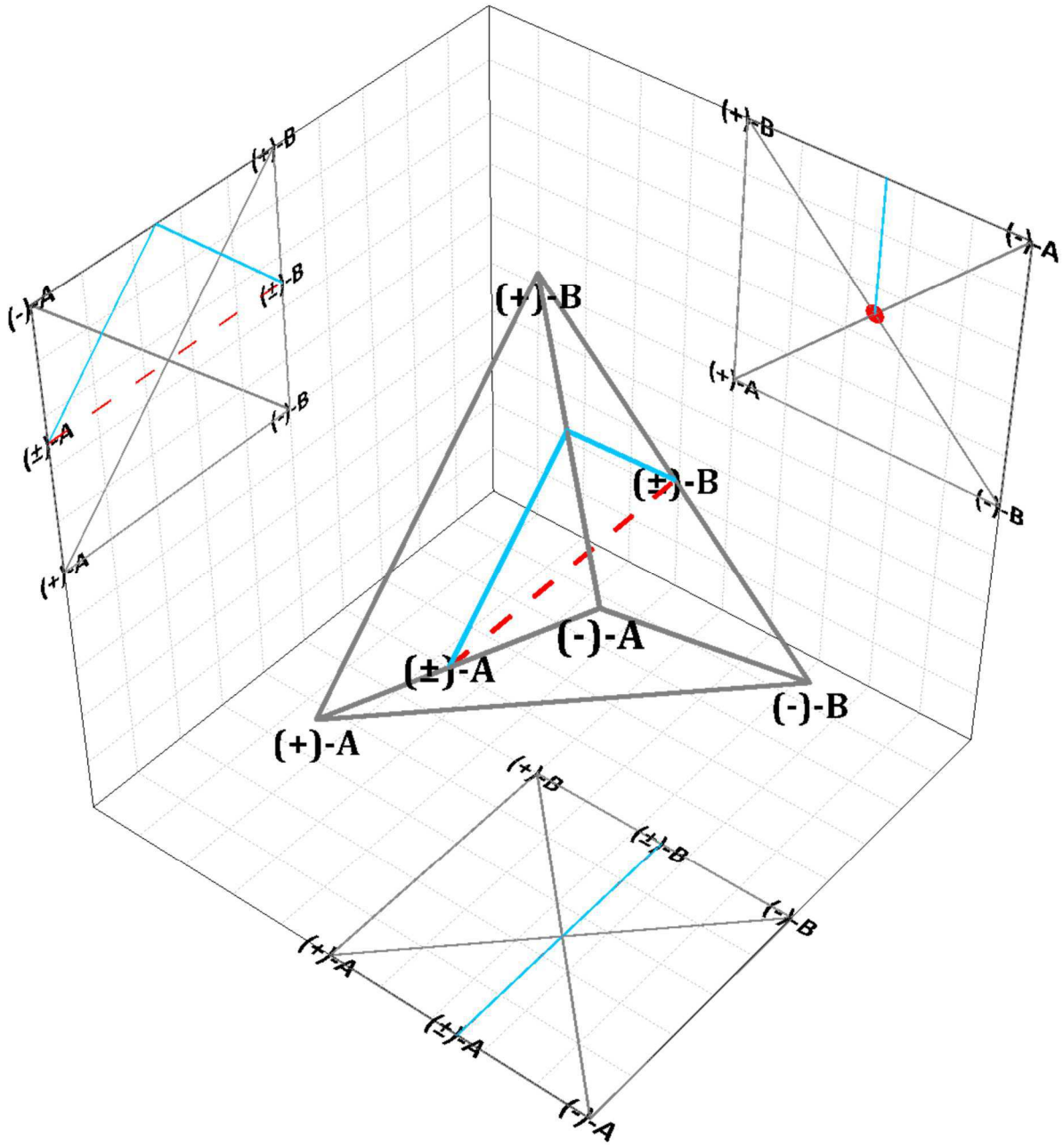

Figure 59. Deracemized tetrahedron for CIDD observed between two isostructural racemic compounds.

Another model can be proposed between a racemic compound and a conglomerate (Figure 60 & 61). Intuitively, structures must be very similar.

Over the 50% composition, a crystal continues to be enriched in the same enantiomer. Thus, if the proportion between the two components evolves, their e.e do not evolve and stay at +100% and -100%.

In the tetrahedron, the phases follow the **(+)-A/(-)-B** and **(-)-A/(+)-B** edges. Below the 50%, tie-lines are in same plane but over 50% they are progressively shifted to the pure **(+)-B/(-)-B** section.

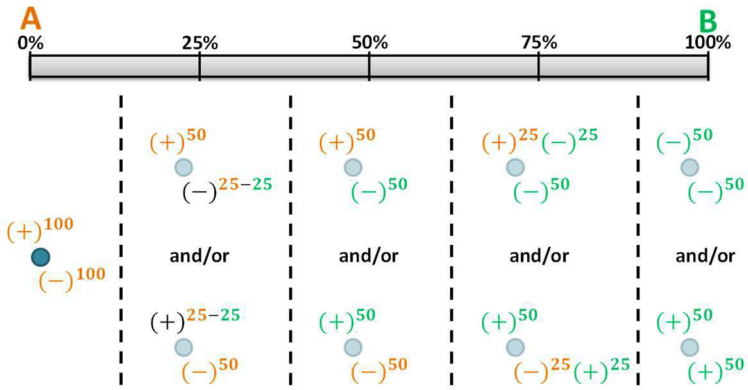

*Figure 60. Schematic CIDD observed between a racemic compound (**A**) and a conglomerate (**B**).*

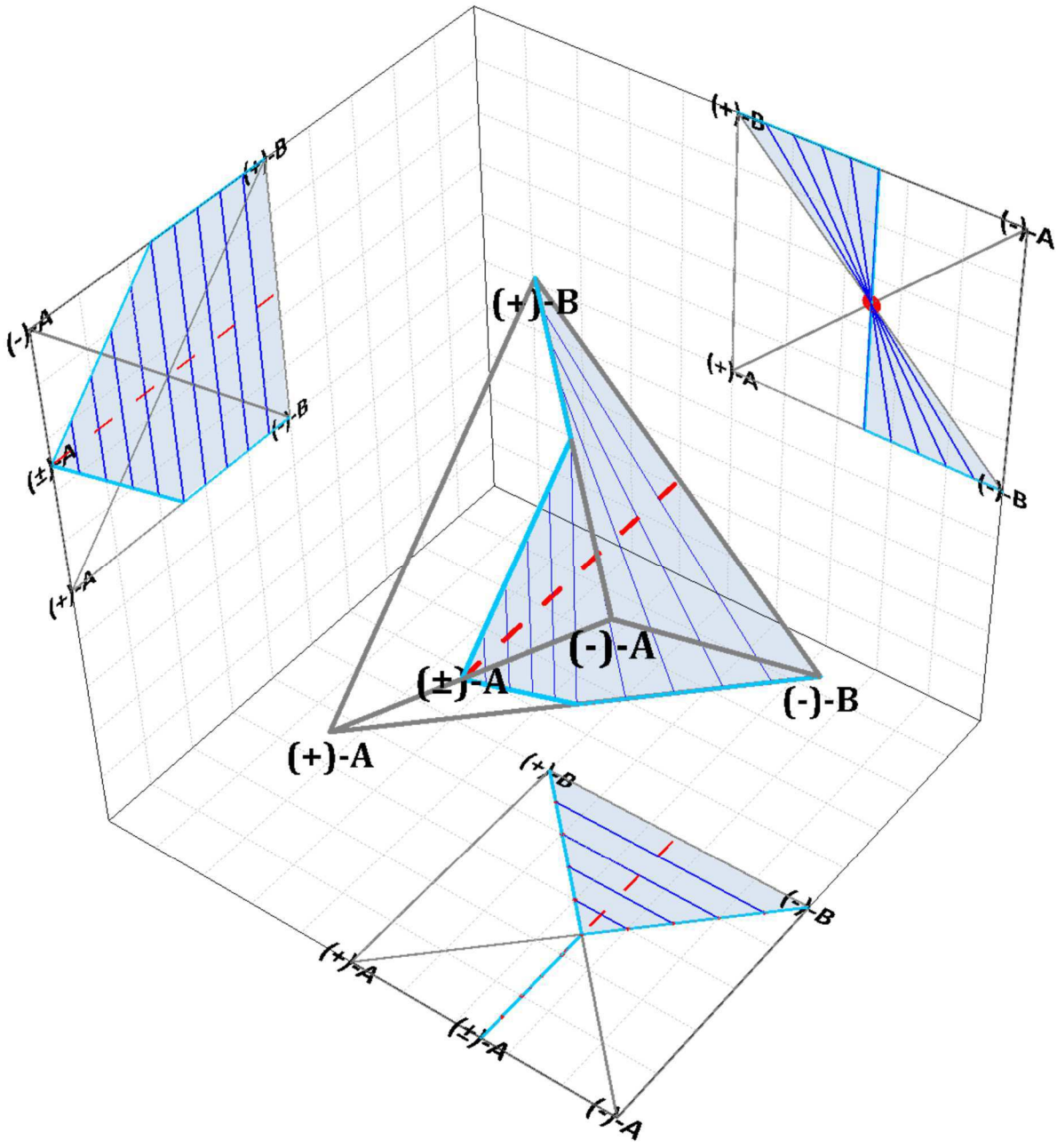

*Figure 61. Tetrahedron for CIDD observed between a racemic compound (**A**) and a conglomerate (**B**).*

As for previous model, deracemization means that only one family is possible (Figure 62).

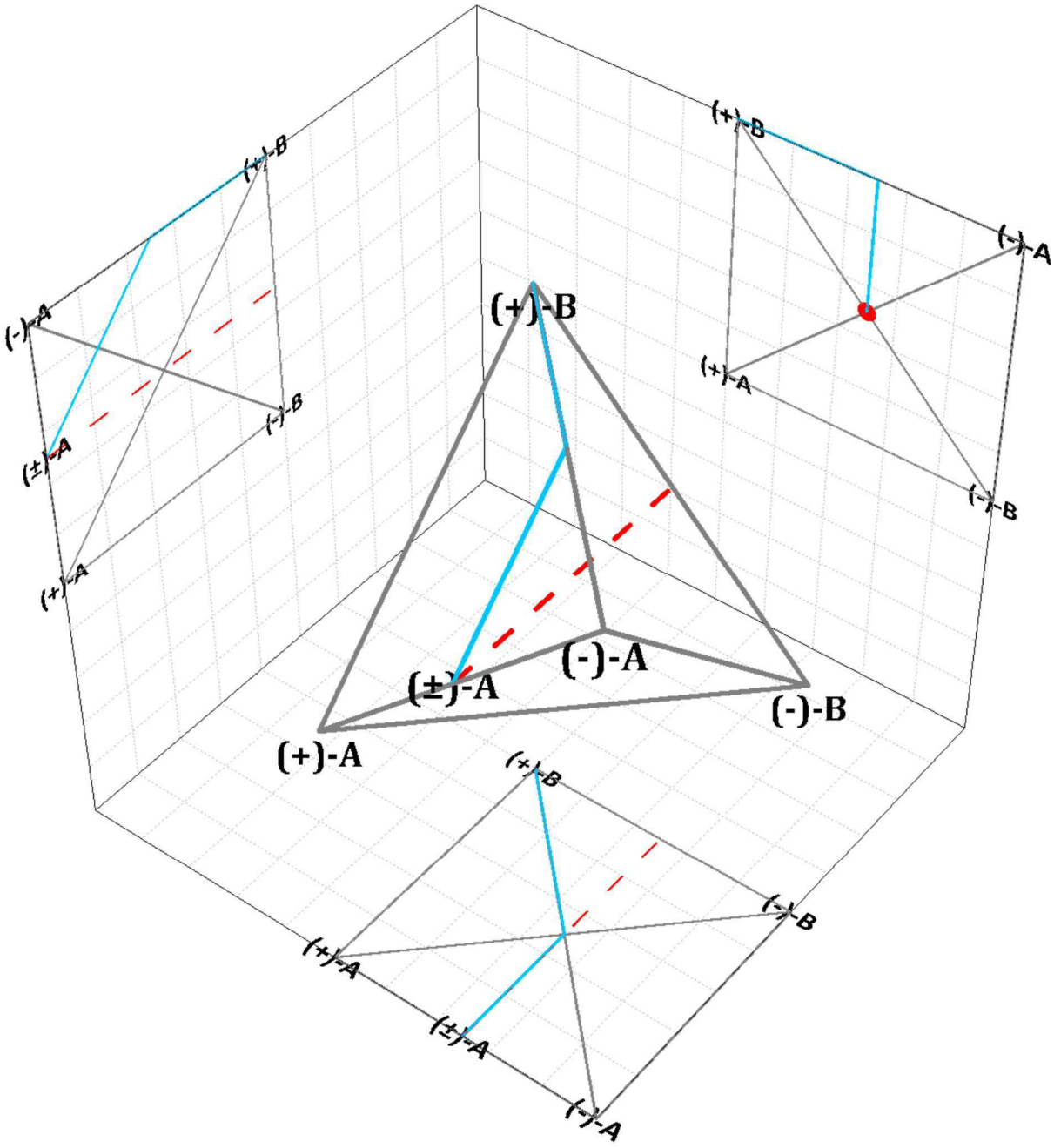

*Figure 62. Deracemized tatrahedron for CIDD observed between a racemic compound (**A**) and a conglomerate (**B**).*

Conclusion

Several points must be mentioned to conclude this chapter.

The first one concerns the initial aim of this study: the establishment of the racemic isoplethal section of a quaternary system composed of a couple of atropisomers. Stable and metastable equilibria interlaced in this section:

- The stable equilibrium involves a five phases eutectic invariant between two families of mirror image partial solid solutions and the liquid phase. The width of those partial solid solutions is quite large on the p-Me side (up to 46%) and less extended on the p-Cl part (circa 20%).
- A first metastable equilibrium consists of the two mirror image orthorhombic complete solid solutions, which are simply the continuity of the partial solid solutions.
- The last equilibrium is an apparent simple ternary eutectic invariant. Obtained by manual mixing, this equilibrium is robustness as long as the system is not in contact with a liquid phase.

Another interesting fact is that the kinetic of recrystallization is impacted by multiplying the possible heterogenous nucleation sites. This could be applicable to future works to accelerate recrystallization and to screen possible metastable polymorphs.

More interesting is the implication of the dissymmetric distribution on the crystallographic sites in the triclinic partial solid solutions. A continuum seems to exist between the centrosymmetric and the non-centrosymmetric structures, but the lack of the symmetry has another impact since it is responsible of a new kind of chirality: C*hirality Induced by Dissymmetric Distribution (CIDD).*

The mechanism behind this chirality is uncertain: does it concern only compounds presenting atropisomerism or can it be applicable to other chirality? Does the "coformer" inducing this dissymmetric repartition need to be itself chiral? etc

Finally, the different results collected for the phase equilibria and the *Chirality Induced by Dissymmetric Distribution* multiply the deracemization possibilities for this system. Indeed, one can think to apply deracemization processes[4,8,10,23] to:

- pure p-Me: observations during single crystals growth practically proved the feasibility of deracemization (very large single crystals can be obtained).
- p-Me partial solid solutions: the same deracemization conditions as that for pure p-Me would lead to the deracemization of the Orthorhombic partial solid solutions. By

this way, p-Cl, which is not initially discriminate at all (racemic compound) can be certainly deracemized inside the p-Me matrix (up to 46%).

- p-Cl partial solid solutions: the incorporation of the p-Me inducing a partial chiral discrimination inside the Triclinic structure, partial deracemization is theoretically feasible.

Bibliography

(1) Prelog, V. Chirality in Chemistry. *Croat. Chem. Acta* **2006**, *79* (3), XLIX–LVII.

(2) Viedma, C. Experimental Evidence of Chiral Symmetry Breaking in Crystallization from Primary Nucleation. *J. Cryst. Growth* **2004**, *261* (1), 118–121.

(3) Viedma, C. Chiral Symmetry Breaking During Crystallization: Complete Chiral Purity Induced by Nonlinear Autocatalysis and Recycling. *Phys. Rev. Lett.* **2005**, *94* (6), 065504.

(4) Viedma, C. Selective Chiral Symmetry Breaking during Crystallization: Parity Violation or Cryptochiral Environment in Control? *Cryst. Growth Des.* **2007**, *7* (3), 553–556.

(5) Noorduin, W. L.; Vlieg, E.; Kellogg, R. M.; Kaptein, B. From Ostwald Ripening to Single Chirality. *Angew. Chem. Int. Ed.* **2009**, *48* (51), 9600–9606.

(6) Noorduin, W. L.; van Enckevort, W. J. P.; Meekes, H.; Kaptein, B.; Kellogg, R. M.; Tully, J. C.; McBride, J. M.; Vlieg, E. The Driving Mechanism Behind Attrition-Enhanced Deracemization. *Angew. Chem. Int. Ed.* **2010**, *49* (45), 8435–8438.

(7) Spix, L.; Alfring, A.; Meekes, H.; van Enckevort, W. J. P.; Vlieg, E. Formation of a Salt Enables Complete Deracemization of a Racemic Compound through Viedma Ripening. *Cryst. Growth Des.* **2014**, *14* (4), 1744–1748.

(8) Rougeot, C.; Guillen, F.; Plaquevent, J.-C.; Coquerel, G. Ultrasound-Enhanced Deracemization: Toward the Existence of Agonist Effects in the Interpretation of Spontaneous Symmetry Breaking. *Cryst. Growth Des.* **2015**, *15* (5), 2151–2155.

(9) Steendam, R. R. E.; Dickhout, J.; van Enckevort, W. J. P.; Meekes, H.; Raap, J.; Rutjes, F. P. J. T.; Vlieg, E. Linear Deracemization Kinetics during Viedma Ripening: Autocatalysis Overruled by Chiral Additives. *Cryst. Growth Des.* **2015**, *15* (4), 1975–1982.

(10) Suwannasang, K.; Flood, A. E.; Rougeot, C.; Coquerel, G. Using Programmed Heating–Cooling Cycles with Racemization in Solution for Complete Symmetry Breaking of a Conglomerate Forming System. *Cryst. Growth Des.* **2013**, *13* (8), 3498–3504.

(11) Suwannasang, K.; Coquerel, G.; Rougeot, C.; Flood, A. E. Mathematical Modeling of Chiral Symmetry Breaking Due to Differences in Crystal Growth Kinetics. *Chem. Eng. Technol.* **2014**, *37* (8), 1329–1339.

(12) Suwannasang, K.; Flood, A. E.; Coquerel, G. A Novel Design Approach To Scale Up the Temperature Cycle Enhanced Deracemization Process: Coupled Mixed-Suspension Vessels. *Cryst. Growth Des.* **2016**, *16* (11), 6461–6467.

(13) Li, W. W.; Spix, L.; de Reus, S. C. A.; Meekes, H.; Kramer, H. J. M.; Vlieg, E.; ter Horst, J. H. Deracemization of a Racemic Compound via Its Conglomerate-Forming Salt Using Temperature Cycling. *Cryst. Growth Des.* **2016**, *16* (9), 5563–5570.

(14) Katsuno, H.; Uwaha, M. Mechanism of Chirality Conversion by Periodic Change of Temperature: Role of Chiral Clusters. *Phys. Rev. E* **2016**, *93* (1).

(15) Ricci, J. E. *The Phase Rule and Heterogeneous Equilibrium*, Dover publications.; New York, 1966.

(16) J. Jaques; A. Collet; S. H. Wilen. *Enantiomers, Racemates, and Resolutions*; Krieger Publishing Company: Malabar, 1994; Vol. 86.

(17) Le Minh, T.; von Langermann, J.; Lorenz, H.; Seidel-Morgenstern, A. Enantiomeric 3-Chloromandelic Acid System: Binary Melting Point Phase Diagram, Ternary Solubility Phase Diagrams and Polymorphism. *J. Pharm. Sci.* **2010**, *99* (9), 4084–4095.

(18) Szulc, J.; Witkiewicz, Z.; Dąbrowski, R. Comparison of Methods for Determining the Eutectic Compositions of Ternary Liquid - Crystalline Mixtures. *Mol. Cryst. Liq. Cryst.* **1984**, *109* (2–4), 125–142.

(19) Duddu, S. P.; Grant, D. J. W. Formation of the Racemic Compound of Ephedrine Base from a Physical Mixture Ot Its Enantiomers in the Solid, Liquid, or Vapor State. *Pharm. Res.* **1992**, *9* (8), 1083–1091.

(20) Brandel, C.; Amharar, Y.; Rollinger, J. M.; Griesser, U. J.; Cartigny, Y.; Petit, S.; Coquerel, G. Impact of Molecular Flexibility on Double Polymorphism, Solid Solutions and Chiral Discrimination during Crystallization of Diprophylline Enantiomers. *Mol. Pharm.* **2013**, *10* (10), 3850–3861.

(21) Lorenz, H.; von Langermann, J.; Sadiq, G.; Seaton, C. C.; Davey, R. J.; Seidel-Morgenstern, A. The Phase Behavior and Crystallization of 2-Chloromandelic Acid: The Crystal Structure of the Pure Enantiomer and the Behavior of Its Metastable Conglomerate. *Cryst. Growth Des.* **2011**, *11* (5), 1549–1556.

(22) Threlfall, T. L. Turning DSC Charts of Polymorphs into Phase Diagrams: A Tutorial Paper. *Org. Process Res. Dev.* **2009**, *13* (6), 1224–1230.

(23) Engwerda, A. H. J.; van Schayik, P.; Jagtenberg, H.; Meekes, H.; Rutjes, F. P. J. T.; Vlieg, E. Solid Phase Deracemization of an Atropisomer. *Cryst. Growth Des.* **2017**, *17* (10), 5583–5585.

Contribution to Chiral Discrimination in the Solid State &
Access to Pure Enantiomer via Crystallization

General Conclusion

Laboratoire SMS, Université de Rouen Normandie

François-Xavier Gendron

29/06/2018

Thermodynamics of phase equilibria on chiral entities is at the origin of the original aspects of this work. Figures 1 below illustrates these new results.

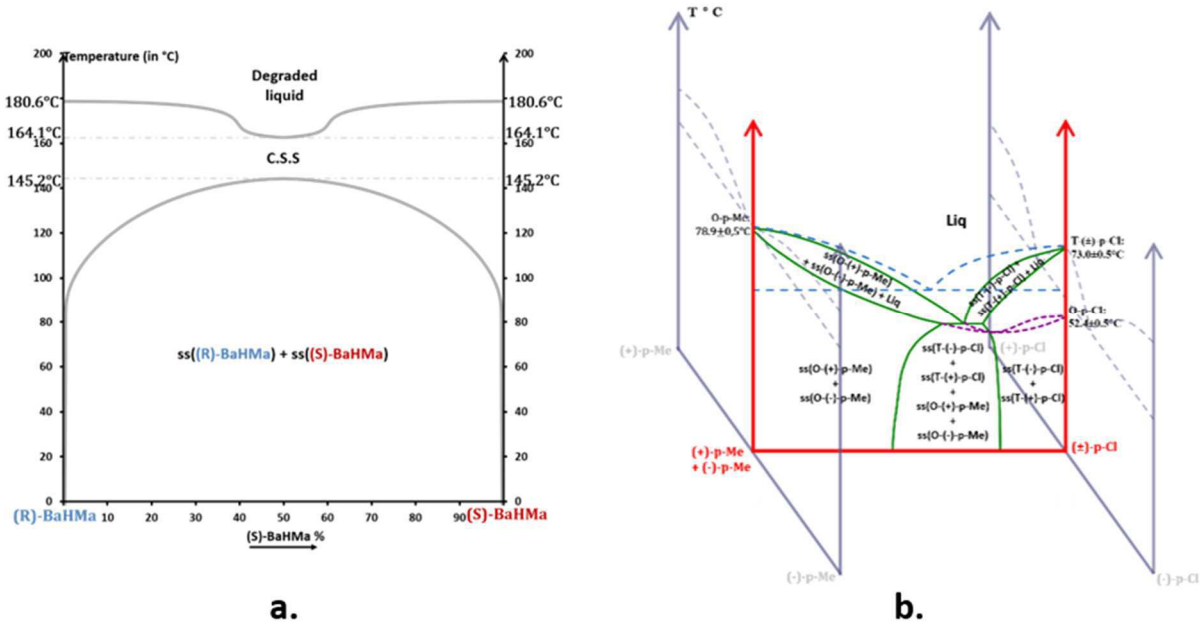

Figure 1. a. The R-S BaHMa phase diagram and b. The p-Me/p-Cl racemic isoplethal section.

In the first case (Figure 1-a), the chiral discrimination was investigated *via* the formation of salts, solvates and co-crystals. The target was to tune a preparative access to the pure enantiomers (R) of Baclofen by means of Preferential Crystallization. No usual conglomerate forming system has been found with this γ amino-acid. Nevertheless, the screen revealed the evidence of a complete solid solution of its hydrogenomaleate salt at high temperature prior melting – decomposition. This salt undergoes an extensive miscibility gap in the solid state so that, at room temperature, the symmetrical monophasic domains are narrow between 98.5%e.e and 100%e.e. To our knowledge this is the first experimental study of a binary system between enantiomers corresponding to this predicted phase diagrams but so far without any example.[1] The narrow symmetrical monophasic domains contribute to the success of the auto-seeded preferential crystallization which was demonstrated at the 40mL scale. Therefore, even if there is a complete solid solution at high temperature (Tc is circa at 145°C), the chiral discrimination at room temperature, up to at least 70°C, leads to a preparative resolution process more productive than those achieved with partial solid solutions only.[2,3] It shows that the screen of conglomerates by using thermal analysis only could lead to miss several nice opportunities for preparative resolutions of racemic mixtures by means of preferential crystallization. Therefore, spotting chiral discrimination by spectroscopic methods at room temperature such as a combination of Second Harmonic Generation and X-ray diffraction should be preferred.

The second study of this work shows a chiral discrimination resulting from particular phase equilibria existing in a degenerated quaternary system.

Below are listed the interesting properties observed between this couple of atropisomers:

- Three types of behaviors have been spotted for the racemic isoplethal section. In addition of the stable and metastable equilibria, there is an apparent equilibrium, without detectable solid solution which result from poor diffusion and mixing in the solid state. This simple eutectic without miscibility on the solid state results from self-consistent data, nevertheless, it seems inconsistent when combined with the other equilibria detected.
- The addition of milled glass to the solute in the DSC crucible has triggered a fast heterogeneous primary nucleation of the pure components and the solid solutions. In our system, the effect was purely kinetic providing roughly a two order of magnitude faster rate of crystallization, we can assume that for other organic systems this simple method could be useful and it is likely that new metastable solid phases could be spotted as well.
- Maybe the most interesting result revealed in this work is the proposition of a new kind of chirality. This chirality is the consequence of a dissymmetric distribution of chemically related atropisomers around a pseudo center of symmetry. By contrast to the corresponding chemically pure couple of atropisomers for which there is perfect center of symmetry, the genuine inversion center vanishes in the solid solution because of dissymmetric statistical occupancy factors over independent crystallographic sites in the domain of the solid solution for $X \neq 100\%$. At the extreme, we can imagine a conglomerate forming system, with enantiomers of opposite absolute configurations of for their two components A and B i. e. 50% mol. composition of the solid solution with: A(+)-B(-) and A(-)-B(+) around a 'false' center of symmetry. The same concept could be applied to any inversion symmetry such as: -2 = mirror and glide mirrors, -3, -4 and -6. We proposed to name this phenomenon: *Chirality Induced by Dissymmetric Distribution CIDD*.
- Even if the p-Cl atropisomer crystallizes in a stable stoichiometric racemic compound, it is very likely that it could be deracemized inside the matrix of the other atropisomer (i.e. p-Me) up to 40%. This observation might be extended to other

couple of racemizable molecules irrespective their types of chirality when the host structure crystallizes as a conglomerate.

One can expect a similar partial deracemization for CIDD. Of course, it would be both: easier to spot a more interesting case in a preparative perspective i.e. the extreme case considered in the previous paragraph. In the practical case depicted in this PhD manuscript, crystals of opposite handedness –determined by the flack parameter- have been spotted; there is then a good probability to partially deracemize these mirror related phases.

(1) Coquerel, G. Review on the Heterogeneous Equilibria between Condensed Phases in Binary Systems of Enantiomers. *Enantiomer* **2000**, *5*, 481–498.

(2) Renou, L.; Morelli, T.; Coste, S.; Petit, M.-N.; Berton, B.; Malandain, J.-J.; Coquerel, G. Chiral Discrimination at the Solid State of Methyl 2-(Diphenylmethylsulfinyl)Acetate. *Cryst. Growth Des.* **2007**, *7* (9), 1599–1607.

(3) Wermester, N.; Aubin, E.; Pauchet, M.; Coste, S.; Coquerel, G. Preferential Crystallization in an Unusual Case of Conglomerate with Partial Solid Solutions. *Tetrahedron Asymmetry* **2007**, *18* (7), 821–831.

Abstract

The need for access to pure enantiomers has largely increased since the nineties. Processes using crystallization are often cheaper and as efficient as other processes. Thus, the improvement of existing techniques and the need for new processes are attractive for scientist and industry.

Two studies have been performed in this thesis:

- The first one concerns the improvement of an existing technique. Indeed, conglomerate Preferential Crystallization efficiency is well known. Nonetheless, its application to mirror image partial solid solutions is more difficult. Here is presented the first example of PC performed on a complete solid solution at high temperature which shows a solid solutions demixion at low temperature: the baclofen hydrogenomaleate salt (an API). Moreover, it is the first experimental observation of such phase equilibria and PC of mirror image solid solutions whose results are comparable to classical PC.
- The second topic did not involve directly enantiomer separation but promising chiral discriminations have been obtained. The phase diagram between the racemic composition of two couples of atropisomers has been defined. Beside multiples equilibria observed, two results concerning the chiral discrimination can be highlighted: the first one is the possibility to deracemize a compound A initially not discriminated (racemic compound) inside the matrix of a compound B (which forms a stable conglomerate). The second is the observation of a new kind of chirality: *Chirality Induced by Dissymmetric Distribution (CIDD).*

Résumé

Le besoin d'accès aux énantiomères purs a largement augmenté depuis les années 90. Les procédés ayant recours à la cristallisation sont souvent moins cher mais tout aussi efficace que les autres procédés.

Deux études ont été réalisées dans cette thèse :

- La première concerne l'amélioration d'un procédé déjà établi. En effet, l'efficacité de la Cristallisation Préférentielle (PC) de conglomérat est connue. Néanmoins, son application à des solutions solides images l'une de l'autre dans un miroir est plus complexe. Est présenté le premier exemple de PC réalisée sur un système à solution solide complète démixant à basse température : le sel d'hydrogénomaléate de baclofène (un API). De plus, il s'agit de la première preuve expérimentale d'un tel équilibre de phases et de PC de solutions solides dont les résultats sont comparables à la cristallisation préférentielle traditionnelle.
- Le second sujet ne traite pas directement de la séparation d'énantiomère mais de prometteuses discriminations chirales ont été obtenues. Le diagramme d'équilibre de phases entre les compositions racémiques de deux couples d'atropoisomères a été étudié. Deux résultats en lien avec la discrimination chirale ont été établis : le premier est la possibilité de déracémiser un composé A initialement non-discriminé (composé racémique) à l'intérieur de la matrice d'un composé B discriminé (conglomérat). Le second est l'observation d'un nouveau type de chiralité : *Chiralité Induite par Dissymmétrie de Distribution (CIDD).*